Tandem Mass Spectrometric Analysis of a Series of Bacterial Lipid As Belonging to the *Vibrionaceae* Family

A thesis submitted to the School of Graduate Studies in partial fulfillment of the requirements for the degree of the Ph.D. of Science.

By

Mervt Almostafa

Department of Chemistry
Memorial University of Newfoundland and Labrador

03/2017

St. John's. Newfoundland and Labrador

Canada

Abstract

This study presents the mass spectrometry structural elucidations of the extracted heterogeneous lipid As mixtures, obtained from native lipopolysaccharides (LPSs) isolated from different types of the *Vibrionaceae* family. As this Gram-negative bacteria family is well known to cause many serious animal diseases and human diseases. This investigation was originally aimed to investigate the treatment of bacterial infected fish with phages as a potential treatment for pathogenic bacterial infections.

In this thesis, I shall discuss the electrospray ionization mass spectrometry (ESI-MS) and low-energy collision induced dissociation tandem mass spectrometry analysis (CID-MS/MS); and MALDI-TOF-MS/MS (high-energy CID-MS/MS) of a heterogeneous mixture of lipid A_s. These lipids As were isolated from the rough lipopolysaccharide (LPS) of the mutant wild strain of the Gram-negative bacteria *Aeromonas. liquefaciens* SJ-19, *Aeromonas. hydrophilla* SJ-55, and *Aeromonas. salmonicidia* SJ-113. These strains of bacteria were grown in the presence of phages and were isolated by the aqueous phenol method from this series of LPS of the rough wild strain of Gram-negative bacteria. Hydrolysis of the different LPS was accomplished with 1% acetic acid, and purification was by chromatography (Gel filteration affinity) using Sephadex G-50 and SephadexG-15.

These MS and MS/MS complex structural investigation were accomplished via the use of different hybrid MS instruments such as: ESI-MS with a fourier transform ion cyclotron (FTICR), a triple quadrupole (QqQ), and MALDI-TOF/TOF-MS instruments.

In that respect, low- and high-energy CID-MS/MS (known as tandem-in-space) and FTICR-MS/MS (known as tandem-in-time) mass spectrometry analyses were chosen for

the structural elucidation of this different series of lipid As isolated from *A. liquefaciens* SJ-19, *hydrophilla* SJ-55, and *salmonicidia* SJ-113a. Excellent elucidation structural results were obtained by using low collision induced (CID-MS/MS) analyses of the various heterogeneous mixtures of lipid As precursor deprotonated molecules with the two different triple quadrupole (QqQ) and FTICR-MS/MS instruments. The concomitant uses of high-energy CID-MS/MS obtained with the MALDI-TOF/TOF-MS instrument allowed the further elucidation of these complex biomolecules and can be effectively used for any structural identifaction studies.

Identifying the exact structures of these microheterogenious lipid As, obtained from Gram-negative bacteria grown in presence of phages, were by using mass spectrometry and tandem mass spectrometry techniques using different MSMS instruments, allowed to conclude that the biosynthesis of these series of mutant rough LPSs were indeed affected and produced a heterogeneous mixtures of different lipid As. Finally, this structural elucidation study provided us with a better understanding of the stereospecific gas-phase mass spectral fragmentation pathways; also, the exact sequence of these series of lipid A obtained from the rough bacteria LPSs, which have not yet been precisely established.

Acknowledgments

I would like to acknowledge my supervisors, Professors Joseph Banoub and Travis Fridgen, for their guidance, patience, and support throughout this thesis.

Thanks also to my committee member Prof. Christina Bottaro, for helping me in various ways during this project.

The acknowledgments can't be complete without thanking the past and present members in Prof. Banoub's group for their friendship and helpful discussion over the years.

I also would like to acknowledge the Department of Chemistry and Memorial University, and I would like to acknowledge the resources provided by the Department of Fisheries and Oceans (DFO), St. John's where I conducted my research. In addition, I would like to thank the government of Saudi Arabia and King Faisal University for their financial support for my Ph.D. studies.

Dedication

To My Mother

My Husband

My Lovely kids

(Sadeem, Mohammed, and Lian)

My Sisters

My Brothers

And My Friend

List of publication submitted and accepted that described the core of this work

1. M. Almostafa, B. Allehyane, S. Egli, C. Bottaro, T. Fridgen, J. Banoub. Tandem mass spectrometry determination of the putative structure of a heterogeneous mixture of Lipid As isolated from the lipopolysaccharide of the Gram-negative bacteria Aeromonas liquefaciens SJ-19a. *Rapid Commun. Mass Spectrom*. **2016**; 30: 1043-1058.
2. M. Almostafa, T. Fridgen, J. Banoub. Tandem mass spectrometry analysis of the putative structure of a heterogeneous mixture of Lipid An isolated from the lipopolysaccharide of the gram-negative bacteria Aeromonas hydrophilla SJ-55Ra. *Rapid Commun. Mass Spectrom*. (**2017**). Submited and in process.

Table of Contents

List of Tables

List of Figures

List of Schemes

List of Appendixs

List of Abbreviations

Alternating current	AC
Atmospheric pressure	AP
Atmospheric pressure chemical ionization	APCI
Chemical ionization	CI
Collision activated dissociation	CAD
Collision induced dissociation	CID
Desorption/ ionization	DI
Desorption electrospray ionization	DESI
Direct current	DC
Electron capture dissociation	ECD
Electron ionization	EI
Electrospray ionization	ESI
Electron transfer dissociation	ETD
Fast Atom Bombardment	FAB
Fourier transforms	FT
Fourier transform ion cyclotron resonance	FT-ICR
Full width at half maximum	FWHM
Galactose	Gal
Glucose	Glc
High performance liquid chromatography	HPLC

Infrared multiphoton dissociation	IRMPD
Inner membrane	IM
In-source decay	ISD
Ion trap	IT
Ion cyclotron resonance	ICR
Laser desorption ionization	LDI
L-*glycero*-D-manno-heptose	Hep
Lipopolysaccharide	LPS
Liquid chromatography	LC
Mass spectrometry	MS
Mass to charge ratio	*m/z*
Matrix assisted laser desorption ionization	MALDI
Outer membrane	OM
Phosphate-buffered salinc	PBS
Post-source decay	PSD
Quadrupole	Q
Quadrupole ion trap	QIT
Quadrupole orthogonal time-of-flight	Qq/TOF
Quadrupole-hexapole-Quadrupole	QhQ
Radio-frequency	RF
Secondary ionization mass spectrometry	SIMS
Select ion monitoring	SIM

Sustained off-resonance irradiation	SORI
Surface-induced dissociation	SID
Tandem mass spectrometry	MS/MS
Time-of-flight	TOF
Triple quadrupole	QqQ
Uridine diphosphate	UDP
α-3-deoxy-D-manno-oct-2-ulosonicacid	Kdo

Chapter 1

Introduction

1.1. Bacteria cell membrane

Bacteria are well known as the causes of many serious human and animal diseases (Zhang-Sun *et al.*, 2015, Silhavy *et al.*, 2010, and Schwechheimer *et al.*, 2015). There are various numbers of bacterial species associated with fish diseases, which are responsible for considerable economic losses for the aquaculture industry (Elaneed *et al*., 2005, Sullam *et al*., 2012, and Declercq *et al.*, 2013).

The bacteria cell envelope is composed of a multilayered component which protects their organisms from any unpredictable hostile environment. In 1884, Christian Gram classified the bacteria into two groups; the Gram-positive bacteria and the Gram-negative bacteria, depending on their cell wall structures (Silhavy *et al*., 2010). The Gram-positive bacteria cell envelope is differentiated from the Gram-negative bacteria in their structures, mostly in their outer membranes. However, the Gram-negative bacteria cell membrane composed of a thin cell wall containing a few layers of peptidoglycan surrounded by two lipids layers (inner and outer membrane) as it is shown in (Figure 1.1.1). On the other hand, the Gram-positive bacteria cell membrane is composed of thick peptidoglycan layers and a phospholipid layer (inner membrane), with the absence of the outer membrane as it shown in (Figure 1.1.1) (Silhavy *et al*., 2010 and Mistou *et al*., 2016).

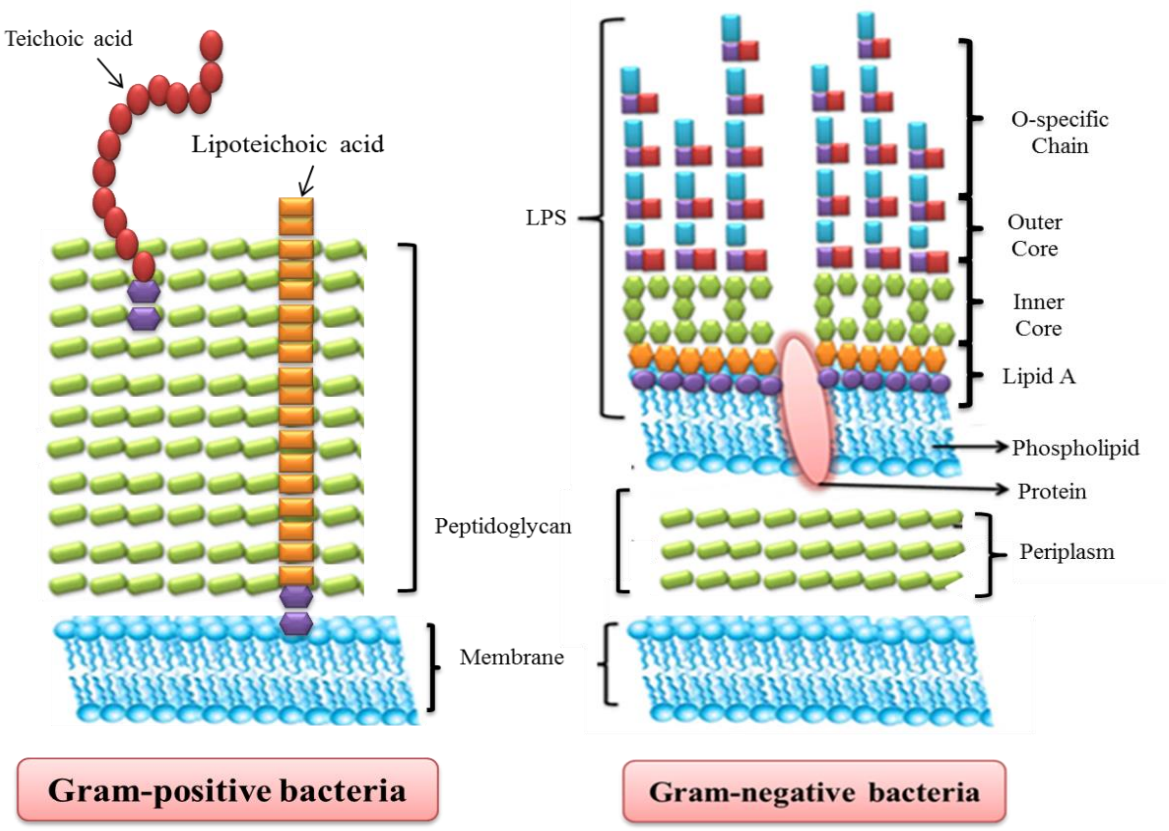

Figure 1.1.1: Illustration showing the structure of the Gram-positive and Gram-negative cell envelops. The Gram-negative bacteria outer membrane consists of a bilayer composed of lipopolysaccharide (LPS), the inner membrane and in between them the periplasm. Gram-positive bacteria outer membrane consists of the inner membrane and a thick peptidoglycan layer. This scheme was completely redrawn and was partially based on Silhavy *et al*., 2010.

A typical Gram-negative bacterial envelope consists of an outer membrane, an inner membrane, and the space between them is filled by the peptidoglycan and is called the periplasmic space. The outer membrane is composed of a bilayer containing a phospholipid layer and a lipopolysaccharide (LPS) layer (Figure.1.1.1).

1.1.1. Lipopolysaccharides (LPS)

Lipopolysaccharides (LPSs) are amphiphilic components in the outer leaflet of the external membranes of the Gram-negative bacteria cell membrane. LPS covers up to 75% of the cell surface (Molinaro *et al*., 2015). It is embedded in the phospholipid part of the bilayer membrane extending outward. LPS functions as a protective barrier for the bacteria. The LPS was also described as endotoxin by "the father of endotoxin", the German Investigator R. Pfeiffer at the end of the 1800s. LPS plays a key role in the pathogenesis of Gram-negative infections in hosts by triggering the activation of the immune systems (Rietschel *et al.*, 2003, and Silhavy *et al*., 2010).

LPS consists of three-domains: The *O*-specific polysaccharide (*O*-antigen), the core oligosaccharide, and Lipid A. The *O*-antigen is covalently associated with the core oligosaccharide (and both parts constitute the hydrophilic moiety). The core oligosaccharide glycosylate lipid A which is the hydrophobic moiety of the LPS (Figures 1.1.1 and 1.1.2) (Silhavy *et al*., 2010, Molinaro *et al*., 2015, and Mistou *et al*., 2016).

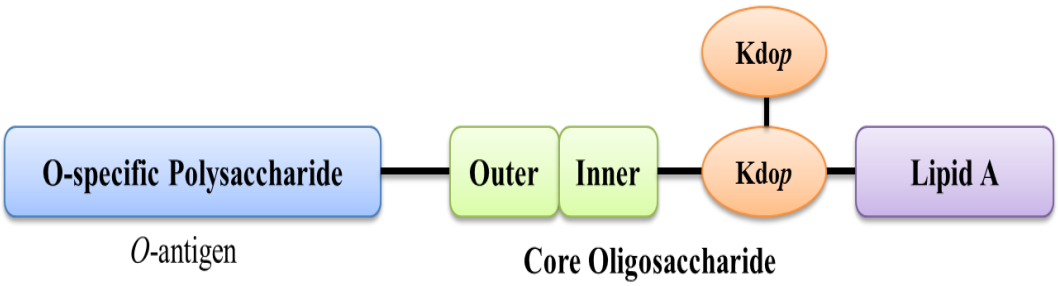

Figure 1.1.2: Illustration showing the structure of the lipopolysaccharide (LPS) within the Gram-negative bacteria cell membrane.

1.1.1.1. The *O*-specific chain (*O*-antigen) polysaccharide

The *O*-specific chain (also called the *O*-antigen) is a repetitive polysaccharide polymer formed of repeating oligosaccharide units. This *O*-antigen is exposed directly to the host during bacterial infection. The number of repeating oligosaccharide units of the *O*-polysaccharide may vary from 4 to 50 units, and each unit is formed of 2-8 monosaccharide residues (Figure 1.1.3). *O*-specific chain structure and composition are different among numerous genera and bacterial serotypes (Matsuura 2013, and Shang *et al*., 2015). The presence or absence of *O*-antigen determines whether the bacteria LPS is considered rough or smooth. Full-length *O*-antigen chains would render the LPS smooth, whereas the absence of *O*-antigen chains would make the LPS rough. Semi-rough LPSs are composed of one *O*-chain unit attached to the core-lipid A oligosaccharide (Banoub *et al.*, 2010, and Matsuura 2013).

1.1.1.2. The core oligosaccharide

The core oligosaccharide is located between the *O*-antigen region of the LPS and lipid A region, and it is the most conserved region more than the highly variable *O*-specific chain (Brade *et al*., 1988). The core oligosaccharide is made up mainly of glucose, galactose and N-acetyl-D-Glucosamine (D-GlcNAc) forming an oligosaccharide. The core oligosaccharide can be divided into two regions: the outer core and the inner core.

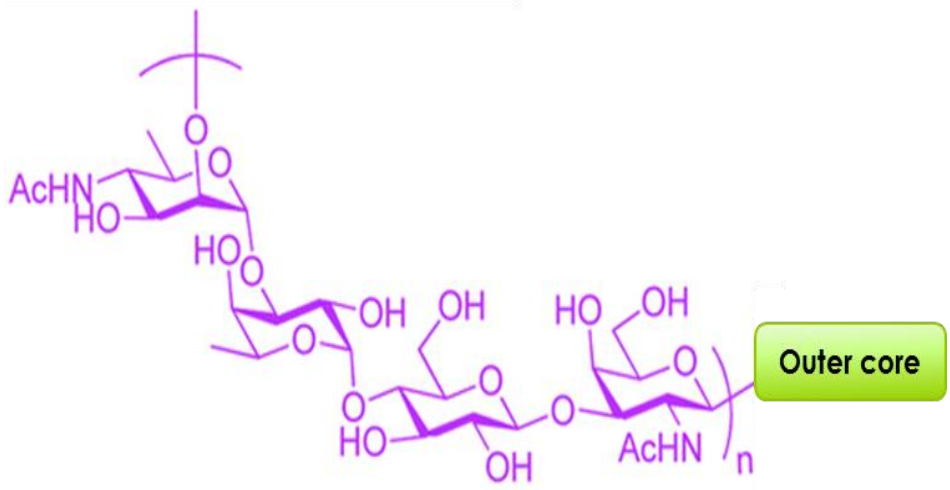

Figure 1.1.3: Illustration showing the structure of the *O*-specific chain of *E. coli* O157:H7 LPS. This scheme was completely redrawn and was partially based on Shang *et al.*, 2015.

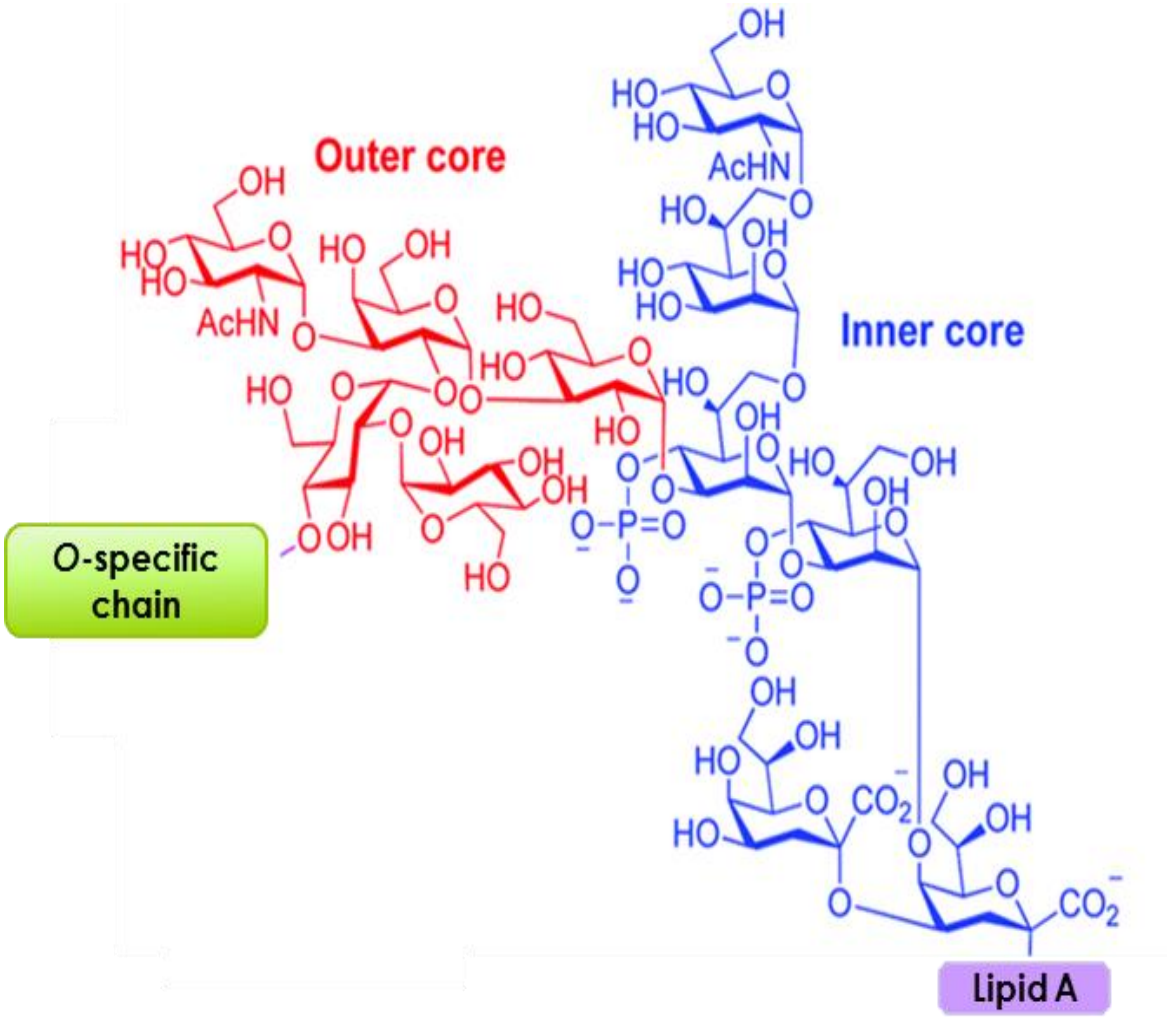

Figure 1.1.4: Illustration showing the structure of the core-oligosaccharide. This scheme was completely redrawn and was partially based on Shang *et al.*, 2015.

The outer core consists of hexoses residues that are attached to a 7-carbon sugar, namely the L-*glycero*-D-manno-heptose (LD-Hep) residue in the inner core by β-D-(1→3) bond and 3-deoxy-D-manno-octulosonic acid (Kdo) residues at the O-6 position (Figure 1.1.4). These 7-carbon sugar can also be phosphryated as shown in (Figure 1.1.4) (Henderson *et al*., 2016, Shang *et al*., 2015).

1.1.1.3. Lipid A

Lipid A is the innermost region of the LPS, and its hydrophobic nature allows it to anchor to the bacterial outer membrane. Lipid A is required for the toxicity of Gram-negative bacteria (Doerrler *et al*., 2006, and Ingram *et al*., 2010). Lipid A has the same role as a potent stimulus for the innate immune system. It is usually involved in the activation of cell-binding proteins such as Toll-like receptor 4 (TLR4)-MD-2 complexes which are responsible for the immune-stimulatory activity.

It is known that the toxic lipid A is considered as one of the most effective immunostimulatory molecules of eukaryotic cells originating from bacteria and can be considered as a tool for vaccines, immuno-stimulant, suppressive agent (Doerrler *et al*., 2006, Ingram *et al*., 2010, and Molinaro *et al*., 2015). The first lipid A structure has been approached by Westphal and Luderitz in 1954 and was finally confirmed in 1983 (Rietschel *et al*., 1999 and Molinaro *et al.*, 2015). Since that time, researchers have been investigating the structure of lipid A. Basically, lipid A consists of two glucosamine (D-GlcN) units forming a disaccharide attached by the β-D-(1→6) linkage. All the remaining O-3, O-3′, N-2 and N-2′ groups of this disaccharide backbone are acylated with fatty acids via both ester

and amide linkage, which will be termed as the throughout this thesis as the primary fatty acid. Both ester and amide linked acyl groups (or the primary fatty acyl group), contain a C-3 hydroxyl group fatty acids are commonly present in the hydroxylated form. Hence the hydroxyl group which can be esterified with additional fatty acid residues, formimg branched fatty acid acyl groups; therefore, the substituent acyl group of the principal fatty acid acy group, will be known as the secondary fatty acid. Usually, the D-GlcN units of the lipid A may contain one or two phosphate groups usually phosphorylated at both the O-1 and the O-4′ position of the β-D-Glc*p*N-(1→6)-β-D-Glc*p*N disaccharide backbone. These features are often used as the basis for distinguishing and classifying Gram-negative bacteria (Figure 1.1.5) (Doerrler *et al*., 2006, Michaud *et al*., 2013, Maeshima *et al*., 2013, and Kelley *et al*., 2013). Variation in the lipid A structure increases by changes in acylation, phosphorylation, and glycosylation. These changes can be affected by factors such as pH, Mg^{2+} concentration, and the presence of cationic peptides (Zähringer *et al*., 1999, Caroff *et al*., 2003, El Aneed *et al*., 2005, Kilár *et al*., 2013, and Wang *et al*., 2015).

There are many analytical methods to structurally characterize lipid A complexes, such as X-ray crystallography (Raetz *et al.*, 2007), and NMR spectroscopy (Suda *et al.*, 2001, and Lukasiewicz *et al.*, 2006). However, these techniques possess inherent insufficiencies, including requiring large quantities of isotope-labeling and crystallization issues (Molinaro *et al*., 2015). On the other hand, mass spectrometry (MS) has many advantages in sensitivity, specificity, speed, and specialty. For these reasons, MS plays a critical role in lipid A characterization and identification (Banoub *et al.*, 2010 and Kilár *et al.*, 2013).

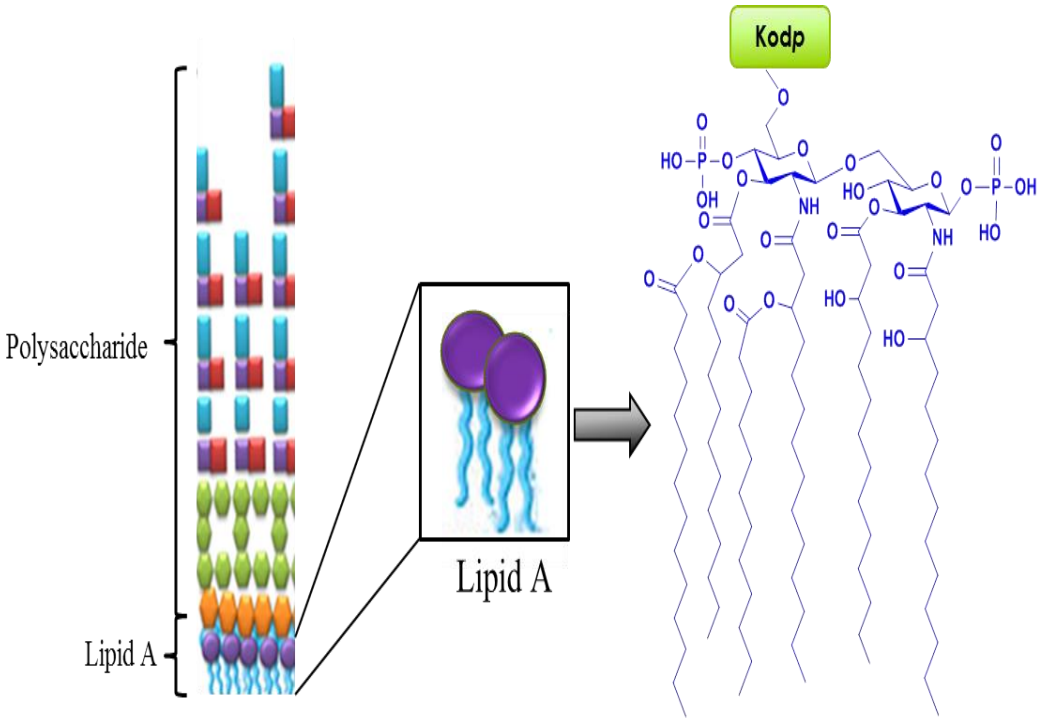

Figure 1.1.5: Illustration showing the structure of lipid A.

1.1.2. Lipopolysaccharides (LPS) Biosynthesis

LPS complex structure is reflected by its complicated biosynthesis and transfer processes. LPS synthesis has been studied most extensively in *E. coli* (Raetz *et al*., 2009, Wang *et al*., 2010, Molinaro *et al*., 2015, and Wang *et al*., 2015). These processes occur in different cellular regions (Figure 1.1.6).

Although LPS is located on the surface of bacterial cells, its synthesis is initiated in the cytoplasm and is transferred to the surface of bacteria. Multiple catalyzed enzymatic reactions are involved in this biosynthesis. It has been proven that the biosynthesis of all LPSs originate form one selective precursor small molecule UDP-*N*-acetylglucosamine (UDP-GlcNAc) (Raetz *et al*., 2009, Whitfield *et al*., 2014, and Wang *et al*., 2015).

This biosynthetic first step is mediated by a series of nine enzymes namely: LpxA, LpxB, LpxC, LpxD, LpxH, LpxK, LpxL, LpxM, and KdtA. All the enzymes involved in the LPS biosynthesis have relatively high specificity for their respective substrates.

With respect to the biosynthesis of lipid A, it was shown that the creation of the building block component of lipid A is initiated by UDP-GlcNAc. As shown in (Figure1.1.6) the first three steps of the lipid A pathway occurs in the cytoplasm. The first step of lipid A biosynthesis is involved in the transfer of the *R*-3-hydroxymyristoyl moiety from *R*-3-hydroxymyristoyl-acyl carrier protein (ACP) to the glucosamine 3-OH group of UDP-GlcNAc. This transfer will occur by means of the acyltransferase (LpxA). In the second step, the product obtained is then deacetylated with the LpxC enzyme. Consequently, the third pathway, is initiated by the LpxD enzyme, which joins a second

hydroxymyristate moiety onto the lipid A precursor, and consume the same β-hydroxymyristoyl-ACP substrate. The fourth and fifth steps in the lipid A biosynthesis pathway are catalyzed by the peripheral membrane proteins LpxH and LpxB. As shown in Figure 1.1.6, the enzyme LpxH will create lipid X by cleaving most of the UDP moiety and replace it with a single phosphate group at the position O-1 on the remaining lipid portion. This is followed by a combination of the LpxB portion to lipid X form the preceding lipid metabolite, UDP-2,3-bis(β-hydroxymyristoyl)-D-glucosamine, to form lipid A disaccharide-1-P. Finally, the kinase LpxK phosphorylates lipid A disaccharide at the O-4 position to form lipid IVA.

The next step of the LPS biosynthesis is the assembly of the Kdo2-lipid A component, which takes place in the cytoplasm and on the inner surface of inner membrane These remaining steps are catalyzed by integral membrane enzyme as shown in (Figure 1.1.6). Next, the enzyme KdtA is involved in the incorporation of either two or three 3-deoxy-D-manno-octulosonic acid (Kdo) residues at the O-6 position of the lipid IV_A to produce Kdo2-lipid IV_A. Further catalyzed reactions occur by the enzymes LpxL and LpxM incorporate lauroyl, myristoyl, or palmitoyl chains to the Kdo2-lipid A, thus giving the final Kdo2-lipid A product six acyl chains.

Respectively, the enzyme LpxL adds a secondary lauroyl residue (C12) and the LpxM enzyme adds a myristoyl residue (C14). Finally, the LpxP enzyme is involved in adding a palmitoyl residue (C16) to the glucosamine unit (Williams et al., 2007, Whitfield *et al*., 2014, Putker *et al*., 2015, and Wang *et al*., 2015).

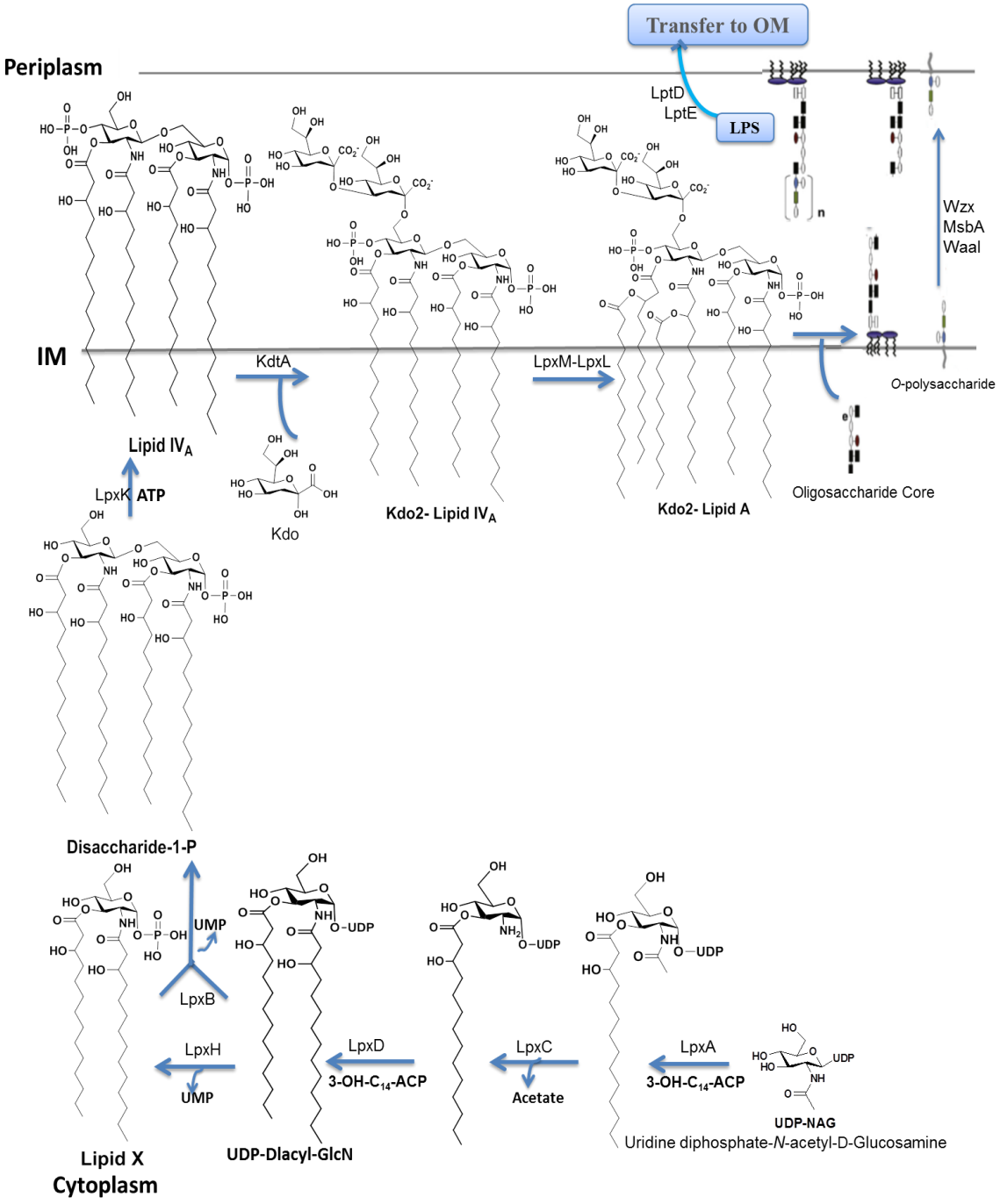

Figure 1.1.6: Structure and biosynthetic pathway of LPS. The catalyzed reactions occur by various enzymes. The structure of lipid A is shown in detail, but structures of core oligosaccharides and *O*-antigen are simplified as symbols since there are many variations in these two regions. This scheme was completely redrawn and was partially based on Wang *et al*., 2015 and Putker *et al*., 2015.

After the synthesis of the Kdo2-lipid A oligosaccharide, the core oligosaccharide is assembled on Kdo2-lipid A at the cytoplasmic surface of the inner membrane and then flipped from the inner leaflet of the inner membrane to the outer leaflet of the inner membrane by MsbA (Klein *et al*., 2009).

Similarly, the *O*-antigen is accumulated on the cytoplasmic surface of the inner membrane. The enzyme Wzx flips the *O*-antigen from the cytoplasmic face to the periplasmic face of the inner membrane. Also, the enzyme WaaL is used to bind the *O*-antigen and the core-lipid A together to create nascent LPS.

All the LPS components are synthesized in the cytoplasm and periplasm, and then are transferred to the outer leaflet of outer membranes by the enzymes glycosyltransferases and polymerases. The enzymes LptA, LptB, LptC, LptF and LptG are involved to transport the nascent LPS from the periplasmic face of the inner membrane to the inner surface of the outer membrane, whereas the LptD and LptE enzymes are used to assemble LPS into the outer surface of the outer membrane (Figure 1.1.6) (Abeyrathne., *et al*., 2005, Whitfield *et al*., 2014, Putker *et al*., 2015, and Wang *et al.*, 2015).

Although complex multiplicity of enzymes is sequentially used during this biosynthesis, each bacterium has its unique way in synthesising and modifying their LPS structure, even its most conserved part lipid A.

It is well known that the structure modification of lipid A might help the bacteria to evade recognition by the innate immune receptor TLR4 (Wang *et al.*, 2015). Nevertheless, the incomplete biosynthesis of lipid A is mainly responsible for directing and regulating the type of fatty acid substitution of the lipid A (Raetz *et al*., 2007).

1.2. Bacteriophages

Bacteriophages are a class of viruses that specifically infect bacteria, and act as intracellular parasites by multiplying inside bacteria and using their biosynthetic machinery. This infection leads to the lysis of the bacteria. Phage is a complex virus composed of protein coat that encapsulate a DNA or RNA genome and Tail (Figure 1.2.1). Bacteriophages were discovered by the British worker Twort and French-Canadian worker d'Hérelle in 1915. In 1917 d'Hérelle named in general viruses as "bacteriophages" and explored their ability to use them for treatment purpose (Viertel *et al*., 2014). Bacteriophages, or phages, have been used for the treatment of infectious diseases by researchers soon after their discovery in the early 20th century. After the discovery of antibiotics in the 1940s, the phage therapy slowed in the West, while it continued in countries such as the former Soviet Union and East Europe (Viertel *et al*., 2014 and Chanishvili. 2012).

Lately, the lack of effective antibiotics and the increasing number of antibiotic-resistant bacterial infections lead to a re-emergence of interest in Western countries in phages as potential therapeutic agents (Viertel *et al*., 2014, Golkar *et al*., 2014, and Chanishvili. 2012). Phages have considerable potential as conventional methods to replace the antibiotics. Phages with their infinite diversity have the potential to rapidly replicate independently at the site of infection, where they are mostly needed to lyse the pathogens. In addition, the phages can be found throughout nature, and they are environmentally friendly and harmless to human beings.

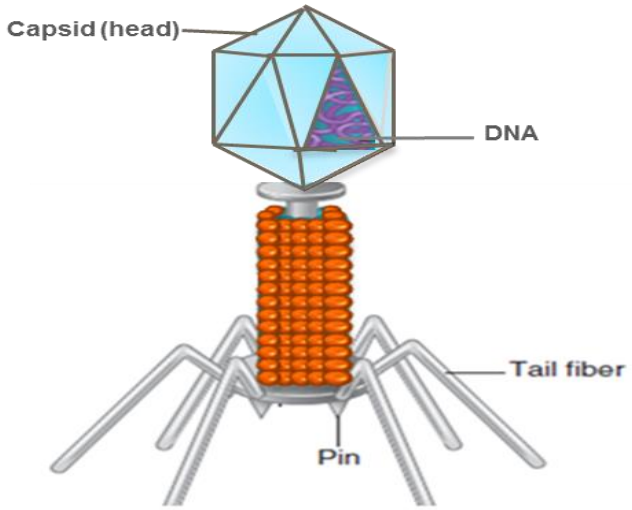

Figure 1.2.1: Structure of typical bacteriophages. This scheme was completely redrawn and was partially based on Hanlon. 2007.

Phages are highly specific to their hosts with no side effects, unlike the antibiotics which target both pathogens bacteria and beneficial. Based on natural selection, isolating and identifying phages are quickly processed compared to antibiotic development, which can take several years with high cost effects (Viertel *et al*., 2014, Golkar *et al*., 2014, Chanishvili. 2012, Perera *et al*., 2015, and Torres-Barceló., *et al*., 2016).

Phages have been used as substitutes for antibiotics in food safety, agriculture, fish culture, and farming settings to solve the spread of antibiotic-resistant bacteria. For example, recently the Food and Drug Administration (FDA) in the United States permitted commercial phage to treat common bacterial pathogens such as *Salmonella* (Torres-Barceló *et al*., 2016). Exportation of fish is one of the biggest assets to commercial wealth in Canada. There are various bacterial species causing fish diseases in aquaculture ventures. These marine and freshwater diseases are known to decrease the population of fish farm, both marine and freshwater (Elaneed *et al*., 2005, Banoub *et al*., 2010 and Torres-Barceló *et al*., 2016).

Bacteriophages can offer natural treatment to eliminate specific foodborne bacteria in foods (Endersen *et al*., 2014). Bacteria can become resistant to both antibiotics as well as to the phages. Phages resistance rate is ten folds less than that of antibiotics. The resistance occurs by developing mutate phages which can be forestalled by using phages cocktails (preparations containing multiple types of phages) (Perera *et al*., 2015, and Torres-Barceló. *et al*., 2016).

1.2.1: Lytic cycle and lysogenic cycle

The life cycle of bacteriophages has been investigated to understand how viruses affect the cells and cause immediate death of the cell through cell lysis. The phage attaches basically to the host by the intermediacy of a specific bacterial surface fibers.

Like most viruses, bacteriophages basically carry only the genetic information to replicate their nucleic acid and synthesis of their protein coats within the host cell. Next, the phages become part of the host chromosome and replicate within the cell genome by packaging its progeny phage particles inside the host (Figure 1.2.2).

Bacterial cells can undergo one of two types of infections by phages named lytic infections and lysogenic infections. The lytic cycle is initiated by replication of the phage genome and the tail proteins, which are synthesized inside the host cell. The bacterial cell will lyse and the new produced phages will be released (as is shown in Figure 1.2.2).

In the case of the lysogenic cycle, the phage genome inserts itself into the bacterial chromosome, and remains inactive to create a prophage which does not lysis the cell. During the host cell replication, prophages are replicated together with the bacterial host chromosome then switch into lytic production (Figure 1.2.2) (Hanlon., 2007, Oliveira *et al*. 2012, Keen 2012, Feiner *et al*., 2015, and Hoai *et al*., 2016).

It is well known that the biosynthesis of LPS is completely altered by infection with bacteriophages. The physical interactions between tailed phages and Gram-negative bacterial pathogens have been used as models in the development of phage therapeutic strategy (Drulis-Kawa *et al.*, 2012, Kim *et al*., 2014, and Chaturongakul *et al*., 2014).

The main purpose of infecting Gram-negative bacteria with bacteriophages is to stop their growth by destroying their cell membranes by lysing. The bacterial receptors of the phages, which are responsible for the phage-bacteria interactions, are the phage tail proteins which associate with the bacterial glycolipid LPS (Chaturongakul *et al*., 2014, and Joo *et al*., 2015).

Therefore, the proteins and LPS present in the bacterial outer membrane may both serve as bacteriophage receptors. The survival of phages depends only on their ability to infect their bacterial hosts without killing them. The interactions between the phages and the Gram-negative bacteria regulate the host specificity and the heterogeneity of all the components of the LPS (Joo *et al*., 2015, and Shin *et al*., 2012). Accordingly, it was interesting to look at the precise molecular structure of the outermost LPS layer, which is usually the receptor site for bacteriophages.

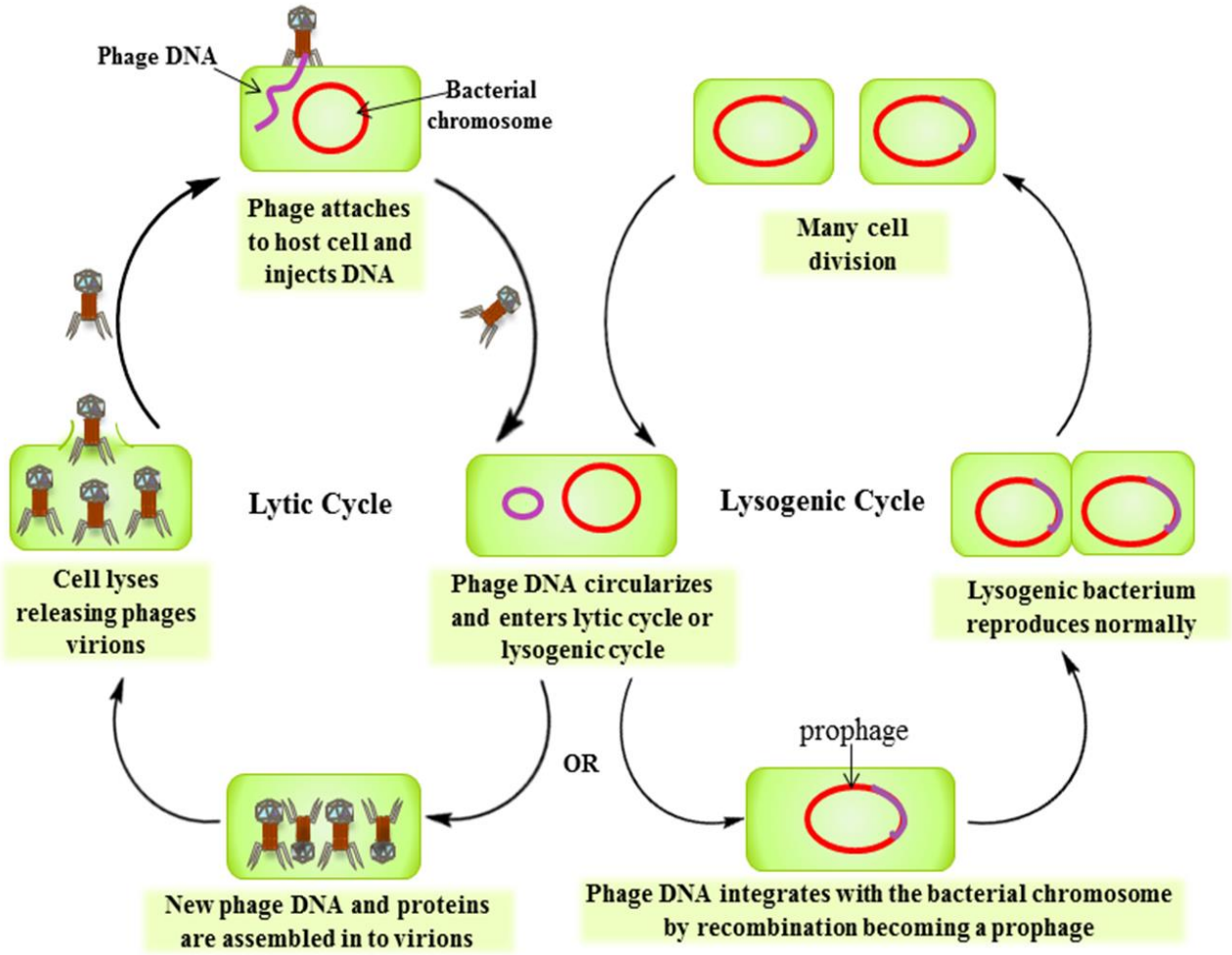

Figure 1.2.2: Schematic of lytic, lysogenic cycles. This scheme was completely redrawn and was partially based on Hanlon, 2007.

1.3. Mass Spectrometry

MS was first introduced in the late 1880s by the physicist Eugen Goldstein, by discovering a new type of radiation with positively charged gas particle streams travelling from the anode through channels towards the cathode (Goldstein 1913). In 1913, Sir Joseph John Thomson built the first mass spectrometer (MS) (Thomson 1913). In 1942 Aston used MS to determine the weight of the elements and their isotopic ratios (Aston 1942, and Downard 2007). In 1956 McLafferty demonstrated the first coupling between gas chromatography and mass spectrometry (McLafferty 1957).

MS is an excellent analysis method that helps identify molecular structure of unknown/known analytes. There are different methods of ionization for MS analysis (- and + ion modes) such as electron ionization (EI), Chemical ionization (CI), fast atom bombardment (FAB), and electrospray ionization (ESI). The ionization techniques can be used for molecular structure elucidation. After the ionization in the ion source of the mass spectrometer, the ions formed are then separated using electric or magnetic fields per their mass-to-charge ratio (*m/z*). In the mass spectrum, the x-coordinate represents the *m/z* values while the y-axis indicates the % relative ion abundances.

Generally, the MS instrument is composed of three principal units; the ionization source, the mass analyzer, and the detector (Figure 1.3.1). The sample is injected into the ionization source by either direct injection or by various methods including chromatography (GC) (Kitson 1996), and high performance liquid chromatography

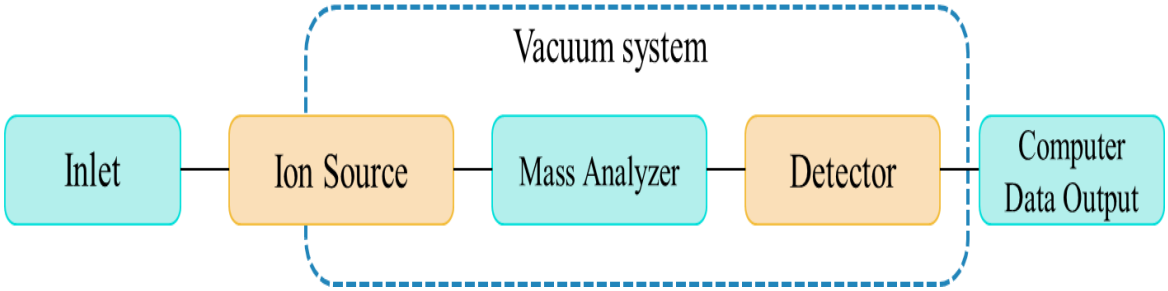

Figure 1.3.1: Components of a Mass Spectrometer including ion source, mass analyzer, and detector.

(HPLC) (Arpino 1989). The job of the GC and HPLC is to separate the analyts mixture into single molecules, which are ionized after entering the ionization chamber. After the analyte is introduced into the ionization source, it becomes a charged ionic species that may remain intact or fragment further into smaller ions. This process is followed by acceleration of all ions by a constant voltage, and accordingly the ions are sorted by their *m/z* values in the analyzer region. These analyte ions are then detected by the detector, in which every analyte molecule produces a characteristic (Figure.1.3.1).

1.3.1. Ionization Methods

Mass spectrometry can be used to study wide classes of molecules, ranging from small volatile species up to very large polar molecules. As they have different properties, *e.g.* molecular weight, volatility, polarity, bond strength, etc., all of them cannot be ionized by just one technique, but a wide range of ionization techniques are nowadays available.

In general, there are two major types of ionization techniques, hard and soft. Hard ionization techniques such as electron ionization (EI) impart high quantities of energy in the subject molecule producing large degrees of fragmentation (Portolés *et al.*, 2011). The most common example of hard ionization is electron ionization, which was first described in 1918 by the Canadian-American Physicist Sir Arthur J. Dempster (Dempster *et al*., 1918). In EI high energy electrons are used to affect the ion cloud of the analyte molecule, oxidizing it, typically by one electron. The electrons are produced by passing an electric current (70 eV) through a wire filament or the cathode. The ions produced will be attracted to the other side of the chamber toward an anode. The number of electrons emitted by the

filament is controlled by the amount of the current applied. Following ionization, the charged analyte molecules can also fragment in the source due to excess energy imparted to the molecule beyond its ionization energy, and sometimes the identity of the molecular ion is lost. This drawback makes EI unsuitable for large biomolecules which cannot be vaporized (Luffer *et al*., 1990, and Portolés *et al.,* 2011).

Chemical ionization (CI) belongs to the "soft ionization techniques". CI was developed due to some of the limitations associated with EI. In CI the interaction between energetic electrons and neutral molecules, such as methane form charged reagents such as CH_5^+. The reagents will interact with the analytes by either donating or abstracting a proton forming either the protonated and/or deprotonated species, or adducts which help determining and confirming the molecular weight of the analytes (Munson *et al.,* 1966, Fenn 2003).

Ionization of the intact analyte that do not produce extensive-ions is soft an ionization technique. These ionization methods included fast atom bombardment (FAB) also known as liquid secondary ion mass spectrometry (LSIMS). FAB and/or LSIMS is a technique that is involved in focusing a fast, high energy primary current beam of neutral atoms/molecules or ions which strike a sample film placed on a metal support, to produce ions. The beam kinetic energy will be transferred to the sample and cause desorption of secondary ions which are extracted and focused towards the mass spectrometer. FAB or LSIMS requires the use of a matrix, most commonly glycerol. The presence of the matrix ions enhances this desorption; though it complicates the interpretation of the mass spectrum (Barber *et al.,* 1981 and Morris *et al*., 1981).

Equally, matrix assisted laser desorption ionization (MALDI) was developed by focusing a laser to strike a sample that was co-crystallized with a matrix chosen, partially, on its ability to absorb the laser radiation (Tanaka *et al.,* 1988). More on MALDI will be discussed in section 1.3.1.1.

There is a quite new branch of mass spectrometry, called atmospheric ambient mass spectrometry consisting of direct sampling and ionization of the analytes at ambient conditions with no or minimal effort for sample preparation. The best example of ambient ionization is electrospray ionization (ESI) technique, which was developed by Fenn. ESI became one of the most popular ionization techniques for proteins and other biomolecules due to its ability to produce multiply charged ions, which permitted determination of their molecular weights with instruments whose mass range is limited. In ESI, singly and multi-charged ions are produced when a high voltage is applied to a liquid forced through a metal capillary and forming a spray (Fenn *et al.,* 1989). A high temperature carrier gas (usually N_2) nebulizer is used to evaporate the solvent molecules from the analyte ions prior to entering the analyzer.

In 1975 Carroll developed the atmospheric pressure chemical ionization (APCI) as an ionization method (Carroll *et al*., 1974). In APCI a corona discharge voltage is applied to the formed spray which then creates ions (Carroll *et al.,* 1974 and Zaikin *et al*., 2006). The corona discharge voltage is placed on a needle inside the source.

Desorption electrospray ionization (DESI) is also an atmospheric pressure ion source. In DESI the ions are produced by using an aqueous spray directed at an insulating sample or an analyte deposited on an insulating surface. The samples are spotted onto a

surface, which makes it applicable to solid samples, liquids, frozen solutions, and to adsorbed gases. It has been demonstrated that DESI ions are formed outside the mass spectrometer source by desorption of the analyte, and then the ions detected once they are drawn into the mass spectrometer (Takáts *et al.*, 2004 and Chen *et al*., 2005).

Direct analysis in real time (DART) ionization was introduced by Cody (Cody *et al.*, 2005). In DART direct detection of various chemical analytes present on solids surface, liquids and gases can be achieved without the need for sample preparation. In the DART source, a gas (usually He or N_2) flow containing metastable particles from the ion source onto a sample and is responsible for the desorption and ionization (Cody *et al.*, 2005 and Chernetsova *et al*., 2011).

Many other novel ionization techniques belong to the ambient ionization ionization group. Some new examples are: extractive electrospray ionization (EESI) (Chen *et al*.,2006), low temperature plasma probe (LTP) (Harper *et al.*, 2008), paper spray ionization (PSI) (Yang *et al*., 2011), and many others (Alberici *et al.*, 2010 and Martin *et al*., 2014).

It should be mentioned with all honours, that in 1987, Tanaka discovered the matrix-assisted lasers desorption/ionization (MALDI) and Fenn developed the electrospray (ESI), and they received jointly the *Nobel Prize* in 2002 (Tanaka *et al.*, 1988; Fenn *et al.*, 1989).

In the introduction of this thesis, I will present the two major types of the soft ionization in more detail namely: ESI and MALDI.

1.3.1.1. Matrix-Assisted Laser Desorption Ionization (MALDI)

MALDI is a soft ionization technique that was derived from laser desorption mass spectrometry (LD-MS), which is an efficient method to produce gaseous ions by focusing a pulsed laser on a sample surface. The laser pulses can ablate material from the surface of the solid analyte and then ionize the sample. The evolution of LD-MS into MALDI-MS occurred with the realization that a matrix was necessary for helping the ionization of the analytes and without gas-phase fregmentation. The use of a MALDI matrix play a critical role in terms of providing and promoting both desorption and ionization mechanisms. In the first step, the sample is dissolved in a solvent containing the analyte solution and the matrix. The most common matrices used are: 2,5-dihydroxybenzoic acid (DHB) (Karas *et al*., 1990), sinapinic acid (SA) (Beavis *et al*., 1989), α-cyano-4-hydroxycinnamic acid (CHCA), and 2,4,6-trihydroxyacetophenone (THAP) (Figure 1.3.2) (Beavis *et al*., 1992). The analyte and the matrix are usually allowed to co-crystalize before analysis, though the necessity for crystalizing matrices is debatable.

Following the introduction of the MALDI plate into the source of the mass spectrometer, the second step occurs under high vacuum conditions and is initiated by irradiation with the laser beam. Usually in all MALDI instruments, the analytes are ionized by using a laser, commonly the nitrogen laser operating at 337 nm. Upon, absorption of the laser irradiation, the matrix is heated and becomes energized, which leads to the excitation of the matrix molecules by donating or extraction a proton, henceforth producing protonated and deprotonated molecules, respectively (Hoffmann *et al*. 2007, and Schiller *et al.,* 2007).

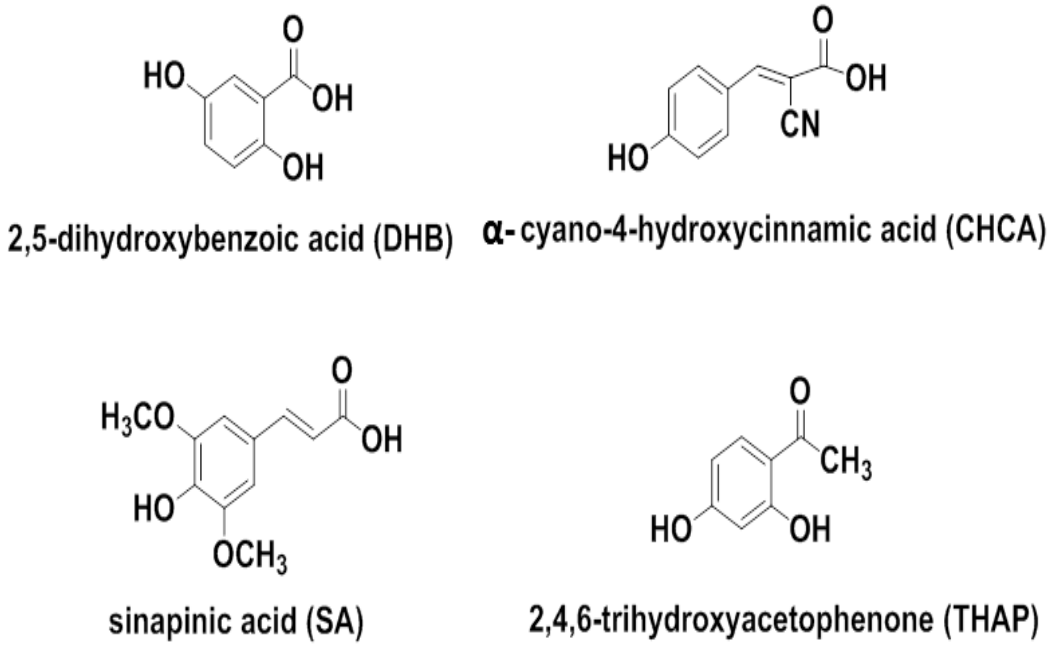

Figure 1.3.2: The chemical structures of four commonly used matrices in MALDI-MS analysis.

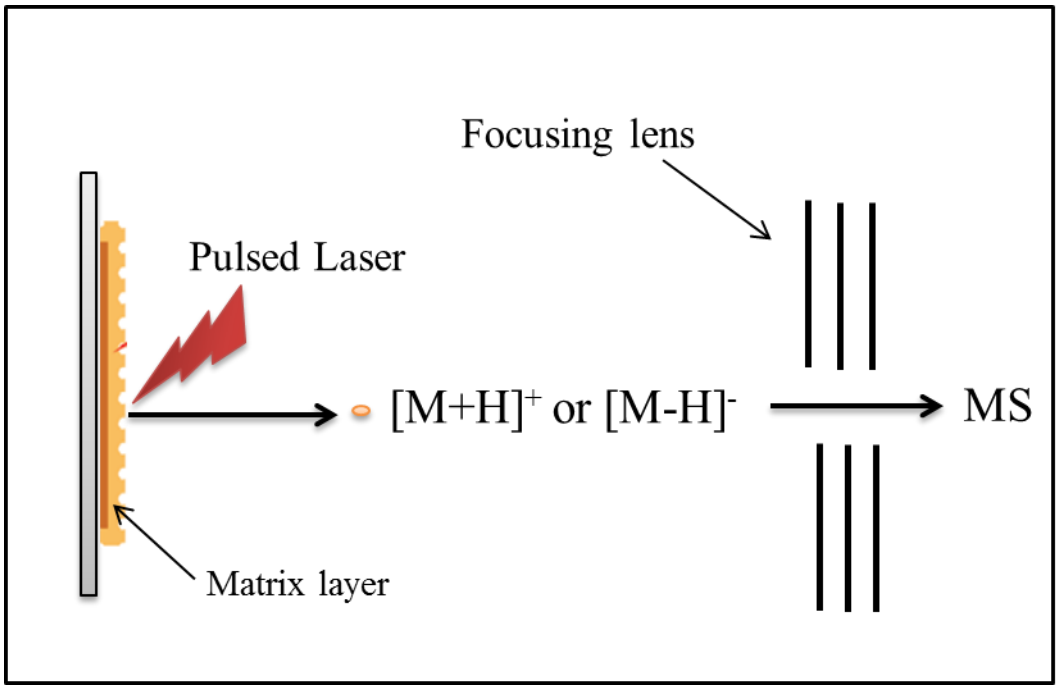

Figure 1.3.3: Representations showing the procedure of desorption/ionization of the analytes by a laser beam during MALDI. This scheme was completely redrawn and was partially based on Downard, 2004.

During laser irradiation (**hν**), the molecules of the matrix (**MH**) are excited according the following equation (M is the matrix)

$$\mathbf{MH + h\nu \rightarrow [MH]^*}$$

Following excitation, the heated and ionized matrix transfers its energy to the analyte and proton which causes its desorption, ionization and ejection into the gas phase. The desorbed ionized molecules are then transferred into the gas-phase as either protonated, deprotonated, or charged adducts (Figure 1.3.3).

MALDI is well suited for most of the mass analyzers such as the time-of-flight (TOF), various hybrid QqTOF, IT-TOF and Fourier transform ion cyclotron resonance (FTICR) analyzers. MALDI-TOF-MS has become a useful analytical tool mainly in the analysis of biomolecules, because, the TOF analyzer can analyze ions over a wide mass range (Cotter 1992, Chen *et al*., 2016).

1.3.1.2. Electrospray ionization (ESI)

ESI is one of the best soft techniques of ionization at atmospheric pressure. In electrospray, the analyte is dissolved in conventional solvents such as methanol, acetonitrile and water prior introduction in the ionization source either from an HPLC column and/or direct introduction via a syringe (Gaskell. 1997). After injection of the analyte in the source, ESI is produced by applying a strong electrical field through a metal capillary tube and the counter electrode of the ionization source by applying a potential difference 2-6 kV.

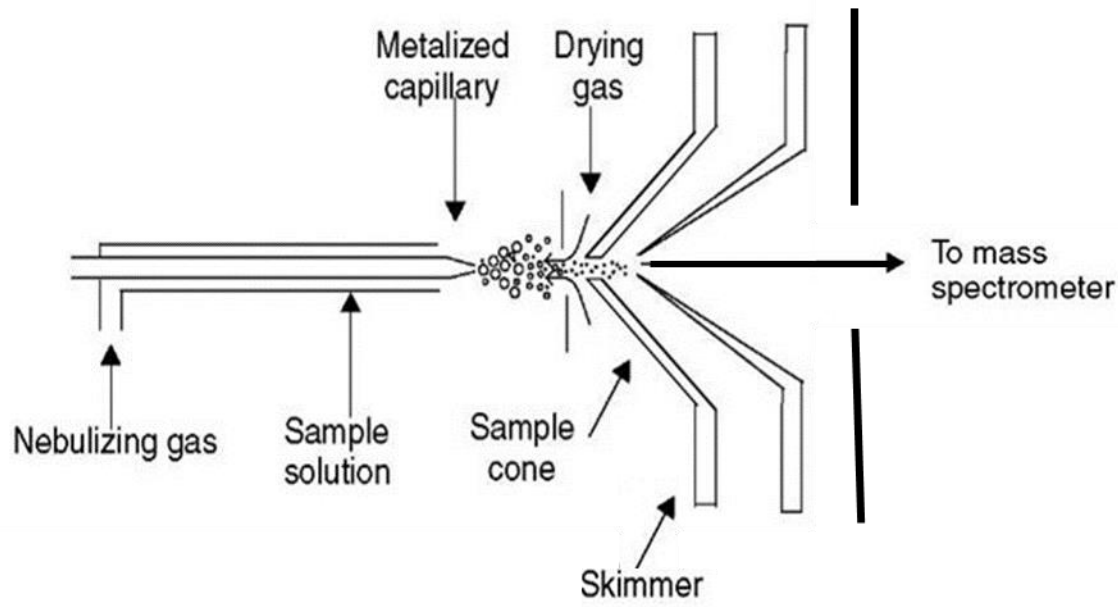

Figure 1.3.4: The atmospheric pressure electrospray ionization process occurs by emission of charged droplets forced into the capillary which is highly charged capillary. This scheme was completely redrawn and was partially based on Fenn 2003.

This electric field induces a charge accumulation at the liquid surface located at the end of the capillary tube and will create charged droplets. A gas injected coaxially facilitates the formation of the ion spray which occurs by forcing and transfering the ions from solution into the gaseous phase, before entrance in the analyzer. A heated gas (most often N_2) injected at a low flow rate and/or through the skimmers helps solvent molecule evaporation and formation of a spray. The sizes of the charged droplets are continuously reduced by solvent evaporation. The charged ions in the droplet will migrate to the outward surface due to Coulombic repulsion forces (Figure 1.3.4). This will lead to increases the surface charge density and a decrease of the droplet radius. (Gaskell 1997, and Kebarle *et al*., 2000). As the droplets continue to evaporate, the diameters of the droplets carry on shrinking until it reaches the Rayleigh charge limit. At this point, release of the charged analyte ions occur into the gas phase (as shown in Figure 1.3.4) (Kebarle *et al*., 2009 and Konermann *et al*., 2014).

There are different mechanisms proposed for biomolecule ESI ionization: the most common two are the ion evaporation model (IEM) and the charged residue model (CRM). In the IEM, the ejection of the analytes from the droplet surface accrues via field emission (Figure 1.3.5). It was shown that IEM of unfolded proteins causes the formation of high ESI charge state ions. In the charged residue model (CRM), the free ions are formed upon droplet evaporation to dryness, this ESI process is known to form singly charged ions (Figure 1.3.5). CRM is known to be the dominant mechanism for higher mass biological molecules. Whereas, IEM is the preferred mechanism of formation of gas phase ions of

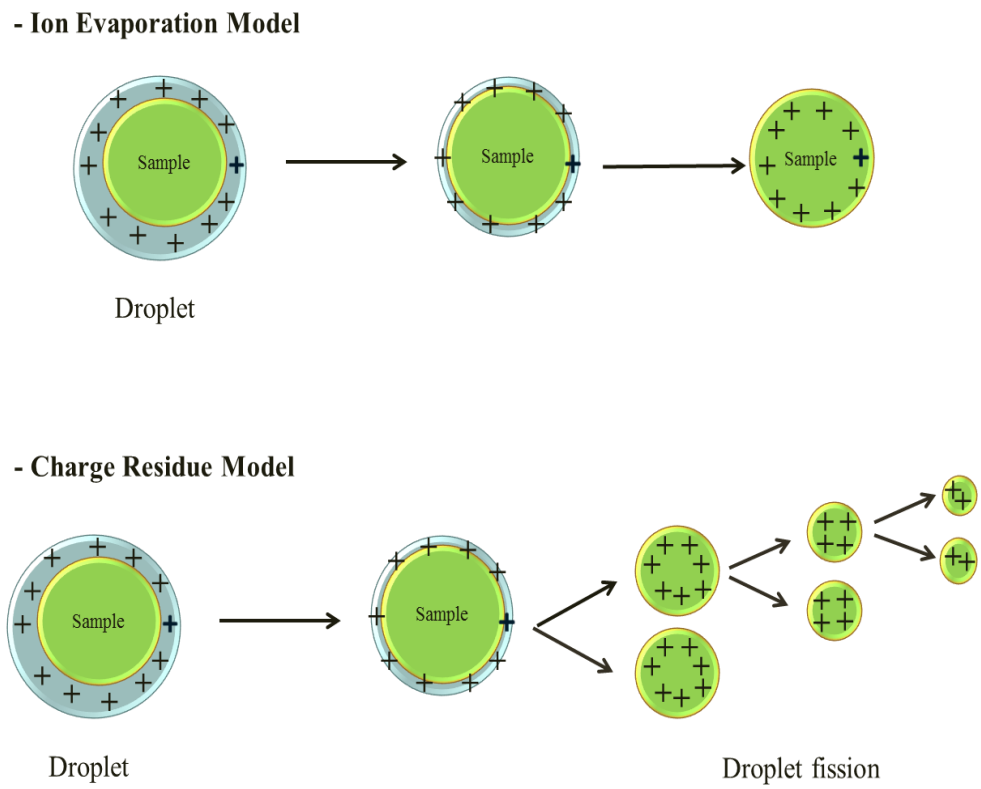

Figure 1.3.5: Schematic representation of the formation of ions during electrospray ionization. This scheme was completely redrawn and was partially based on Metwally *et al*., 2016.

small molecules, that are singly charged (Figure 1.3.4) (Fenn *et al*., 1989, Smith *et al.*, 2006, Konermann *et al.*, 2014, and Mehmood *et al.* 2016).

ESI is the most common ionization method of biological molecules, due to its ability to transfer large intact biomolecules in their ion form into the gas phase, without destroying their structure. Even non-covalent interactions can be conserved during thelectrospray ionization process. Moreover, the ability of ESI charged ions to be singly or multiply charged makes it a powerful technique in biomolecule research. Obtaining multiply charged ions can improve the sensitivity at the detector, and it allows the analysis of high-molecular-weight molecules to be measured by using the mass-to-charge ratio *m/z* (Hilton *et al*., 2012, Smith *et al*., 2006, Fenn. 2003, and Brodbelt. 2014).

1.3.2. Mass analyzers

The gas phase ions produced in the ionization source are transferred in the mass analyzer, where the ions are separated based on their mass-to-charge (*m/z*) ratios. As there are various types of ions sources, there are several types of mass analyzers that have been developed since 1990s. The choices among the different mass analyzers reside in the type of analyte molecules or biomolecules that need to be separated and/or the type of information desired (Griffiths *et al*., 2008).

Each mass analyzer has its advantages and its limitations. Different types of mass analyzers will be discussed in this introduction with a description of their principles. Once the ions are formed in the ion source, they are accelerated towards the mass analyzer where their separation according to their *m/z* occurs. To fulfil their aim, analyzers use forces which

influence ion movement, and; *a)* a magnetic field; *b)* an electric field; *c)* TOF and *d)* radiofrequency a radiofrequency (Downard. 2004).

Analyzers can be divided into two main groups: those based on ion separation *in space*, sometimes also referred to as *beam-type* analyzers, and those separating ions *in time*. Double sector instruments, having a magnetic and an electric field, quadrupole and time of flight belong to the first group. In this case ions travel for some centimeters (roughly 30-100 cm in quadrupole) or meters (roughly 2-5 m in sectors or 2-17 m in TOF) and along the way they are submitted to one or two of the forces described above (Burgoyne *et al*., 1996, Steel *et al*., 1998, Cotter *et al*., 1999). Analyzers separating ions *in time* are trapping devices: ion traps (linear or tridimensional ion trap), Orbitrap, and Fourier Transform Ion Cyclotron Resonance (FTICR). In these cases, the ion path may be from cm to meters long, depending on trapping time (Marshal *et al*., 1991, and Makarov. 2000). Usually, analyzers measure either single full scan of ions such as the case in sectors, quadrupole and ion trap, the flight time of the ions (TOF) and/or the frequencies (frequency of axial oscillations (Orbitrap), cyclotron frequency (FT-ICR). In the last case, the Fourier transform mathematical operations are applied for generating mass spectra from time domain transients produced by the image current (Marshal *et al*., 1991).

1.3.2.1. Quadrupole (Q) analyzer

The quadrupole analyzer is widely used as a "mass filter" and it is a device which separates the ions by their (*m/z*) using the stability of the trajectories in oscillating electric

fields. It is composed of four parallel electrical rods capable of separating ions based on (*m/z*). The polarities of each pair of opposite rods are different and also alternate. Basically, the operation of the quadrupole depends on applying a direct current (DC) potential and a radiofrequency (RF) potential between these rods, which leads to the ion oscillation between the rods as they move along the z-axis (Figure 1.3.6). In fact, when these two opposite rods have an applied potential of (U+Vcos(ωt)) and the other two rods have a potential of -(U+Vcos(ωt)), where Φ is the voltage applied to the rods, U is a DC voltage, and Vcos(ωt) is an AC voltage. The following equation defines the voltage across the rods:

$$\Phi = +(U+V\cos\omega t) \text{ and } \Phi = -(U+V\cos\omega t)$$

The applied voltages affect the trajectory of ions traveling down the flight path centered between the four rods. For given DC and AC voltages, only ions of a certain mass-to-charge ratio pass through the quadrupole filter and all other ions are thrown out of their original path. A mass spectrum is obtained by monitoring the ions passing through the quadrupole filter as the voltages on the rods are varied (Steel *et al*., 1998, Downard. 2004, Hoffmann *et al*. 2007, and March *et al*., 1989).

When the ions are accelerated lengthwise the z axis, they enter the space between the quadrupole rods and they maintain their velocity along this axis. Nonetheless, they are also submitted to acceleration along x and y axes that result from the forces induced by the electric fields, according to the following equation:

$$F_x = m\frac{\mathrm{d}^2 x}{\mathrm{d}t^2} = -ze\frac{\partial \Phi}{\partial x}$$

$$F_y = m\frac{\mathrm{d}^2 y}{\mathrm{d}t^2} = -ze\frac{\partial \Phi}{\partial y}$$

Φ is a function of Φ_0:

$$\mathbf{\Phi_{(x,y)} = \Phi_0\,(x^2 - y^2)/r_0^2 = (x^2\text{-}y^2)(U\text{-}V\cos\omega t)/r_0^2}$$

After differentiation and rearrangement of the above equation, we can derive the equations of motion (Paul equation):

$$\frac{\mathrm{d}^2 x}{\mathrm{d}t^2} + \frac{2ze}{mr_0^2}(U - V\cos\omega t)\,x = 0$$

$$\frac{\mathrm{d}^2 y}{\mathrm{d}t^2} - \frac{2ze}{mr_0^2}(U - V\cos\omega t)\,y = 0$$

Please note that if the trajectory of an ion is stable only when the values of *x* and *y* never reach r_0, this means that ion will never hit the rods. To obtain the values of either *x* or *y* during the time, these equations need to be integrated. The following equation was established in 1866 by the physicist Mathieu to describe the propagation of waves in membranes:

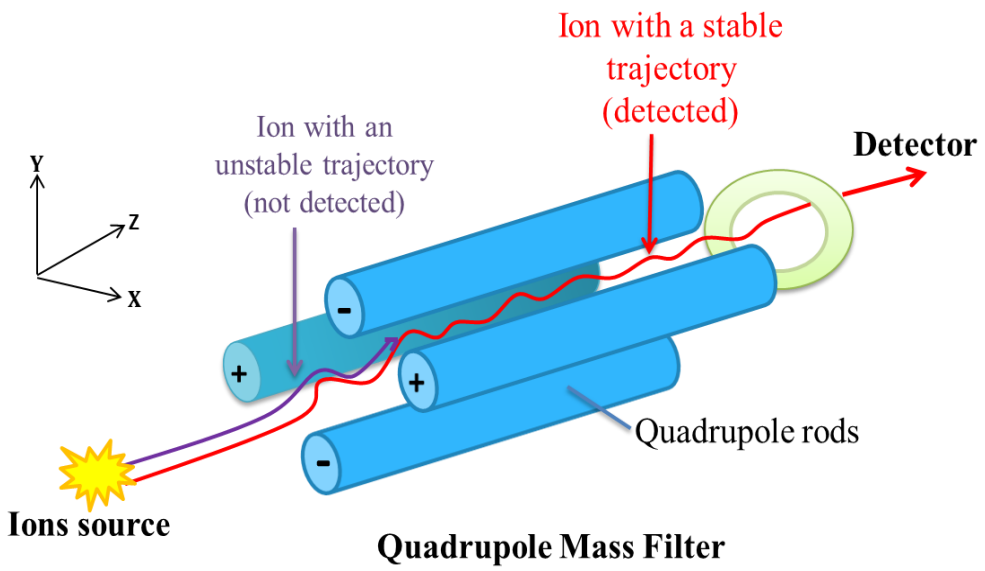

Figure 1.3.6: Schematic diagram of quadrupole mass analyzer and the x, y, and z axis where ions drift through the array of rods. This scheme was completely redrawn and was partially based on Downard, 2004.

$$\frac{d^2u}{d\xi^2} + (a_u - 2q_u \cos 2\xi)\, u = 0 \qquad \xi = \frac{\omega t}{2}$$

The Mathieu equation can only be solved numerically. The important characteristic of the solutions of this equation indicate that there are only stable (real) for a certain range of values of U and V. The regions of stable solutions are shown below as a function of U and V. The Mathieu stability diagram in two dimensions (x and y) is shown in Figure 1.3.7. Regions of simultaneous overlap are labeled A, B, C, and D. Stability areas for an ion along x or y (above) and along x and y (below); u represents either x or y. The region (shaded grey) where the stable solutions of both (a) [x-motion] and (b) [y-motion] intersect is where the quadrupole mass filter operates (March. 1997).

In summary, the general principle of operation of the quadrupole mass filter can be pictured qualitatively as follows: light *m/z* ions can follow the alternating component of the field. For the x-direction, these ions will stay in phase with the RF drive, gain energy from the field and oscillate with increasingly large amplitude until they encounter one of the rods and are discharged. Consequently, the x-direction is considered as the effective high-pass mass filter in which only high *m/z* values will be transmitted to the other end of the quadrupole without striking the x-electrodes. On the other hand, in the y-direction, heavy ions will be unstable because of the defocusing effect of the DC component, but some lighter ions will be stabilized by the AC component if its magnitude is such as to correct the trajectory whenever its amplitude tends to increase.

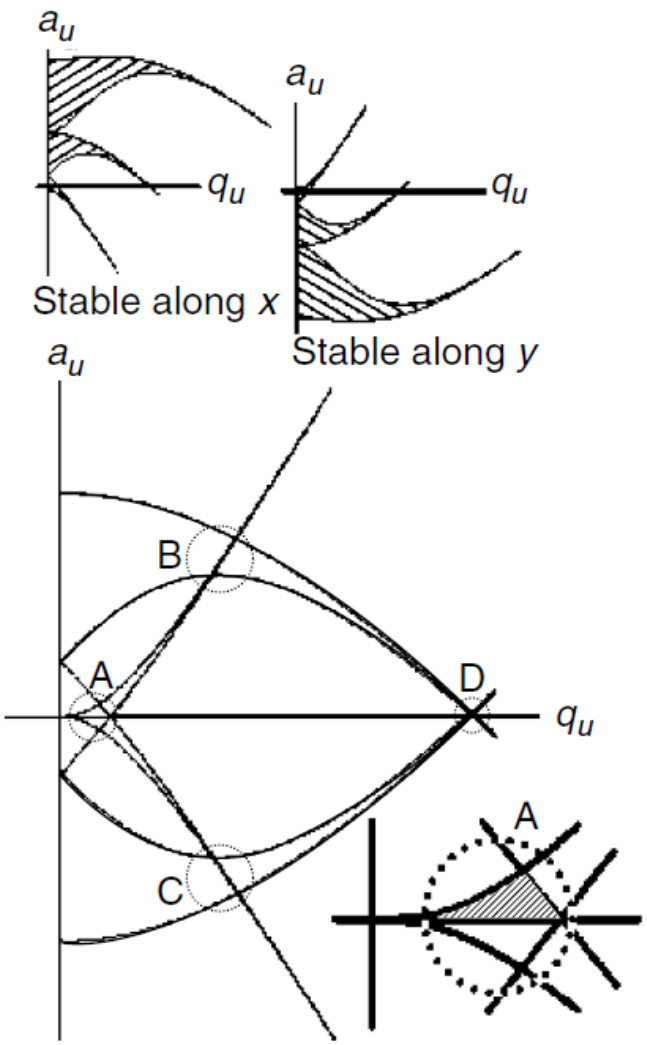

Figure 1.3.7: The Mathieu stability diagram in two dimensions (x and y). Regions of simultaneous overlap are labeled A, B, C, and D. Stability areas for an ion along x or y (above) and along x and y (below); u represents either x or y. Reproduced (modified) from March, R.E *et al.*, 1989 with permission.

For these reasons, the y-direction is a low-pass mass filter: only low masses will be transmitted to the other end of the quadrupole without striking the y electrodes. By a suitable choice of RF/DC ratio, the two directions together give a mass filter which can resolve individual atomic masses.

The quadrupole analyzer possesses many advantages such as the low cost, small size, robustness, transmission efficiency, and ease of maintenance. On the other hand, quadrupole analyzers have limitation in terms of mass range (2000 to 4000 Da) and resolving power (1 FWHM), and the ability to perform MS/MS analysis on their own (Downard. 2004).

1.3.2.2. Time-of-flight (TOF) analyzer

The TOF analyzer is a device that separates the formed ions after ionization, according to their *m/z* values and their velocities. After exit from the source, all ions are accelerated by a constant electric field and hence possess the same kinetic energy. Following entrance in the field-free region of the TOF analyzer. the ions possessing different masses will be separated according to their flight velocities.

The determination of the mass-to-charge ratios will be achieved by measuring the time that the ions move through the field-free region between the source and the detector. Consequently, the ions are accelerated by the same voltage (V_s), and travel through the analyzer (d) reaching the detector without using any other acceleration source or process. Once the ion leaves the ion source with a mass (m) along with a total charge q = Ze, it

would ultimately have an additional kinetic energy (KE). The connection between both the mass/charge ratio as well as the time of flight can be expressed as:

$$\mathbf{KE = 1/2mv^2 = qV_s}$$

The TOF analyzer has many advantages including fast acquisition rates, spectral continuity, exceptional dynamic range, and nearly unlimited upper-mass limit (mass range) without sacrificing speed or sensitivity. Nevertheless, the poor resolution sometimes obtained with this type of instrument, has been a major flaw compared to other mass analyzers. The factors that affect the mass resolution are the following: the length of the ion formation pulse (time distribution), the size of the volume where the ions are formed (space distribution) and the variation of the initial kinetic energy of the ions (kinetic energy distribution). This drawback can be improved with using two major developments called delayed pulsed extraction and the potential use of the reflectron sytem. The delayed ion extraction corrects the (KE) dispersion of the ions with the same *m/z* ratio and thus improves the resolution of the TOF analyzer without degradation of sensitivity compared with conventional extraction (Mamyrin & Shmikk, 1979). In addition, the resolution drawback can be overcome by availing of the reflectron. The use of an electrostatic ion mirror is introduced (also called the reflectron) to increase both the resolving power and hence, accuracy in measurement of the mass. The uses of the reflectron system were originally proposed by Mamyrin (Mamyrin *et al.*, 1973). With the reflecton system the ions having same *m/z* values and nearly different kinetic energies, are introduced in the analyzer in almost the same time and reach the detector at the same time (Figure 1.3.8).

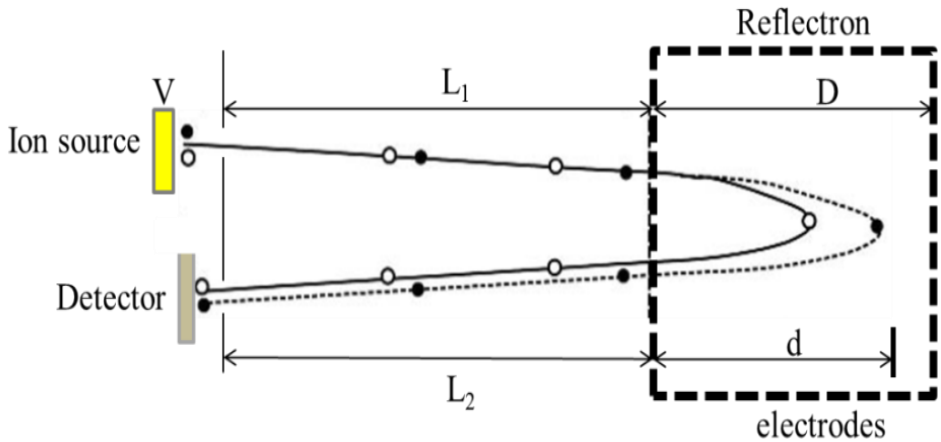

Figure 1.3.8: Schematic description of a TOF instrument equipped with a reflectron. ● = ions of a given mass with correct kinetic energy; o = ions of the same mass but with a kinetic energy that is too low. This scheme was completely redrawn and was partially based on Downard, 2004.

To sum it up, as ions traveling in a longer path of the reflectron, we can obtain better resolution as well as accurate mass measurements (Figure 1.3.8) (Mamyrin *et al*., 1973 and Clauser *et al*., 1999).

1.3.2.3. Fourier-transform ion cyclotron resonance mass spectrometry (FTICR-MS)

Since the introduction of the Fourier-transform ion cyclotron resonance analyzer (FTICR) in 1974 by Comisarow and Marshall, the interest in using this instrumentation has increased consequently (Dietmar *et al*., 2000, Nikolaev *et al.*, 2014, and Junot *et al.*, 2010). FTICR-MS is considered as to possess the highest mass resolution, and accuracy coupled to high sensitivity of analysis.

The functioning principle of the FTICR analyzer depends on the frequency measurement of the ion in the ICR cell which is subjected to a magnetic field (cyclotron frequency). To convert ion motion into their cyclotron motion, a magnetic field is necessary. This magnetic field is provided either with a permanent magnet, electromagnet, or a superconductive magnet. The permanent magnets and electromagnets only produce weak magnetic field strengths. However, once we increase the strength of the magnetic field, the performance of the FTICR-MS instrument improves as well as the mass resolution (Marshall *et al*., 1998). For these reasons, there has been an increase in the use of strong superconductive magnets, such as magnets with field strengths of 11.5 T (Tesla) or even 20 T.

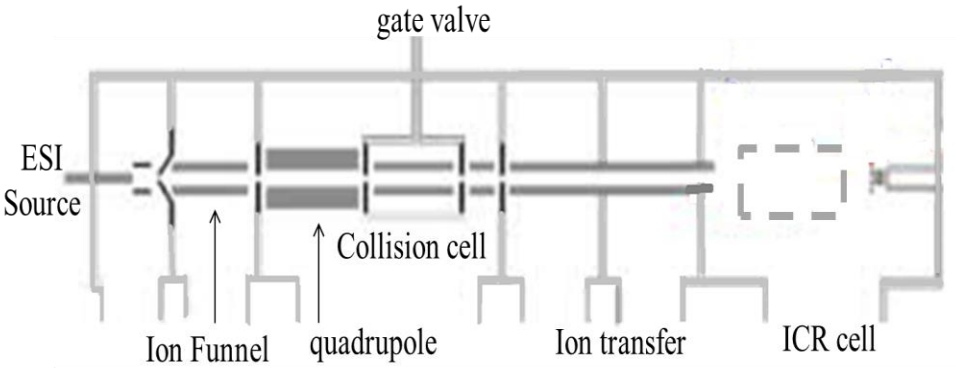

Figure 1.3.9: Schematic illustration of a Bruker FT-ICR mass spectrometry. This scheme was completely redrawn and was partially based on (Laskin *et al*., 2003).

The Fourier transform ion cyclotron resonance mass spectrometer (FTICR-MS or FT-MS) used in this research consists of several main subunits in the instrument: an ion source (usually electrospray source), various ion optics to transfer the ions into the magnetic field as the RF-Only quadrupole ion guide, which direct the ions into the (ICR) cell or Penning trap (Figure 1.3.9) (Dietmar *et al*., 2000, Laskin *et al*., 2003, and Downard, 2004).

The heart of FTICR analyzer is the ICR cell, where the measurements of the (*m/z*) ratio of an ion accumulate. The ICR cell is composed of three opposing pairs of plates. These plates are called the trapping, the exciting, and the detecting plates (as shown in Figure 1.3.10). Trapping the ions in the ICR cell enhances the time of detection and thus sensitivity and resolution. The ions can be trapped and stored for up to hours in the ICR cell by applying a small voltage to the trapping plates (usually +/− 1-2 Volts, depending on the polarity of the ions). At the same time the excitation plates and the detection plates are held at ground potential (Dietmar *et al*., 2000).

Ions can be stored for long periods in the analyzer cell only in a very high vacuum environment. The ultrahigh mass resolution analysis occurs at a pressure of (10^{-6} to 10^{-10} mbar). The several processes that occur in the FTICR analyzer can be summarized as follows. Once the ions enter the ICR cell, they will experience harmonic oscillations in the electric field between the trapping plates. In order to create a trapping motion, the ions are submitted to a strong magnetic field (B) induces them into a stable cyclic motion represented by the cyclotron frequency.

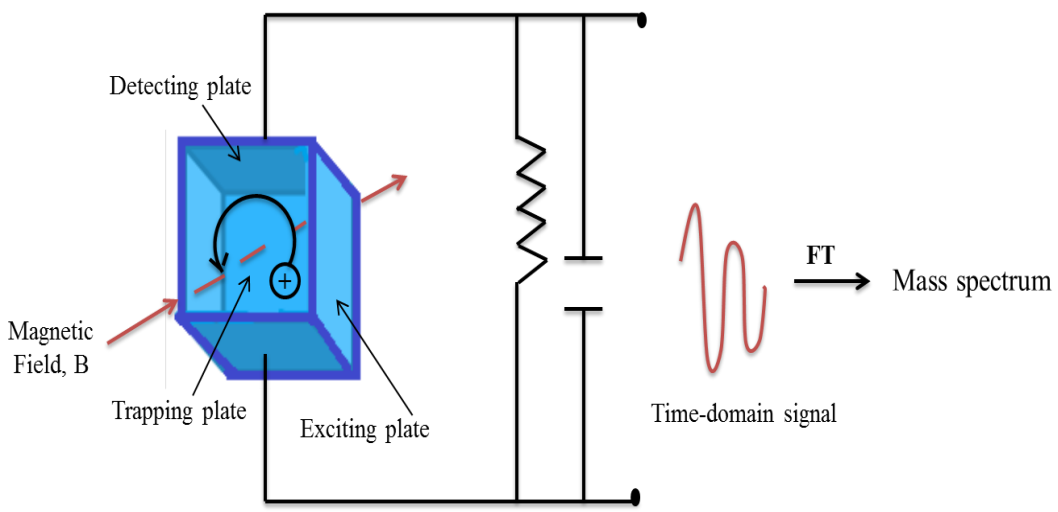

Figure 1.3.10: Schematic diagram of an ion cyclotron resonance (ICR) analyzer. This scheme was completely redrawn and was partially based on Marshall *et al*., 1998.

In a magnetic field (B), ions of charge (q) and velocity (ν) experience the Lorentz force (F_L). This (F_L) force is perpendicular to both the ions velocity and the magnetic field lines.

$$\mathbf{F_L = q\nu \times B}$$

The Lorentz force (F_L) is directed inward and balanced by the centrifugal force (F_Z), which is directed outward (as illustrated in Figure.1.3.11). The ion mass is represented by (m), the ions velocity (ν_{xy}) in the x-y-plane and the orbital radius (r).

$$\mathbf{F = m\upsilon^2/r}$$

Both forces will balance the ions and then stabilize them.

$$\mathbf{q\upsilon B = m\upsilon^2/r \text{ or } qB = m\upsilon/r}$$

A complete circular trajectory can be represented by (**2πr**) having a frequency (**υ**):

$$\boldsymbol{\upsilon = \omega/2\pi r}$$

Hence, the angular velocity (**ω**) becomes equal to:

$$\boldsymbol{\omega_c = 2\pi\upsilon = \upsilon/r = qB/m}$$

The frequency and the angular velocity of the ion depend on the ratio (qB/m).

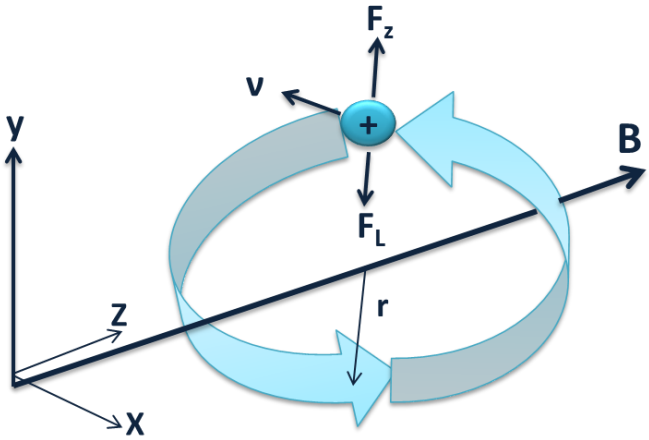

Figure 1.3.11: Schematic diagram of cyclotron motion of ions in the magnetic field induced by the. Counterbalance of the centrifugal force F_z and Lorentz force F_L. This scheme was completely redrawn and was partially based on Schmid *et al*., 2000.

Nevertheless, the radius of the ion trajectory increases in proportion to the velocity. If the radius becomes larger than the cell radius, the ion will be expelled (Marshall *et al*., 1991, Schmid *et al*., 2000, and Marshal *et al*., 2002). Each different ion rotates with its unique frequency in a small radius. The ions with the same *m/z* will experience increasing in their kinetic energy (KE), and will be exited coherently as "ion packets" to a larger radius, and this happens by increasing the applying voltages of the excitation plates.

In the ICR cell, once particular ions with the same *m/z* values are excited with an electromagnetic wave having the same frequency, they will move coherently in a larger radius packet and became closer to the detection plates. It should be noted that the higher kinetic energy of the irradiation translates into larger radius motion. As we have two trapping plates connected by a circuit with a cyclotron frequency characteristic of the ions with the same *m/z* value, the creation of an image charge in the detection plates occurs. This image current is formed when the ions packet passes by one plate and then by the second plate. Consequently, the time domain signals are detected and then converted into a mass spectrum.

To summarize the described FTICR sequential steps of ions separation, we can say that after that the ions are trapped in the ICR cell, they are excited by a resonant excitation pulse into a coherent orbit. The excitation amplifier is then turned off and the ions continue to orbit at their final radius. Ions moving near electrodes cause an image charge to form on these electrodes to balance the ions electric field. In the case of a circular orbit, this image charge will oscillate at the ion characteristic resonant frequency, and hence can be detected by a sensitive preamplifier circuit, digitized, and stored in computer memory.

The complex wave detected as a time-dependent function will transfer into a frequency-dependent intensity function through a Fourier transform (FT) (Marshall, 1985, Marshall *et al*., 1998, Shi *et al*., 1999, Marshal *et al*., 2002, and Junot *et al*., 2010).

FTICR is considered as one of the most effective tools for the analysis of biological molecules identification. Recently, FTICR with its sensitivity, full width half mass FWHM resolution, dynamic range, and resolution has been utilized for the identification of lipid A studies (Schmidt *et al*., 2000, Nikolaev *et al*., 2014, and Junot *et al*., 2010).

1.3.4. Tandem mass spectrometry:

Tandem mass spectrometry (MS/MS) is a powerful technique of structural investigation allowing unravelling the exact structure, sequencing, and identity of the analyte. Tandem mass spectrometry involves multiple separation steps of the ion and their fregmenation rather than a single step, by using more than one mass analyzer (Figure 1.3.12).

The main principle of tandem mass spectrometry technique is depicted in Figure1.3.12. In the first analyzer, the isolation of the ions occurs to select one ion of a given mass called “the precursor ion”. The mass selected precursor ions pass through a region where they are activated by increasing their kinetic energy and causes them to fragment apart to produce product ions. This is usually achieved by collision of the precursor ions with a neutral gas, a process called collisional activation or collision induced dissociation (CID). Also, increasing the pressure in the collision cell increases the CID-

fragmentation of the precursor ions. Accordingly, the precursor ion will be fragmented into product ions. The product ions are then sorted by the second analyzer which separates these ions based on their *m/z* values, which then can be detected by the detector (McLafferty *et al*., 1983, and Busch *et al*., 1988). There are various methods to activate the precursor ions and increase their internal energy in order to dissociate and fragment the precursor in order to provide structural information.

The most commonly used activation method in the tandem mass spectrometry (MS) is collision induced dissociation (CID) (Wells *et al*., 2005). McLafferty and Jennings were the first researchers that have introduced the tandem mass spectrometry technique and the collision induced dissociation (CID) analysis (McLafferty *et al.,* 1967, and Jenning *et al.*, 1968). When a solid material is used for the activation of the ion, then this technique is called surface-induced dissociation (SID) (Cooks *et al*., 1994). In addition, electron capture dissociation (ECD) was also introduced as another MS/MS fragmentation technique, in which they use a direct introduction of low-energy electrons to interact with the gas-phase ions (Zubarev *et al*., 1998). Like ECD, electron-transfer dissociation (ETD), transfers electrons to induce fragmentation of large, multiply-charged cations (Hart-Smith *et al*., 2014). CID remains the most common ion activation method. CID methods are distributed into three types based on the collision energy and activation time scale; high energy, low energy, and very low energy.

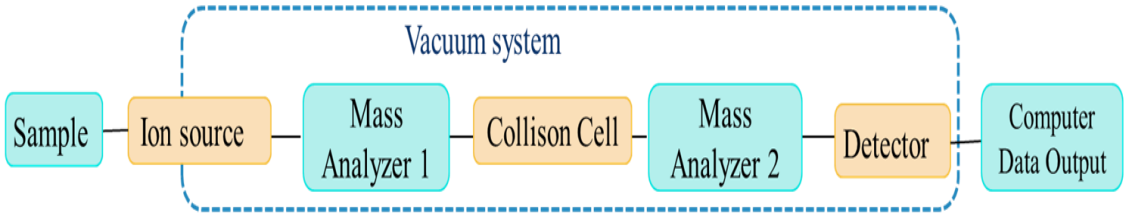

Figure 1.3.12: Schematic diagram of the main components of tandem mass spectrometry (MS/MS).

Recently, there have been enormous advances in developing hybrid tandem mass spectrometers. The purpose of these instruments is to combine the strength of different analyzer to enhance the separation of the precursor ion and product ions. In these types of instrument, the first analyzer function as an ion focusing device that guides the precursor ion to other components of the device. Almost all possible combinations of several different types of analyzer have been reported (ex, triple quadrupole instrument (QqQ), ion trap-quadrupole (IT-Q-TOF), or a quadrupole linked to a Time-of-flight (QqQ-TOF-MS) hybrid instruments.

1.3.3.1 CID-QqQ-MS/MS (Low-energy)

It has been shown that the time scale of the CID-activation is based on the rapidity of energy deposition on the precursor ion, which in fact translates into how fast this precursor ion dissociates or rearranges (McLuckey *et al*., 1997). Therefore, low- energy CID methods are slow when multiple collisions occur. The low-energy collision in tandem mass spectrometry analyses usually occur in the 1–100 eV range. Usually, within few hundred microseconds to a few milliseconds, activation of tens to hundreds collisions occur. Therefore, these collisions happen with long intervals between individual each individual collision which leads to more activation and dissociation. This is exemplified in Table 1.3.1 which presents three time regimens for activation methods used in MS/MS.

This type of low-energy CID is commonly used in triple quadrupoles (QqQ) (Figure 1.3.13). The product ions formed by dissociation of the precursor ion can experience further

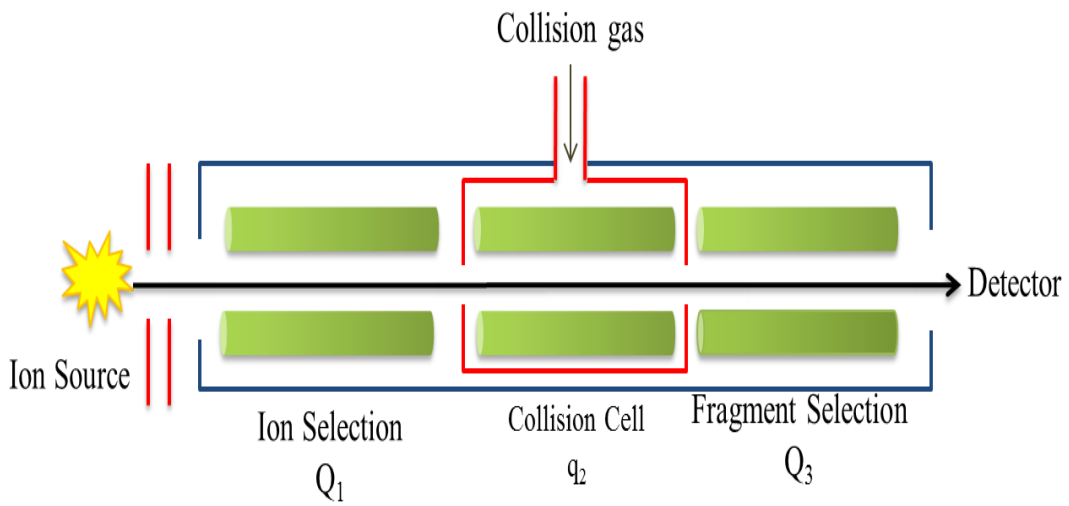

Figure 1.3.13: Triple Quadrupole mass spectrometry. This scheme was completely redrawn and was partially based on McLafferty *et al*., 1983.

Figure of merit	High-energy CID (fast activation)	Low-energy CID (slow activation)	Very low-energy CID (very slow activation)
Instruments used	Magnetic/electric sectors, TOF/TOF	Tandem quadrupoles, (e.g., QqTOF, QqQ)	Quadrupole ion trap, FT-ICR
Collision energy	2–10 keV	1–200 eV	1–20 eV
Collision number	1-5	10-100	100s
Activation time scale	1-10 µs	0.5-1 ms	10-100 ms
Instrument time scale (kinetic window)/minimum observable reaction rate	10-100 µs/10^6-10^4 s^{-1}	0.1-1 ms/10^4-10^3 s^{-1}	10 ms-1s/10^2-1 s^{-1}
Efficiency	<10%	5–50%	50–100%

Table 1.3.1. Summary of the typical parameters for the three commonly used CID regimens.

activation by subsequent collisions and then also dissociate at higher gas pressures. Once the product ions are formed, they can be reactivated by collision and can fragment further. This step can be repeated to provide MS^n spectra.

In this thesis, I will discuss the advantages and disadvantages of implementing the CID analysis. During the CID-process, after collision with the neutral collision gas, the precursor ion kinetic energy is transferred into internal energy, which caused the precursor ion to dissociate into various product ions. This technique is called collision-induced dissociation or collision-activated dissociation (CID or CAD) (McLafferty *et al*., 1983, and Shukla *et al*., 2000).

1.3.3.2. CID-MS/MS (Very Low Energy)

Very low collision energy MS/MS experiments occur in the order of few eV collision energies and hundreds of collisions are required, whereas, as precursor ion activation time needs to be much longer, (hundreds of milliseconds to second). Consequently, very low-energy CID-MS/MS analyses are considered to occur with very slow activation and slow heating methods (Table 1.3.10) (Gauthier *et al*., 1991). It is commonly used in trapping devices, such as quadrupole ion traps (IT) and Fourier-transform ion cyclotron resonance (FTICR) instruments.

1.3.3.2.1. QIT-MS/MS

Quadrupole ion trap (QIT) consists of central doughnut-shape ring electrode and a pair of end cap electrodes (Figure 1.3.14). Ions will enter through the end-cap electrode and then directed to the detector, by applying appropriate DC (U) and RF (V) voltages to electrodes to create a dynamic parabolic region inside the trapping volume. In a quadrupole ion trap (IT), the isolation and acceleration of precursor ions are achieved by using the ‘‘on-resonance’’ excitation method. In the “on resonance method”, the isolated precursor ion is excited by applying a small potential across the end-caps. Ion activation times of the order of tens of milliseconds can be used without significant ion losses, therefore, multiple collisions can occur. The product ions are detected by subsequent ejection from the trap (Figure 1.3.13) (Wieboldt *et al*., 1997, and Stafford, 2002).

1.3.3.2.2 CID-FTICR-MS/MS

When an FTICR-MS instrument is used for MS/MS experiments, the ions are directed to the ICR cell where they are exposed to a very low pressure (10^{-10} mbar). An electric field (AC) can be applied to excite the desired ions or to expel the not wanted ions by discharge on the wall. The selected ions can then be fragmented by using a collision gas which induces the fragmentation. The product ions are then formed close to the centre and detected. The processes of selection, fragmentation, and detection, can be performed repetitively. This will allow the increase in sensitivity, the resolution and more importantly can provide MS^n capability, without reloading ions from the source. In FTICR-MS high

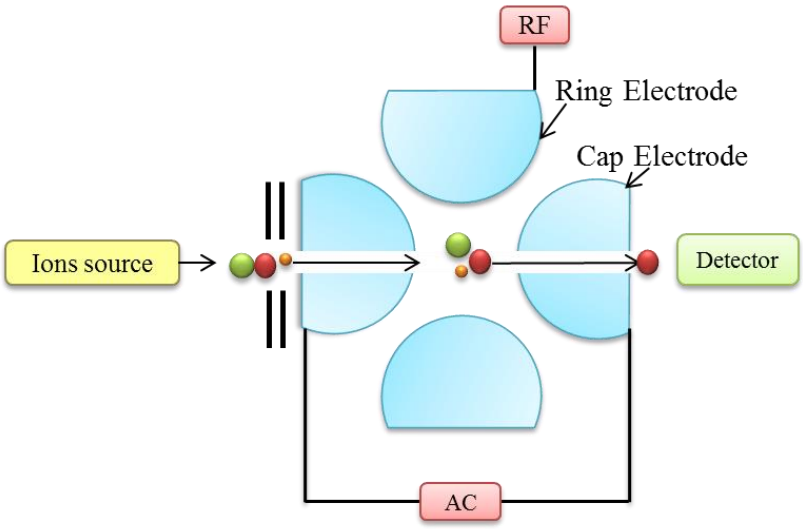

Figure 1.3.14: Schematic diagram of quadrupole ion trap mass analyzer (QIT). This scheme was completely redrawn and was partially based on Downard, 2004.

resolution can be obtained on both precursor and product ions (Wieboldt *et al*., 1997, and Stafford, 2002).

It should be noted that in many FTICR tandem mass spectrometers collision activation is a stepwise process. Initially, the ions enter the ICR cell with low kinetic energies and are trapped effectively without any fragmentation. The chosen precursor ions are excited, gain higher kinetic energy and move to larger radii. This excitation is followed by either one of the following processes: collision-induced dissociation (CID), sustained off-resonance irradiation collision-induced dissociation (SORI/CID), infrared multiphoton dissociation (IRMPD), and electron capture dissociation (ECD) (Scigelova *et al*., 2011, and Brodbelt. 2014).

In this thesis, we will use SORI/CID technique in order to produce the fragment ions. Therefore, we will discuss the advantages and disadvantages of implementing the SORI/CID.

1.3.3.3. MALDI-TOF-TOF-MS/MS analysis (High energy)

When using MALDI-TOF-TOF-MS/MS instruments, high collision energy CID possessing very high translational energy is usually used to fragment the precursor ions into product ions. Henceforth, the precursor ions with a kinetic energy of a few keV can enter the collision cell under low-vacuum conditions. It should be noted that this high-energy CID-MS/MS is considered as a fast method of activation as the deposited energy is related to the number of collisions. For these reasons, the use of single or a few (5–10)

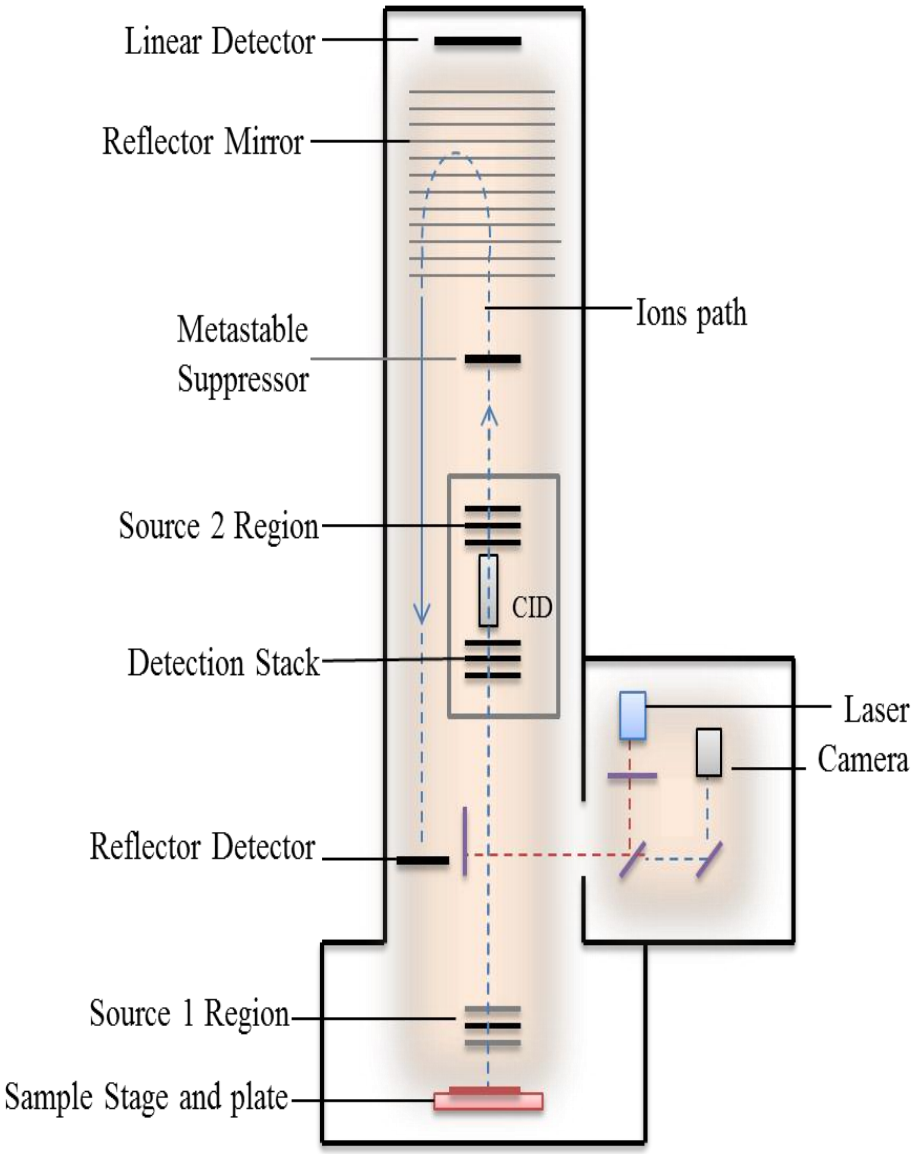

Figure 1.3.15: Schematic representation of MALDI-TOF/TOF-MS/MS. This scheme was completely redrawn and was partially based on Sleno *et al*., 2004.

collisions are typically used to input high energy (Table 1.3.10), (McLuckey *et al*., 1997). As previously mentioned, the high-energy collision cell is located between two TOF mass analyzers (as illustrated in Figure 1.3.15) (Sleno *et al*., 2004).

1.3.3.4. Different types of MS/MS analysis

There are various types MS/MS experiments that can be performed (Figure 1.3.16). The first type is the product-ion scan (or CID-MS/MS experiment) which is one of the four main scan experiments, and the most common mode of MS/MS operation. The product ion scan spectrum contains only those product ions that are formed from a mass-selected precursor ion. The first mass analyzer is used to transmit only the selected precursor ion, and the second mass spectrometer is scanned over a required *m/z* range.

Another type of MS/MS scan used is the precursor-ion scan. That type of scan allows the identification of all the precursor ions that fragment to a common product ion. This can be achieved by adjusting the second mass analyzer to transmit a chosen product ion, and then the first mass analyzer will scan over a certain *m/z* range to transmit only those precursor ions that fragment to produce the chosen product ion.

Additionally, a natural-loss scan is another scan type, in which all the precursor ions endure the loss of a specified common neutral species. Both mass analyzers are scanned at the same time, but with a mass offset that associates with the mass of the specified neutral group. This scan is typically suitable for closely related compounds, which is often result in forming the same product ion.

Finally, the fourth scan type is multiple-reaction monitoring (MRM) scanning in which both mass analyzers can simultaneously measure a set of preselected analyte *m/z* precursor ion →*m/z* product ion transition. Monitoring more than one reaction is termed multiple-reaction monitoring (MRM). Both type of reaction monitoring is suitable for quantitative measurements of analytes within complex mixtures (Figure 1.3.16) (McLafferty. 1981, and Lin *et al*., 2014).

1.3.3.5. Definition of tandem in-space and in-time

Tandem mass spectrometry was developed as a tandem-in-space method when using sector mass spectrometers. Later, it was expanded as consecutive arrangements of mass/energy analyzers, where the selection of the precursor ion and the formation of the product ions could be performed by two or more analyzers that were coupled together sequentially, such as multiple quadrupoles (Q) (Yost *et al*., 1978), time-of-flight (TOF) (McLafferty *et al*., 1980) and various combinations.

This was followed by the development of tandem-in-time instruments, in which the selected precursor ion was dissociated consecutively within the same space by using a radiofrequency, such as the quadrupole ion trap (March *et al*., 1995), and the ion cyclotron resonance (ICR) mass spectrometers (Cody *et al*., 1982). During the trapping process, the precursor ions contain relatively low-kinetic energy, and following excitation, their energy is activated by multiple collision activation methods which convert their internal energy to translational energy (Melvin *et al*., 1974, and Schmid *et al*., 2000).

In this thesis, I will employ both types of the described tandem mass spectrometry instruments. The most common type of tandem-in-space mass spectrometer used in this investigation will be performed with a low-energy CID a triple quadrupoles instrument such as (ESI-QqQ-MS/MS).

In addition, low-energy collision dissociation tandem-in-time mass spectrometer will be used with an by ESI-FTICR-MS/MS (McLuckey *et al*., 1992, Harrison *et al*., 1999, Hakansson *et al*., 2003, and Vukelića *et al*., 2007). For high-energy tandem mass spectrometric analysis, CID-MALDI-TOF/TOF-MS/MS will be used.

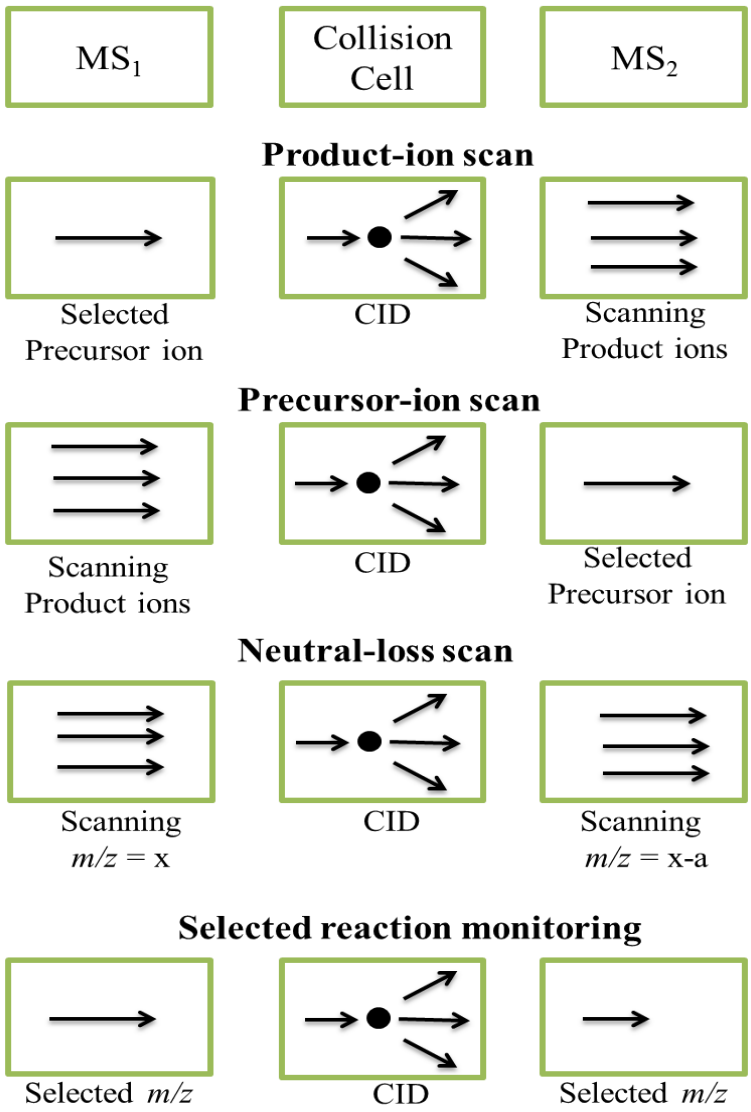

Figure 1.3.16: Block diagram of scan modes of MS/MS. This scheme was completely redrawn and was partially based on Sleno *et al*., 2004.

1.3.4. Characterization of Lipid A by mass spectrometry and tandem mass spectrometry.

Mass spectrometry (MS) has been developed as one of the premier tools for elucidation of lipid A structures. The amphiphilic nature of lipid A species makes them intensely difficult to separate and ionize. The number and the length of lipid A fatty acids vary among different species. For example, the analysis of lipid A isolated from the LPS of *B. parapertussis pagP* using MALDI-TOF- and ESI-FTICR-MS (- ion mode), revealed the presence of a singly deprotonated GlcN disaccharide di-phosphorylated hexa-acylated lipid A structure, containing two phosphate groups at O-1 and O-4´ and six fatty acids, including two (C14:0(3-OH)) acyl chains, one (C14:0), two (C16:0) acyl chains, and one (C10:0(3-OH)) acyl chains (Hittle *et al*., 2015). Also, ESI-FTICR-MS (- ion mode) of lipid A isolated from the LPS of the *Salinivibrio sharmensis*, revealed the presence of a singly deprotonated GlcN disaccharide di-phosphorylated hexa-acylated lipid A structure, containing two phosphate groups at O-1 and O-4’ and six fatty acids, including three (C14:0(3-OH)) acyl chains and one (C12:0(3-OH)) acyl chains (Carillo *et al*., 2013).

While MALDI-QqTOF-MS (- ion mode) analysis of the lipid A obtained from LPS of *H. alvei* 1192 revealed the presence of a singly deprotonated GlcN disaccharide di-phosphorylated hexa-acylated forms of lipid A carrying four (C14:0(3-OH), one (C14:0) and one (C12:0) fatty acids, containing two phosphate groups at O-1 and O-4´ (Lukasiewicz *et al*., 2010). The chemical structure of lipid A isolated from LPS of the *A. salmonicida* SJ-83, was investigated using ESI-QqTOF-MS hybrid instrument (negative-

ion mode) afforded a major doubly charged ion and its corresponding singly charged ion as a minor species. The GlcN disaccharide structure was composed of di-phosphorylated hexa-acylated lipid A structure, containing two phosphate groups at O-1 and O-4´ and six fatty acids, including four (C14:0(3-OH)) acyl chains, (C14:0) acyl chins, and one (C12:0) acyl chains (El-Aneed *et al*., 2005).

1.4. The objective of the thesis

The main purpose of this research is focused on the uses of several types of tandem mass spectrometry techniques (tandem-in space, tandem in-time, high- and low-energy collision induced dissociation tandem mass spectrometry analysis) to investigate the structure of a series of lipid As extracted from different type of bacteria of the *Vibrionanaceae* family. In this thesis, it should be clarified that the investigated series of lipid As, were obtained from LPSs isolated from the outer membrane of the Gram-negative bacteria pathogen *Aeromonas Liquefaciens* SJ-19, *hydrophilla* SJ-55, and *Salmonicidia* SJ-113. In addition, it should be mentioned that the bacteria were infected with one type of a bacteriophage virus (ATCC # PTA-8357). This voluntary infection of this series of bacteria was completed, to investigate the possible physical interactions, between the phages and the bacteria in order to understand, whether this phage-bacteria interaction, affected the biosynthesis of the outer membrane LPSs. This study initially was aimed for the possible development of phage therapeutic strategy in the aquaculture industry.

Most of the published studies on infection of bacteria with phages, have been mainly focused on elucidating the respective structures of the *O*-specific antigens and core oligosaccharide portions of the affected virus induced LPSs structures which results from the interactions of the phage receptors and the LPS outer cell surface, membrane (Perry *et al*., 1979, Banoub *et al*., 2010, Rakhuba *et al*., 2010, and Viertel *et al*., 2014).

In that respect, it should be mentioned, that to our knowledge, that there has never been any work published on the variation of the lipid A structures following the isolation of LPSs from bacteria infected with bacteriophages, this was never investigated before. For

these reasons, the effect of the bacteriophages on the bacteria, and specifically on the structures of this series of Lipi A_s will be investigated by MS techniques and evaluated in this document.

Chapter 2

Materials and Methods

The original strain of *Aeromonas liquefaciens, hydrophilla,* and *salmonicidia* were obtained from Dr H. N. Atkinson (The South Australian School of Technology Oceans, Australia). The cultures were grown to medium-to-late stationary phase in Trypticase Soy Broth without added glucose (Baltimore Biological Laboratories Inc.) for almost 20 h at 25°C. The bacteriophage product used in our studies is ListShield™; AP2 for *A. liquefaciens,* AH1 for *A. hydrophilla,* and AHER1 for *A. Salmonicidia*. Following individual infection with the (ATCC # PTA-8357) phage, each species was divided into three bacterial colonies which are then selected from biochemically pure cultures of *Aeromonas liquefaciens* SJ-19, *hydrophilla* SJ-55, and *salmonicidia* SJ-113.

It should be mentioned that for these Gram-negative bacteria the overall strain of these species were isolated as morphologically different clones. The first series of clones (Strain 19a), (Strain 55a), and (Strain 113a), grew when infected with the phage, and were referred to as phage resistant. The second series of clones (Strain 19b), (Strain 55b), and (Strain 113b), when cultivated in the presence of the same phage, were unable to be reproduced, and were referred to as phage sensitive.

These strains were added to the collection of the Northwest Atlantic Fisheries Center, St. John's as (SJ-19, SJ-55, SJ-113) (original), and (SJ-19a, SJ-55a, SJ-113a) (resistant). These organisms were initially plated on Trypticase Soy Agar (Baltimore

Biological Laboratory, Baltimore, MD, USA) to check purity and colonial morphology. Stock cultures were grown in Trypticase Soy Broth without dextrose, divided into 1 mL aliquots, and frozen and stored at (-80 °C). The protocol for medium-scale culture of the bacteria in the presence of phages was generally identical for each strain (Michon *et al*., 1984, and Almostafa *et al*., 2016).

2.1. Purification of the lipopolysaccharides

The extractions of the LPSs were achieved using the hot-phenol method (of Whestphal and Jann) and freeze-dried. The stored cells (10 g) were suspended in deionized water (175 ml) and heated to 70° C. The addition of an equal volume of heated phenol (90 %) to the mixtures was finalized by stirring the mixtures for 20 min at 70° C. Then the mixtures were cooled on ice and centrifuged using Sorvall SS-34 rotor (3500 rpm, 1475 x g). The isolation was for the aqueous layers by aspiration and the procedure was repeated twice.

The aqueous layers were combined and dialysed against water to remove any traces of phenol. Consequently, the evaporation (under vacuum) was done to reduce the water volume of the combined water mixtures and finally centrifuged at 39,000 rpm (105,000 x g) for 3 h.

The LPSs were finally lyophilized and isolated and further purified using polymyxin-coated Affi-prep beads (Bio-Rad Laboratories, Richmond, CA, USA). Fifteen milligrams of LPSs were suspended in 15 ml of phosphate-buffered saline (PBS, PH=7.4). LPSs solutions were mixed with washed polymyxin beads (the beads were originally

washed first with 0.1 M NaOH and then with distilled water. The mixtures were incubated overnight with agitation using an orbital shaker (1500 rpm). The mixtures were then centrifuged (2500 x g) for 10 min and the supernatants were collected. The beads were then washed twice with 15 ml and 5 ml 0.1 M NaOH. The supernatants were combined and LPSs were dialysed against water and finally lyophilized (Caroff *et al*., 2003, Banoub *et al*., 2010).

2.2. Hydrolysis of the lipopolysaccharides

LPSs (100 mg) were hydrolyzed with 1% acetic acid for 90 min at 100°C. Then, the LPSs were centrifuged at 3000 x g for 30 min induce the precipitation of lipid A_s, while the polysaccharides were present in aqueous media.

Lipid A_s were removed and washed with water and the *O*-specific polysaccharide or the rough mutant core oligosaccharides were recovered from the supernatant by chromatography on Sephadex G-50 (Pharmacia Ltd.). Fractions were visualized using a differential refractive index detector (Waters Associates) (Banoub *et al*., 2010, Kilár *et al*., 2013, Wang *et al*., 2015, and Almostafa *et al*., 2016).

2.3. Gas chromatography-mass spectrometry (GC-MS) for fatty acid analysis

GC-MS analysis was performed on a Varian Saturn 2000 GC MS/MS instrument equipped with a Zebron capillary column (30m x 0.25 mm). Helium was used as the carrier

gas. Lipid A was treated with 2 M HC1 in methanol (methanolysis) for 3 hrs at 100° C. Methyl esters were extracted into hexane and analyzed by GC-MS in comparison with standard methyl esters (Supeleo, Bellefonte, PA, USA). GC (1 µL injection) analysis of methyl esters was performed with the following temperature program: 100° C for 5 min, 100° to 280° C at 5° C/ min, hold at 280° C for 5 min (Kitson *et al*., 1996, Portolés *et al*., 2011, Banoub *et al*., 2010, and Almostafa *et al*., 2016).

2.4. Mass spectrometric analysis of the extracted mixture of lipid A_s

2.4.1. Electrospray triple-quadrupole mass spectrometry (ESI-QqQ-MS) of the extracted mixture of lipid A_s.

Electrospray ionization mass spectrometry (ESI-MS) and low-energy collision-induced dissociation (CID-MS/MS) analysis were performed using a Waters XEVO TQ-S (QqQ) system (Waters Corp., Milford, MA, USA) equipped with an ESI source operated in negative ion mode. The operating voltage on the ESI capillary was 2200 V and the cone voltage was set at 31 V. The ESI source was maintained at 75 °C and the desolation temperature at 200 °C.

All the CID-MS/MS analysis were carried out with the same collision energy of 30 eV. The Xevo TQ-S is equipped with a ScanWave™ collision cell (q), which provides enhanced product ion spectral acquisition capability. The mass accuracy of the reported masses is 0.01 *m/z* units based on the mass assignment of ±0.05 m/z units over a 24 h period (Kilár *et al*., 2013, and Almostafa *et al*., 2016).

The lipid As mixtures of the Gram-negative bacteria *Aeromonas liquefaciens* (SJ-19a), *hydrophilla* (SJ-55a), and *salmonicidia* (SJ-113a) were dissolved in chloroform and methanol (1:1) and 0.1% trimethylamine/pure Milli-Q water, and (SJ-19a: 1.6 mg/mL), (SJ-55a: 1.7 mg/mL), and (SJ-113a: 1.4 mg/mL). Then they were directly injected (10 µl flow) into the ESI source in negative (-ve) ion mode.

2.4.2. Electrospray quadrupole Fourier transform ion cyclotron mass spectrometry (ESI-FTICR-MS) of the extracted mixture of lipid A_s

Electrospray ionization Fourier transform ion cyclotron resonance (ESI-FTICR) mass spectrometry was performed in the negative ion mode using an APEX QE (Bruker Daltonik GmbH, Bremen, Germany) with a 7 Tesla actively shielded magnet. The samples were sprayed at a flow rate of 250 µL min^{-1}. The capillary entrance voltage was set to 4 kV and nitrogen was used as drying gas at a temperature of 200 °C. The instrument was externally calibrated with appropriate standards. Sustained off-resonance irradiation collision induced dissociation (SORI-CID) experiments were performed by isolating the ions under study inside the ICR cell ($P = 10^{-10}$ mbar) and exposing them to Ar at higher pressures ($P \approx 10^{-5}$–10^{-6} mbar). At these pressures, in the 250 ms excitation time, there are of the order of 10s to 100s of collisions (Brodbelt. 2014, and ALmostafa *et al*., 2016).

The lipid As mixtures of the Gram-negative bacteria *Aeromonas liquefaciens* SJ-19a, *hydrophilla* SJ-55a, and *salmonicidia* SJ-113a were dissolved in chloroform and methanol (1:1) and 0.1% trimethylamine/pure Milli-Q water, and (SJ-19a: 1.6 mg/mL),

(SJ-55a: 1.7 mg/mL), and (SJ-113a: 1.4 mg/mL). Then they were directly injected into the ESI source in negative (-ve) ion mode.

2.4.3. Matrix-assisted laser/desorption ionization time-of-flight mass spectrometry (MALDI-TOF-MS) of the extracted mixture of lipid As

2,5-dihydroxybenzoic acid (DHB) matrix was used at a concentration of 5 mg/ml in a 2:2:1 mixture (v/v/v) of methanol, acetonitrile, and water. Lipid A was used at a concentration of 2 mg/ml in a (1:1) mixture (v/v) of chloroform and methanol. The sample was prepared by mixing equal volumes of DHB solution and lipid A solution. The spot was done by using 1 µl of this mixed solution and spotted onto a MALDI plate and then left to crystallize and dry in desiccators before being loaded into the MALDI-MS instrument.

Mass spectra of the lipid A isolated from *Aeromonas liquefaciens* SJ-19a, *hydrophilla* SJ-55a, and *salmonicidia* SJ-113a were acquired in reflectron negative ion mode. The MALDI-TOF/TOF-MS spectrometer (MALDI 4800, Applied Bioscience) (MALDI-Quality™ Matrix Solutions, Agilent Technologies) was used for this experiment. The MS data were acquired in the mass range 600 to 1900 *m/z*. The MALDI-TOF/TOF-MS instrument was equipped with a nitrogen laser (337 nm). All the spectra were accumulated as 600 individual laser shots. The accelerating potential was 25KV. The focusing guide wire was held at a potential 0.18%. The laser intensity of 4200 was used. The MALDI-TOF/TOF-MS possessed a high mass accuracy (5 ppm) and resolution of 15000-25000 (FWHM). The minimum signal to noise ratio was 35.

High-energy collision dissociation MS/MS (CID-MS/MS) experiments were conducted using the same instrument. Product ion scans of selected masses were induced by a high CID collision cell. The resulting product ions were analyzed by the second TOF analyzer. The tandem mass spectrometric analysis was achieved with N_2 as collision gas and at collision energy of 1 kV, which corresponds to the difference between the accelerating potential (8 kV) and the floating cell (7 kV) (Schiller *et al.*, 2007, Lukasiewicz *et al*., 2006, Kilár *et al*., 2013, and Almostafa *et al*., 2016).

Chapter 3

Mass Spectral analysis of the mixture of lipid A_n isolated from the LPS of *A. liquefaciens* SJ-19.

Aeromonas Liquefaciens is a genus of Gram-negative, anaerobic, non-spore-forming bacilli bacterium belonging to the Gram-negative *Vibrionaceae* family (Aoki *et al.*, 1971, and Michon *et al*., 1984). This bacterium fits in a group of closely related motile *Aeromonads*, which mainly cause hemorrhagic septicemia in cultured pond-fish and salmonids (Michon *et al.*, 1984 and Janda *et al*., 2010). The LPS of SJ-19a was obtained from the rough mutant Gram-negative bacteria *A. liquefaciens* grown in the presence of phage and it was classified as phage resistant.

3.1. Gas chromatography-mass spectrometry (GC-MS) of the fatty methyl ester released from the lipid A_n mixture isolated from the LPS of the *A. liquefaciens* SJ-19.

The qualitative analysis of fatty acids was carried out by GC-EI-MS to identify separately the amide and the ester-bound fatty acids. The (R)-3-hydroxytetradecanoic acid (C14:0(3-OH)) was identified as an amide-linked fatty acid, whereas the (R)-3-hydroxytetradecanoic acid (C14:0(3-OH)) (3-hydroxymyristic acid) and dodecanoic acid (lauric acid) (C12:0) were identified as amide-linked fatty acids (Perry *et al*., 1979, Rebeil *et al*., 2004, and Almostafa *et al*., 2016). In addition to the methyl ester derivative of 3-

methoxytetradecanoic acid, the fatty acid methyl esters obtained by trans-esterification with sodium methoxide also showed the presence of the (C14:0(3-OH)) acid, which was substituted by the tetradecanoic acid (C14:0) (myristic acid) in the native lipid A. Similarly, the (C14:0(3-OH)) acid was also shown to be substituted by lauric acid. The absolute configuration of the GlcN residues in lipid A was determined as D on the deacylated, dephosphorylated lipid A fraction, using (R)-2-butanol (Perry *et al*., 1979, Rebeil *et al*., 2004, and Almostafa *et al*., 2016).

3.2. ESI-QqQ-MS analysis of the extracted mixture of lipid A_n isolated from the LPS of *A. liquefaciens* SJ-19a

The *A. liquefaciens* SJ-19a bacteria dissolved in chloroform and methanol was electrosprayed in the negative ion mode. The ESI-QqQ-ToF-MS is shown in (Figure 3.1.1). The lipid A_n component of the *A. liquefaciens* SJ-19a bacteria is not merely composed of a single lipid A entity. In reality, it is a complex mixture of many structurally-related components produced by the incomplete biosynthesis of this lipid A.

The ESI-QqQ-MS (- ion mode) of the lipid A_n (where n=1-5) mixture showed the presence of *inter-alia* seven different fragment ions at *m/z* 1716.30, *m/z* 1688.19, *m/z* 1506.10, *m/z* 1279.73, *m/z* 1097.63 *m/z* 892.56, and *m/z* 666.06. This indicates the presence of a heterogeneous mixture of lipid A_n (Scheme.3.1.1).

We have assigned these fragment ions as the series of $[M_n\text{-}H]^-$ deprotonated mono-phosphorylated molecules, represented as the following: $LipA_1$ at *m/z* 1716.30, $LipA_2$ at

m/z 1688.19, $LipA_3$ at *m/z* 1506.10, $LipA_4$ at *m/z* 1279.73, and $LipA_5$ at *m/z* 1097.63 (Figure 3.1.1 and Table 3.1.1). In addition, we also observed two deprotonated molecules at *m/z* 892.56 and *m/z* 666.06. It is important to note that our tentative structural assignments of this series of deprotonated molecules have relied on comparison with well know Lipid A structures by a manual and expert-driven process. This was done without help of any software such as LipidView™ Software produced by Sciex. It is vital to mention that this mixture of lipid A_n did not give any distinctive mass spectra when electrosprayed in the positive ion mode.

From the above assignments, it became clear that the structures of the heterogeneous lipid A_n mixture contained a phosphate group which was located either on the O-4′ or O-1 positions of the β-D-Glc*p*N-(1→6)-α-D-Glc*p*N disaccharide backbone of lipid A.

From comparison with known literature, the deprotonated molecules were tentatively assigned that the 3-hydroxy-myristic acid (C14:0(3-OH)) fatty acid chains that acylate the various free positions of the β-D-Glc*p*N-(1→6)-α-D-Glc*p*N backbone of the fully biosynthesized $LipA_1$; these fatty acid chains were certainly attached to the O-3, O-3′, N-2 and N-2′ positions of this lipid A.

Also, it was proposed that two of these (C14:0(3-OH)) fatty acyl groups were substituted with either myristic and/or lauric acid (Scheme 3.1.1). By scrutinizing other known structures of lipid A, these two branched (Cl4:0(3-*O*-C12:0)) and (Cl4:0(3-*O*-C14:0)) fatty acyl groups are probably located on the O-3′and N-2′ positions (or *vice-versa*) of the non-reducing end group of the β-D-Glc*p*N-(1→6)-α-D-Glc*p*N disaccharide backbone

of this lipid A_n mixture (Scheme 3.1.1) (Lukasiewicz *et al*., 2010, Banoub *et al*., 2010, Kilár *et al*., 2013, Brodbelt *et al*., 2014, and Almostafa *et al*., 2016).

The deprotonated molecule $[M_1\text{-H}]^-$ at *m/z* 1716.30 was assigned as the mono-phosphorylated hexa-acylated forms carrying four primary 3-hydroxy-myristic acid (C14:0(3-OH)) fatty acids, in which two of them were substituted by either lauric and /or myristic acids forming the branched fatty acids (Cl4:0(3-*O*-C12:0)) and (Cl4:0(3-*O*-C14:0)). This series of fatty acyl groups can be distributed on the O-3, O-3′, N-2, and N-2′ position, not necessary in that order (Scheme 3.1.1).

Similarly, the deprotonated molecule $[M_2\text{-H}]^-$ of $LipA_2$ at *m/z* 1688.19 was attributed to the mono-phosphorylated hexa-acylated molecules. Accordingly, we presume that this molecule was formed by four (C14:0(3-OH)) 3-hydroxy-myristic acids, in which two of these fatty acids were esterified with two separate molecules of lauric acid (C12:0) at the 3-hydroxyl position of (C14:0(3-OH)) myristic acids. Once more, by comparing with other known structures of lipid A, these two branched (Cl4:0(3-*O*-C12:0)) fatty acids are probably located on the O-3′and N-2′ positions (or *vice-versa*) of the non-reducing end group of the $LipA_2$ disaccharide backbone (Scheme 3.1.1).

The most abundant deprotonated molecules at *m/z* 1506.10 and at *m/z* 1279.73 were tentatively assigned as $LipA_3$ and $LipA_4$. The deprotonated molecule $[M_3\text{-H}]^-$ of $LipA_3$ at *m/z* 1506.10 was assigned as the mono-phosphorylated penta-acylated form of the β-D-(1→6)-Glucosamine disaccharide carrying four primary 3-hydroxy-myristic acid (C14:0(3-OH)) fatty acids, in which one of them was substituted by lauric acids forming the branched fatty acids (Cl4:0(3-*O*-C12:0)), which we tentatively assigned to be located

at N-2′ of the non-reducing end residue of β-D-GlcpN-(1→6)-α-D-GlcpN disaccharide of $LipA_3$ (Scheme 3.1.1).

The deprotonated molecule of $LipA_4$ $[M_4\text{-H}]^-$ at *m/z* 1279.73 was assigned as containing a mono-phosphorylated tri-acylated form of the β-D-Glc*p*N-(1→6)-α-D-Glc*p*N disaccharide, carrying three primary 3-hydroxy-myristic acid (C14:0(3-OH)) fatty acids, in which one of them was substituted by lauric acids forming the branched fatty acids (Cl4:0(3-*O*-C12:0)), probably located at the N-2′ position of this lipid A. It should be noted that $LipA_4$ at *m/z* 1279.73 appears to be related to the deprotonated molecules $LipA_3$ at *m/z* 1506.10, which can be formed by elimination of one myristic fatty acid (C14:0(3-*O*-C14:0)) (-228 Da) from $LipA_3$ (Scheme 3.1.1).

The deprotonated molecule $[M_5\text{-H}]^-$ at *m/z* 1097.63 was assigned as $LipA_5$ mono-phosphorylated tri-acylated β-D-Glc*p*N-(1→6)-α-D-Glc*p*N disaccharide containing three 3-hydroxy-myristic acid (C14:0(3-OH)) fatty acids, which can be tentatively distributed on the O-3, N-2, and N-2′ positions (Scheme 3.1). Nevertheless, one can presume that the deprotonated molecule $LipA_5$ at *m/z* 1097.63 can be related to the deprotonated molecules $LipA_4$ at *m/z* 1279.73, and probably created by elimination of one lauric fatty acid (C14:0(3-*O*-C12:0)) (-182 Da). In addition, we have also observed the deprotonated molecule at *m/z* 892.56 which was tentatively assigned as $[\text{C-(C14:0)ketene-H}]^-$. This latter deprotonated molecule was attributed to the deprotonated molecule mono-phosphorylated D-GlcN species containing a 3-hydroxy-myristic (C14:0(3-OH)) fatty and a branched (Cl4:0(3-*O*-C12:0)) fatty acid group located on N-2.

Another deprotonated molecule at *m/z* 666.06 was assigned as [C-(C14:0(3-*O*-C14:0))ketene-H]$^-$. This latter deprotonated molecule was recognized as the mono-phosphorylated D-GlcN species, containing one branched (Cl4:0(3-*O*-C12:0)) fatty acyl group on the N-2 position (Scheme 3.1.1). It is reasonable to assume that the formation of these C-fragment ions at lower *m/z* values can be produced by the incomplete biosynthesis of the lipid A (Please understand, that these deprotonated molecules were named Fragment ions, to respect only the Domon and Costello nomenclature) (Domono and Cosetello 1988). Other logical reasons are: the partial degradation of lipid A during work-up, and the acid liability of some acyl chains and phosphate group at O-1 position during the acid hydrolysis.

At this stage of this investigation, we have tentatively identified a series of complete and incomplete O-3, O-3', N-2 and N-2 acylated the β-D-Glc*p*N-(1→6)-α-D-Glc*p*N disaccharide backbone of the lipid A_{1-5} structures sharing common properties. Once more, by analogy with known structures of lipid A, we have identified the presence of two primary hydroxytetradecanoic acids (14:0(3-OH)) at N-2 and O-3 positions present on the β-D-Glc*p*N-(1→6)-α-D-Glc*p*N disaccharide backbone of this mixture of lipidA_{1-5}. In addition, we have proposed the presence of branched fatty acid (C14:0(3-*O*-C14:0)) at the position O-3′, and (Cl4:0(3-*O*-C12:0)) at the position N-2′. All this series of LipA_{1-5} contained one phosphate group.The confirmation of our tentative assignments and the putative structures for the five deprotonated molecules LipA_1 to LipA_5 and the other various fragment ions were achieved by low-energy collision dissociation tandem mass spectrometry analysis. In this thesis we have followed the Domon and Costello carbohydrate nomenclature to define

and characterize all the deprotonated molecules produced by their gas-phase fragmentation in the ESI-MS and CID-MS/MS analysis (Domon and Costello 1988). It is well known that the glycosidic cleavage can be induced by the ESI-MS and provides useful structural information and reveals the sugar sequencing of the lipid A backbone.

It is vital to mention that the structure of the lipid A isolated from the rough LPS from *A. Liquefaciens* SJ-19 (original strain) was mainly composed majorly of one entity which was identified by ESI-MS and CID-MS/MS measured with a QqQ-mass spectrometer as the deprotonated molecule $[M-H]^-$ at *m/z* 1798.36. This deprotonated molecule was assigned as the O-1 and O-4′ bis-phosphorylated hexa-acylated forms of the β-D-Glc*p*N-(1→6)-α-D-Glc*p*N disaccharide carrying four primary 3-hydroxy-myristic acid (C14:0(3-OH)) fatty acids on the O-3′, O-3′, N-2 and N-2′ position. The O-3′ position of the myristyl group is substituted by myristic acid forming the branched (Cl4:0(3-*O*-C14:0)) fatty acyl group, whereas the N-2 myristyl group is substituted at the 3-position by lauric acid forming the (Cl4:0(3-*O*-C12:0)) branched fatty acyl group (Lukasiewicz *et al*., 2010, Banoub *et al*., 2010, Kilár *et al*., 2013, John *et al*., 2014, and Brodbelt *et al*., 2014).

3.2.1. Low-energy CID-MS/MS analysis of the extracted mixture of lipid A_n isolated from the LPS of a *A. liquefaciens* SJ-19a using the QqQ-MS/MS instrument

Low-energy CID-MS/MS (tandem-in-space) analysis using the triple quadrupole (QqQ) instrument conducted on the five-different precursor $[M-H]^-$ deprotonated mono-phosphorylated anions at *m/z* 1716.30 ($LipA_1$), *m/z* 1688.19 ($LipA_2$),

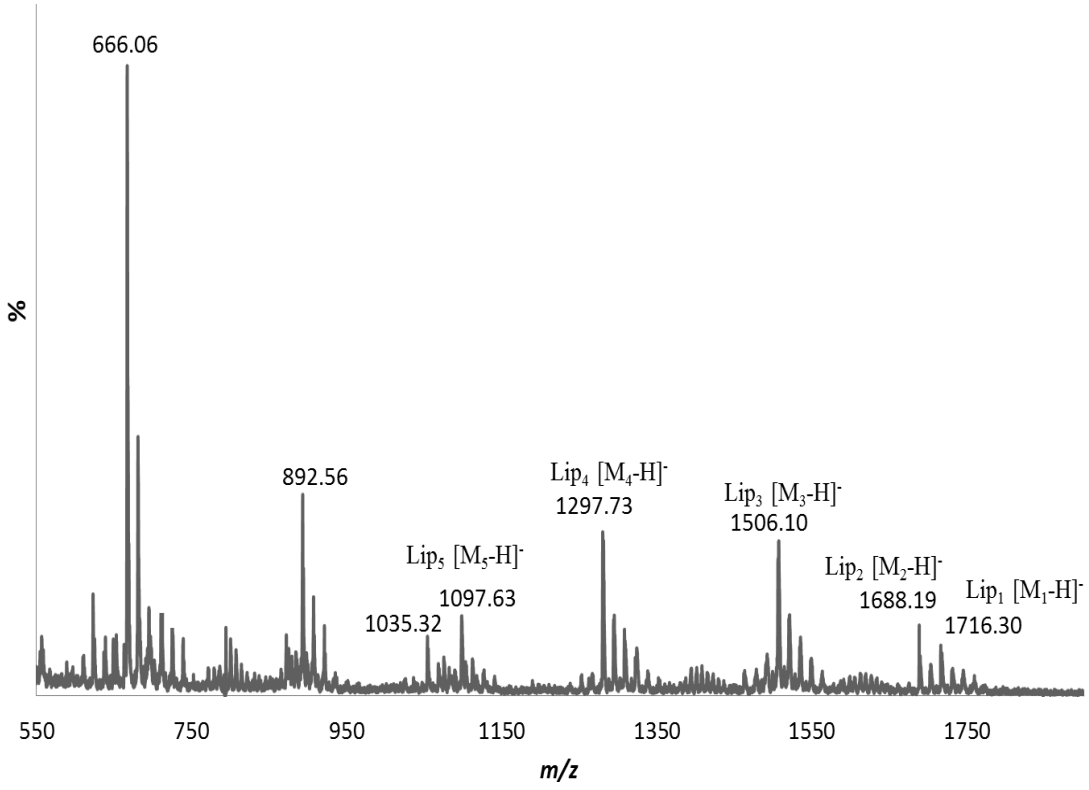

Figure 3.1.1: ESI-QqQ-MS of the native lipid A_n extract from the LPS of A. *liquefaciens* SJ-19a.

Table 3.1.1: Assignments of the deprotonated mono-phosphorylated molecules observed in ESI-QqQ-MS, ESI-FTICR-MS and CID-MALDI-TOF/TOF-MS (- ion mode) of native mixture of lipid A_{1-5} extracted from the LPS of *A. liquefaciens* SJ-19a.

Deprotonated Molecules	Empirical Formula	ESI-QqQ-MS		ESI-FTICR-MS		MALDI-TOF/TOF-MS	
		m/z Observed; Calculated (%)	δ ppm	*m/z* Observed; Calculated (%)	δ ppm	*m/z* Observed; Calculated (%)	δ ppm
$[M_1 -H]^-$	$C_{94}H_{176}N_2O_{22}P$	1716.30; 1716.24 (27.5)	-10	1716.2491;1716.2458 (29.1)	-2	1716.2512; 1716.2458 (16)	3.1
$[M_2 -H]^-$	$C_{92}H_{172}N_2O_{21}P$	1688.19; 1688.21 (30.7)	-11.8	1688.2209;1688.2145 (30.3)	-2	1688.2085; 1688.2145 (18)	-3.5
$[M_3 -H]^-$	$C_{80}H_{150}N_2O_{21}P$	1506.10; 1506.05 (93.5)	33.1	1506.0511; 1506.0574 (95.2)	-4.1	1506.0497; 1506.0574 (97.3)	-5.1
$[M_4 -H]^-$	$C_{66}H_{124}N_2O_{19}P$	1279.73; 1279.85 (97.3)	-15.6	1279.8593; 1279.8541 (96.5)	4	1279.8486; 1279.8541 (100)	-4.2
$[M_5 -H]^-$	$C_{54}H_{102}N_2O_{18}P$	1097.63; 1097.68 (36.4)	-45.5	1097.6930; 1097.6871 (40.8)	5.3	1097.6810; 1097.6871 (35)	-5.5
$[C-(C12:0)ketene-H]^-$	$C_{46}H_{87}NO_{13}P$	-	-	-	-	920.6198; 920.6234 (90.4)	-3.9
$[C-(C14:0)ketene-H]^-$	$C_{46}H_{87}NO_{13}P$	892.56; 892.59 (46.8)	-33.6	892.5975; 892.5921 (50.4)	5.4	-	-
$[C-(C14:0(3-O-C14:0))ketene-H]^-$	$C_{32}H_{61}NO_{11}P$	666.06; 666.43 (100)	-55	666.4396; 666.4390 (97.1)	0.9	-	-

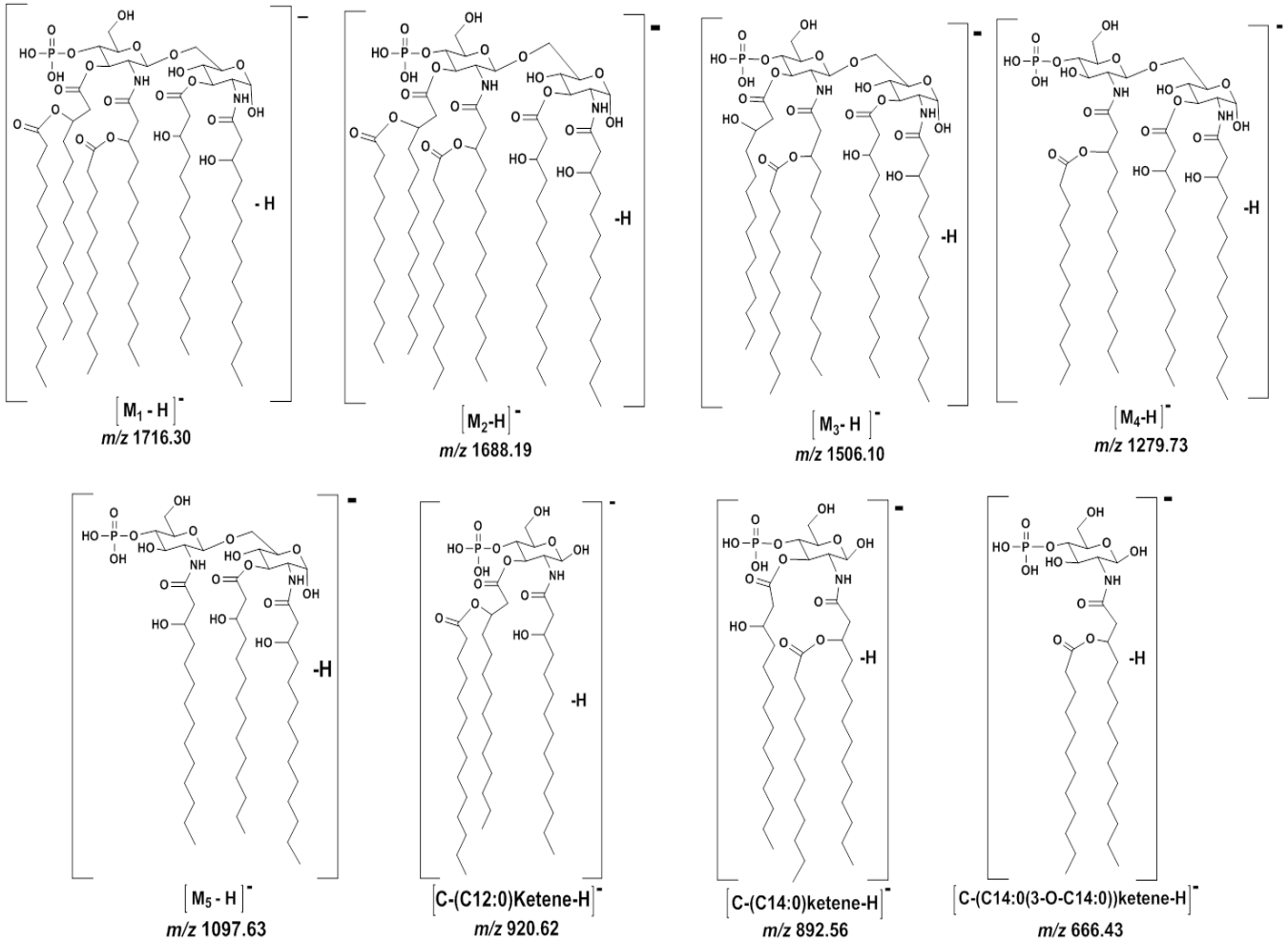

Scheme 3.1.1: Schematic representation of suggested structures of the deprotonated molecules of the lipid As mixture extracted from *A. liquefaciens* SJ-19a.

m/z 1506.10 ($LipA_3$), *m/z* 1279.73 ($LipA_4$), and *m/z* 1097.63 ($LipA_5$) afforded series of distinct and diagnostic product ions. It is well-known that the competitive hydrolysis of the primary and/or secondary fatty esters located on β-D-Glc*p*N-(1→6)-α-D-Glc*p*N disaccharide backbone of lipid A occurs in a step-wise fashion. Apparently, the ester-linked fatty groups at O-3 and O-3′ are more readily hydrolysable than the fatty acyl amide groups. This is due to the greater stability of the fatty acyl amide groups located at N-2 and N-2′, which makes them more difficult to be released (Banoub *et al*., 2010, Kilár *et al*., 2013). In general, it is well known that the CID-MS/MS gas-phase fragmentation routes of lipid A derivatives are usually governed by cleavages arising from the glycosidic bond followed by inter-ring bond cleavages (Domon and Costello., 1988).

The product ion scan of deprotonated molecules at *m/z* 1716.30 $LipA_1$ allowed us to investigate the fatty acyl group distributions that were observed in ESI-QqQ-MS analysis of $LipA_1$, as illustrated in (Figure 3.1.2). Accordingly, the CID-MS/MS of the deprotonated molecules at *m/z* 1716.30 produced the following series of product ions at *m/z* 1516.02, *m/z* 1488.08, *m/z* 1226.92, *m/z* 1053.82, *m/z* 1017.12, and *m/z* 692.39 (Figure 3.1.2, Scheme 3.1.2 and Table 3.1.2) (Lukasiewicz *et al*., 2010). The most abundant product ion at *m/z* 1516.02 was assigned as the $[M_1\text{-(C12:0)acid-H}]^-$ ion, and was formed by the elimination of lauric acid from the branch (Cl4:0(3-*O*-C12:0)) fatty acids (-200 Da), which was attached to the N-2′ position of the lipid A disaccharide backbone. This product ion supports our suggested notion that the branched (Cl4:0(3-*O*-C12:0)) fatty acid group was acylating the N-2′ $LipA_1$. Likewise, the product ion at *m/z* 1488.08 was assigned as the $[M_1\text{-(C14:0)acid-H}]^-$ ion, which was created by elimination of myristic acid form the

branched fatty (C14:0(3-*O*-C14:0)) acid acyl group located at O-3′ (-228 Da). The product ion at *m/z* 1226.92 was formed by the consecutive losses of the branched fatty (C14:0(3-*O*-C14:0)) located on position O-3′ (-454 Da) and two molecules of water. This product ion was assigned as $[M_1$-(C14:0(3-*O*-C14:0))acid-$2H_2O$-H$]^-$ ion (-490 Da). The product ion at *m/z* 1053.62 was formed by elimination of a molecule of the branched fatty (C14:0(3-*O*-C14:0)) ketene (-436 Da) from the O-3′ position and by loss of a 3-hydroxyl myristic ketene (-226 Da) from O-3. This product ion was assigned as $[M_1$-(C14:0(3-*O*-C14:0))ketene-(C14:0(3-OH))ketene-H$]^-$ ion as shown in (Figure 3.1.2, Table 3.1.2, and Scheme 3.1.2). It is noteworthy to mention that the primary product ion at *m/z* 1053.62 will create the secondary product ion at *m/z* 1017.12 by elimination of two molecules of water from the hydroxyl groups located on both the O-3 and O-3′ positions. The product ion at *m/z* 692.39 was formed by the glycosidic cleavages of the β-D-Glc*p*N-(1→6)-α-D-Glc*p*N disaccharide backbone, to afford the reducing D-GlcN-OH species obtained following consecutive losses of myristic (-210 Da) and lauric acid (-200 Da) molecules from the branched fatty acids (C14:0(3-*O*-C14:0)) and (C14:0(3-*O*-C12:0)) respectively located at O-3 and N-2 positions. This product ion was assigned as [C-(C14:0)ketene-(C12:0)acid-H$]^-$ ion. This MS/MS studies supports the suggested structure assignment of the deprotonated molecule ($LipA_1$), and indicates that the H_2PO_3 group is located at the O-4′ position of the non-reducing end of the disaccharide backbone. It also confirms the presence of the two molecules of 3-hydroxyl myristic acids located at the positions O-3, and N-2 of the reducing end of the disaccharide backbone.

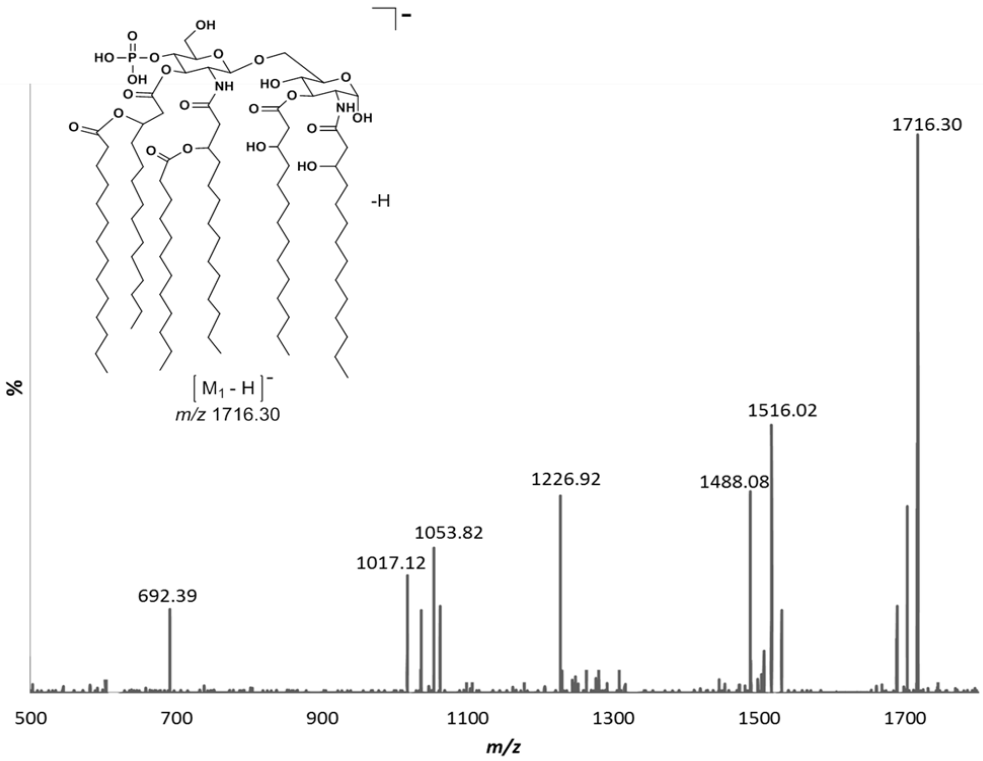

Figure 3.1.2: CID-MS/MS of the precursor deprotonated $[M_1\text{-}H]^-$ molecules at *m/z* 1716.30.⁕

⁕ Please note, that some product ions were not assigned as these were produced by other isobars isolated during the MS/MS analysis.

Table 3.1.2: Assignments of the product ions observed from CID-MS/MS, SORI-CID-MS/MS, and MALDI-CID-TOF/TOF-MS/MS of the precursor deprotonated $[M_1\text{-}H]^-$ molecules at *m/z* 1716.30.

Precursor deprotonated $[M_1\text{-}H]^-$ molecules at *m/z* 1716.30						
Empirical Formula	**ESI-QqQ-MS/MS**		**ESI-FTICR-MS/MS**		**MALDI-TOF/TOF-MS/MS**	
	m/z **Observed; Calculated (%)**	**δ ppm**	***m/z*** **Observed; Calculated (%)**	**δ ppm**	***m/z*** **Observed; Calculated (%)**	**δ ppm**
$C_{92}H_{172}N_2O_{21}P$	-	-	-	-	1688.2145; 1688.2265 (18)	7.1
$C_{82}H_{153}N_2O_{20}P$	1516.07; 1516.02 (50)	-32.9	-	-	-	-
$C_{80}H_{148}N_2O_{20}P$	1488.04; 1488.08 (38.8)	33.6	1488.0465; 1488.0469 (28)	-3.1	1488.0465; 1488.0512 (55)	3.2
$C_{66}H_{119}N_2O_{16}P$	1226.88; 1226.92 (38.9)	32.6	-	-	1085.5602; 1085.5630 (19.6)	2.5
$C_{66}H_{120}N_2O_{17}P$	-	-	243.8403; 1243.8399 (75.8)	-0.3	1243.8430; 1243.8398 (19.7)	-2.5
$C_{52}H_{98}N_2O_{17}P$	1053.76; 1053.82 (25.9)	56.9	-	-	-	-
$C_{52}H_{94}N_2O_{15}P$	1017.63; 1017.12 (21)	-50	-	-	-	-
$C_{52}H_{96}N_2O_{16}P$	-	-	1035.6581; 1035.6975 (35.0)	3.8	-	-
$C_{43}H_{63}NO_{11}P$	692.42; 692.39 (19.9)	-43.3	-	-	-	-

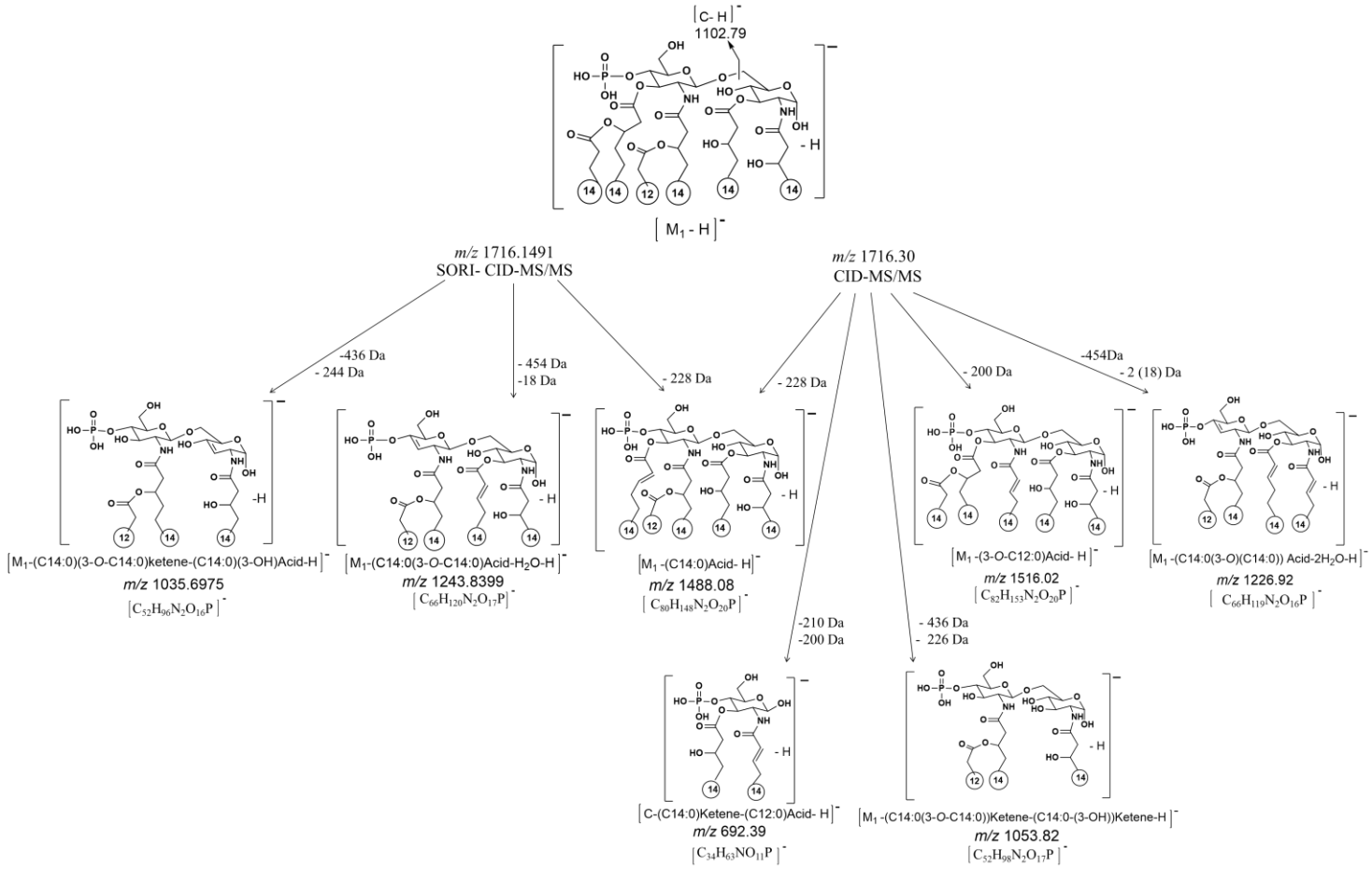

Scheme 3.1.2: Proposed fragmentation pathways obtained by CID-QqQ-MS/MS and SORI-CID-FTICR-MS/MS of the precursor deprotonated $[M_1–H]^-$ molecules at *m/z* 1716.30.

Whereas the branched (C14:0(3-*O*-C14:0)) and (C14:0(3-*O*-C12:0)) fatty acids were located on O-3′ and N-2′ positions of the non-reducing end of the β-D-Glc*p*N-(1→6)-α-D-Glc*p*N disaccharide backbone of this lipid A_1 (El-Aneed *et al*., 2006, Lukasiewicz *et al*., 2010, John *et al*., 2014, and Brodbelt *et al*., 2014).

The product ion scan of the deprotonated mono-phosphorylated $LipA_2$ molecules at *m/z* 1688.19 afforded the product ions at *m/z* 1488.10, *m/z* 1444.02, *m/z* 1305.82, *m/z* 1243.79, *m/z* 1017.59, and *m/z* 871.46 (Figure 3.1.3, Table 3.1.3 and Scheme 3.1.3) (El-Aneed *et al*., 2006, and Lukasiewicz *et al*., 2010). The product ion at *m/z* 1488.01 was assigned as the $[M_2$-(C12:0)acid-H$]^-$ ion, which was created by elimination of the lauric acid form the branched fatty (C14:0(3-*O*-C12:0)) acid located either the O-3′ or N-2′ position (-200 Da). The product ion at *m/z* 1444.02 was assigned as $[M_2$-(C14:0(3-OH))acid-H$]^-$ ion. It was created by the loss of a 3-hydroxyl myristic acid (-244 Da) which was located at O-3 position of the $LipA_2$ precursor ion. The product ion at *m/z* 1305.82 was assigned as the $[M_2$-(C12:0)acid-(C12:0)ketene-H$]^-$ ion. It was generated by both eliminations of lauric acid (-200 Da) and lauryl ketene (-182 Da) from the precursor ion at *m/z* 1688.19; these two losses originated from both the branched (C14:0(3-*O*- C12:0)) and (C14:0(3-*O*-C12:0)) fatty acyl groups located respectively O-3′ and N-2′ of the non-reducing of the disaccharide backbone of lipid A (Figure 3.1.1). Similarly, the product ion at *m/z* 1243.79 was assigned as $[M_2$-(C14:0(3-*O*-C12:0))acid-H_2O-H$]^-$ ion, and it was formed by consecutive losses of the branched fatty (C14:0(3-*O*-C12:0)) acid (-426 Da) located on position O-3′ and a molecule of water from the precursor ion at *m/z* 1688.19.

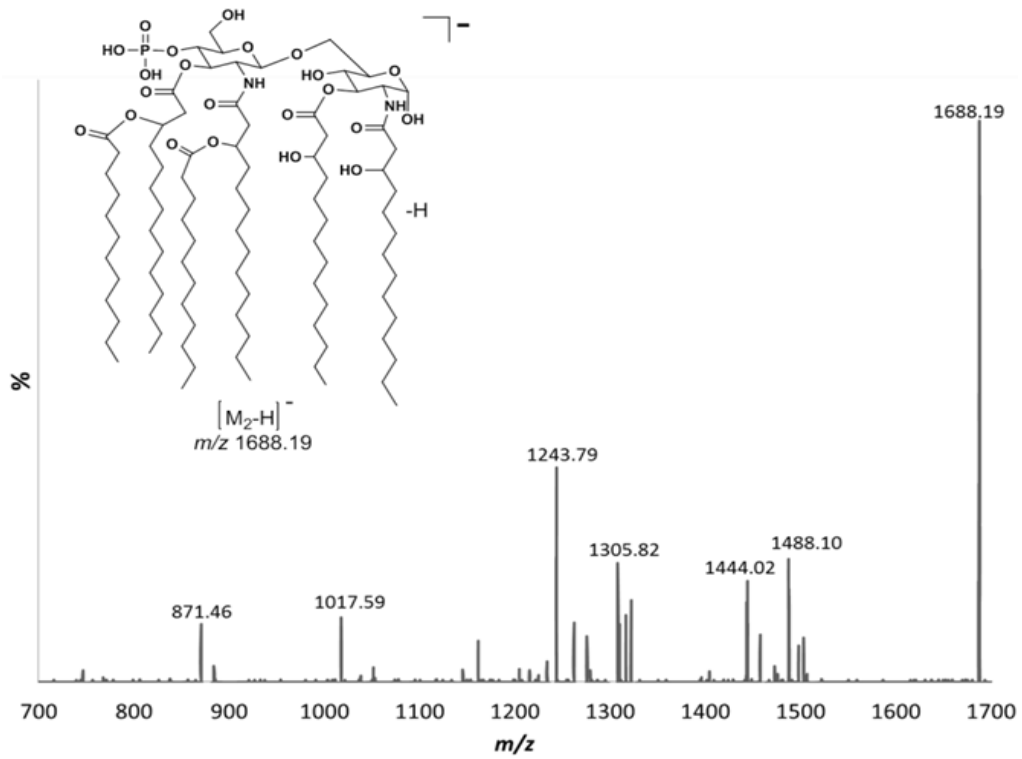

Figure 3.1.3: CID-MS/MS of the precursor deprotonated $[M_2\text{-}H]^-$ molecules at *m/z* 1688.19.*

* Please note, that some product ions were not assigned as these were produced by other isobars isolated during the MS/MS analysis.

Table 3.1.3: Assignments of the product ions observed from CID-MS/MS, SORI-CID-MS/MS, and MALDI-CID-TOF/TOF-MS/MS of the precursor ion $[M_2\text{-}H]^-$ at *m/z* 1688.19.

Precursor deprotonated $[M_2\text{-}H]^-$ molecules at *m/z* 1688.19						
Empirical Formula	**ESI-QqQ-MS/MS**		**ESI-FTICR-MS/MS**		**MALDI-TOF/TOF-MS/MS**	
	m/z **Observed; Calculated (%)**	**δ ppm**	***m/z*** **Observed; Calculated (%)**	**δ ppm**	***m/z*** **Observed; Calculated (%)**	**δ ppm**
$C_{80}H_{148}N_2O_{20}P$	1488.03; 1488.10 (24.9)	47	1488.0379; 1488.0379 (32.0)	0.6	1488.0379; 1488.0324 (45.3)	-3.6
$C_{78}H_{145}N_2O_{19}P$	1444.97; 1444.02 (21.9)	-34.6	-	-	1444.9815; 1444.9743 (20.1)	-4.9
$C_{68}H_{126}N_2O_{19}P$	1305.88; 1305.82 (23.9)	-45.9	-	-	-	-
$C_{66}H_{120}N_2O_{17}P$	1243.84; 1243.79 (39.6)	-32.1	1243.8430; 1243.8851 (52.8)	3.6	1243.8430; 1243.8512 (26)	5.7
$C_{52}H_{96}N_2O_{16}P$	-	-	1035.6681; 1035.6599 (15.2)	-7.5	-	-
$C_{52}H_{94}N_2O_{15}P$	1017.64; 1017.59 (19.5)	-39.3	-	-	-	-
$C_{40}H_{76}N_2O_{16}P$	871.94; 871.46 (17.2)	-34.4	-	-	-	-

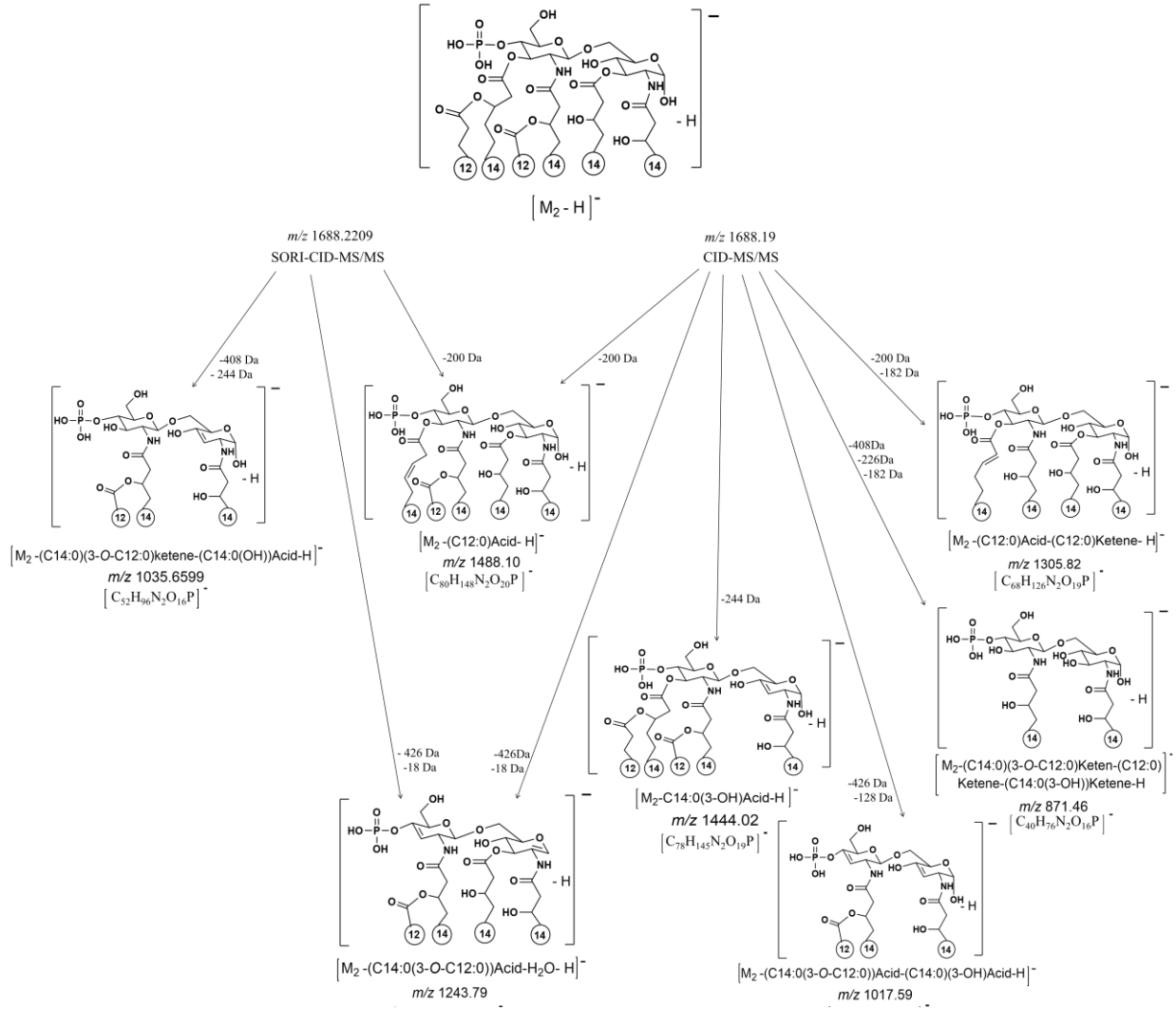

Scheme 3.1.3: Proposed fragmentation pathways obtained by CID-QqQ-MS/MS and SORI-CID-FTICR MS/MS of the precursor monophosphorylated $LipA_2$ $[M_2–H]^-$ ion at *m/z* 1688.19.

The product ion at *m/z* 1017.59 was assigned as [M_2-(C14:0(3-*O*-12:0))acid-(C14:0(3-OH))acid-H]$^-$ ion. It was formed by successive elimination of the branched fatty (C14:0(3-*O*-C12:0)) acid form the O-3′ position (-426 Da), and a 3-hydroxyl myristic acid (-244 Da), which is located at O-3 of the $LipA_2$ precursor ion. As well, the product ion of at *m/z* 871.46, assigned as [M_2-(C14:0(3-*O*-C12:0))ketene-(C12:0)ketene-(C14:0(3-OH))ketene-H]$^-$ ion. It was formed by the consecutive losses of the branched fatty (C14:0(3-*O*-C12:0)) ketene (-408 Da) located at the O-3′ position, lauryl ketene molecule (-182 Da) from the branched fatty acids (C14:0(3-*O*-C12:0)) located on the N-2′ position. The concomitant loss of 3-hydroxyl myristic ketene molecule (-226 Da) located at the O-3 position of the β-D-GlcpN-(1→6)-α-D-GlcpN disaccharide backbone of this $LipA_2$ precursor ion. The structure of this product ion confirms the presence of the branched (C14:0(3-*O*-C12:0)) fatty acid ester group on the N-2′ position (El-Aneed *et al*., 2006, and Lukasiewicz *et al*., 2010).

The product ion scan of the deprotonated $LipA_3$ molecules at *m/z* 1506.10 gave the series of product ion at *m/z* 1488.01, *m/z* 1461.95, *m/z* 1415.98, *m/z* 1305.85, and *m/z* 666.39 (Figure 3.1.4, Table 3.1.4 and Scheme 3.1.4). The product ion at *m/z* 1488.01 was obtained by the loss of a molecule of water from the precursor ion. The product ion at *m/z* 1461.95 was formed by the elimination of a molecule of propane (-44 Da), which most probably arose from the fatty acid chain located on O-3′. This product ion was assigned as [M_3-C_3H_8-H]$^-$. Similarly, the product ion at *m/z* 1415.95 was assigned as the [M_3-C_5H_{12}-H_2O-H]$^-$ ion, which was produced by the loss of pentane (-72 Da), most probably from the fatty acid of $LipA_3$ located at the N-2′ and a molecule of water from the precursor ion.

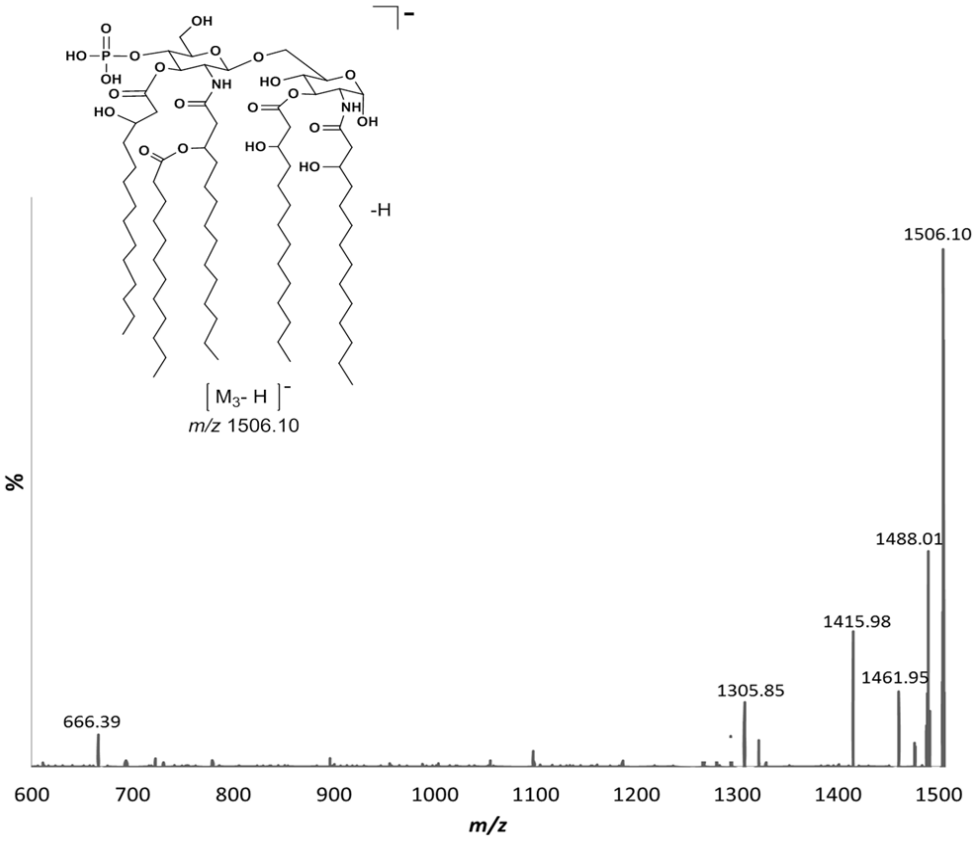

Figure 3.1.4: CID-MS/MS of the precursor deprotonated $[M_3\text{-}H]^-$ molecules at *m/z* 1506.10.*

* Please note, that some product ions were not assigned as these were produced by other isobars isolated during the MS/MS analysis.

Table 3.1.4: Assignments of the product ions observed from CID-MS/MS, SORI-CID-MS/MS, and MALDI-CID-TOF/TOF-MS/MS of the precursor ion $[M_3\text{-}H]^-$ at *m/z* 1506.1

Precursor deportonated $[M_3\text{-}H]^-$ molecules at *m/z* 1506.10						
Empirical Formula	**ESI-QqQ-MS/MS**		**ESI-FTICR-MS/MS**		**MALDI-TOF/TOF-MS/MS**	
	m/z **Observed; Calculated (%)**	**δ ppm**	***m/z*** **Observed; Calculated (%)**	**δ ppm**	***m/z*** **Observed; Calculated (%)**	**δ ppm**
$C_{80}H_{147}N_2O_{20}P$	1488.03; 1488.01 (28)	20.1	-	-	-	-
$C_{77}H_{142}N_2O_{21}P$	1461.98; 1461.95 (16.8)	20.5	-	-	-	-
$C_{75}H_{137}N_2O_{20}P$	1415.95; 1415.98 (30)	21.2	-	-	-	-
$C_{68}H_{126}N_2O_{19}P$	1305.88; 1307.85 (20)	-22.9	-	-	-	-
$C_{66}H_{123}N_2O_{18}P$	-	-	1261.8436; 1261.8349 (91.1)	-6.8	1261.8436; 1261.8510 (120)	5.8
$C_{66}H_{120}N_2O_{17}P$	1017.64; 1017.59 (19.5)	-39.3	-	-	1243.8430; 1243.8398 (45)	-2.5
$C_{52}H_{96}N_2O_{16}P$	-	-	-	-	1035.6681; 1035.6597 (55)	-8.1
$C_{32}H_{61}NO_{11}P$	666.40; 666.39 (15)	-45.0	-	-	-	-

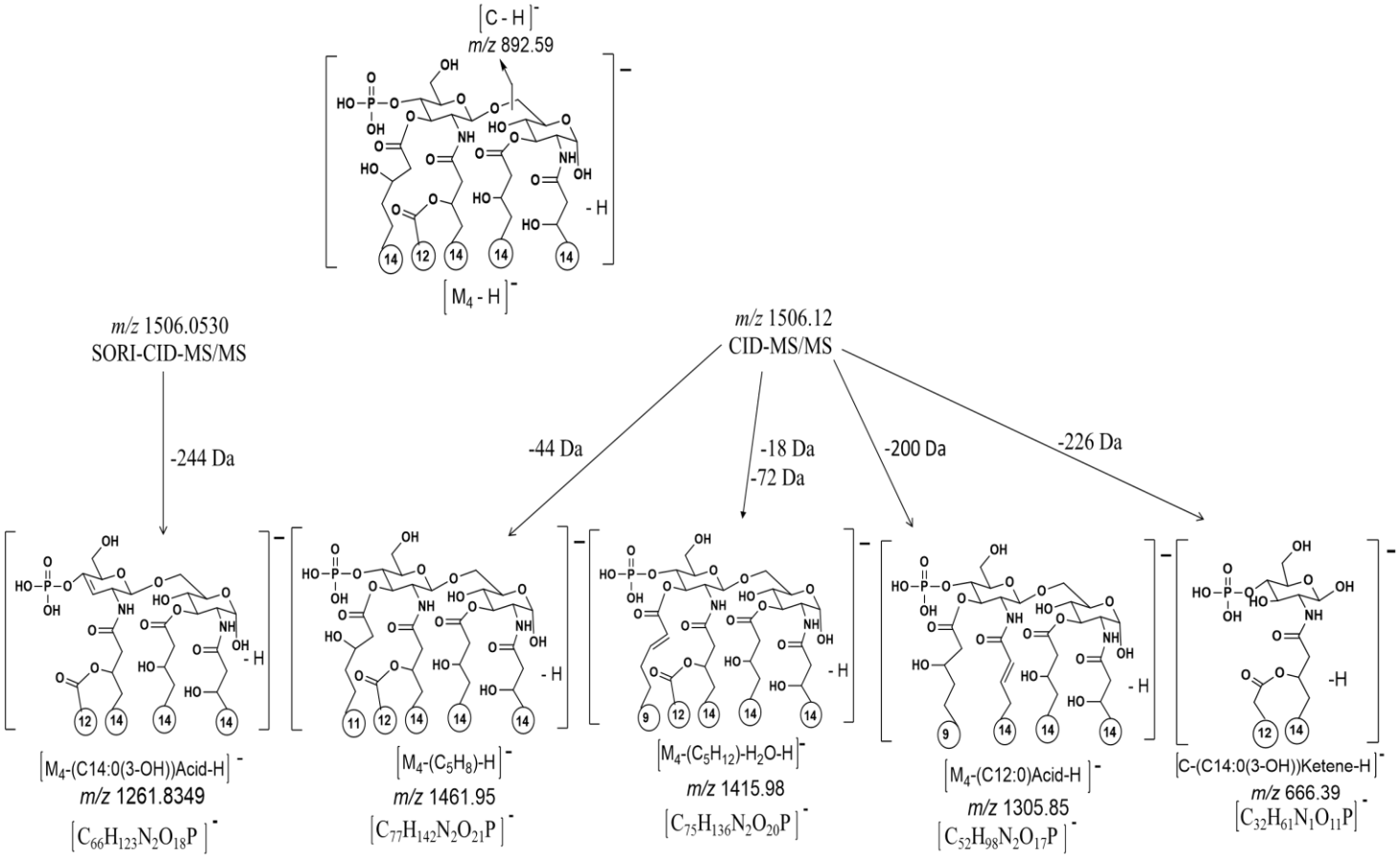

Scheme 3.1.4: Proposed fragmentation pathways obtained by CID-QqQ-MS/MS and SORI-CID- FTICR MS/MS of the precursor monophosphorylated $LipA_3$ $[M_3–H]^-$ ion at *m/z* 1506.10.

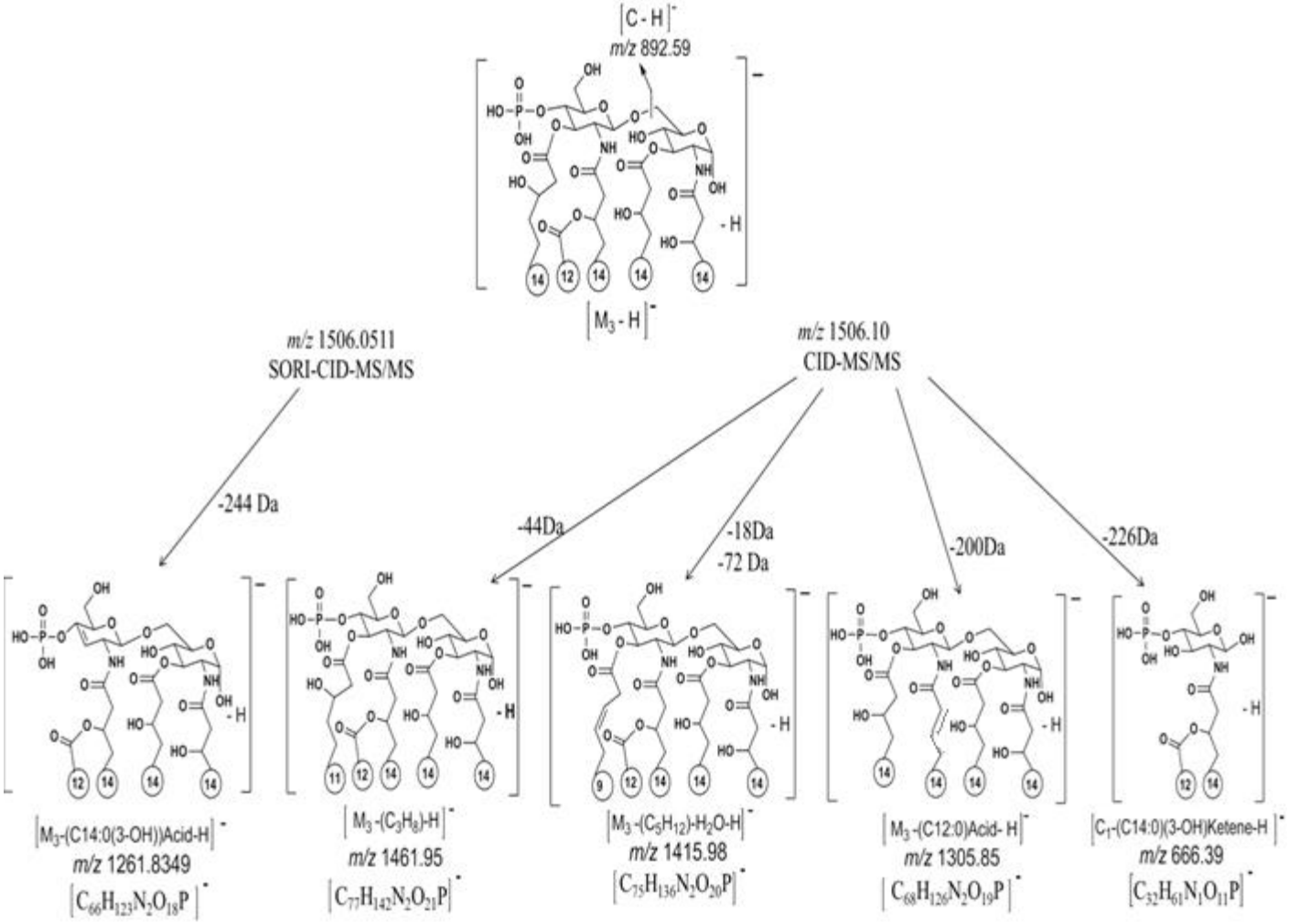
[C - H]⁻
m/z 892.59
[M3 - H]⁻
m/z 1506.0511
SORI-CID-MS/MS
m/z 1506.10
CID-MS/MS
-244 Da
-44Da
-18Da
-72 Da
-200Da
-226Da
[M3-(C14:0(3-OH))Acid-H]⁻
m/z 1261.8349
[C66H123N2O18P]⁻
[M3 -(C3H8)-H]⁻
m/z 1461.95
[C77H142N2O21P]⁻
[M3 -(C5H12)-H2O-H]⁻
m/z 1415.98
[C75H136N2O20P]⁻
[M3 -(C12:0)Acid- H]⁻
m/z 1305.85
[C68H126N2O19P]⁻
[C1-(C14:0)(3-OH)Ketene-H]⁻
m/z 666.39
[C32H61N1O11P]⁻

The product ion at *m/z* 1305.85 was assigned as the $[M_3\text{-(C12:0)acid-H}]^-$ ion and was formed by the loss a molecule of lauric acid (-200 Da) from the branched (C14:0(3-*O*-C12:0)) fatty acyl group located at the N-2′ position of $LipA_3$ (El-Aneed *et al*., 2006, and Lukasiewicz *et al*., 2010).The last product ion at *m/z* 666.39 was produced from the C-fragmentation routes described by Domon and Costello which was formed by glycosidic cleavages of the β-D-(l→6)-GlcN disaccharide, followed by the loss of a 3-hydroxy-myristic ketene molecule (-226 Da) from the O-3 position of the D-GlcN residue (Domon and Costello, 1988). This product ion was assigned as the $[\text{C-(C14:0(3-}O\text{-C14:0))ketene-H}]^-$ ion (Figure 3.4, Table 3.4 and Scheme 3.4). Please note that the $[\text{C-(C14:0(3-}O\text{-C14:0))ketene-H}]^-$ product ion contains a phosphate group located on O-4 (Domon and Costello., 1988, El-Aneed *et al*., 2006, Banoub *et al*., 2010, and Kilár *et al*., 2013). Accordingly, this finding strongly confirms that the suggested structures for $lipA_2$ contains an H_2PO_3 group located at the non-reducing end of the $LipA_3$ at O-4′, and it also confirms the location of the branched lauric acid at N-2′.

The product ion scan of the deprotonated mono-phosphorylated $LipA_4$ molecules $[M_4\text{-H}]^-$ (base peak) at *m/z* 1279.73 gave a series of product ions at *m/z* 1261.79, *m/z* 1035.60, and *m/z* 791.50 (Figure 3.1.5, Table 3.1.5 and Scheme 3.1.5). The product ion at *m/z* 1261.79 was formed by the loss of a molecule of water from the precursor ion (-18 Da). The product ion at *m/z* 1035.60 was assigned as the $[M_4\text{-(C14:0(3-OH))acid-H}]^-$ ion, which was created by the eliminating of 3-hydroxy-myristic acid (C14:0(3-OH)) (-244 Da) located at the position O-3 of the reducing GlcN end. The last product ion at *m/z* 791.50 was assigned as the $[M_4\text{-(C14:0(3-OH))ketene-(C12:0))ketene-HPO}_3\text{-H}]^-$ ion.

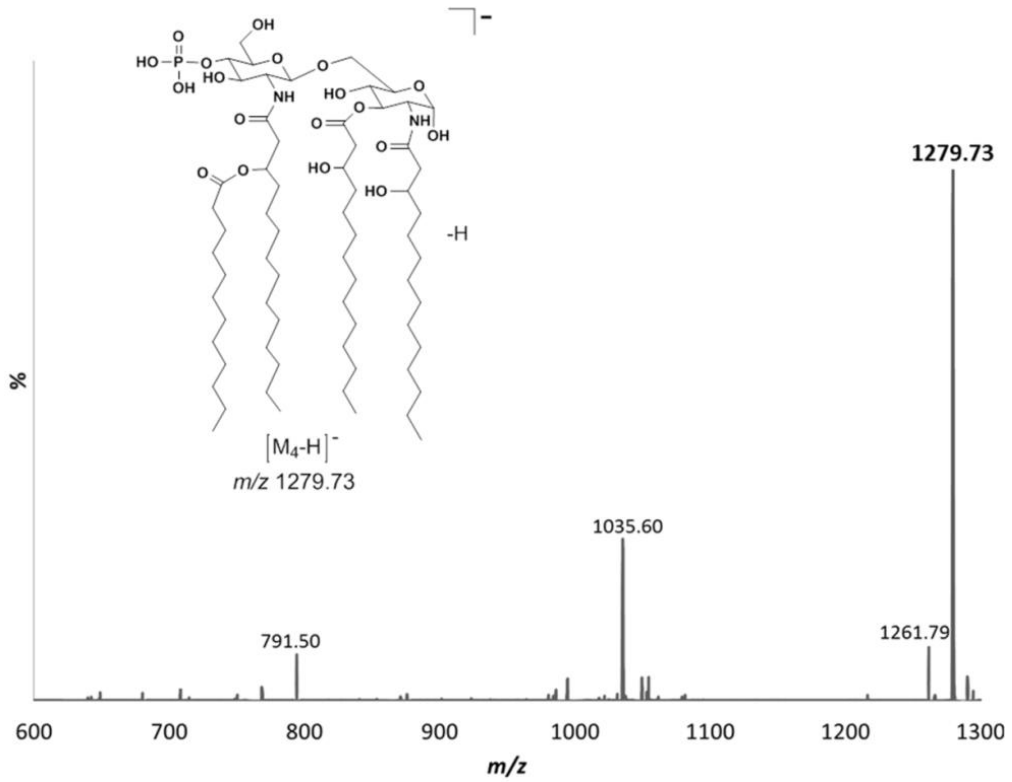

Figure 3.1.5: CID-MS/MS of the precursor deprotonate $[M_4\text{-}H]^-$ molecules at *m/z* 1279.73.*

* Please note, that some product ions were not assigned as these were produced by other isobars isolated during the MS/MS analysis.

Table 3.1.5: Assignments of the product ions observed from CID-MS/MS, SORI-CID-MS/MS, and MALDI-CID-TOF/TOF-MS/MS of the precursor ion $[M_4\text{-}H]^-$ at *m/z* 1297.73.

Precursor deprotonated $[M_4\text{-}H]^-$ molecules at *m/z* 1279.73						
Empirical Formula	**ESI-QqQ-MS/MS**		**ESI-FTICR-MS/MS**		**MALDI-TOF/TOF-MS/MS**	
	m/z **Observed; Calculated (%)**	**δ ppm**	***m/z*** **Observed; Calculated (%)**	**δ ppm**	***m/z*** **Observed; Calculated (%)**	**δ ppm**
$C_{66}H_{123}N_2O_{18}P$	**1261.84; 1261.79 (19.1)**	**-39.6**	**-**	**-**	**1261.8436; 1261.8511 (28)**	**-1.3**
$C_{54}H_{100}N_2O_{17}P$	**-**	**-**	**-**	**-**	**1079.6765; 1079.6732 (25)**	**-3**
$C_{68}H_{126}N_2O_{19}P$	**1035.66; 1035.60 (39.4)**	**-57.9**	**1035.6681; 1035.6622 (91.0)**	**-1.8**	**1035.6681; 1035.6721 (105)**	**3.8**
$C_{52}H_{94}N_2O_{15}P$	**-**	**-**	**-**	**-**	**1017.6397; 1017.6343 (46.5)**	**-5.3**
$C_{40}H_{75}N_2O_{13}$	**791.53; 791.50 (19.4)**	**-37.8**	**-**	**-**	**-**	**-**

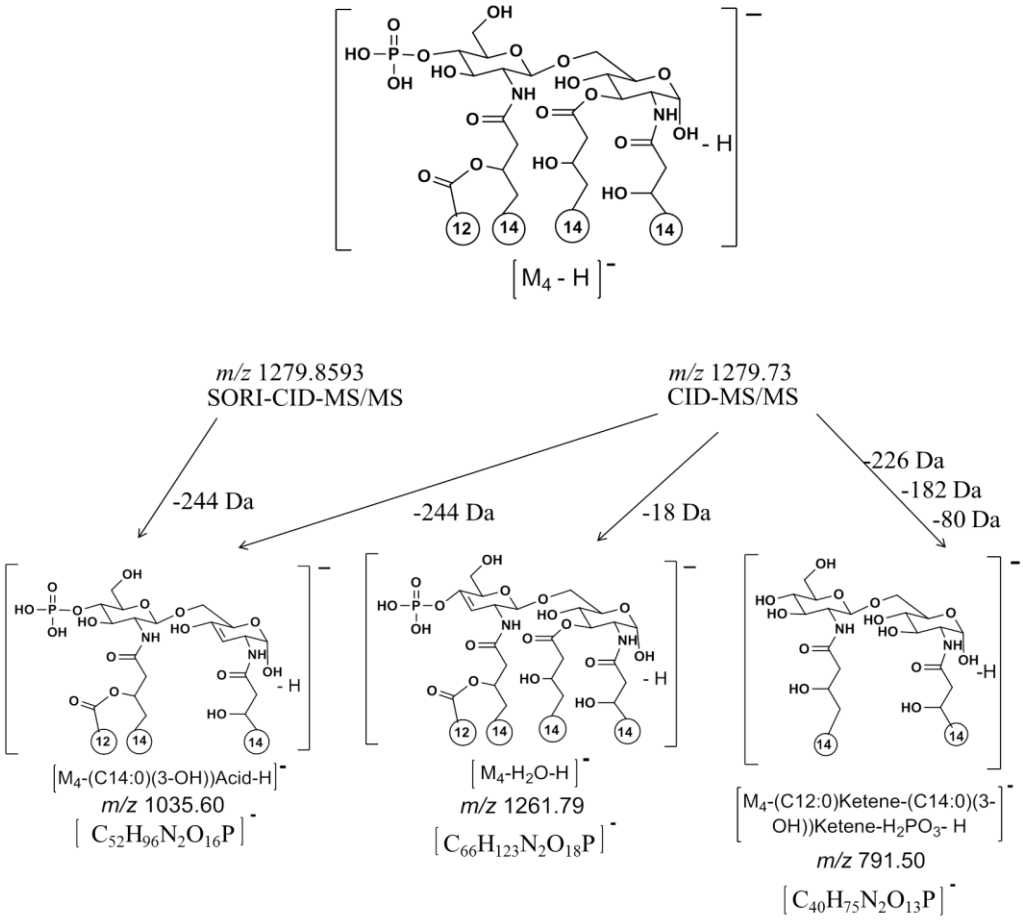

Scheme 3.1.5: Proposed fragmentation pathways obtained by CID-QqQ-MS/MS and SORI-CID-FTICR MS/MS of the precursor monophosphorylated $LipA_4$ $[M_4–H]^-$ ion at *m/z* 1279.73.

It was created by the consecutive losses of the lauryl ketene (-182 Da) from the branched fatty (C14:0(3-*O*-C12:0)) acid (-182 Da) located on N-2′, followed by 3-hydroxy-myristyl ketene (-226 Da) located at the position O-3 and finally by elimination of the neutral HPO_3 (-80 Da) moiety.

These findings support that our suggested $LipA_4$ structure contains a H_2PO_3 group at the O-4′ position of the non-reducing D-GlcN residue, and that the 3-hydroxy-non reducing end myristic ester groups are located on the N-2 and N-2′ of β-D-Glc*p*N-(1→6)-α-D-Glc*p*N disaccharide backbone of lipid A_4 (El-Aneed *et al*., 2006, Lukasiewicz *et al*., 2010, John *et al*., 2014, and Brodbelt *et al*., 2014).

The product ion scan of $LipA_5$ at *m/z* 1097.63 gave series of product ions at *m/z* 853.48, *m/z* 691.49, and *m/z* 581.36 (Figure 3.1.6, Table 3.1.6 and Scheme 3.1.6). The product ion at *m/z* 853.48 was assigned as the $[M_5\text{-(C14:0(3-OH))acid-H}]^-$ ion. It was created by the elimination of 3-hydroxy-myristic acid (C14:0(3-OH)) (-244Da) located at the position O-3 of the reducing GlcN end of the $lipidA_5$ disaccharide. The product ion at *m/z* 691.49 was assigned as the $[M_5\text{-(C14:0(3-OH))acid-}(C_2H_4)\text{-}H_2PO_4\text{-}2H_2O\text{-H}]^-$ ion. It was created by the consecutive loss of the 3-hydroxy-myristic acid (C14:0(3-OH)) (-244 Da) located at the position O-3, a molecule of C_2H_4 (-28 Da) as part of the fatty acid chain located at N-2′ and H_3PO_4 (-98 Da) released from the O-4′ position of the D-GlcN non-reducing end of $LipA_5$. The last product ion at *m/z* 581.36 was assigned as the $[M_5\text{-(C14:0(3-OH))acid-}(C_{10}H_{18})\text{-}H_2PO_4\text{-}H_2O\text{-H}]^-$ ion. It was created by the consecutive eliminations of the 3-hydroxy-myristic acid (C14:0(3-OH)) (-244 Da) located at the position O-3, of $nC_{10}H_{18}$ (-138 Da) as part of the fatty acid chain located at N-2′, and

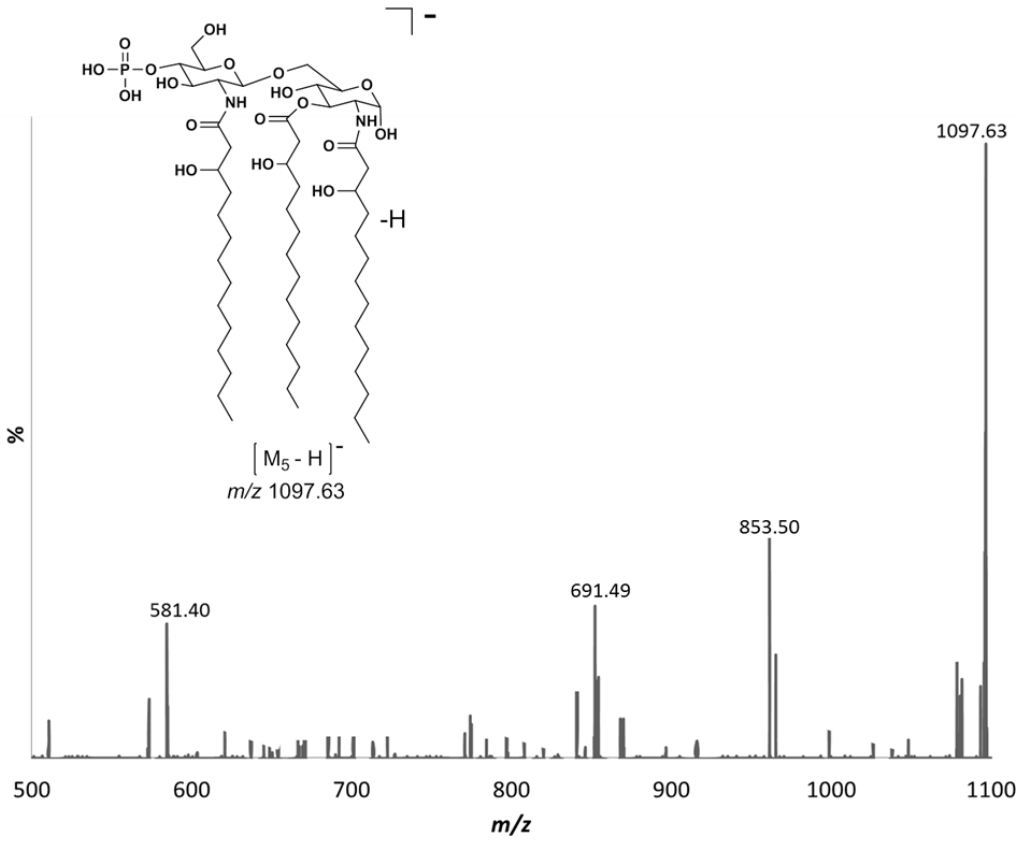

Figure 3.1.6: CID-MS/MS of the precursor deprotonated $[M_5\text{-}H]^-$ molecules at *m/z* 1097.63.⁕

⁕ Please note, that some product ions were not assigned as these were produced by other isobars isolated during the MS/MS analysis.

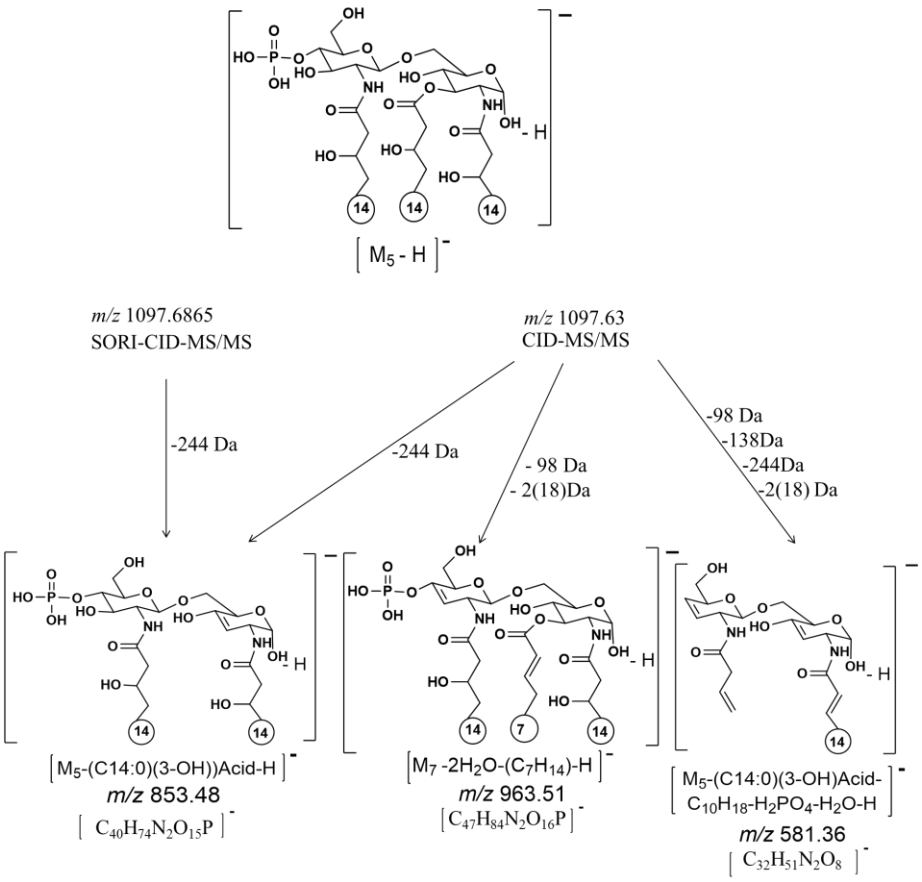

Scheme 3.1.6: Proposed fragmentation pathways obtained by CID-QqQ-MS/MS and SORI-CID-FTICR MS/MS of the precursor monophosphorylated $LipA_5$ $[M_5–H]^-$ ion at *m/z* 1097.63.

Table 3.1.6: Assignments of the product ions observed from CID-MS/MS, SORI-CID-MS/MS, and MALDI-CID-TOF/TOF-MS/MS of the precursor ion $[M_5\text{-}H]^-$ at *m/z* 1097.63.

Precursor deprotonated $[M_5\text{-}H]^-$ molecules at *m/z* 1097.63						
Empirical Formula	**ESI-QqQ-MS/MS**		**ESI-FTICR-MS/MS**		**MALDI-TOF/TOF-MS/MS**	
	m/z **Observed; Calculated (%)**	**δ ppm**	***m/z*** **Observed; Calculated (%)**	**δ ppm**	***m/z*** **Observed; Calculated (%)**	**δ ppm**
$C_{40}H_{74}N_2O_{15}P$	853.48; 853.50 (29.7)	23	853.4832; 853.4897 (107)	7.0	853.4832; 853.4843 (21)	1.2
$C_{38}H_{64}N_2O_9$	691.45; 691.49 (22.7)	57	-	-	-	-
$C_{32}H_{51}N_2O_8$	581.34; 581.36 (30.4)	3.4	-	-	-	-
$C_{22}H_{42}NO_{11}P$	-	-	-	-	527.2495; 527.2514 (12.2)	3.6

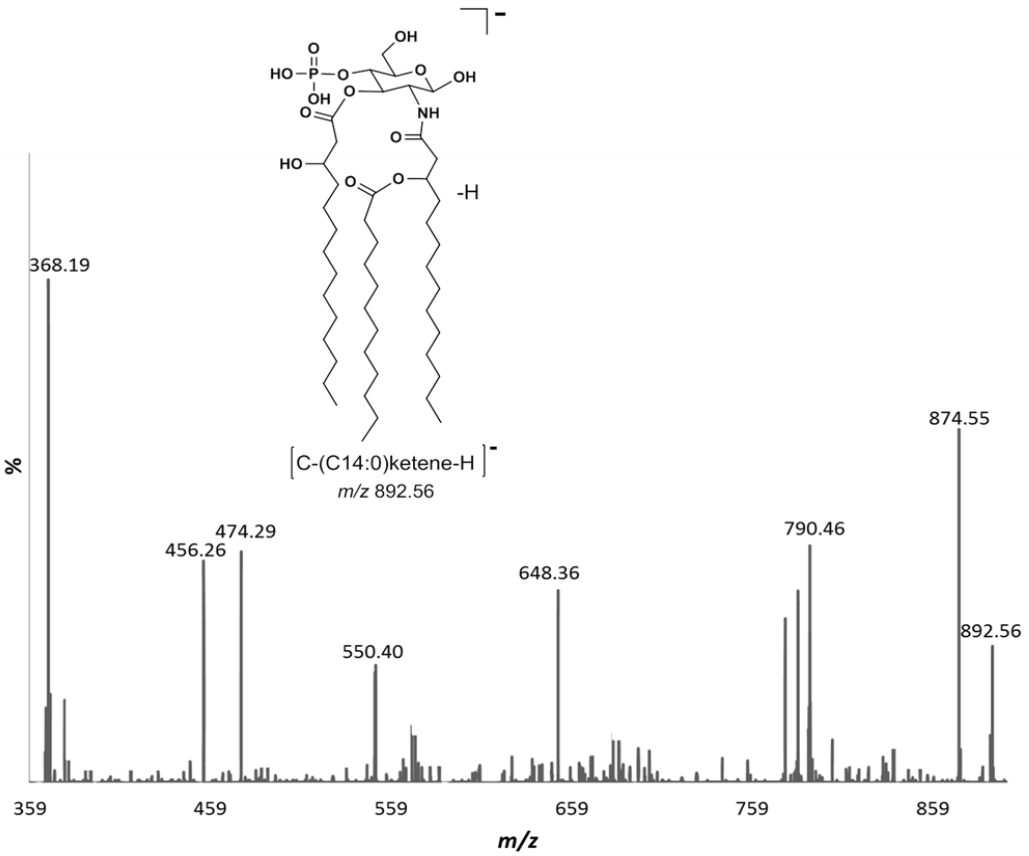

Figure 3.1.7: CID-MS/MS of the precursor deprotonated [C-(C14:0)ketene-H]$^-$ molecules at *m/z* 892.56.*

* Please note, that some product ions were not assigned as these were produced by other isobars isolated during the MS/MS analysis.

Table 3.1.7: Assignments of the product ions observed from the CID-MS/MS and SORI-CID-MS/MS analysis of the precursor deprotonated [C-(C14:0)ketene-H]$^-$ molecules at *m/z* 892.56.

	Precursor deprotonated [C-(C14:0)ketene-H]$^-$ molecules at *m/z* 892.56			
	CID-QqQ-MS/MS		SORI-FTICR-MS/MS	
Empirical formula	Product ion *m/z* Calculated; Observed (%)	δ ppm	Product ion *m/z* Calculated; Observed (%)	δ ppm
$C_{46}H_{85}NO_{12}P$	874.58; 874.55 (60.4)	-34.3	-	-
$C_{40}H_{73}NO_{12}P$	790.49; 790.46 (20.9)	-37.9	-	-
$C_{32}H_{59}NO_{10}P$	648.38; 648.36 (48.7)	30.8	648.3955; 648.3931 (84.0)	-3.7
$C_{32}H_{58}NO_6$	550.43; 550.40 (20.4)	-54.5	-	-
$C_{24}H_{44}NO_8$	474.30; 474.29 (40.9)	21	-	-
$C_{20}H_{38}NO_9P$	-	-	466.2284; 466.2275 (16.7)	-1.9
$C_{24}H_{42}NO_7$	456.28; 456.26 (40.1)	-43.9	-	-
$C_{20}H_{36}NO_8P$	-	-	448.2179; 448.2165 (14.4)	-3.1
$C_{20}H_{34}NO_5$	368.21; 368.19 (79.9)	-54.1	-	-

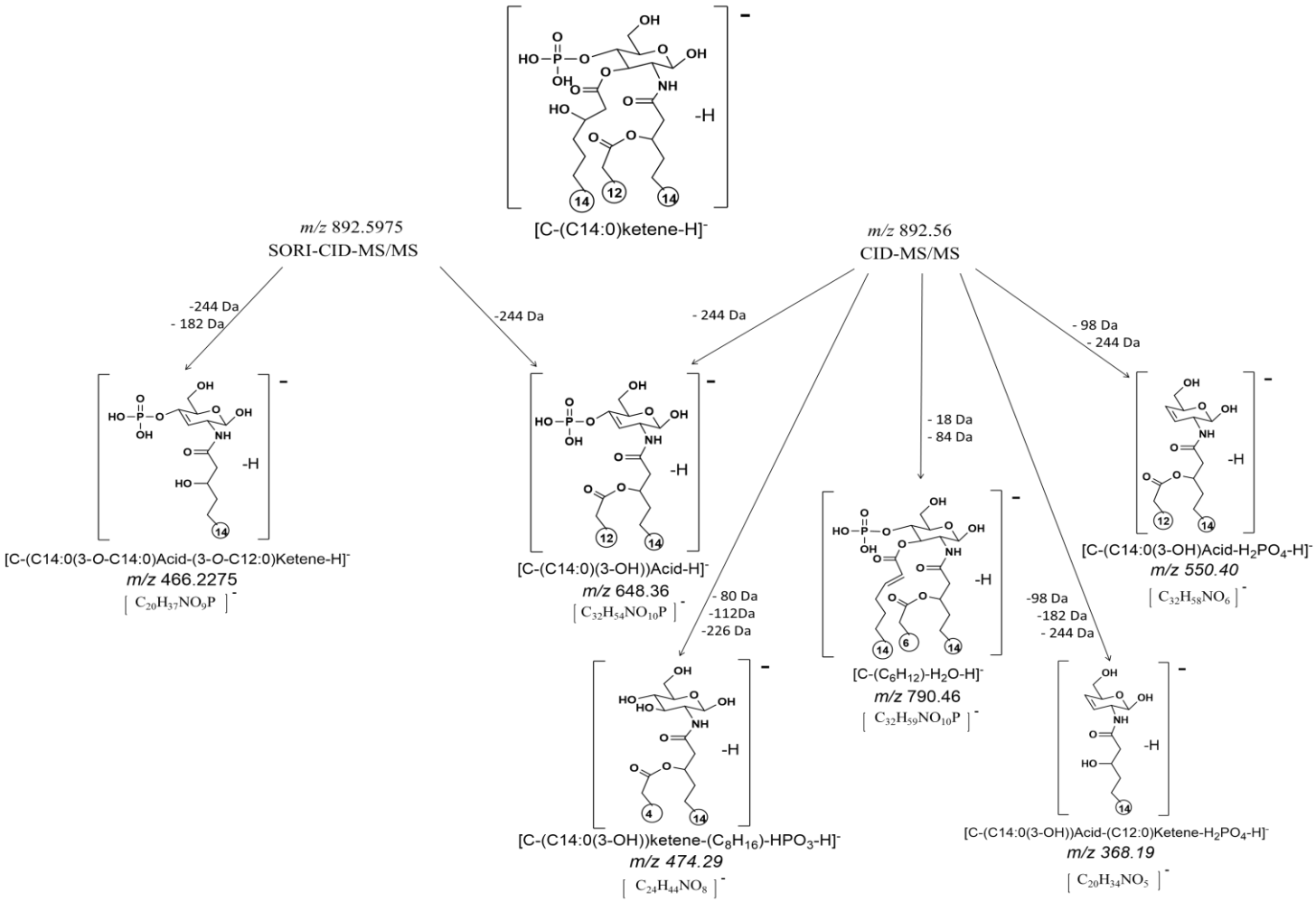

Scheme 3.1.7: Proposed fragmentation pathways obtained by CID-QqQ-MS/MS and SORI-CID- FTICR MS/MS analyses of the precursor deprotonated [C-(C14:0)ketene-H]$^-$ molecules at *m/z* 892.56.

H_3PO_4 (-98 Da) and two molecules of water (-36 Da). Lastly, we also investigated the nature of the two deprotonated molecules at *m/z* 892.56, and *m/z* 666.06 observed in the ESI-MS of this lipid A_n mixture. We have tentatively assigned these deprotonated molecules as being created by the $[C\text{-}H]^-$ ion series, whose presence are probably an indication of the incomplete biosynthesis of the lipid $A_{1\text{-}5}$ series of the LPS *A. liquefaciens* SJ-19a (Please understand, that these deprotonated molecules were named Fragment ions, to respect only the Domon and Costello nomenclature) (Domono and Cosetello 1988).

For simplification, we have tied these deprotonated molecules to the $[M\text{-}H_{1\text{-}5}]^-$ molecules and adopted a similar nomenclature. Hence, the product ion scan of the deprotonated $[C\text{-}(C14{:}0)\text{ketene-}H]^-$ molecule at *m/z* 892.56 gave a series of product ions at *m/z* 874.55, *m/z* 790.46, *m/z* 648.36, *m/z* 550.40, *m/z* 474.29, *m/z* 456.26, and *m/z* 368.19 (Figure 3.1.7, Scheme 3.1.7, and Table 3.1.7). The product ion at *m/z* 874.55 was created by the loss of a water molecule from the precursor ion. The product ion at *m/z* 790.46 was assigned as $[C\text{-}(C14{:}0)\text{ketene-}C_6H_{12}\text{-}H_2O\text{-}H]^-$ ion. It was generated by the consecutive eliminations of n-hexane as a part of the fatty acid (-84 Da) probably located at N-2 and a molecule of water. Similarly, the product ion at *m/z* 648.36 was assigned as the $[C\text{-}(C14{:}0)\text{ketene-}(C14{:}0(3\text{-}OH))\text{acid-}H]^-$ ion. It was created by the loss 3-hydroxy-myristic acid (C14:0(3-OH)) (-244 Da) located at the position O-3. The product ions at *m/z* 550.40 was assigned as $[C\text{-}(C14{:}0)\text{ketene-}(C14{:}0(3\text{-}OH))\text{acid-}H_2PO_4\text{-}H]^-$ ion. It was generated by the loss of both the 3-hydroxy-myristic acid (-244 Da) at O-3 position, and H_3PO_4 (-98 Da) at the O-4′ position of the GlcN monosaccharide residue. The ion at *m/z* 474.29 was assigned as $[C(C14{:}0(3\text{-}OH))\text{ketene-}(C_8H_{16})\text{-}HPO_3\text{-}H]^-$ ion. It was generated by the loss of

both the 3-hydroxy-myristic acid located at O-3 (-226 Da), and n-octane (C_8H_{16}) (-112 Da) as part of the fatty acid chain located at N-2, in addition to the loss of HPO_3 (-80 Da) from the non-reducing D-GlcN residue. The product ion at *m/z* 456.26 was assigned as [C-(C14:0(3-OH))ketene-(C_8H_{16})-H_2PO_4-H]$^-$ ion. It was generated by the consecutive losses of 3-hydroxyl-myristic acid **(-**226 Da) located at O-3, n-octane (-112 Da) as part of the fatty acid chain located at N-2, and H_3PO_4 (-98 Da) at the position O-4 ′ of the GlcN monosaccharide residue (El-Aneed *et al*., 2006, Lukasiewicz *et al*., 2010, John *et al*., 2014, and Brodbelt *et al*., 2014).

This series of product ions indicates the presence of a fatty acid possessing different length, and highlight the elimination of H_3PO_4 from the O-4′ position of the GlcN monosaccharide residue. The last product ion at *m/z* 368.19 was assigned as [C-(C14:0(3-OH)acid-(C12:0)ketene-H_2PO_4-H]$^-$ ion. It was formed by the consecutive losses of the 3-hydroxy-myristic acid (C14:0) (-244 Da) at O-3, a molecule of lauryl ketene (-182 Da) from the branched (C14:0(3-*O*-C12:0)) ester at the N-2 position, followed by loss of H_3PO_4 (-98 Da) from O-4 position of the GlcN monosaccharide residue (Figure 3.1.7, Scheme 3.1.7, and Table 3.1.7).

Once more, we have again a strong support indicating that the lipid A_{1-5} structures contained a H_2PO_3 group at O-4′ of the D-GlcN non-reducing end residue of the β-D-Glc*p*N-(1→6)-α-D-Glc*p*N disaccharide backbone. Also, the presence of primary myristic esters located at both the O-3′ and N-2′ positions of this lipid A_{1-5} mixture. It also means that the position of the branched lauric acid ester is located on the N-2 position of the

reducing GlcN residue present in the β-D-Glc*p*N-(1→6)-α-D-Glc*p*N disaccharide backbone.

Finally, the CID-MS/MS afforded the precursor deprotonated mono-phosphorylated [C-(C14:0(3-*O*-C14:0))ketene-H]$^-$ molecules at *m/z* 666.06 afforded the following series of product ions at *m/z* 648.40, *m/z* 630.36, *m/z* 560.29, *m/z* 550.30, and *m/z* 520.25 (Figure 3.1.8, Table 3.1.8 and Scheme 3.1.8). The presence of this category of molecules in our lipid A_n mixture provides an indication of the incomplete biosynthesis of this bacterial lipid A_n component. The product ion at *m/z* 648.40 was formed by the loss of a water molecule from the precursor ion. The product ion at *m/z* 630.36 was formed by the loss of two molecules of water (-36 Da). It was assigned as [C-(C14:0(3-*O*-C14:0))ketene-2(H_2O)-H]$^-$ ion. The product ion at *m/z* 560.29 was assigned as [B_1-(C14:0(3-*O*-C14:0))ketene-(C_5H_{10})-2H_2O-H]$^-$ ion. It was assigned by the sequential eliminations of two molecules of water and a molecule of n-pentane (-70 Da) molecules from the branched (C14:0(3-*O*-C12:0)) fatty acid at N-2 position. The product ion at *m/z* 550.30 was assigned as [C-(C14:0(3-*O*-C1:0))ketene-(H_2PO_4)-H_2O-H]$^-$ ion. It was formed by sequential the loss of H_3PO_4 (-98 Da) from the O-4 position and a molecule of water. The product ion at *m/z* 520.25 was assigned as [C-(C14:0(3-*O*-C14:0))ketene-(C_9H_{20})-H_2O-H]$^-$ ion. It was formed by the loss of both nC_9H_{20} (-128 Da) from the branched (C14:0(3-*O*-C12:0)) fatty acid at N-2 position and a molecule of water as previously stated. The product ions formed from the precursor ion at *m/z* 666.06 confirm our suggested lipid $A_{1\text{-}5}$ structures, contained in their respective positions: The H_2PO_3 group at O-4′ position, and two molecules of 3-hydroxyl-myristic acid at O-3 and N-2 of their lipid $A_{1\text{-}5}$. In addition, the branched fatty

acid substituents, namely (C14:0(3-*O*-C14:0)) and (C14:0(3-*O*-C12:0)) the O-3′, and N-2′ positions of their lipid A_{1-5} backbones.

It is interesting to note that the CID-MS/MS analysis of the deprotonated molecules $[M_{1-5}-H]^-$ at *m/z* 1716.30 ($LipA_1$), *m/z* 1688.19 ($LipA_2$), *m/z* 1506.10 ($LipA_3$), *m/z* 1279.73 ($LipA_4$), and *m/z* 1097.63 ($LipA_5$) afforded distinctive series of product ions. In addition, it is important to comprehend that there was no cross connectivity between the different precursor deprotonated molecules. This indicates that the genesis of each of these species of precursor ions was distinctive. Moreover, each of these precursor deprotonated molecules created specific product ions. Once more, this finding seems to confirm that the origins of the precursor ions were indeed caused by an incomplete biosynthesis of the LPS and not by chemical degradation of any kind (El-Aneed *et al*., 2006, and Lukasiewicz *et al*., 2010).

In general, it is important to note that during the low-energy CID-MS/MS analyses conducted with the QqQ-tandem instrument on these series of deprotonated molecules, we were able to confirm that the formation of each deprotonated molecule recorded in single stage ESI-QqQ-MS instrument, were indeed single unique diagnostic molecules that were not produced by further fragmentation from contiguous higher masses deprotonated molecules. In addition, these product ion scans created series of product ions that excluded the possibility, that they could be related to each other.

Finally, precursor ion scans of these deprotonated molecules formed during the ESI-QqQ-MS showed that there were no connectivities and/or genesi relations between these different deprotonated molecules (see Appendix).

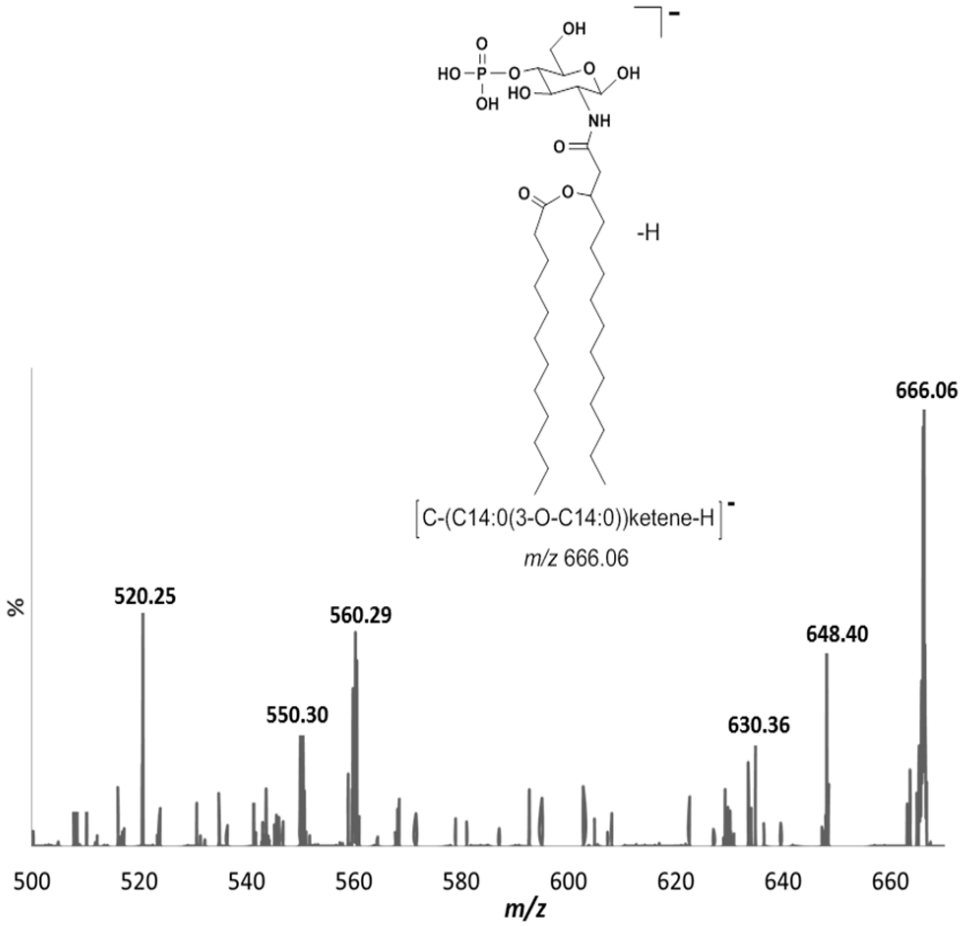

Figure 3.1.8: CID-MS/MS of the precursor deprotonated [C-(C14:0(3-*O*-C14:0))ketene-H]$^-$ molecules at *m/z* 666.06.⁕

⁕ Please note, that some product ions were not assigned as these were produced by other isobars isolated during the MS/MS analysis.

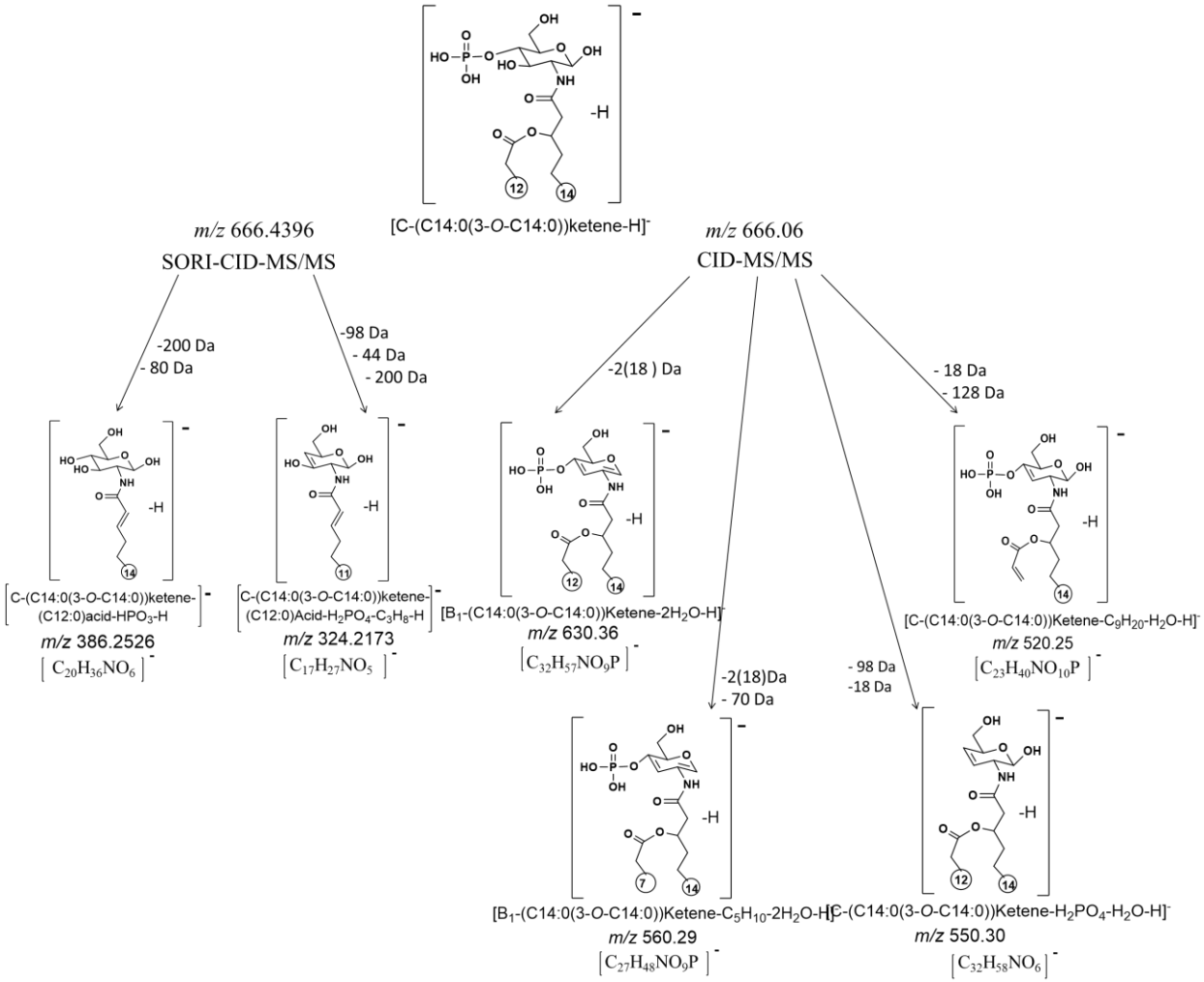

Scheme 3.1.8: Proposed fragmentation pathways obtained by CID-QqQ-MS/MS and SORI-CID- FTICR MS/MS of the precursor mono-phosphorylated ion [C-(C14:0(3-*O*-C14:0))ketene-H]$^-$ *m/z* 666.06.

Table 3.1.8: Assignments of the product ions observed from CID-MS/MS and SORI-CID-MS/MS of the precursor ion at *m/z* 666.06.

	Precursor deprotonated [C-(C14:0(3-*O*-C14:0))ketene-H]$^-$ molecules at *m/z* 666.06			
	CID-QqQ-MS/MS		SORI-FTICR-MS/MS	
Empirical formula	Product ion *m/z* Calculated; Observed (%)	δ ppm	Product ion *m/z* Calculated; Observed (%)	δ ppm
$C_{32}H_{59}NO_{10}P$	648.38; 648.40 (53.1)	30	648.3282; 648.3235 (26.7)	-7.2
$C_{32}H_{57}NO_9P$	630.38; 630.36 (22.6)	-31.5	-	-
$C_{27}H_{48}NO_9P$	560.31; 560.29 (50.5)	-35.6	-	-
$C_{23}H_{58}NO_6$	550.27; 550.30 (25.9)	54.5	-	-
$C_{23}H_{40}NO_{10}P$	520.23; 520.25 (51.9)	38.4	-	-
$C_{20}H_{36}NO_6$	-	-	386.2548; 386.2526 (102)	-5.6
$C_{17}H_{27}NO_5$	-	-	324.2180; 324.2173 (53.5)	-2.1

3.3. ESI-FTICR-MS analysis of heterogeneous lipid A_n mixture isolated from the LPS of *A. liquefaciens* SJ-19a

The ESI-MS analysis of the mixture of lipid $A_n$was also conducted with an FTICR-mass spectrometer in order to create a spectrum with high mass resolving power. Because FT-ICR-MS is based on a time measurement and because the trapped ion frequencies are independent of the kinetic energy, this technique provides the highest resolving power and mass accuracy currently available which allow to determine the elemental composition of the analyzed produced ions (Marshall, *et al*., 1998, Marshall, *et al*., 1999, Palumbo *et al*., 2011, van Agthoven *et al*., 2015, and Almostafa *et al*., 2016). As expected, this ESI-MS (- ion mode) obtained for lipid A of *A. liquefaciens* SJ-19a displayed an incomplete biosynthesis as illustrated by the multiple deprotonated molecules.

Similarly to the ESI-QqQ-MS, the ESI-FTICR-MS (- ion mode) showed the presence of *inter-alia* seven fragment ions, five of which were assigned to different $[M-H]^-$ deprotonated mono-phosphorylated anions $LipA_1$ at *m/z* 1716.2491, $LipA_2$ at *m/z* 1688.22091, $LipA_3$ at *m/z* 1506.0511, $LipA_4$ at *m/z* 1279.8593, and $LipA_5$ at *m/z* 1097.6930, whereas, the last deprotonated molecules at *m/z* 892.5975 and *m/z* 666.4396 were assigned as belonging the $[C-H]^-$ indicating the presence of a heterogeneous mixture of lipid A_n (Figure 3.2.1, Scheme 3.1.1 and Table 3.1.1).

When comparing the ESI-spectra recorded with QqQ-mass and the FTICR-mass spectrometer instruments, we noticed that the deprotonated molecules of the $LipA_{1-5}$ mixture had different abundances.

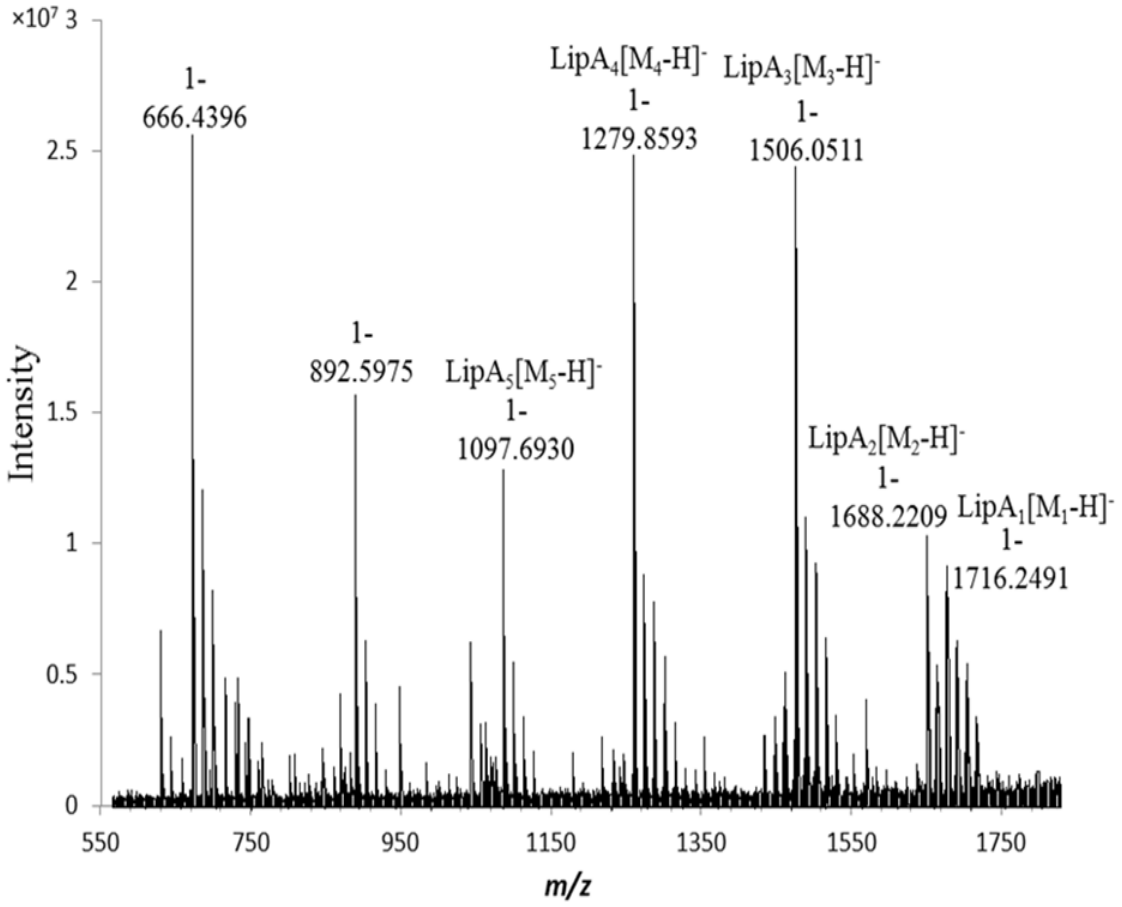

Figure 3.2.1: ESI-FTICR-MS (- ion mode) of the native lipid A_n mixture extracted from *A. liquefaciens* SJ-19a**.**

In the ESI-FTICR-mass spectrum, we noticed that the deprotonated molecule assigned to the $LipA_3$ at *m/z* 1506.0511 was the most abundant (El-Aneed *et al*., 2006, Lukasiewicz *et al*., 2010, John *et al*., 2014, and Brodbelt *et al*., 2014).

3.3.1 Measurement of the FT-ICR-MS isotopic distributions of the deprotonated molecules of lipid A_n isolated from the LPS of *A. liquefaciens* SJ-19a

The influence of spectral accuracy of the deprotonated molecular ions on elemental composition calculations was investigated by high-resolution mass spectrometer. For that reason, high mass accuracy together with high isotopic abundance accuracy proved to be generally important to obtain only few molecular formula candidates from an accurate mass measurement. The automated correction of isotope pattern abundance errors using peak shaping and correction algorithms resulted in better identification rates of the molecular formulas. It should be mentioned that the determination of the molecular formula or elemental composition requires a clean mass spectrum with no interfering noise or co-eluting compounds (Kind *et al*., 2010, and Jaitly *et al*., 2009).

The algorithm includes a decision making step for proton and alkali metal adducts, automated determination of charge states and overlapping peaks, and an isotopic pattern matching. The freely available software SIRIUS (Sum formula Identification by Ranking Isotope patterns using mass spectrometry) has a user-friendly graphical interface and can be used on LINUX, MAC, and Windows platforms.

The isotopic distribution of this series of deprotonated lipid A_n (where n=1-5), namely: $LipA_1$ at *m/z* 1716.2491, $LipA_2$ at *m/z* 1688.22091, $LipA_3$ at *m/z* 1506.0511, $LipA_4$ at *m/z* 1279.8593, and $LipA_5$ at *m/z* 1097.6930, and in addition to the two deprotonated molecules at *m/z* 892.5975 and *m/z* 666.4396, is indicated in the (Figure 3.3.1 and Figure 3.3.2) (Kind *et al*., 2010, and Jaitly *et al*., 2009). Therefore, the calculated elemental compositions of the deprotonated molecule $[M_1\text{-}H]^-$, $[M_2\text{-}H]^-$, $[M_3\text{-}H]^-$, $[M_4\text{-}H]^-$, and $[M_5\text{-}H]^-$, matched their experimental isotopic abundances using the algorithm "Gaussian 09 software package", which allowed us to calculate the isotopic fine structures and allow the modeling of Gaussian peak shapes according to the selected resolving power of the instrument (Kind *et al*., 2010, and Jaitly *et al*., 2009). In order to examine the difference in CID-gas-phase fragmentations between the QqQ and the FTICR-instruments, we subjected this series of deprotonated molecules to SORI-CID-FTICR-MS/MS analysis in order to confirm their exact structures.

3.3.2 SORI-CID-FTICR-MS/MS analysis of lipid A isolated from the LPS of *A. liquefaciens* SJ-19a

It is well known that MS/MS analysis of different lipid A have provided researchers with information about the number and location of phosphoryl groups and by defining the nature of the ion charges (singly and doubly charged ions). In addition, it provides information about the fatty acids on the lipid A backbone, which can be identified by the sequential release of primary and/or secondary fatty acids, and cross-ring and inter-ring fragments.

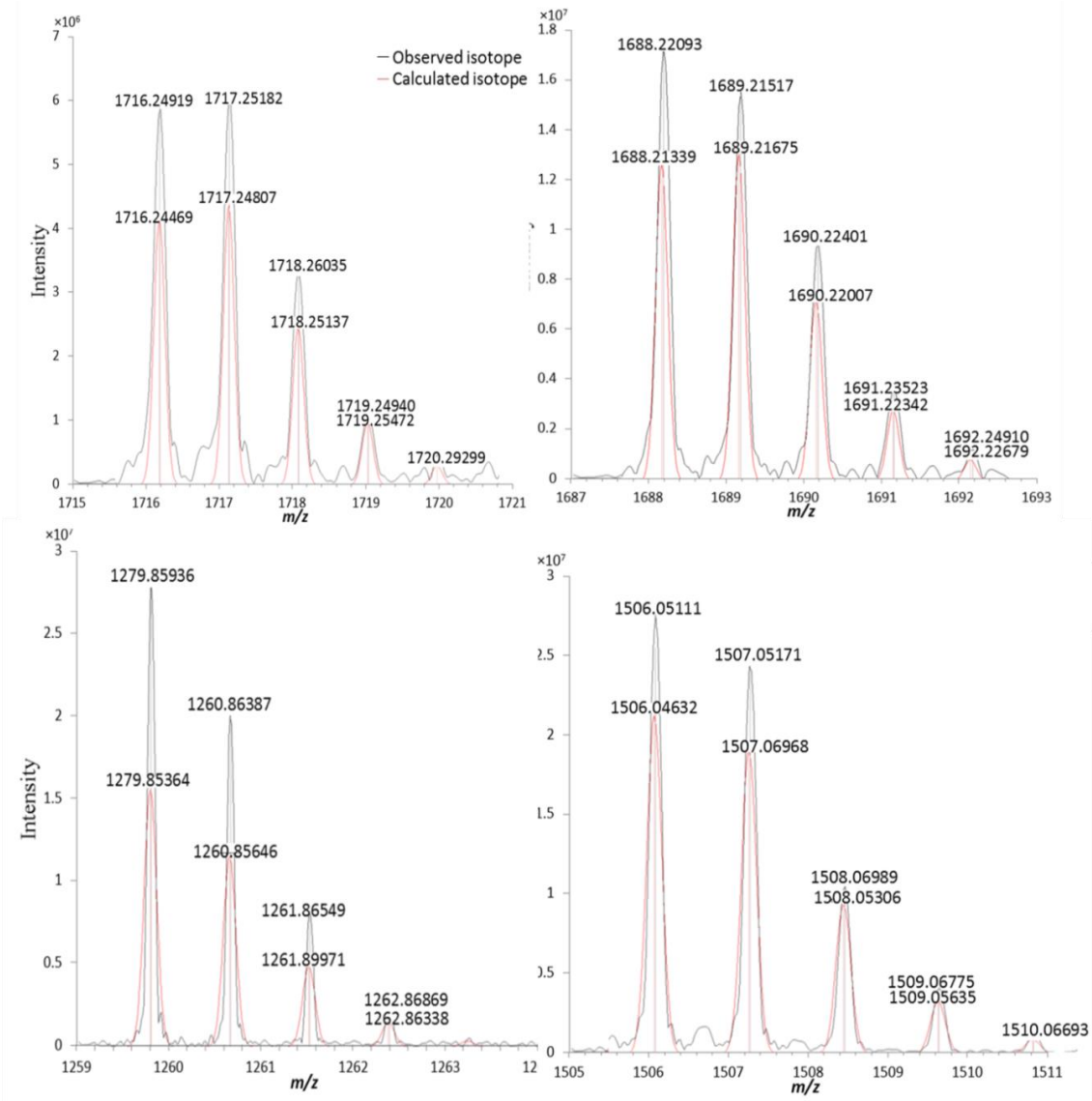

Figure 3.3.1: Theoretical isotope distribution overlapped on top of the observed pattern of the lipid A_n extract from the LPS of *A. liquefaciens* SJ-19a.

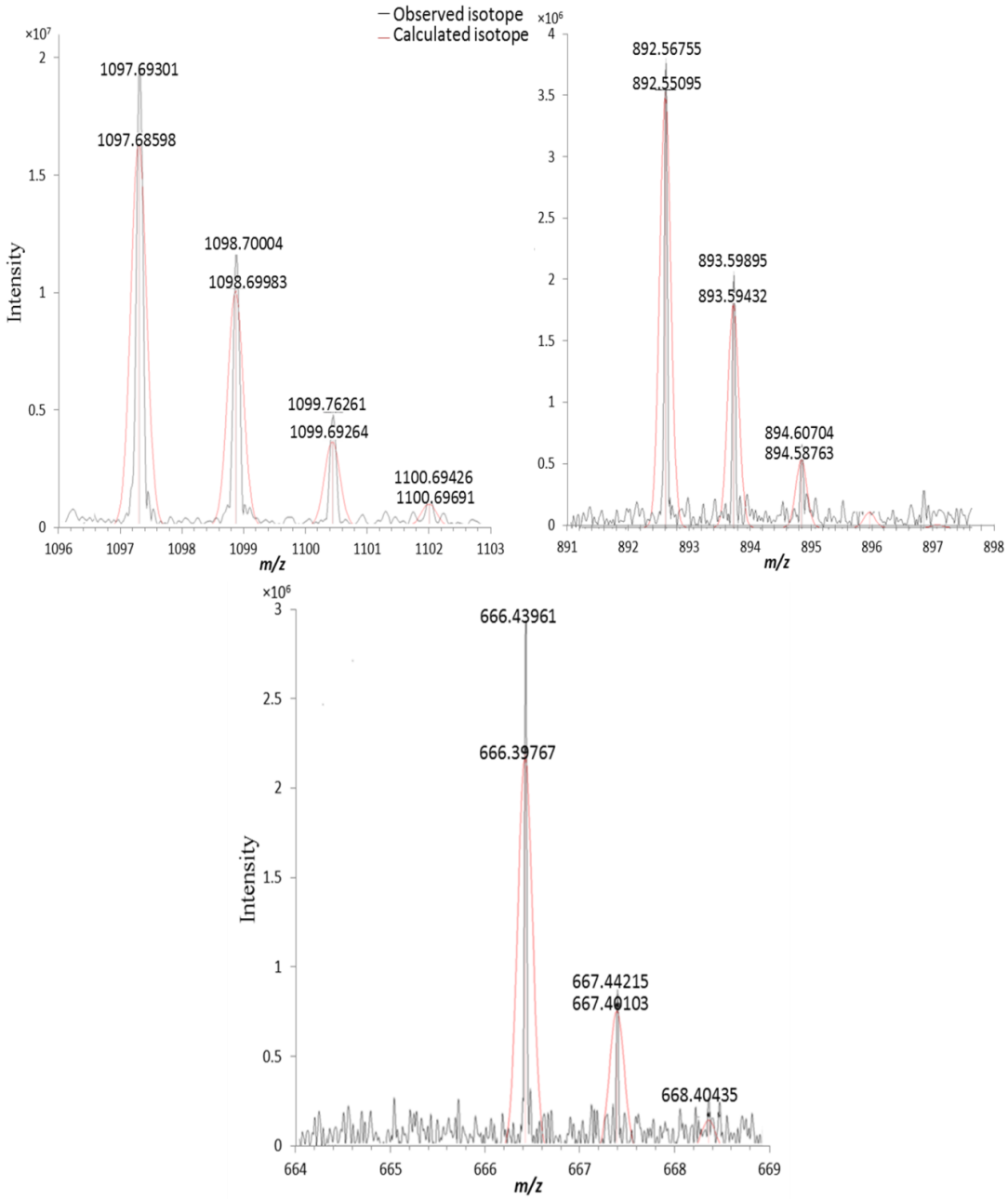

Figure 3.3.2: Theoretical isotope distribution overlapped on top of the observed pattern of the lipid A_n extract from the LPS of *A. liquefaciens* SJ-19.

Please note that there was a never encountered doubly charged ion. The use of the low-energy collision induced dissociation mass spectrometry (SORI-CID-MS/MS) was with a Fourier transform ion cyclotron resonance mass spectrometer instrument to establish the MS/MS fragmentation routes.

The product ion scan of the deprotonated molecules of $LipA_1$ at *m/z* 1716.2491 gave the product ions at *m/z* 1488.0469, *m/z* 1243.8399, and *m/z* 1035.6975. The product ion at *m/z* 1488.0469 was assigned as the $[M_1$-(C14:0)acid-H$]^-$ ion, which was created by the elimination of myristic acid form the branched fatty (C14:0(3-*O*-C14:0)) acid acyl group located at O-3′ (-228 Da). The product ion at *m/z* 1243.8399 was assigned as $[M_1$-(C14:0)acid-C14:0(3-OH)acid-H$]^-$ ion. It was formed by consecutive losses of myristic acid form the branched fatty (C14:0(3-*O*-C14:0)) acid acyl group located at O-3′ (-228 Da), and ketene 3-hydroxy-myristic acid (C14:0(3-OH)) (-244 Da) located at the position O-3 of the reducing GlcN end. The product ion at *m/z* 1035.6599 was assigned as the $[M_1$-(C14:0(3-*O*-C12:0))ketene-(C14:0(3-OH))acid-H$]^-$ ion, which was created by the elimination of a molecule of the branched fatty (C14:0(3-*O*-C12:0)) (-436 Da) and ketene 3-hydroxy-myristic acid (C14:0(3-OH)) (-244 Da) located at the position O-3 of the reducing GlcN end (Figure 3.3.3, Scheme 3.1.2 and Table 3.1.2).

The product ion scan of the deprotonated $LipA_2$ molecules at *m/z* 1688.2209 gave the product ions at *m/z* 1488.0379, *m/z* 1243.8851 and *m/z* 1035.6599 (Figure 3.3.4, Table 3.1.3 and Scheme 3.1.3).

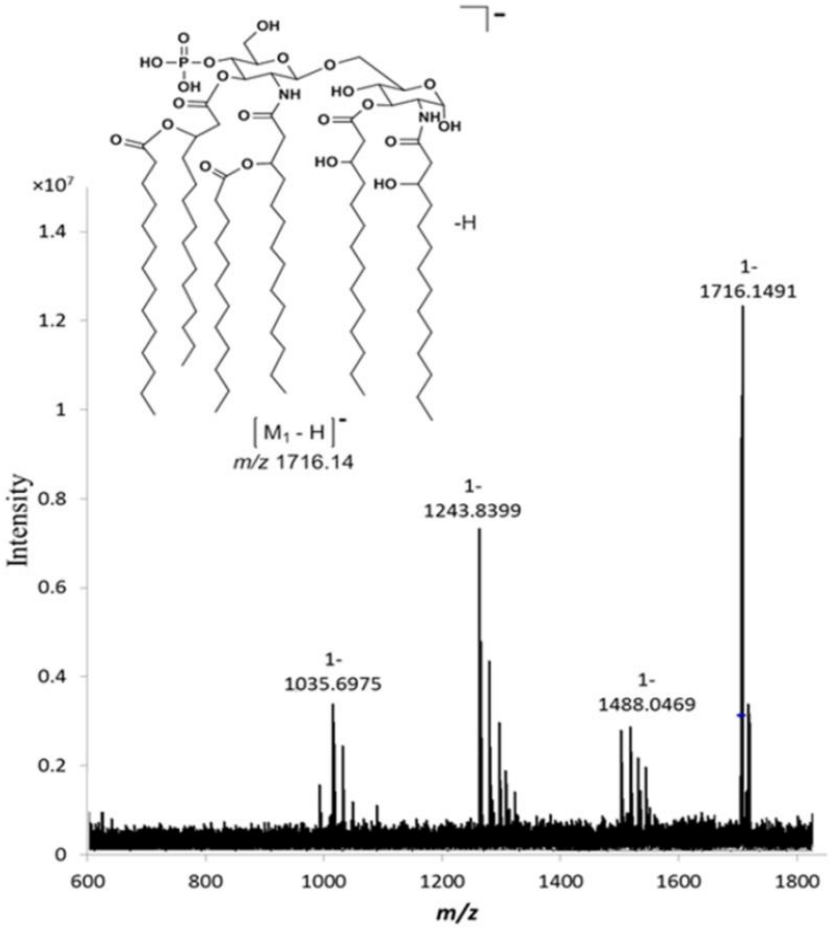

Figure 3.3.3: SORI-CID-MS/MS of the precursor deprotonated $[M_1\text{-}H]^-$ molecules at *m/z* 1716.2491.

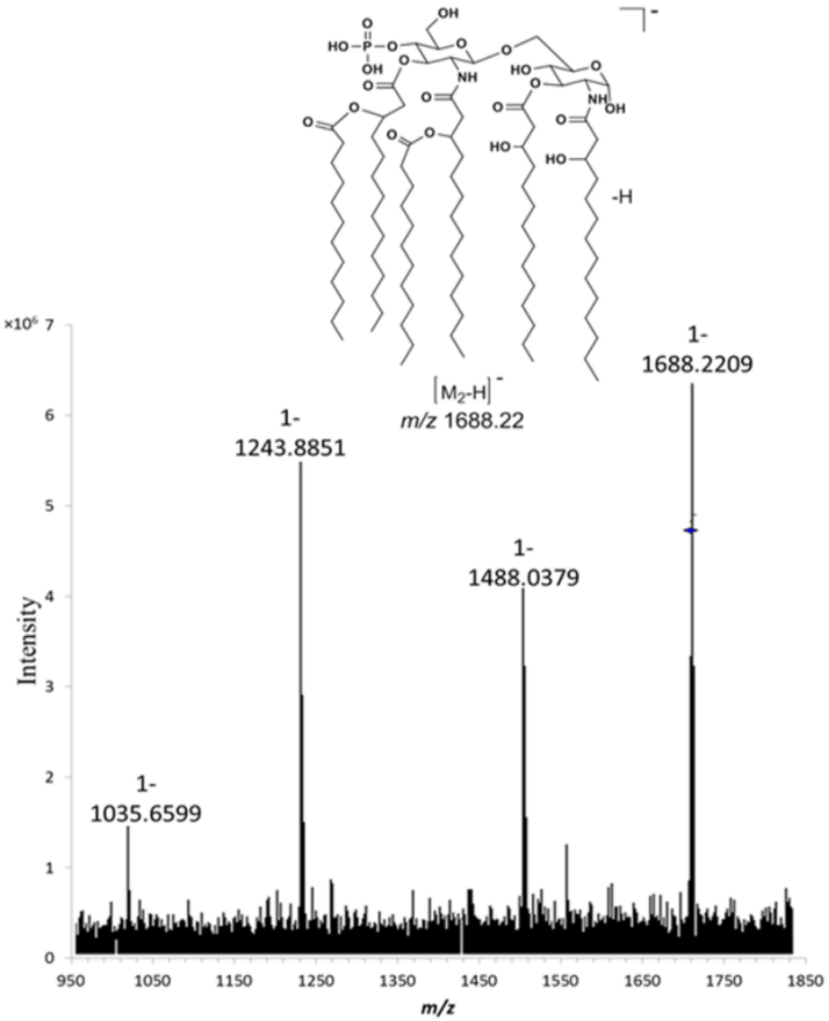

Figure 3.3.4: SORI-CID-MS/MS of the precursor ion $[M_2\text{-}H]^-$ at *m/z* 1688.2209.

The product ion at *m/z* 1488.0379 was assigned as the $[M_2$-(C12:0)acid-H$]^-$ ion, which was created by elimination of the lauric acid form the branched fatty acid (C14:0(3-*O*-C12:0)) located either the O-3′ or N-2′ position (-200 Da). The product ion at *m/z* 1243.8851 was assigned as $[M_2$-(C14:0(3-*O*-C12:0))acid-H_2O-H$]^-$ ion, and it was formed by consecutive losses of the branched fatty (C14:0(3-*O*-C12:0)) acid (-426 Da) located on position O-3′ and a molecule of water from the precursor ion at *m/z* 1688.2209. The product ion at *m/z* 1035.6599 was assigned as the $[M_2$-(C14:0(3-*O*-C12:0))ketene-(C14:0(3-OH))acid-H$]^-$ ion, which was created by elimination of a molecule of the branched fatty (C14:0(3-*O*-C12:0)) (-408 Da) and ketene 3-hydroxy-myristic acid (C14:0(3-OH)) (-244 Da) located at the position O-3 of the reducing GlcN end (El-Aneed *et al*., 2006, Shaffer *et al*., 2007, Lukasiewicz *et al*., 2010, John *et al*., 2014, and Brodbelt *et al*., 2014).

The product ion scan of the precursor deprotonated molecules of $LipA_3$ *m/z* 1506.0511 gave the major product ion at *m/z* 1261.8349, which was formed by the elimination of 3-hydroxy-myristic acid (-244 Da) from the precursor ion and (Figure 3.3.5, Table 3.1.4, and Scheme 3.1.4). This product ion was assigned as $[M_3$-(C14:0(3-OH))acid-H$]^-$ ion. It should be noted that this elimination can be in fact occur from either at the O-3 and O-3′ positions located respectively in the reducing end or non-reducing end of the lipid A disaccharide backbone (El-Aneed *et al*., 2006, Shaffer *et al*., 2007, Lukasiewicz *et al*., 2010, John *et al*., 2014, and Brodbelt *et al*., 2014).

Additionally, the product ion scan of $LipA_4$ at *m/z* 1279.8593 afforded the product ion at *m/z* 1035.6622 was assigned as the $[M_4$-(C14:0(3-OH))acid-H$]^-$ ion. It was created

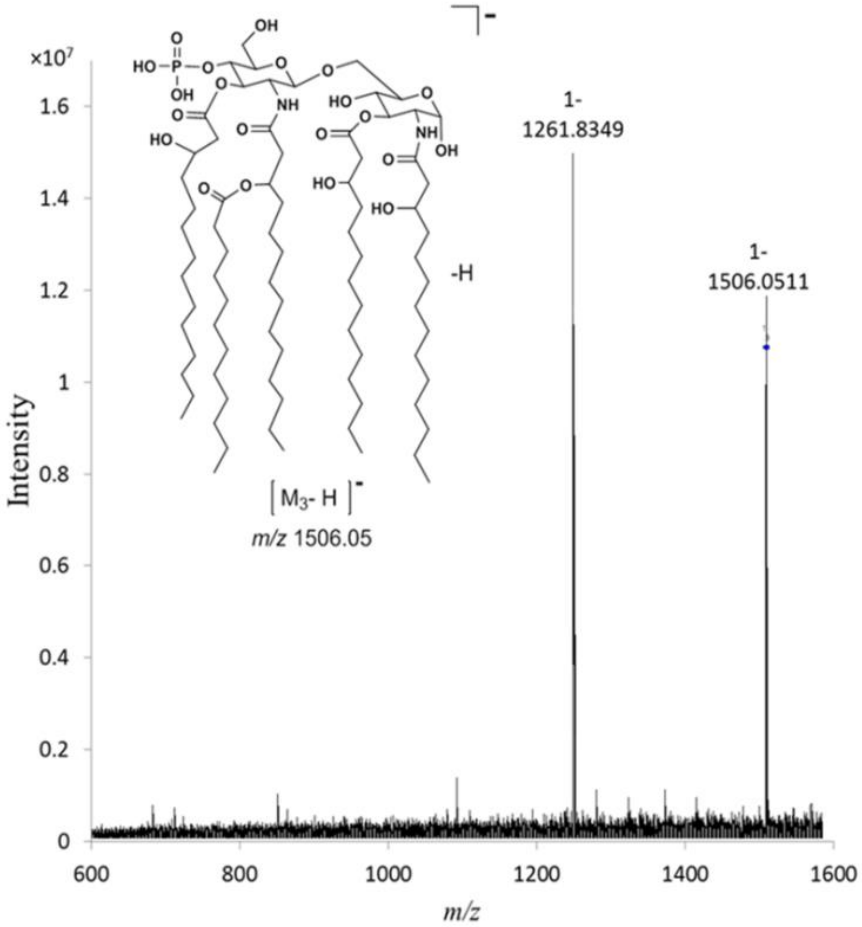

Figure 3.3.5: SORI-CID-MS/MS of the precursor ion $[M_3\text{-}H]^-$ at *m/z* 1506.0511.

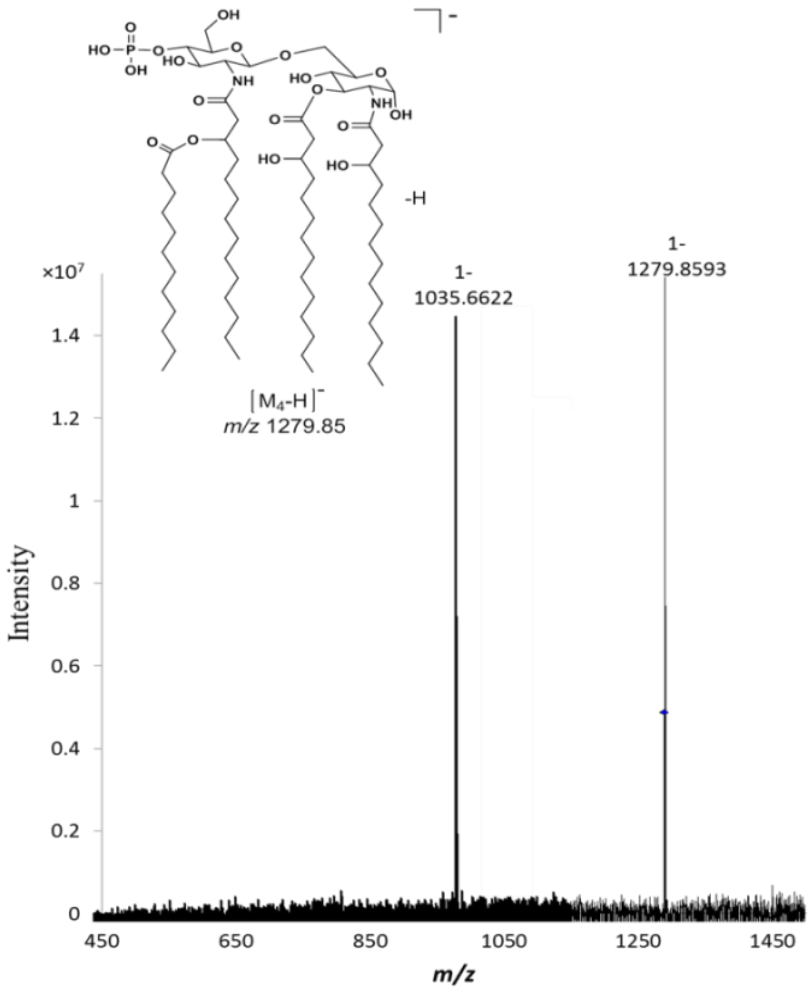

Figure 3.3.6: SORI-CID-MS/MS of the precursor ion $[M_4\text{-}H]^-$ at *m/z* 1279.8593.

by the elimination of 3-hydroxy-myristic acid (C14:0(3-OH)) (-244 Da) located at the position O-3 of the reducing GlcN end (Figure 3.3.6, Table 3.1.5 and Scheme 3.1.5).

Similarly, the product ion scan of deprotonated molecules of $LipA_5$ at *m/z* 1097.6865 gave the product ion at *m/z* 853.4897 was assigned as the $[M_5$-(C14:0(3-OH))acid-H$]^-$ ion, which was created by the elimination of 3-hydroxy-myristic acid (C14:0(3-OH)) (-244Da) located at the position O-3 of the reducing GlcN end of the lipidA_5 disaccharide (Figure 3.3.7, Table 3.1.6 and Scheme 3.1.6) (El-Aneed *et al*., 2006, Lukasiewicz *et al*., 2010, John *et al*., 2014, and Brodbelt *et al*., 2014).

The following diagnostic deprotonated molecules, which were previously encountered in the ESI-QqQ-MS measurement of the lipid A_n mixture, were also produced by measurement with the FTICR-mass spectrometer instrument. They were assigned as $[C-H]^-$ at *m/z* 892.5975 and *m/z* 666.4396. Accordingly, in order to confirm their putative structures and to confirm the presence of the phosphate group position, we acquired their product ion scans.

SORI-CID-MS/MS of the deprotonated molecules at *m/z* 892.5975, which were assigned previously as $[C-(C14:0)ketene-H]^-$, gave the product ions at *m/z* 648.3931, *m/z* 466.2275 and *m/z* 448.2165 (Figure 3.3.8, Table 3.1.7, and Scheme 3.1.7). The product ion at *m/z* 648.3931 was assigned as the $[C-(C14:0)ketene-(C14:0(3-OH))acid-H]^-$ ion. It was formed by the elimination of the 3-hydroxy-myristic acid (C14:0(3-OH)) (-244 Da) from the O-3 of the precursor ion. The product ions at *m/z* 466.2275 was attributed as the $[C-(C14:0)ketene-(C14:0(3-OH))acid-(C12:0)ketene-H]^-$ ion. It was formed by consecutive elimination of the 3-hydroxy-myristic acid (C14:0(3-OH)) (-244 Da) from the O-3, and

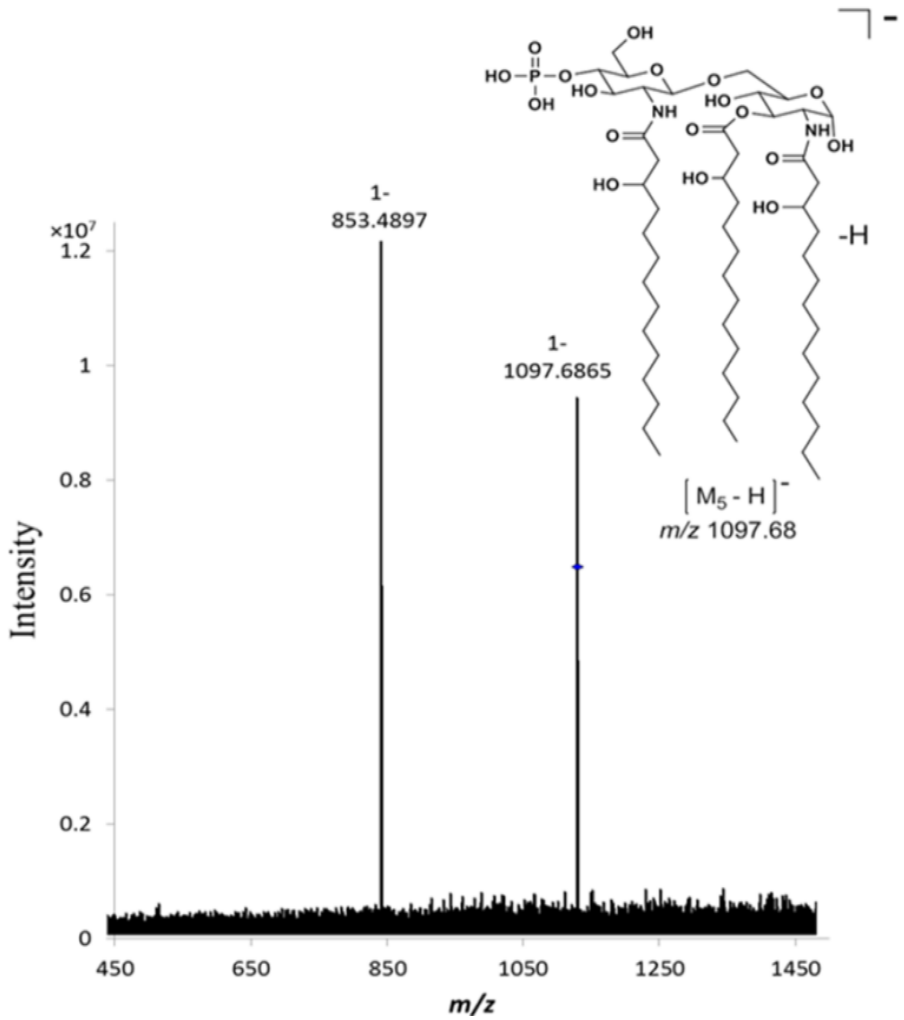

Figure 3.3.7: SORI-CID-MS/MS of the precursor ion $[M_5\text{-}H]^-$ at *m/z* 1097.6865.

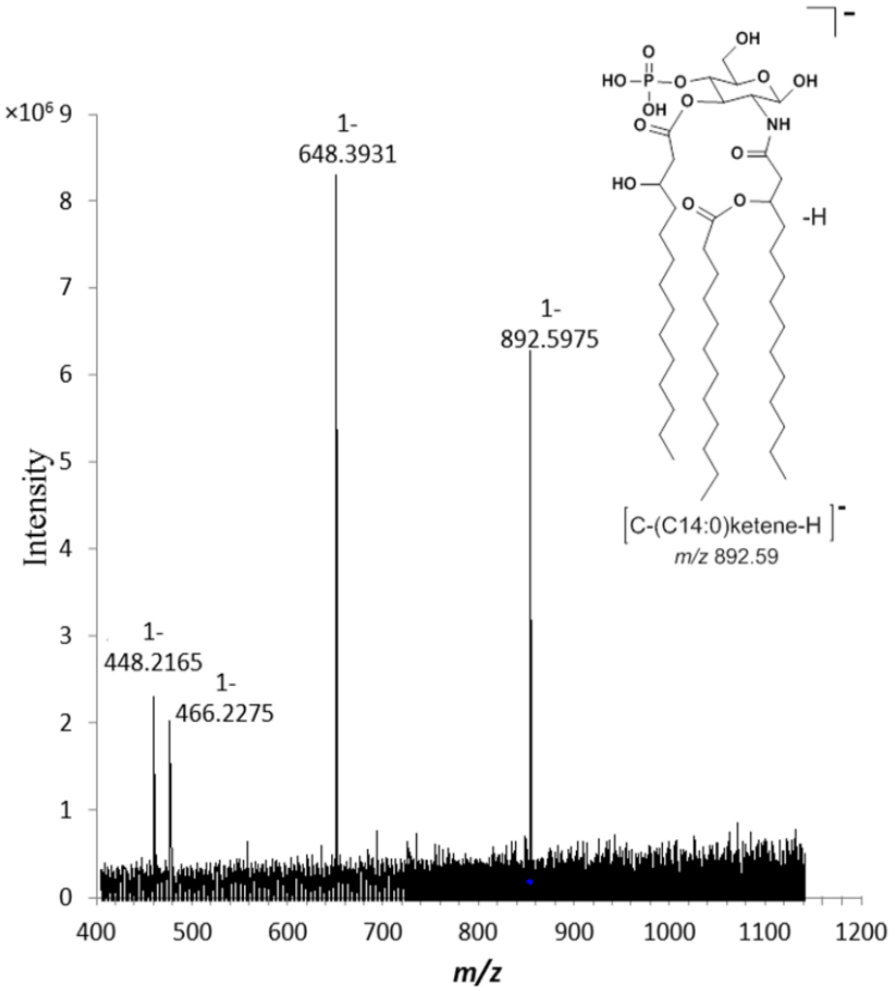

Figure 3.3.8: SORI-CID-MS/MS of the precursor ion of $[C\text{-}(C14{:}0)ketene\text{-}H]^-$ at *m/z* 892.5975.

of lauric ketene (-182 Da) form the branched fatty acids (C14(3-*O*-C12:0)) at the N-2 position of the non–reducing GlcN residue obtained from the precursor ion at *m/z* 892.5975. Though, the product ion at *m/z* 448.2165 was assigned as [C-(C14:0(3-*O*-C14:0))acid-(C12:0)acid-H]$^-$. It was formed by consecutive eliminations of both 3-hydroxyl-myristic acid (C14:0) (-244 Da) at O-3 position and lauric acid molecule (-200 Da) from the branched (C14:0(3-*O*-C12:0)) at the N-2 position of lipid A. It is clearly evident that this product ion contains a PO_4 group located at the non-reducing end O-4′.

Similarly, the SORI-CID-MS/MS of the precursor deprotonated [C-(C14:0(3-*O*-C14:0))ketene-H]$^-$ molecule at *m/z* 666.4396 gave the product ions at *m/z* 648.3235, *m/z* 386.2526 and at *m/z* 326.2173, respectively (Figure 3.3.9, Table 3.1.8, and Scheme 3.1.8). The product ion *m/z* 648.3235 was formed by the elimination of a molecule of water, from the precursor ion. The product ion at *m/z* 386.2526 was assigned as [C-(C14:0(3-*O*-C14:0))ketene-(C12:0)acid-HPO_3-H]$^-$ ion. It was formed by the consecutive eliminations of the lauric acid (-200 Da) from the branch (Cl4:0(3-*O*-C12:0)) fatty acids. It was attached to the N-2′ position, of HPO_3 (-80 Da) located at O-4′ position of the lipid A disaccharide backbone. The product ion at *m/z* 324.2173 was assigned as [C-(C14:0(3-*O*-C14:0))ketene-(C12:0)acid-H_2PO_4-C_3H_8-H]$^-$ ion (-340 Da). It was formed by the consecutive eliminations of the lauric acid (-200 Da) from the branched (Cl4:0(3-*O*-C12:0)) fatty acid which was attached to the N-2′ position, by the loss of H_3PO_4 (-98 Da) at O-4 ′ position, and by loss of n-propane (-44 Da) from the alkyl chain (C14:0) located at N-2′. The SORI-CID-MS/MS of the precursor ion at *m/z* 666.4396 and its associated product ions strongly confirms that

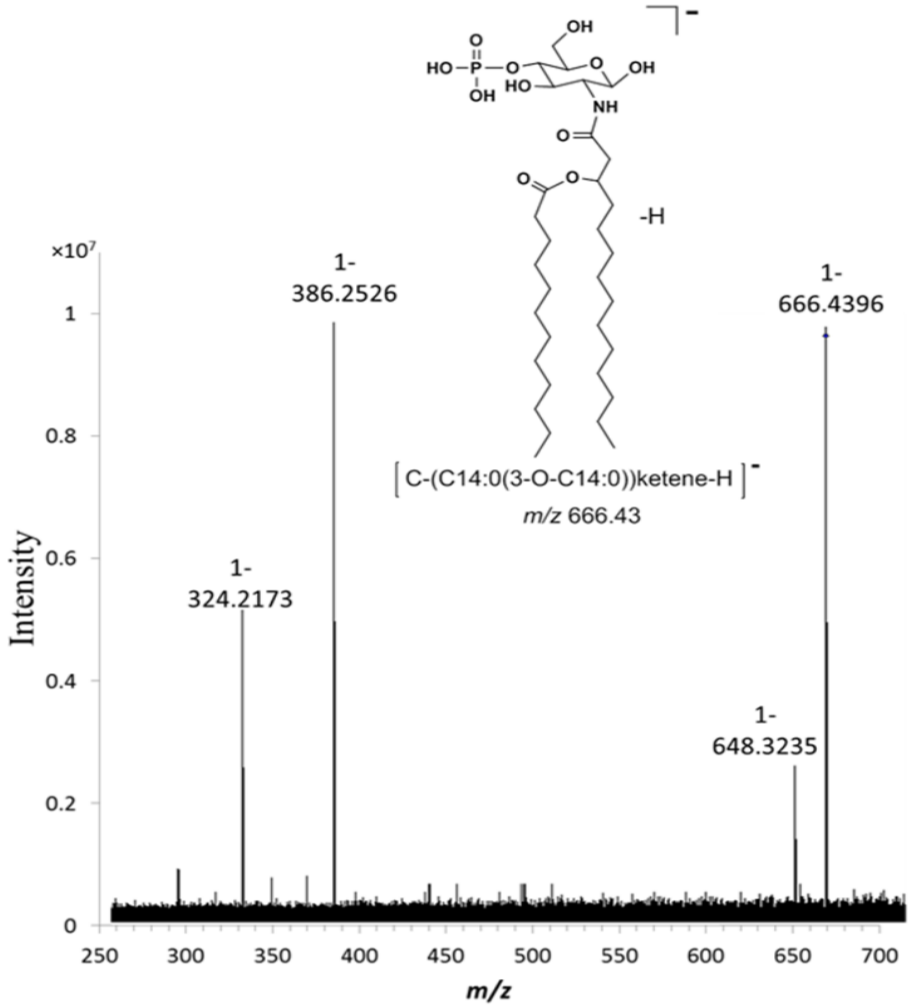

Figure 3.3.9: SORI-CID-MS/MS of the precursor ion of [C-(C14:0(3-*O*-C14:0))ketene-H]$^-$ at *m/z* 666.4396.

our suggested structures of the $LipA_{1-5}$ are certainly correct, and specify that these structures contain a PO_4 group located at the non- reducing end of the lipid A at O-4′. Finally, it also defines the location of the branched lauric acid at N-2′ (El-Aneed *et al*., 2006, Shaffer *et al*., 2007, Lukasiewicz *et al*., 2010, John *et al*., 2014, and Brodbelt *et al*., 2014).

3.3.3. Comparison between low-energy CID-QqQ-MS/MS and SORI-CID-MS/MS of the deprotonated molecules obtained from the mixture of lipid A_n isolated from the LPS of *A. liquefaciens* SJ-19a

Comparing between the CID-MS/MS analysis with the QqQ-MS/MS and SORI-MS/MS, we have noticed that the number of distinctive product ions decreased with SORI-MS/MS analysis, when compared to CID-MS/MS analysis with the QqQ-mass spectrometer instrument. As all of the previous schemes (3.1.2 – 3.1.8) showed, we have noticed that all the of the product ions which obtained from SORI-CID-MS/MS were produced by the primary fatty acid fragmentation not the branched, most of the time the elemenation occure at O-3 and O-3´ posetion. Fore This was probably due to the trapping in the ultra-high-vacuum ICR cell of the formed precursor deprotonated molecules. Accordingly, there are many more collisions with much lower kinetic energy, than in the collision cell (q) of the QqQ-mass spectrometer. Also, SORI-CID-MS/MS is a soft tandem mass spectrometric technique, in which, only the precursor ion is accelerated, whereas in the quadrupole, the product ions are also accelerated.

In SORI-CID-MS/MS, the product ions formed from the precursor are not accelerated, as I the precursor deprotonated molecules alone are the only ones being excited. Once, they dissociate the product ions are not energized. Whereas with the CID-QqQ-MS/MS in the collision cell q, the precursor ions and the formed product ions have time to collide, gain energy, and to further CID-fragment. All the produced product ions are then accelerated through the q (Wieboldt *et al*., 1997, Gauthier *et al*., 1991, and Stafford *et al*., 2002).

3.4. High-energy MALDI-TOF-MS analysis of the extracted mixture of lipid A_n isolated from the LPS of *A. liquefaciens* SJ-19a

The MALDI-TOF-MS (- ion mode) of the lipid A obtained from *A. liquefaciens* SJ-19a was measured in the reflector mode with the TOF/TOF instrument and high laser power. Similarly, MALDI-TOF-MS showed similar spectra to the ones measured with the ESI-QqQ-MS and FTICR-MS instruments, indicating again that the biosynthesis of lipid A was incomplete. Accordingly, as previously discussed in section 3.2 and 3.4, we shall use the same nomenclature of all the analyzed deprotonated molecules.

Hence, we have assigned that this lipid A mixture contained seven common structures corresponding to the different $[M-H]^-$ deprotonated mono-phosphorylated anions $LipA_s$, respectively: at *m/z* 1716.24, $LipA_2$ at *m/z* 1688.2145, $LipA_3$ at *m/z* 1506.0574, $LipA_4$ at *m/z* 1279.8541, and $LipA_5$ at *m/z* 1097.6871, whereas, the last deprotonated molecule at *m/z* 920.6234 which was assigned as belonging to the $[C-H]^-$.

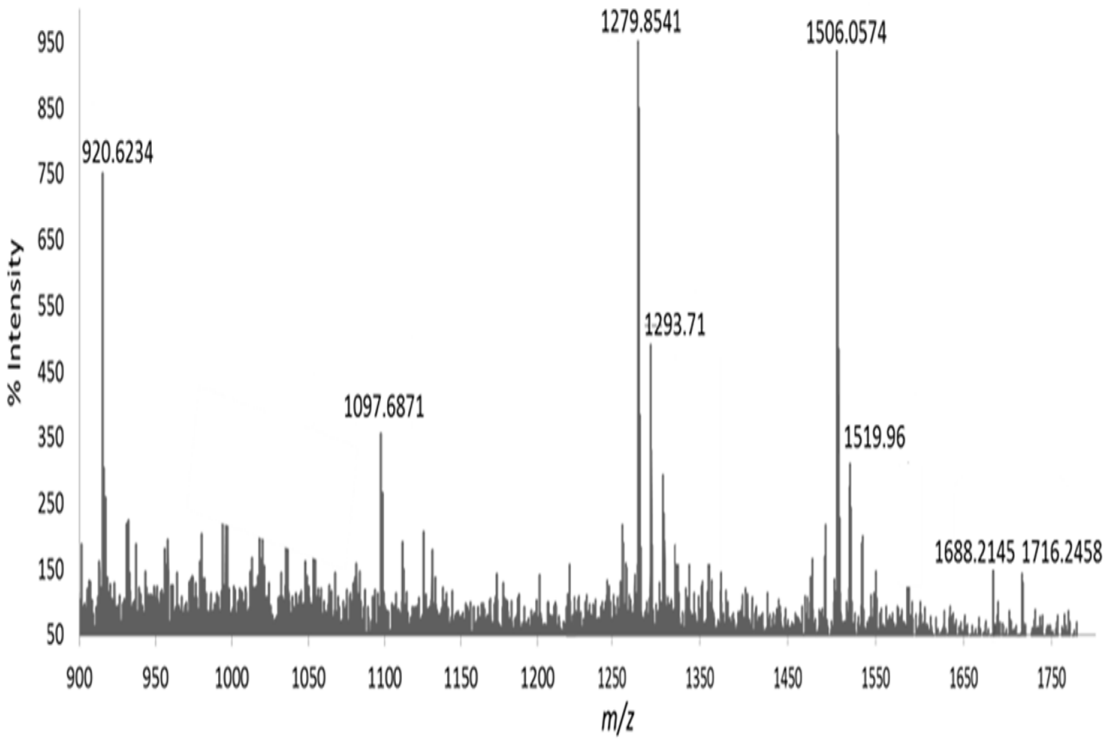

Figure 3.4.1: MALDI-TOF-MS (- ion mode) of the native lipid A_n mixture extracted from *A. liquefaciens* SJ-19a**.**

The ion at *m/z* 920.6234 was assigned as [C-(C12:0)ketene-H]$^-$ (Figure 3.4.1, Scheme 3.1.1 and Table 3.1.1). In the MALDI-TOF-mass spectrum, we noticed that the ions assigned to the $LipA_3$ at *m/z* 1506.0574 and $LipA_4$ at *m/z* 1279.8541 were the most abundant in the mass spectrum. It is important to note that the ion at *m/z* 920.6234 was only observed in the MALDI-TOF-MS as a major peak, as illustrated in (Figure 3.4.1).

3.4.1. High-energy MALDI-CID-TOF/TOF-MS/MS analysis of the extracted mixture of lipid A_n isolated from the LPS of *A. liquefaciens* SJ-19a

The lipid A isolated from *A. liquefaciens* SJ-19a was subjected to high-energy CID-TOF/TOF-MS/MS. The structures of the detected product ions were deduced as previously described in the ESI-MS/MS studies of lipid A. High-energy CID-TOF/TOF-MS/MS of the anion at *m/z* 1716.2458 $LipA_1$ is illustrated in (Figure 3.4.2, Tables 3.1.2, and Scheme 3.1.2). Product ion scan of LipA1 formed the product ions at *m/z* 1688.2265, *m/z* 1488.0512, and *m/z* 1243.8398. The product ion at *m/z* 1688.2265 was assigned as [M_1-(C_2H_4)-H]$^-$ ion and it was created by the losses of a molecule of C_2H_4 (-28 Da) as part of the fatty acid chain located at O-3′. The product ion at *m/z* 1488.0512 was assigned as the [M_1-(C14:0)acid-H]$^-$ ion. It was created by the elimination of myristic acid form the branched fatty (C14:0(3-*O*-C14:0) acid acyl group located at O-3′ (-228 Da). The last product ion at *m/z* 1243.6 was assigned as [M_1-(C14:0) (3-*O*-C14:0))acid-H_2OH]$^-$ ion. It was formed by the consecutive losses of molecule of water and the branched fatty (C14:0(3-*O*-C14:0)) acid acyl group located at O-3′ (-454 Da).

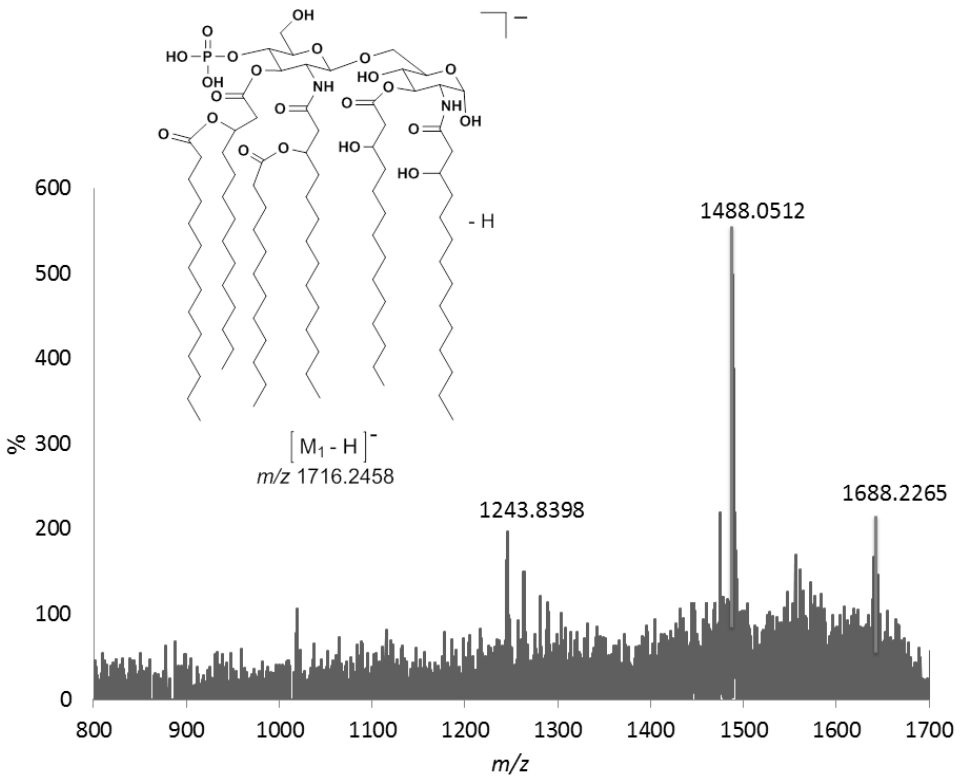

Figure 3.4.2: High-energy CID-TOF/TOF-MS/MS of the precursor ion $[M_1\text{-}H]^-$ ion at *m/z* 1716.2458.

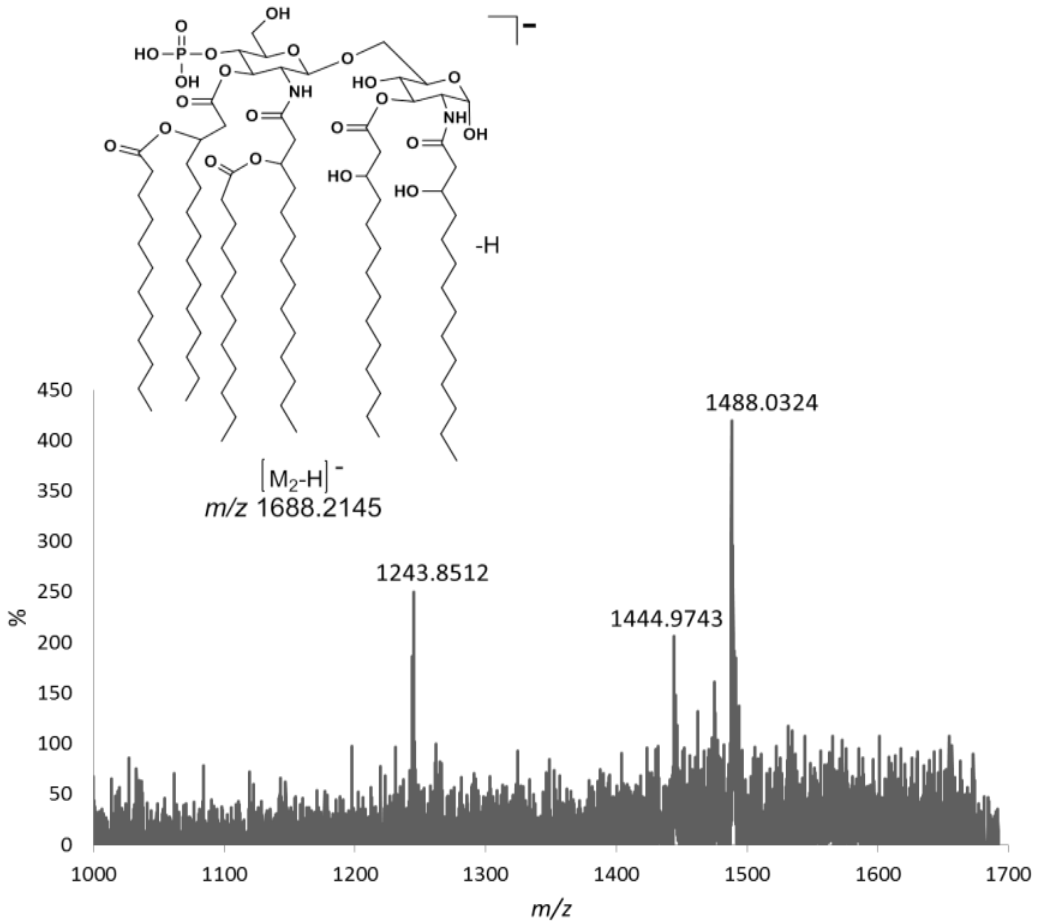

Figure 3.4.3: High-energy CID-TOF/TOF-MS/MS of the precursor ion $[M_2\text{-}H]^-$ ion at *m/z* 1688.2145.

High-energy CID-TOF/TOF-MS/MS of the anion at *m/z* 1688.2145 $LipA_2$ is illustrated in (Figure 3.4.3, Tables 3.1.3, and Scheme 3.1.3). Product ion scan of $LipA_2$ created the product ions at *m/z* 1488.0324, *m/z* 1444.9743, and *m/z* 1243.8512. The product ion at *m/z* 1488.0324 was assigned as the $[M_2$-(C12:0)acid-H$]^-$ ion. It was created by the elimination formed by elimination of lauric acid from the branch (Cl4:0(3-*O*-C12:0)) fatty acids (-200 Da), which was attached to the N-2′ position of the lipid A disaccharide backbone. Which was created by loss of a 3-hydroxyl myristic acid (-244 Da), it was located at O-3 position. The last product ion at *m/z* 1243.8512 was assigned as $[M_2$-(C14:0(3-*O*-C12:0))acid-H_2O-H$]^-$ ion. It was formed by the consecutive losses of a molecule of water and the myristic acid form the branched fatty (C14:0(3-*O*-C12:0)) acid acyl group located at O-3′ (-426 Da).

High-energy CID-TOF/TOF-MS/MS of the anion at *m/z* 1506.0574 $LipA_3$ is illustrated in (Figure 3.4.4, Tables 3.1.4, and Scheme 3.1.4). Product ion scan of $LipA_3$ formed the product ions at *m/z* 1261.8510, *m/z* 1243.8398, and *m/z* 1035.6597. The product ion at *m/z* 1261.8510 was assigned as the $[M_2$-(C14:0(3-OH))acid-H$]^-$ ion, which was created by the elimination of a 3-hydroxyl myristic acid (-244 Da), It was located at O-3 or O-3′ position. The product ion at *m/z* 1243.8398 was assigned as the $[M_2$-(C14:0(3-OH))acid-H_2O-H$]^-$ ion. It was created by the elimination of a molecule of water and a 3-hydroxyl myristic acid (-244 Da) molecule which was located at O-3 or O-3′ position. The product ion at *m/z* 1035.6597 was assigned as the $[M_2$-(C14:0(3-OH))acid-(C14:0)(3-OH))ketene-H$]^-$ ion. It was created by the elimination of a 3-hydroxyl myristic acid (-244 Da) and a 3-hydroxyl myristic ketene (-226 Da) which is located at O-3 and O-3′ position.

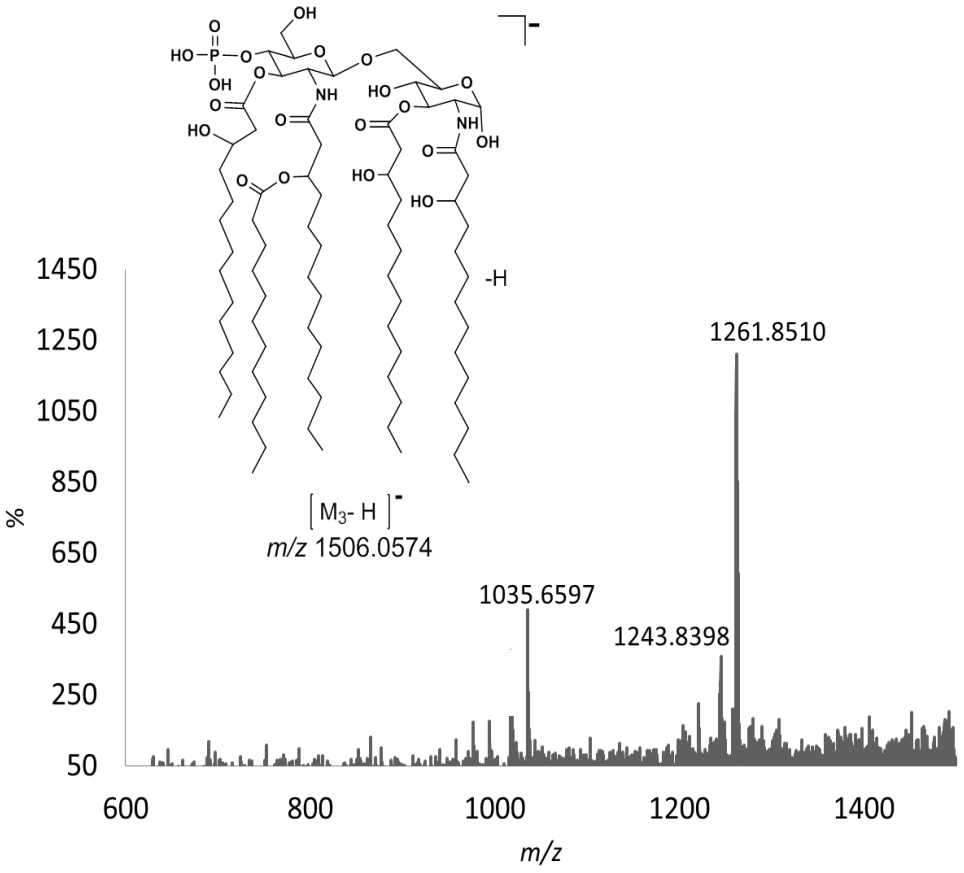

Figure 3.4.4: High-energy CID-TOF/TOF-MS/MS of the precursor ion $[M_3\text{-}H]^-$ ion at *m/z* 1506.0574.

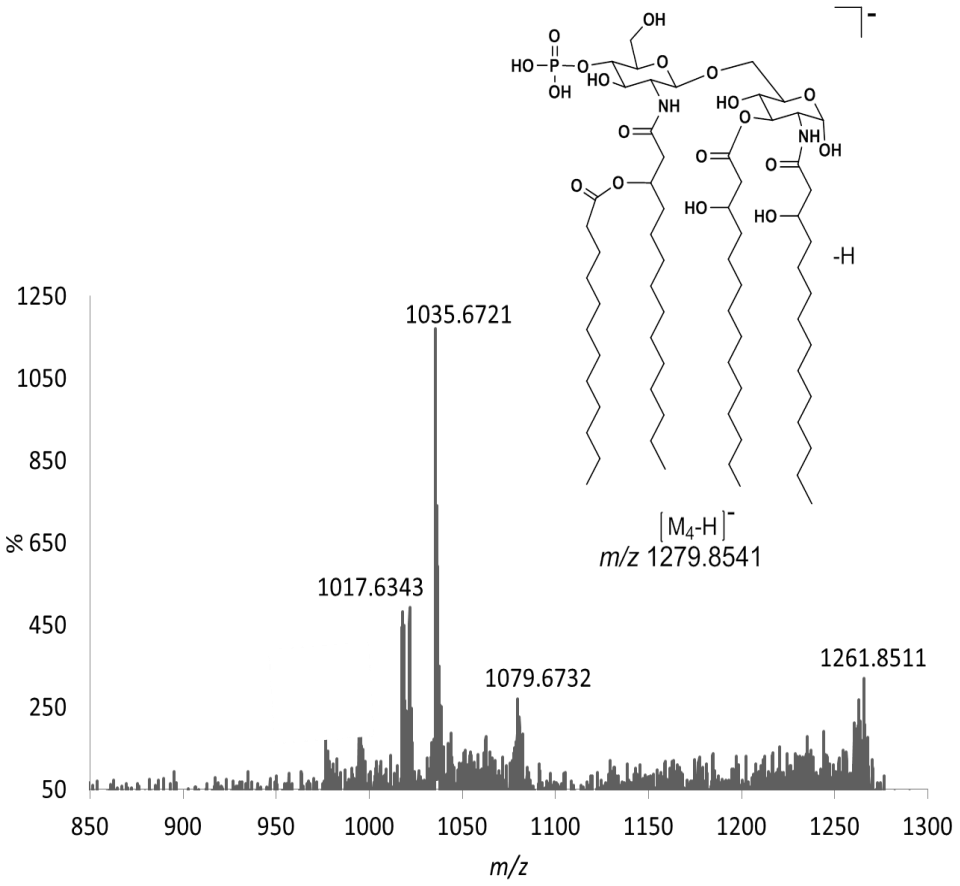

Figure 3.4.5: High-energy CID-TOF/TOF-MS/MS of the precursor ion $[M_4\text{-}H]^-$ ion at *m/z* 1279.8541.

High-energy CID-TOF/TOF-MS/MS of the anion at *m/z* 1279.8541 $LipA_4$ is illustrated in (Figure 3.4.5, Tables 3.1.5, and Scheme 3.1.5).

Product ion scan of $LipA_4$ formed the product ions at *m/z* 1261.8511, *m/z* 1079.6732, *m/z* 1035.6721, and *m/z* 1017.6343. The product ion at *m/z* 1261.8511 was created by the elimination of a molecule of water. The product ion at *m/z* 1079.6732 was assigned as the $[M_2$-(C12:0)acid-H$]^-$ ion; it was created by the elimination of lauric acid from the branch (Cl4:0(3-*O*-C12:0)) fatty acids (-200 Da) attached to the N-2′ position. The product ion at *m/z* 1035.6721 was assigned as the $[M_2$-(C14:0(3-OH))acid-H$]^-$ ion and was formed by elimination of a 3-hydroxyl myristic acid (-244 Da) located at O-3 position. The last secondary product ion at *m/z* 1017.6343 was obtained from the primary product ion at *m/z* 1035.7 by elimination of two molecules of water.

The product ion scan of $LipA_5$ at *m/z* 1097.6871 gave a series of product ions at *m/z* 853.4843 and *m/z* 527.2514 (Figure 3.4.6, Table 3.1.6, and Scheme 3.1.6). The product ion at *m/z* 853.4843 was assigned as the $[M_5$-(C14:0(3-OH))acid-H$]^-$ ion, which was created by the elimination of 3-hydroxy-myristic acid (C14:0(3-OH)) (-244Da), located at the position O-3 of the reducing GlcN end of the $lipidA_5$ disaccharide. The product ion at *m/z* 527.2514 was assigned to be formed by the $[^{0,4}A$-H$]^-$ cleavage of the reducing D-Glucosamine end as shown in (Figure 3.4.6). The primary ion at *m/z* 920.6234 assigned as [C-(C12:0)ketene-H$]^-$ gave the secondary product ions at *m/z* 808.5012 and *m/z* 710.4240. The product ion at *m/z* 808.5012 was assigned as [C-(C12:0)ketene-C_8H_{16}-H$]^-$ ion, which was created by the elimination of n-C_8H_{16} from the fatty acid located at O-3′ (-112 Da).

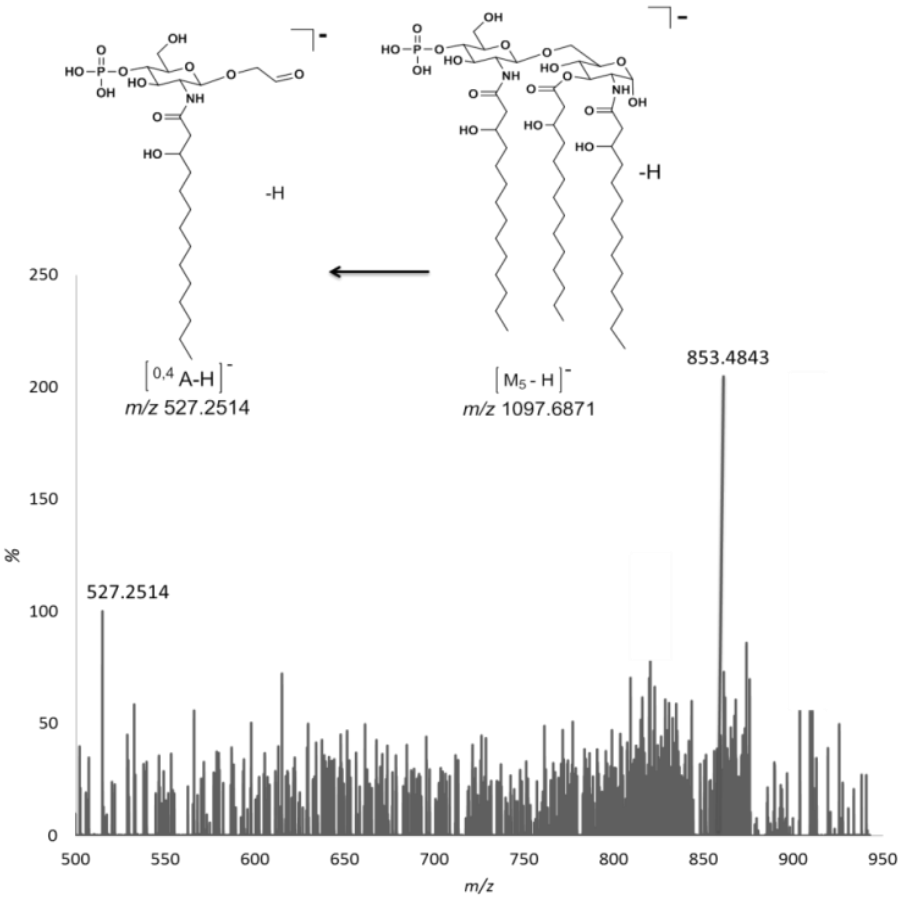

Figure 3.4.6: High-energy CID-TOF/TOF-MS/MS of the precursor ion $[M_5\text{-}H]^-$ ion at *m/z* 1097.6871.

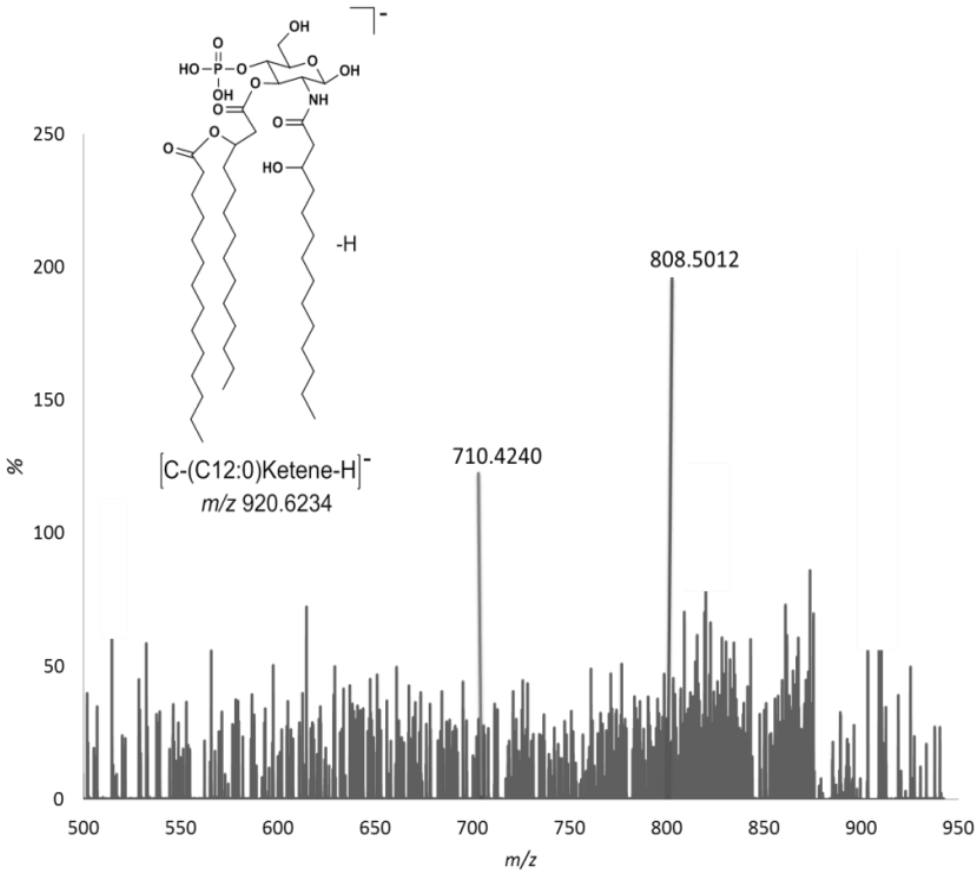

Figure 3.4.7: High-energy CID-TOF/TOF-MS/MS of the precursor ion [C-(C12:0)ketene-H]$^-$ ion at *m/z* 920.6234.

The product ion at *m/z* 710.4240 was assigned as [C-(C12:0)ketene-(C14:0)ketene-H]$^-$ ion and was created by the elimination of a molecule of myristic ketene (-210 Da) from the branched (C14(3-*O*-C14:0)) ester at the O-3′ position (Figure 3.4.7).

3.4.2. Comparison between low-energy CID-QqQ-MS/MS and high-energy CID-TOF/TOF-MS/MS

A quick comparison between the MALDI-CID-TOF/TOF-MS/MS and the ESI-CID-QqQ-MS/MS analysis indicate that the formation of distinctive product ions have decreased with MALDI-CID-TOF/TOF analysis. We have noticed that all the of the product ions which obtained from MALDI-CID-TOF/TOF just like SORI-CID-MS/MS were produced by the primary fatty acid fragmentation not the branched, most of the time the elimination occur at O-3 and O-3´ position (Schemes 3.1.2-3.1.8 and Tables 3.1.2 - 3.1.8). It is well known that high-energy CID-TOF/TOF-MS/MS experiments occur in the collision chamber having low gas pressure and subsequently leads to only single or few collisions. In addition, the high kinetic energy of the ions leads to shorter time scale for dissociation (few microseconds). However, in low-energy CID-QqQ-MS/MS analysis the target gas pressure selected allow multiple (tens to hundreds) collisions. Furthermore, when low-energy CID-QqQ-MS/MS analysis is used, the collisions occur in a longer time scale and the product ions have time to collide, gain energy, and to further fragment, before been accelerated through the q (McLuckey *et al*., 1997 and Sleno *et al*., 2004).

3.5. Summary.

The lipid A isolated from the LPS of *A. Liquefactions* SJ-19a which was grown in presence of phage and was assessed to be phage resistant. This lipid A, when analyzed by ESI- and MALDI-MS, afforded series of deprotonated molecules and fragment ions indicating that the lipid A analyte, was really a mixture of components composed of a series different lipid A_{1-5} molecules. The presence of this series of different lipid A_{1-5} molecules was attributed to the incomplete biosynthesis of the LPS due to the interaction with the phage during the growth of this Gram-negative bacterium. It should be stated that the ESI- and MALDI-MS (negative ion mode) afforded series of deprotonated molecules and fragment ions which were the identical when analyzed with different instruments such as ESI-QqQ-MS, ESI-FTICR-MS, and MALDI-TOF/TOF-MS (Please note that MALDI did not contain *m/z* 893 and *m/z* 666). In ESI-QqQ-MS, we have assigned these fragment ions as the series of $[M_n\text{-}H]^-$ deprotonated mono-phosphorylated molecules, represented as the following individual lipid A of this series (mixture), namely: $LipA_1$ at *m/z* 1716.30, $LipA_2$ at *m/z* 1688.19, $LipA_3$ at *m/z* 1506.10, $LipA_4$ at *m/z* 1279.73, $LipA_5$ at *m/z* 1097.63, *m/z* 892.56 and *m/z* 666.06. It is important to mention, that the structures of this series of incomplete biosynthesized lipid A obtained from LPS *Aeromonas Liquefaciens* SJ-19a (phage resistant), has not been characterized before this work.

In addition, the molecular structures of this heterogeneous mixture of lipid A_n were investigated by tandem mass spectrometry using low-energy collision SORI-CID-MS/MS (tandem in time) and CID-MS/MS (tandem in space) with the aforementioned instruments.

In this study, we have noticed that the SORI-MS/MS analysis of the various precursor deprotonated molecules were much simpler than those of the acquired CID-MS/MS with the high-energy MALDI-CID-TOF/TOF-MS/MS and low-energy CID-QqQ-MS/MS instruments.

The combined MS/MS studies indicate that all the proposed structures of the lipid A_1 to A_5 contained one phosphate group at the position O-4′. They were built by a (H_3PO_4→4-*O*-)-β-D-Glc*p*N-(1→6)-α-D-Glc*p*N disaccharide blueprint, substituted with (C14:0(3-OH)) at the N-2 and O-3 and contained different substitution permutations with (C14:0(3-*O*-12:0)) and (C14:0(3-*O*-14:0)) at the N-2´, and the O-3´ positions (Scheme 3.1.1).

In conclusion, the low-energy CID-QqQ-MS/MS, SORI-CID-FTICR-MS/MS and MALDI-CID-TOF/TOF-MS/MS, allowed to rationalize the different structures of the different lipid $A_{1\text{-}5.}$ These studies also allowed to elucidate the different structures of all diagnostic product ions and showed the presence of C-C heterolytic fragmentation of the fatty acid chains during these various gas-phase CID-fragmentations.

The presence of this series mixture of lipid A_n in the MS spectrum is good indicator to incomplete biosynthesis of lipid A. Also, the presence of the monosaccharide backbone was reported in all of them, such as the deprotonated molecules at *m/z* 892.56, *m/z* 920.62, and *m/z* 666.43.

As mentioned earlier in (Chapter 1, introduction section 1.1.1.3), lipid A structure plays a critical role in the bacteria infection. Bacteriophages interaction with the bacteria cell is complicated process which dose not always result in cell lysis. In this obtaiend series

of lipid A_n mixture, we have shown that the distribution of the various primary fatty acid chain length and the presence of phosphate groups were affected by this virus infection.

In conclusion, it is postulated that mutant LPS SJ-19a strain, obtained by bacteriophage infection of bacteria *A. Liquefactions* SJ-19a, afforded an LPS containing a lipid A, that has been due to the bacteriophages disruption in core biosynthesis process occurring at different stages.

Chapter 4

Mass Spectral analysis of the mixture of lipid A_n isolated from the LPS of *A. hydrophilla* SJ-55a

Aeromonas Hydrophilla is a genus Gram-negative, heterotrophic, aerobic and anaerobic belonging to the *Vibrionaceae* families. This bacterium infects fish in both, warm-water and cold-water fishes, and causes ulcers, tail rot, fin rot, and hemorrhagic septicemia (Michon *et al.,* 1984, and Banoub *et al.,* 1983).

The LPS of SJ-55a was obtained from the rough mutant Gram-negative bacteria *Aeromonas Hydrophilla* grown in the presence of phage, and it was classified as phage resistant as previously described in Chapters 2 and 3.

The following sections discuss the various mass spectrometric analyses that were used for the structural investigation of the complex $lipid_n$ mixture.

4.1. Gas chromatography-mass spectrometry (GC-MS) of the fatty methyl ester released from the lipid A_n mixture isolated from the LPS of the *A. hydrophilla* SJ-55a

The qualitative analysis of fatty acids was carried out by GC-MS to identify separately the amide and the ester-bound fatty acids. The (R)-3-hydroxytetradecanoic acid (C14:0(3-OH)) was identified as an amide-linked fatty acid, whereas the (R)-3-hydroxydodecanoic acid (C12:0(3-OH)) was identified as amide-linked fatty acids (Perry *et al*., 1979, Rebeil *et al*., 2004, and Lukasieweicz *et al*., 2006). In addition to the methyl

ester derivative of 3-methoxytetradecanoic acid, the fatty acid methyl esters obtained by trans-esterification with sodium methoxide also showed the presence of the (C14:0(3-OH)) acid, which was substituted by the tetradecanoic acid (C14:0) (myristic acid) in the native lipid A. Similarly, the (C12:0(3-OH)) acid was also shown to be substituted by myristic acid. The absolute configuration of the GlcN residues in lipid A was determined as D on the deacylated, dephosphorylated lipid A fraction, using (R)-2-butanol. (M. Almostafa., *et al* 2016 and Lukasieweicz *et al*., 2006).

4.2. ESI-QqQ-MS analysis of the extracted mixture of lipid A_n isolated from the LPS of *A. hydrophilla* SJ-55a

The extracted mixture of the lipid A constituting portion of *A. hydrophilla* SJ-55a bacteria is composed of a complex mixture of many structurally-related components, which we presume are produced by the incomplete biosynthesis of this lipid A.

The ESI-QqQ-MS (- ion mode) of the lipid A_n (where n=1-8) mixture shows the presence of *inter-alia eleven* different fragment ions at *m/z* 1796.30, *m/z* 1716.15, *m/z* 1688.26, *m/z* 1506.12, *m/z* 1359.75, *m/z* 1279.87, *m/z* 1097.64, *m/z* 1053.69, *m/z* 892.55, *m/z* 710.40 and *m/z* 666.37. This indicate the presence of a heterogeneous mixture of lipid A_n assigned by the $[M_n\text{-}H]^-$ molecules (Scheme.4.1.1.).

It is well known that structures of pure extract of lipid A contain two phosphate groups which are always located on the O-4′ and O-1 positions of the β-D-Glc*p*N-(1→6)-α-D-Glc*p*N disaccharide backbone of lipid A (Lukasiewicz *et al*., 2006, Lukasiewicz *et al*., 2010, John *et al*., 2014, Banoub *et al*., 2010, and Brodbelt *et al*., 2014).

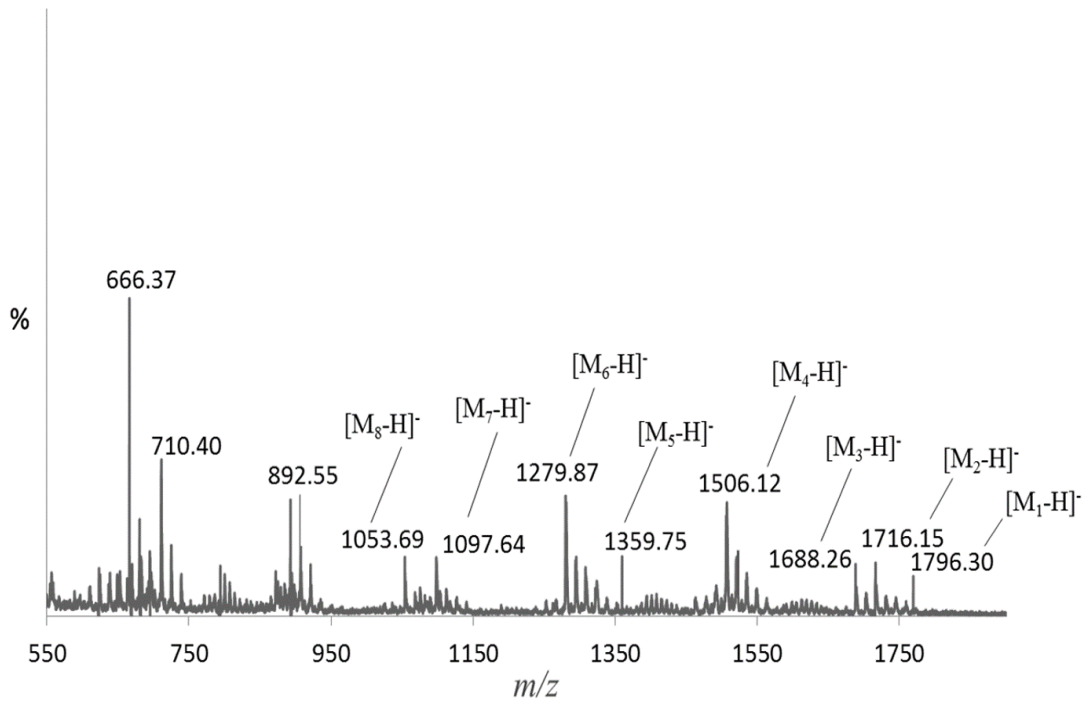

Figure 4.1.1: ESI-QqQ-MS of the native lipid A_n extract from the LPS of *A. hydrophilla* SJ-55a.

For this reason, the three deprotonated molecules $LipA_1$ at *m/z* 1796.30, $LipA_5$ at *m/z* 1359.75, and $LipA_7$ at *m/z* 1097.64 were also assigned as containing both di-phosphorylated groups at the O-1 and O-4 respectively and as such were specifically diagnostic for this mixture of lipid A_n (where n=1-8), obtained from the LPS SJ-55a. However, the remaining deprotonated molecules at *m/z* 1716.15, *m/z* 1688.26, *m/z* 1506.12, *m/z* 1279.87, *m/z* 1053.69, *m/z* 892.55, *m/z* 710.40 and *m/z* 666.37 are mono-phosphorylated molecules and were assigned as follows as following: $LipA_2$ at *m/z* 1716.15, $LipA_3$ at *m/z* 1688.26, $LipA_4$ at *m/z* 1506.12, $LipA_6$ at *m/z* 1279.87, and $LipA_8$ at *m/z* 1053.69 (Figure 4.1.1, Scheme 4.1.1, and Table 4.1.1). We also observed three deprotonated molecules at *m/z* 892.55, *m/z* 710.40, and *m/z* 666.37. These latter deprotonated molecules were recognized as the C-fragment ions at lower *m/z* values, which can be produced by the incomplete biosynthesis of the lipid A (Please understand, that these deprotonated molecules were named Fragment ions, to respect only the Domon and Costello nomenclature) (Domono and Cosetello 1988).

We have tentatively assigned that the putative structures of our lipid A_n mixtures contained 3-hydroxy-myristic acid (C14:0(3-OH)) fatty acid chains that acylate the various free positions of the β-D-Glc*p*N-(1→6)-α-D-Glc*p*N backbone of as the GlcN disaccharide. These 3-hydroxy-myristic acid (C14:0(3-OH)) fatty acid chains were attached to the O-3, O-3′, and N-2 positions of this lipid A. In addition, we presumed that the 3-hydroxy-lauric acid (C12:0(3-OH)) fatty acid chains, acylated the last free positions of the β-D-Glc*p*N-(1→6)-α-D-Glc*p*N backbone of the fully biosynthesized lipid A_n, which was definitely attached to the N-2′ positions of this lipid A. In this lipid A_n mixture, we have proposed that the one of the (C14:0(3-OH)) fatty acyl groups at O-3´could be substituted with

myristic acid as branched fatty acid (C14:0(3-*O*-C14:0)) (Scheme 4.1.1). The primary (C12:0(3-OH)) fatty acyl groups could be substituted with myristic acid as branched fatty acid (C12:0(3-*O*-C14:0)) located at N-2′ positions of the non-reducing end group of the β-D-Glc*p*N-(1→6)-α-D-Glc*p*N disaccharide backbone of this lipid A_n mixture (Scheme 4.1.1) (Lukasiewicz *et al*., 2006, Lukasiewicz *et al*., 2010, Banoub *et al*., 2010, Kilár *et al*., 2013, Brodbelt *et al*., 2014, and Almostafa *et al*., 2016). Based on these presumptions, we assigned the lipid A_n (where n=1-8) mixture as in the following:

The deprotonated molecule $[M_1\text{-H}]^-$ $LipA_1$ at *m/z* 1796.30 was assigned as the di-phosphorylated hexa-acylated completely biosynthetisized lipid A, which is composed of three primary 3-hydroxy-myristic acids (C14:0(3-OH)) fatty acids, one of which, can be substituted with myristic acid, forming the branched fatty acid (Cl4:0(3-*O*-C14:0)) located at the O-3′ position. In addition, we also presumed that the primary 3-hydroxy-lauric acid (C12:0(3-OH)) fatty acid chain, which was acylated with myristic acid, forming the branched fatty acid (Cl2:0(3-*O*-C14:0)) located at the N-2′ position of the non-reducing end group of the $LipA_1$ disaccharide backbone (Scheme 4.1.1) (El-Aneed *et al*., 2006, Lukasiewicz *et al*., 2006, Lukasiewicz *et al*., 2010, John *et al*., 2014, and Brodbelt *et al*., 2014).

Likewise, the deprotonated molecule $[M_2\text{-H}]^-$ $LipA_2$ at *m/z* 1716.15 was tentatively assigned as the mono-phosphorylated hexa-acylated GlcN disaccharide containing three primary 3-hydroxy-myristic acids (C14:0(3-OH)) fatty acids, in which one of them was substituted by myristic acid forming the branched fatty acids (Cl4:0(3-*O*-C14:0)) presumably located at the O-3′ position. In addition, the primary 3-hydroxy-lauric acid

(C12:0(3-OH)) fatty acid chain was acylated by myristic acid, forming the branched fatty acid (Cl2:0(3-*O*-C14:0)) located at the N-2′ position of the non-reducing end group of the $LipA_2$ disaccharide backbone (Scheme 4.1.1) (El-Aneed *et al*., 2006, Lukasiewicz *et al*., 2006, John *et al*., 2014, and Brodbelt *et al*., 2014).

The structure of deprotonated molecule $[M_3\text{-}H]^-$ of $LipA_3$ at *m/z* 1688.26 was tenatively assigned as been composed of a mono-phosphorylated hexaacylated GlcN disaccharide molecule. In that deprotonated molecule, we presume that the hexa-acylated was composed from three primary 3-hydroxy-myristic acids (C14:0(3-OH)) fatty acids, one of which, was substituted by lauric acid forming the branched fatty acid (Cl4:0(3-*O*-C12:0)) located on the O-3 position. We tentatively presumed that the primary 3-hydroxy-lauric acid (C12:0(3-OH)) fatty acid chain was substituted by myristic acid, forming the branched fatty acid (Cl2:0(3-*O*-C14:0)). This branched fatty acid substituent was located at the N-2′ position of the non-reducing end group of the $LipA_3$ disaccharide backbone (Scheme 4.1.1) (El-Aneed *et al*., 2006, Lukasiewicz *et al*., 2006, John *et al*., 2014, and Brodbelt *et al*., 2014).

The deprotonated molecules $LipA_4$ at *m/z* 1506.12 was assigned as the mono-phosphorylated pentaacylated form of the β-D-(1→6)-Glucosamine disaccharide carrying three primary 3-hydroxy-myristic acids (C14:0(3-OH)) fatty acids located at the O-3, N-2, O-3′ position. Whereas, the fourth primary 3-hydroxy-lauric acid (C12:0(3-OH)) fatty acid chains was substituted by myristic acid, forming the branched fatty acid (Cl2:0(3-*O*-C14:0)) located at the N-2′ of the non-reducing end residue of β-D-Glc*p*N-(1→6)-α-D-

Glc*p*N disaccharide of $LipA_4$ (Scheme 4.1.1) (El-Aneed *et al*., 2006, Lukasiewicz *et al*., 2006, John *et al*., 2014, and Brodbelt *et al*., 2014).

The deprotonated molecule of $LipA_5$ $[M_5\text{-H}]^-$ at *m/z* 1359.75 was assigned as containing a di-phosphorylated tri-acylated form of the β-D-Glc*p*N-(1→6)-α-D-Glc*p*N disaccharide, carrying two primary 3-hydroxy-myristic acids (C14:0(3-OH)) fatty acid groups acylating the t O-3 and N-2 position of the reducing end of the disaccharide. The third primary 3-hydroxy-lauric acid (C12:0(3-OH)) fatty acid chain was substituted by myristic acid, forming the branched fatty acid (Cl2:0(3-*O*-C14:0)); and this branched fatty acid acyl group was located at the N-2′ of the non-reducing end residue of β-D-Glc*p*N-(1→6)-α-D-Glc*p*N disaccharide of $LipA_5$ (Scheme 4.1.1).

While, the deprotonated molecule of $LipA_6$ $[M_6\text{-H}]^-$ at *m/z* 1279.87 was assigned as a mono-phosphorylated triacylated form of the β-D-Glc*p*N-(1→6)-α-D-Glc*p*N disaccharide, carrying two primary 3-hydroxy-myristic acid (C14:0(3-OH)) fatty acids located at O-3 and N-2 position of the reducing end of the disaccharide. It should be noted that a third primary fatty acid was identified as the 3-hydroxy-lauric acid (C12:0(3-OH)) fatty acid chain. This latter fatty acid was substituted by myristic acid, forming the branched fatty acid (Cl2:0(3-*O*-C14:0)) located at the N-2′ of the non-reducing end residue of β-D-Glc*p*N-(1→6)-α-D-Glc*p*N disaccharide of LipA6 (El-Aneed *et al*., 2006, Lukasiewicz *et al.*, 2006, John *et al*., 2014, and Brodbelt *et al*., 2014).

The deprotonated molecule of $LipA_7$ $[M_7\text{-H}]^-$ at *m/z* 1097.63 was assigned as containing a mono-phosphorylated tri-acylated form of the β-D-Glc*p*N-(1→6)-α-D-Glc*p*N disaccharide, carrying three primary 3-hydroxy-myristic acid (C14:0(3-OH)) fatty acid

located at N-2, O-3 position of the reducing end, and at N-2´position of the non-reducing end of the disaccharide β-D-Glc*p*N-(1→6)-α-D-Glc*p*N disaccharide.

The deprotonated molecule $[M_8\text{-}H]^-$ at *m/z* 1053.69 was assigned as $LipA_8$ mono-phosphorylated tri-acylated β-D-Glc*p*N-(1→6)-α-D-Glc*p*N disaccharide containing two 3-hydroxy-myristic acid (C14:0(3-OH)) fatty acids, which can be tentatively distributed on the N-2 and O-3 positions of this lipid A. The third primary 3-hydroxy-lauric acid (C12:0(3-OH)) fatty acid chain located at the N-2′ of the non-reducing end residue of β-D-Glc*p*N-(1→6)-α-D-Glc*p*N disaccharide (Scheme 4.1.1) (El-Aneed *et al*., 2006, Lukasiewicz *et al*., 2006, John *et al*., 2014, and Brodbelt *et al*., 2014).

In addition, we have also observed the deprotonated molecule at *m/z* 892.55 which was tentatively assigned as deprotonated $[C\text{-}(C14:0)ketene\text{-}H]^-$ molecule. This latter, contained a primary 3-hydroxy-myristic (C14:0(3-OH)) fatty acid, and another primary 3-hydroxy-lauric acid (C12:0(3-OH)) fatty acid chain, which was substituted by myristic acid, forming the branched fatty acid (Cl2:0(3-*O*-C14:0)) located at the N-2 (Scheme 4.1.1).

Another deprotonated molecule at *m/z* 710.40 was assigned as $[Y\text{-}H]^-$. This was recognized as the mono-phosphorylated D-GlcN species containing two 3-hydroxy-myristic acids (C14:0(3-OH)) fatty acids, which would be tentatively distributed on the O-3 and N-2.

Table 4.1.1: Assignments of the deprotonated molecules observed in ESI-QqQ-MS and ESI-FTICR-MS (- ion mode) of native mixture of lipid A_{1-8} extracted from the LPS of *A. hydrophilla* SJ-55.

Deprotonated Molecules	Empirical Formula	ESI-QqQ-MS		ESI-FTICR-MS		MALDI-TOF/TOF-MS	
		m/z Observed; Calculated (%)	δ ppm	*m/z* Observed; Calculated (%)	δ ppm	*m/z* Observed; Calculated (%)	δ ppm
$[M_1 -H]^-$	$C_{94}H_{177}N_2O_{25}P_2$	1796.30; 1796.21 (18.2)	50.8	1796.2228; 1796.2194 (10)	1.8	1796.2088; 1796.2121 (50)	-1.8
$[M_2 -H]^-$	$C_{94}H_{176}N_2O_{22}P$	1716.15; 1716.24 (27.5)	52.4	1716.2610; 1716.2458 (22.1)	8.8	1716.2569; 1716.2458 (70.3)	5.4
$[M_3-H]^-$	$C_{92}H_{172}N_2O_{21}P$	1688.26; 1688.21 (20.3)	29.6	1688.2253; 1688.2145 (23.4)	6.3	1688.2145; 1688.2145 (10)	4.4
$[M_4 -H]^-$	$C_{80}H_{150}N_2O_{21}P$	1506.12; 1506.05 (35.2)	53.1	1506.0530; 1506.0574 (80.3)	3.7	1506.0499;1506.0574 (14.3)	-4.9
$[M_5-H]^-$	$C_{66}H_{125}N_2O_{22}P_2$	1359.75; 1359.82 (30.9)	51.4	1359.8180; 1359.8205 (46.3)	1.8	1359.8615; 1359.8205 (14.5)	3
$[M_6-H]^-$	$C_{66}H_{124}N_2O_{19}P$	1279.87; 1279.85 (41)	15.6	1279.8489; 1279.8541 (85.5	4	1279.8432; 1279.8541 (45)	-3
$[M_7-H]^-$	$C_{52}H_{102}N_2O_{18}P$	1097.64; 1097.69 (28)	45.	1097.6930; 1097.6944 (40.2)	1.2	1097.6426; 1097.6944 (15	-4.7
$[M_8-H]^-$	$C_{52}H_{99}N_2O_{17}P$	1053.69; 1053.66 (29.4)	28.4	1053.6583; 1053.6609 (59.2)	2.4	-	-
$[C-(C14:0)ketene-H]^-$	$C_{46}H_{87}NO_{13}P$	892.55; 892.59 (55.8)	44.8	892.5979; 892.5993 (39.2)	1.5	-	-
$[Y-H]^-$	$C_{34}H_{65}NO_{12}P$	710.40; 710.42 (54.7)	28.1	710.4259; 710.425 (25.9)	1.2	-	-
$[C-(C14:0(3-O-C14:0))ketene-H]^-$	$C_{32}H_{61}NO_{11}P$	666.37; 666.39 (54.7)	30	666.4013; 666.3988 (54.7)	3.7	-	-

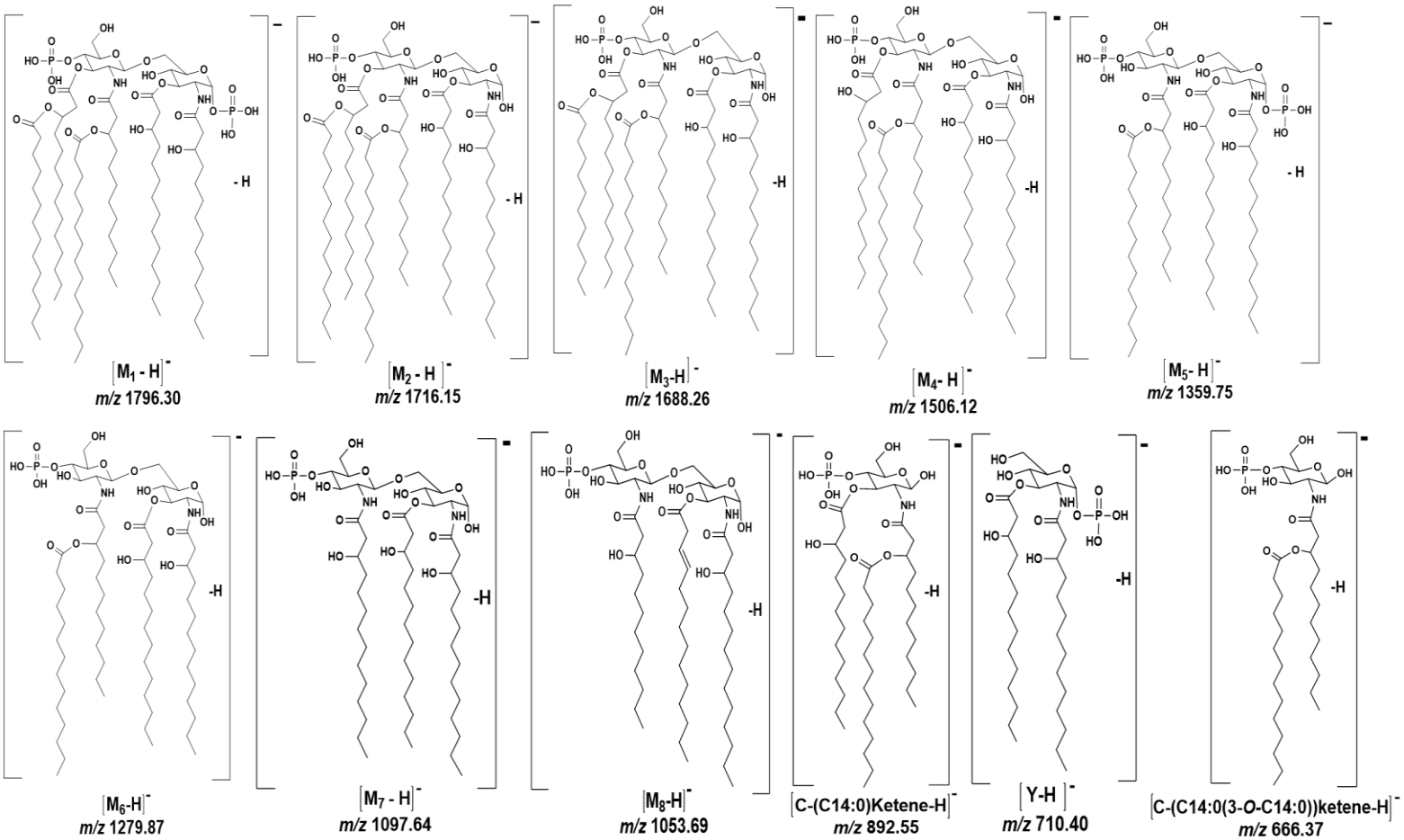

Scheme 4.1.1: Schematic representation of suggested structures of the deprotonated molecules of the lipid A_s mixture extracted from *A. hydrophilla* SJ-55a.

The last deprotonated molecule at *m/z* 666.37 was assigned as [C-(C14:0(3-*O*-C14:0))ketene-H]$^-$. This molecule was recognized as the mono-phosphorylated D-GlcN species, containing one branched (Cl2:0(3-*O*-C14:0)) fatty acyl group on the N-2 position (Scheme 4.1.1).

We presume that the formation of the C-fragment and Y-fragment ions at lower *m/z* values, are produced by the incomplete biosynthesis of the lipid A (El-Aneed *et al*., 2006, Lukasiewicz *et al*., 2006, John *et al*., 2014, and Brodbelt *et al*., 2014).

At this point of this study, we have tentatively identified a series of complete and incomplete O-3, O-3′, N-2 and N-2′ acylated the β-D-Glc*p*N-(1→6)-α-D-Glc*p*N disaccharide backbone of the lipid $A_{1\text{-}8}$ structures sharing common properties.

We have identified the presence of three primary hydroxytetradecanoic acids (C14:0(3-OH)) at N-2, O-3, and O-3′ position present on the β-D-Glc*p*N-(1→6)-α-D-Glc*p*N disaccharide backbone of this mixture of lipid$A_{1\text{-}8}$. The primary 3-hydroxy-myristic acids (C14:0(3-OH)) fatty acids can be acylated with myristic acyl groupss, forming the branched fatty acids (Cl4:0(3-*O*-C14:0)) located at the O-3′ position. In addition, we have also proposed that the primary 3-hydroxy-lauric (C12:0(3-OH)) fatty acid chain was acyalted with myristic acid, forming the branched fatty acid (Cl2:0(3-*O*-C14:0)) located at the N-2′. This series of lipid A_n was shown to contain either two and/or one phosphate groups.

The use of the low-energy collision dissociation tandem mass spectrometry analysis confirms our tentative assignments, and the putative structures for the eight deprotonated

molecules $LipA_1$ to $LipA_8$ and other fragment ions (El-Aneed *et al*., 2006, Lukasiewicz *et al*., 2006, John *et al*., 2014, and Brodbelt *et al*., 2014).

As previously described in this thesis we have used the Domon and Costello carbohydrate nomenclature to define and characterize all the deprotonated molecules; it was produced by their gas-phase fragmentation in the ESI-MS and CID-MS/MS analysis. (Domon and Costello, 1988).

4.2.1. Low-energy CID-MS/MS analysis of the extracted mixture of lipid A_n isolated from the LPS of *A. hydrophilla* SJ-55a using the QqQ-MS/MS instrument

The low-energy CID-MS/MS analysis were conducted using the triple quadrupole (QqQ) instrument (tandem-in-space) on the eight different precursor $[M-H]^-$ deprotonated molecules: at *m/z* 1796.30 ($LipA_1$), *m/z* 1716.15 ($LipA_2$), *m/z* 1688.26 ($LipA_3$), *m/z* 1506.12 ($LipA_4$), *m/z* 1359.75 ($LipA_5$), *m/z* 1279.87 ($LipA_6$), *m/z* 1097.64 ($LipA_7$), and *m/z* 1053.69 ($LipA_8$) (Figure 4.1.2). The product ion scans of these precursor molecules afforded series of distinct and diagnostic product ions, which were produced by competitive cleavages of the primary and/or secondary fatty esters located on β-D-Glc*p*N-(1→6)-α-D-Glc*p*N disaccharide backbone of lipid A.

As mentioned previously in section (3.1.2), it is well known that the ester-linked fatty groups at O-3 and O-3′ are more readily hydrolysable than the fatty acyl amide groups at N-2 and N-2′; in addition, the cleavages arising from the glycosidic bond are followed

by inter-ring bond cleavages (Lukasiewicz *et al*., 2006, Kilár *et al*., 2013, and Brodbelt *et al*., 2014).

The product ion scan of the deprotonated di-phosphorylated $LipA_1$ molecules at *m/z* 1796.30 allowed us to investigate the fatty acyl group distributions detected in ESI-QqQ-MS analysis of $LipA_1$, as shown in (Figure 4.1.2).

The CID-MS/MS of the deprotonated molecules at *m/z* 1796.30 produced the following series of product ions at *m/z* 1732.17, *m/z* 1532.96, *m/z* 1279.90, *m/z* 1097.65, and *m/z* 804.47 (Figure 4.1.2, Scheme 4.1.2 and Table 4.1.2). The product ions at *m/z* 1732.17 was assigned as the $[M_1\text{-}2(H_2O)\text{-}(C_2H_6)\text{-}H]^-$ ion and was formed by the consecutive losses of two molecules of water and a molecule of ethane (C_2H_6,-30 Da) as part of the fatty acid chain properly located at O-3′ of $LipA_1$. Likewise, the product ion at *m/z* 1532.96 was assigned as the $[M_1\text{-}2(H_2O)\text{-}(C14{:}0)acid\text{-}H]^-$ ion, which was created by the elimination of two molecules of water, and myristic acid forming the branched fatty (C14:0(3-*O*-C14:0) acid acyl group located at O-3′ (-228 Da). The product ion at *m/z* 1279.90 was formed form the precursor ion by consecutive loss of the branched fatty (C14:0(3-*O*-C14:0)) located at O-3′ position (-436 Da) and by the elimination of the neutral HPO_3 (-80 Da) moiety located at O-3´. This product ion was assigned as $[M_1\text{-}(C14{:}0(3\text{-}O\text{-}C14{:}0))ketene\text{-}HPO_3\text{-}H]^-$ ion. The product ion at *m/z* 1097.65 was formed form the precursor ion by elimination of a molecule of the branched fatty (C14:0(3-*O*-C14:0)) acid (-454 Da) from the O-3′ position, and followed by the elimination of the 3-hydroxyl myristic acid (-244 Da) from the O-3 position. This product ion was assigned as $[M_1\text{-}(C14{:}0(3\text{-}O\text{-}C14{:}0))acid\text{-}(C14{:}0(3\text{-}OH))acid\text{-}H]^-$ ion.

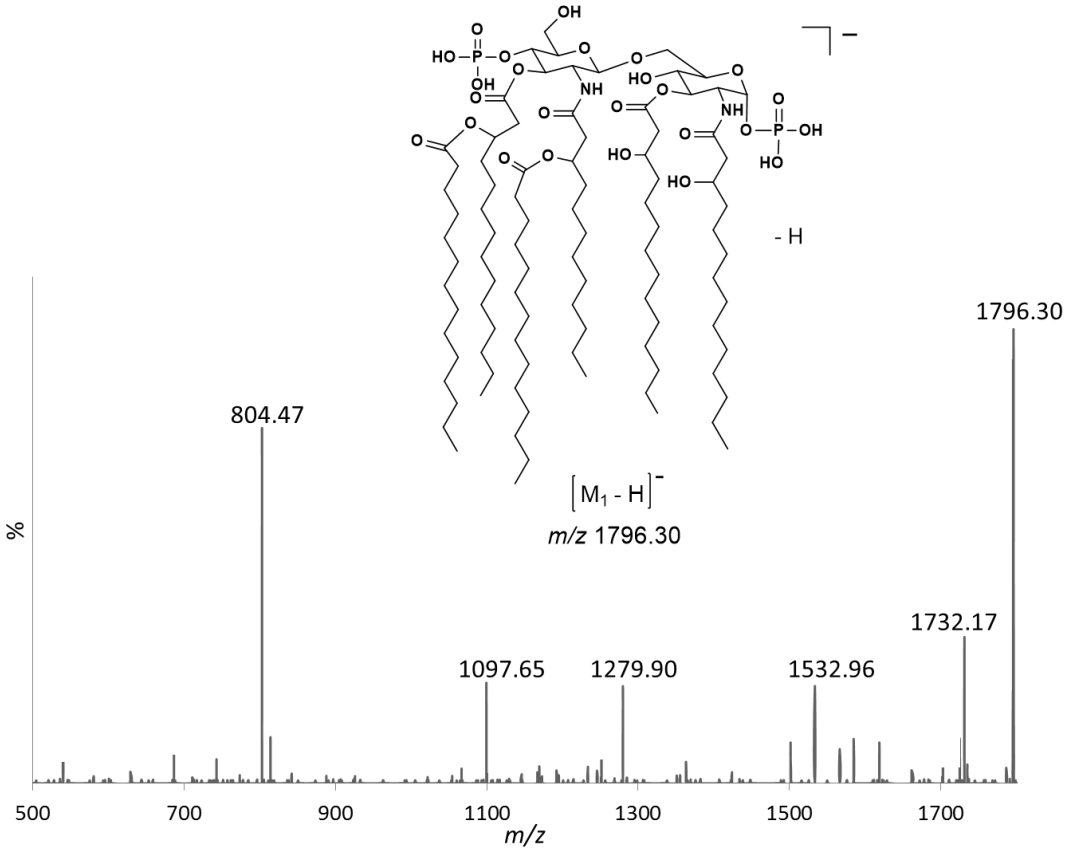

Figure 4.1.2: CID-MS/MS of the precursor deprotonated $[M_1\text{-}H]^-$ molecules at *m/z* 1796.30.*

* Please note, that some product ions were not assigned as these were produced by other isobars isolated during the MS/MS analysis.

Table 4.1.2: Assignments of the product ions observed from CID-MS/MS of the precursor deprotonated $[M_1\text{-}H]^-$ molecules at *m/z* 1796.30.

Product ions of the deprotonated molecules $[M_1\text{-}H]^-$ at *m/z* 1796.30				
Empirical formula	CID-QqQ-MS/MS		MALDI-TOF/TOF-MS/MS	
	Product Ion *m/z* Calculated; Observed (%)	δ ppm	Product Ion *m/z* Observed; Calculated (%)	δ ppm
$C_{92}H_{169}N_2O_{23}P_2$	1732.14; 1732.17 (28.6)	17.3	-	-
$C_{80}H_{145}N_2O_{21}P_2$	1532.98; 1532.96 (20.9)	-13	-	-
$C_{80}H_{150}N_2O_{21}P$	-	-	1506.0529; 1506.0574 (17)	-2.9
$C_{80}H_{148}N_2O_{20}P$	-	-	1488.0465; 1488.0439 (25.4)	-1.7
$C_{66}H_{124}N_2O_{19}P$	1279.85; 1279.90 (20.6)	39	1279.8498; 1279.8541 (16.6)	1.1
$C_{52}H_{96}N_2O_{18}P_2$	1097.68; 1097.65 (22.3)	-27	-	-
$C_{41}H_{75}NO_{12}P$	804.50; 804.47 (78.9)	-37.2	-	-

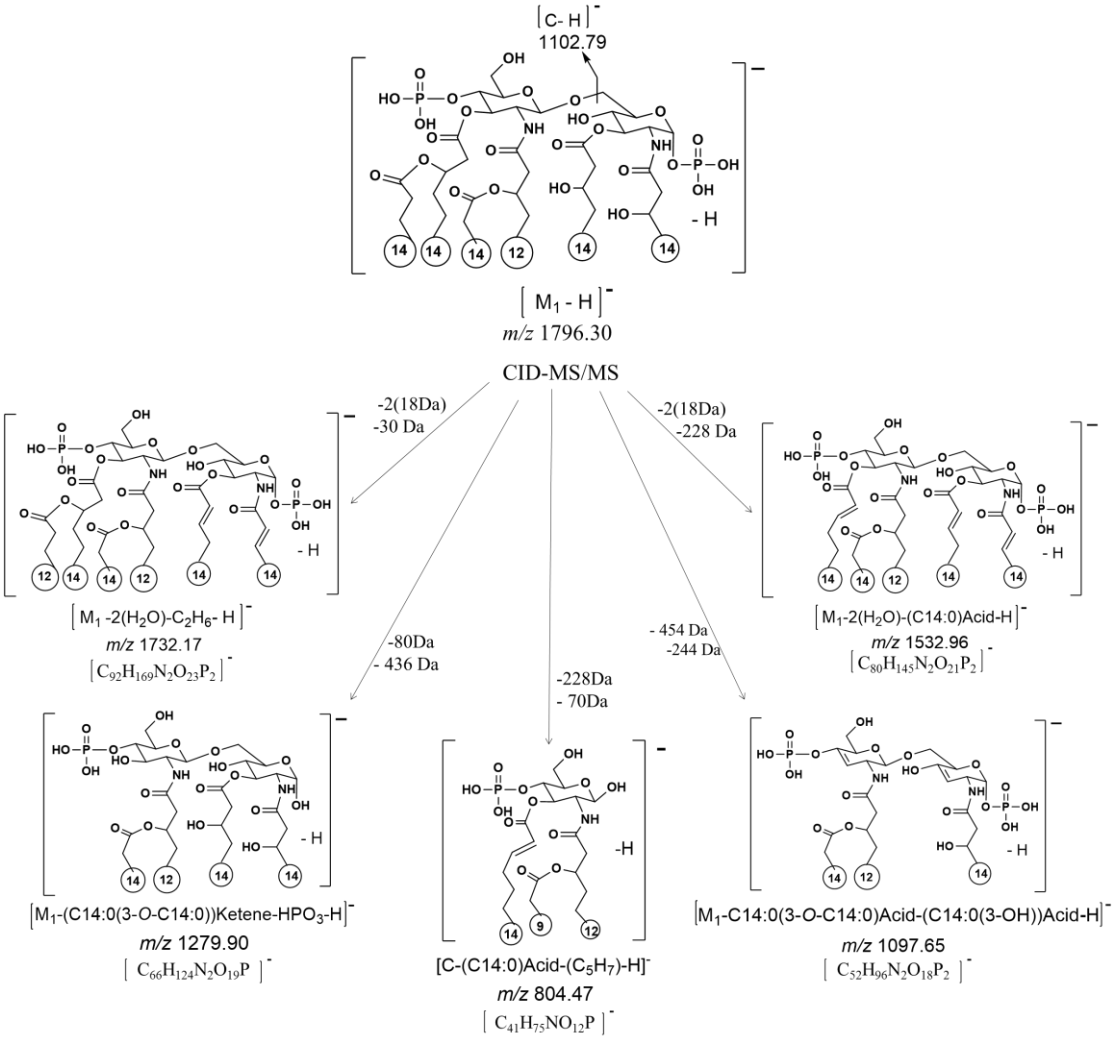

Scheme 4.1.2: Proposed fragmentation pathways obtained by CID-QqQ-MS/MS and SORI-CID-FTICR-MS/MS of the precursor deprotonated $[M_1–H]^-$ molecules at *m/z* 1796.30.

Finally, the product ion at *m/z* 804.47 was formed by the glycosidic cleavages of the β-D-Glc*p*N-(1→6)-α-D-Glc*p*N disaccharide backbone of the precursor deprotonated molecule to afford the reducing D-GlcN-OH species obtained, following consecutive losses of myristic (-228 Da) located at O-3 position and a molecule of C_5H_7 (-70 Da) as part of the fatty acid chain properly located at N-2. This products ion was assigned as [C-(C14:0)acid-(C_5H_7)-H]$^-$ ion. These results are indicating the presence of three molecules of 3-hydroxyl myristic acids at the positions O-3, O-3′ and N-2 of the disaccharide backbone, and a 3-hydroxy-lauric (C12:0(3-OH)) fatty acid chains located at the N-2′, whereas the branched (C14:0(3-*O*-C14:0)) fatty acids were located on O-3′ and N-2′ positions of the non-reducing end of the β-D-Glc*p*N-(1→6)-α-D-Glc*p*N disaccharide backbone of this lipid A_1.

The product ion scan of the deprotonated mono-phosphorylated $LipA_2$ molecules at *m/z* 1716.15 afforded the product ions *m/z* 1462.65, *m/z*1279.80, *m/z* 1035.68, and *m/z* 710.37 (Figure 4.1.3, Scheme 4.1.3, and Table 4.1.3). The product ions at *m/z* 1462.65 was assigned as the [M_2-(C14:0)ketene-C_3H_8-H]$^-$ ion. It was formed by the elimination of myristic acid from the branch (Cl4:0(3-*O*-C14:0)) fatty acids (-210 Da), which was attached to the O-3′ position, and the concomitant loss of molecule of C_3H_8 (-44 Da) as part of the fatty acid chain, properly located at O-3′ position of the β-D-Glc*p*N-(1→6)-α-D-Glc*p*N disaccharide backbone of the lipid A. The product ion at *m/z* 1279.80 was assigned as the [M_2-(C14:0(3-*O*-C14:0))ketene-H]$^-$ ion, which was formed by the elimination of myristic acid and the branched fatty (C14:0(3-*O*-14:0)) acid acyl group located at O-3′ (-436 Da).

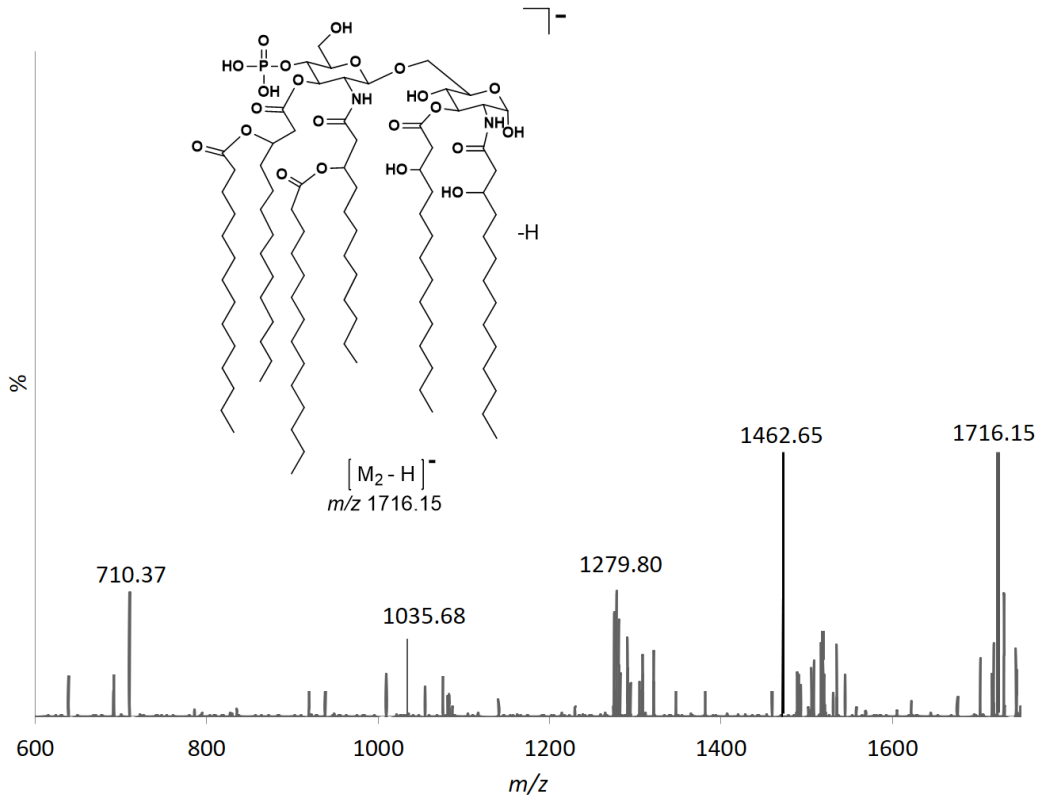

Figure 4.1.3: CID-MS/MS of the precursor deprotonated $[M_2\text{-}H]^-$ molecules at *m/z* 1716.15.*

* Please note, that some product ions were not assigned as these were produced by other isobars isolated during the MS/MS analysis.

Table 4.1.3: Assignments of the product ions observed from CID-MS/MS of the precursor deprotonated $[M_2\text{-}H]^-$ molecules at *m/z* 1716.15.

Product ions of the deprotonated molecules $[M_2\text{-}H]^-$ at *m/z* 1716.15						
Empirical Formula	**ESI-QqQ-MS/MS**		**ESI-FTICR-MS/MS**		**MALDI-TOF/TOF-MS/MS**	
	m/z **Observed; Calculated (%)**	**δ ppm**	***m/z*** **Observed; Calculated (%)**	**δ ppm**	***m/z*** **Observed; Calculated (%)**	**δ ppm**
$C_{80}H_{148}N_2O_{20}P$	-	-	1488.0465; 1488.0460 (29.4)	3.3	1488.0465; 1488.0234 (50)	-1.5
$C_{77}H_{143}N_2O_{21}P$	1462.65; 1462.99 (51.5)	-23.2	-	-	-	-
$C_{78}H_{145}N_2O_{19}P$	-	-	-	-	1444.9815; 1444.9687 (20.1)	-8.8
$C_{66}H_{124}N_2O_{19}P$	1279.87; 1279.80 (29.3)	-54.6	-	-	-	-
$C_{66}H_{120}N_2O_{17}P$	-	-	1243.8403; 1243.8380 (78.3)	-3.1	1243.8403; 1243.8512 (19.7)	-8.9
$C_{52}H_{96}N_2O_{16}P$	1035.65; 1035.68 (18.5)	28.9	1035.6581; 1035.6578 (30.6)	0.3	-	-
$C_{34}H_{66}NO_{12}P$	710.40; 710.37 (22.3)	-42.2	-	-	-	-

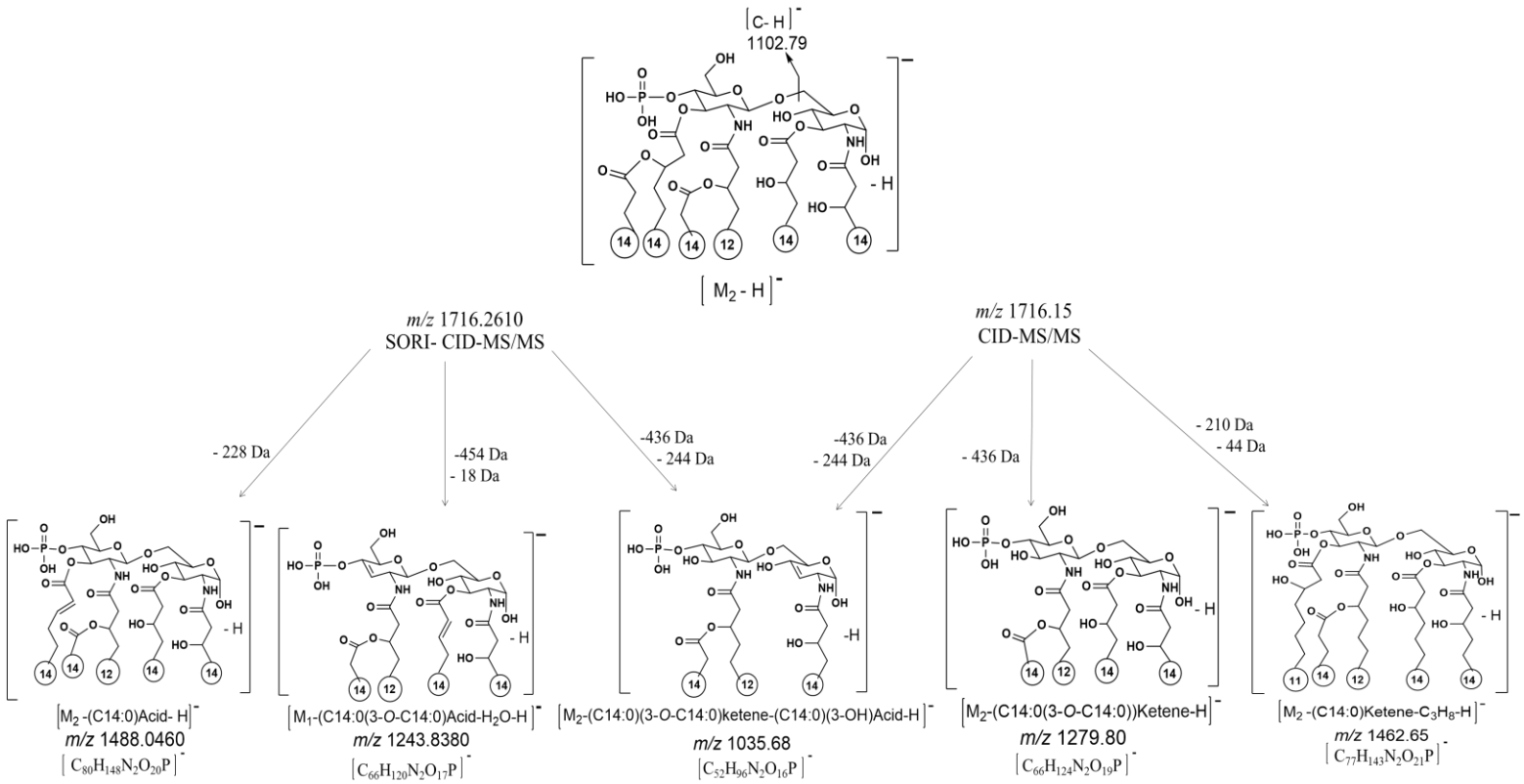

Scheme 4.1.3: Proposed fragmentation pathways obtained by CID-QqQ-MS/MS and SORI-CID-FTICR-MS/MS of the precursor deprotonated $[M_2\text{-}H]^-$ molecules at *m/z* 1716.15.

The product ion at *m/z* 1035.68 was formed by the elimination of a molecule of the branched fatty (C14:0(3-*O*-C14:0)) ketene (-436 Da) from the O-3′ position and by the loss of a 3-hydroxyl myristic acid (-244 Da) from O-3. This product ion was assigned as [M_2-(C14:0(3-*O*-C14:0))ketene-(C14:0(3-OH))acid-H]$^-$ ion, as shown in (Figure 4.1.3, Table 4.1.3, and Scheme 4.1.3). The product ion at *m/z* 710.37 was assigned as [Y-H]$^-$, and it was recognized as the mono-phosphorylated D-GlcN species containing two 3-hydroxy-myristic acid (C14:0(3-OH)) fatty acids, which would be tentatively distributed on the O-3 and N-2 (El-Aneed *et al*., 2006, Lukasiewicz *et al*., 2010, Kilár *et al*., 2013, and Brodbelt *et al*., 2014).

It is important to note that the obtained product ion scan of the deprotonated mono-phosphorylated $LipA_2$ molecules at *m/z* 1716.15 is completely different from the one obtained for the deprotonated molecule of $LipA_1$ isolated from the lipid A_n SJ-19a (Chapter 3). This indicated that both deprotonated molecules for *m/z* 1716 are indeed isobaric and have completely different structures.

This MS/MS studies supports our suggested structure assignment of the deprotonated molecule ($LipA_2$), and indicates that the H_2PO_3 group is located at the O-4′ position of the non-reducing end of the disaccharide backbone. It also confirms the position of the presence of two molecules of 3-hydroxyl myristic acids at the positions O-3, and N-2 of the reducing end of the GlcN disaccharide backbone, and a 3-hydroxy-lauric (C12:0(3-OH)) fatty acid acyl chain which was substituted by myristic acid, forming the branched fatty acids (Cl2:0(3-*O*-C14:0)) located at the N-2′. Whereas the branched (C14:0(3-*O*-

C14:0)) fatty acid appeared to be located on O-3′ positions of the non-reducing end of the β-D-Glc*p*N-(1→6)-α-D-Glc*p*N disaccharide backbone of this lipid A (El-Aneed *et al*., 2006, Lukasiewicz *et al*., 2006, John *et al*., 2014, and Brodbelt *et al*., 2014).

The product ion scan of the deprotonated mono-phosphorylated $LipA_3$ molecules at *m/z* 1688.26 afforded the product ions at *m/z* 1331.79, *m/z* 1243.80, and *m/z* 548.23 (Figure 4.1.4, Table 4.1.4 and Scheme 4.1.4). The product ion at *m/z* 1331.79 was assigned as the $[M_3\text{-(C12:0)acid-}(C_{11}H_{24})\text{-H}]^-$ ion, and it was generated by the eliminations of lauric acid (-200 Da) located at O-3, and the concomitant loss of molecule of $C_{11}H_{24}$ (-156 Da) as part of the fatty acid chain, properly located at N-2′ position of the β-D-Glc*p*N-(1→6)-α-D-Glc*p*N disaccharide backbone of the lipid A. (Figure 4.1.4).he product ion at *m/z* 1243.80 was assigned as $[M_3\text{-(C14:0(3-}O\text{-12:0)))acid-}H_2O\text{-H}]^-$ ion, and it was formed by consecutive losses of the branched fatty (C14:0(3-*O*-C12:0)) acid (-426 Da) located on position O-3′ and a molecule of water from the precursor ion at *m/z* 1688.26. The product ion of at *m/z* 548.23, assigned as $[\text{C-(C12:0)acid-(C14:0)acid-}(H_3PO_4)\text{-H}]^-$ ion; was formed by the consecutive losses of the branched fatty (C14:0(3-*O*-C12:0)) acid (-200 Da) located at the O-3′ position, myristic acid (-228 Da) from the branched fatty acids (C12:0(3-*O*-C14:0)) located on the N-2′ position, and the elimination of the neutral H_3PO_4 (-98 Da) moiety (Figure 4.1.4, Table 4.1.4, and Scheme 4.1.4). The structure of this product ion confirms the presence of the branched (C14:0(3-*O*-C12:0)) fatty acid ester group on the O-3′ position, and the presence of the branched (C12:0(3-*O*-C14:0)) fatty acid ester group on the N-2′ position (El-Aneed *et al*., 2006, Lukasiewicz *et al*., 2010, John *et al*., 2014, and Brodbelt *et al*., 2014).

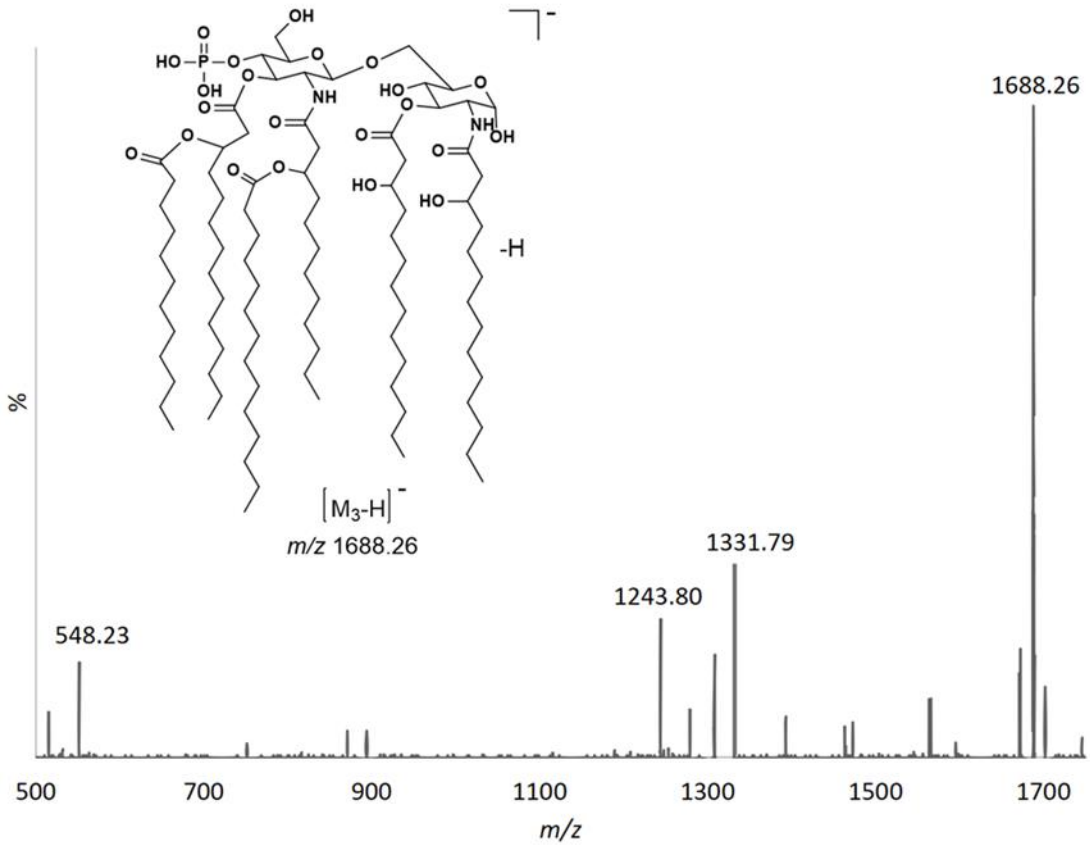

Figure 4.1.4: CID-MS/MS of the precursor deprotonated $[M_3\text{-}H]^-$ molecules at *m/z* 1688.26.*

* Please note, that some product ions were not assigned as these were produced by other isobars isolated during the MS/MS analysis.

Table 4.1.4: Assignments of the product ions observed from CID-MS/MS of the precursor deprotonated $[M_3\text{-}H]^-$ molecules at *m/z* 1688.26.

Product ions of the deprotonated molecules $[M_3\text{-}H]^-$ at *m/z* 1688.26						
Empirical Formula	**ESI-QqQ-MS/MS**		**ESI-FTICR-MS/MS**		**MALDI-TOF/TOF-MS/MS**	
	m/z **Observed; Calculated (%)**	**δ ppm**	***m/z*** **Observed; Calculated (%)**	**δ ppm**	***m/z*** **Observed; Calculated (%)**	**δ ppm**
$C_{86}H_{148}N_2O_{20}P$	-	-	1488.0379; 1488.0382 (42.3)	-0.2	1488.0379; 1488.0403 (45.3)	1.6
$C_{78}H_{145}N_2O_{19}P$	-	-	-	-	1444.9815; 1444.9765 (20.1)	-3.4
$C_{68}H_{126}N_2O_{19}P$	1331.79; 1331.86 (22.4)	-49.0	-	-	-	-6.1
$C_{66}H_{120}N_2O_{17}P$	-	-	-	-	1243.8430; 1243.8520 (26)	7.2
$C_{52}H_{96}N_2O_{16}P$	-	-	1035.6581; 1035.6577 (18.5)	-0.3	-	-
$C_{24}H_{43}NO_{11}P$	548.23; 548.40 (20.6)	-30.2	-	-	-	-

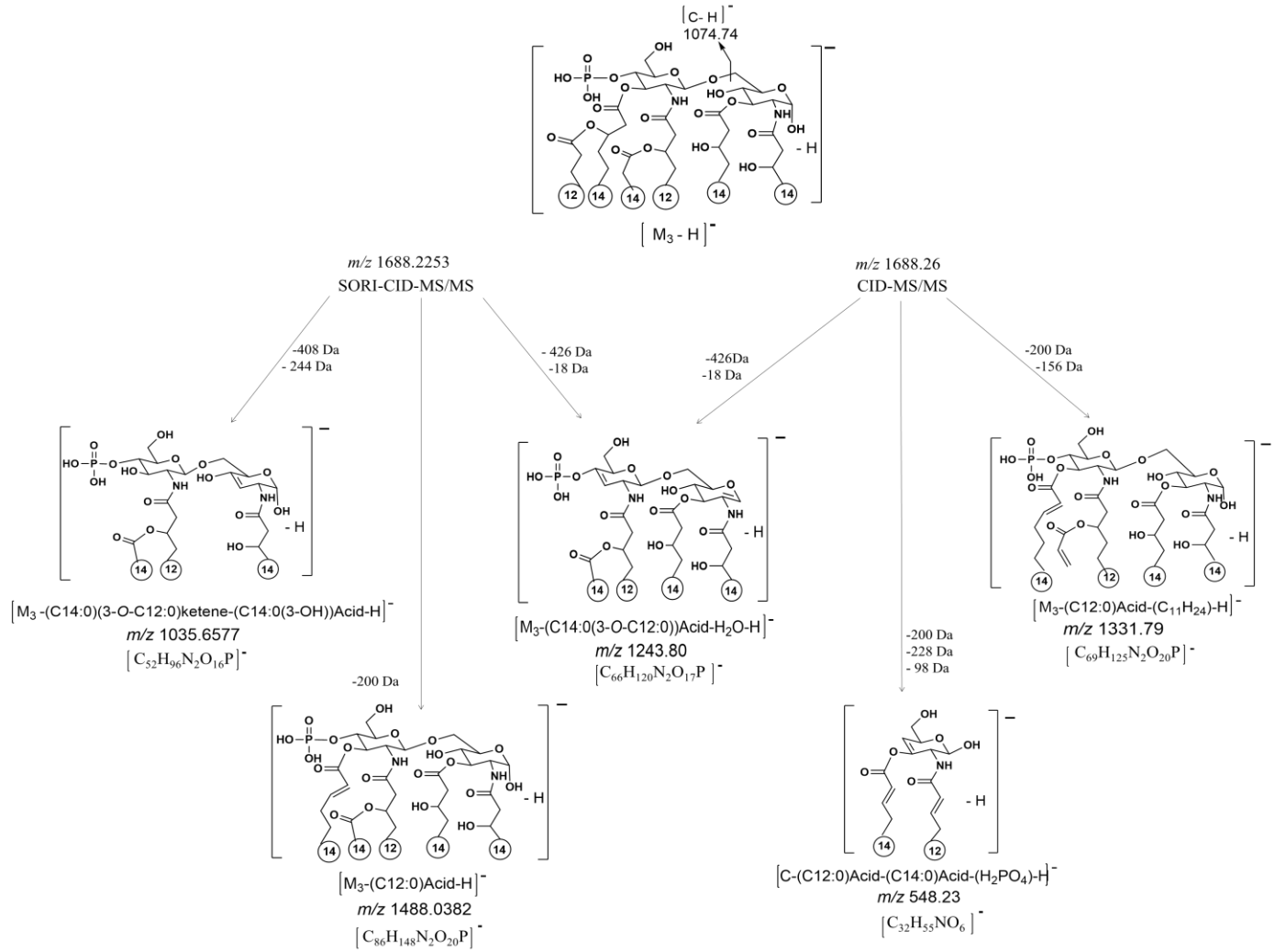

Scheme 4.1.4: Proposed fragmentation pathways obtained by CID-QqQ-MS/MS and SORI-CID-FTICR-MS/MS of the precursor deprotonated $[M_3\text{-}H]^-$ molecules at *m/z* 1688.26.

It is important to note that the obtained product ion scan of the deprotonated mono-phosphorylated $LipA_3$ molecules at *m/z* 1688.26 is completely different from the one obtained for the deprotonated molecule of $LipA_2$ isolated from the lipid A_n SJ-19a (Chapter 3). This indicated that both deprotonated molecules for *m/z* 1688 are indeed isobaric and have completely different structures.

The product ion scan of the deprotonated $LipA_4$ molecules at *m/z* 1506.12 gave the series of product ion at *m/z* 1261.81, *m/z* 1053.63, and *m/z* 690.36 (Figure 4.1.5, Table 4.1.5, and Scheme 4.1.5). The product ion at *m/z* 1261.81 was assigned as the $[M_4$-(C14:0(3-OH))acid-H$]^-$ ion, and was formed by the elimination of 3-hydroxy-myristic acid (C14:0(3-OH)) (-244 Da) located at the position O-3′. The product ion *m/z* 1053.63 was assigned as the $[M_4$-2(C14:0(3-OH))ketene-H$]^-$, and it was formed by the elimination of two of the 3-hydroxy-myristic ketene (C14:0(3-OH)) (-226 Da) located at the position O-3 and O-3′. The last product ion at *m/z* 690.36 was assigned as $[^{0,4}A$-(C14:0(3-OH))acid-H$]^-$ produced by cleavage of the non-reducing mono-phosphorylated D-Glucose residue, and it was formed by the loss of a 3-hydroxy-myristic ketene molecule (-244 Da) from the O-3 position. This latter product ion was indeed produced from the C-fragmentation routes described by Domon and Costello. It is initiated by glycosidic cleavages of the β-D-(l→6)-GlcN disaccharide (Domon and Costello, 1988).

It is important to note that the obtained product ion scan of the deprotonated mono-phosphorylated $LipA_4$ molecules at *m/z* 1506.12 is completely different from the one obtained for the deprotonated molecule of $LipA_3$ isolated from the lipid A_n SJ-19a (Chapter 3).

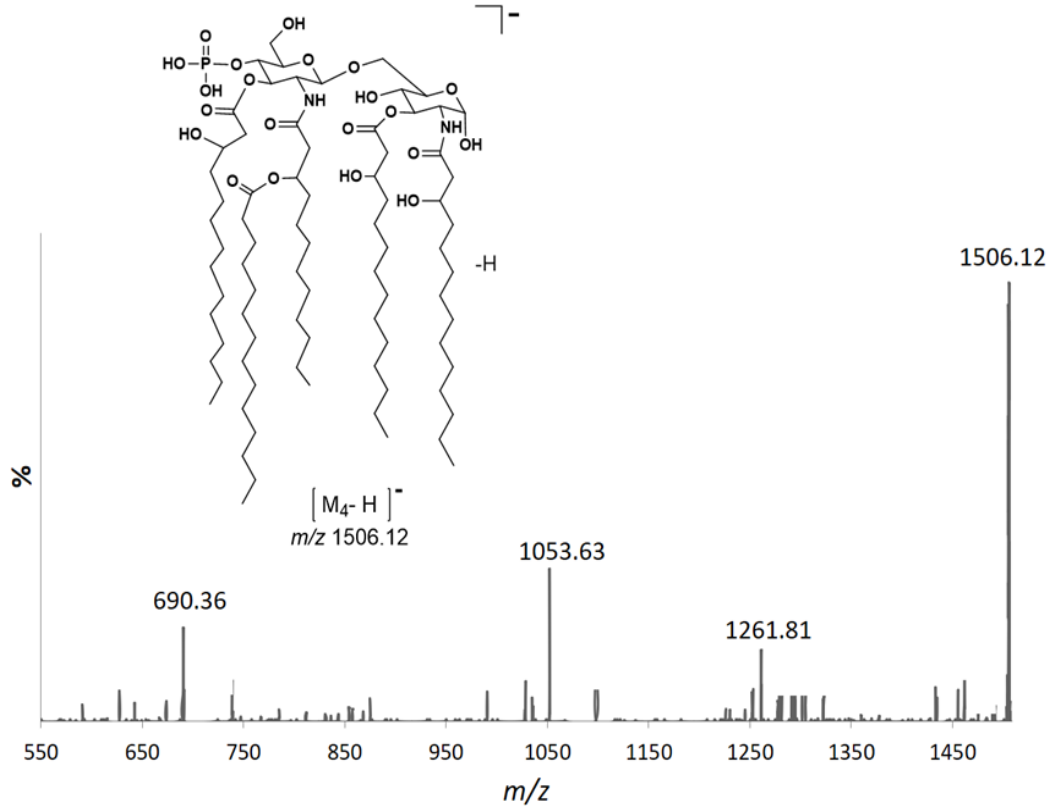

Figure 4.1.5: CID-MS/MS of the precursor deprotonated $[M_4\text{-}H]^-$ molecules at *m/z* 1506.12.∗

∗ Please note, that some product ions were not assigned as these were produced by other isobars isolated during the MS/MS analysis.

Table 4.1.5: Assignments of the product ions observed from CID-MS/MS of the precursor deprotonated $[M_4\text{-}H]^-$ molecules at *m/z* 1505.12.

Product ions of the deprotonated molecules $[M_4\text{-}H]^-$ at *m/z* 1506.12						
Empirical Formula	**ESI-QqQ-MS/MS**		**ESI-FTICR-MS/MS**		**MALDI-TOF/TOF-MS/MS**	
	m/z **Observed; Calculated (%)**	**δ ppm**	***m/z*** **Observed; Calculated (%)**	**δ ppm**	***m/z*** **Observed; Calculated (%)**	**δ ppm**
$C_{86}H_{148}N_2O_{20}P$	-	-	-	-	1488.0465; 1488.0420 (49.3)	-3
$C_{66}H_{122}N_2O_{18}P$	1261.84; 1261.81 (27	-23.7	1261.8436; 1261.8399 (91)	-2.9	1261.8436; 1261.8501 (150)	7.5
$C_{66}H_{120}N_2O_{17}P$	-	-	-	-	1243.8430; 1243.8511 (90)	-8.2
$C_{52}H_{99}N_2O_{17}P$	-	-	-	-	1035.6681; 1035.6614 (50)	-6.3
$C_{34}H_{62}NO_{11}P$	690.39; 690.36 (30)	-43.4	-	-	-	-

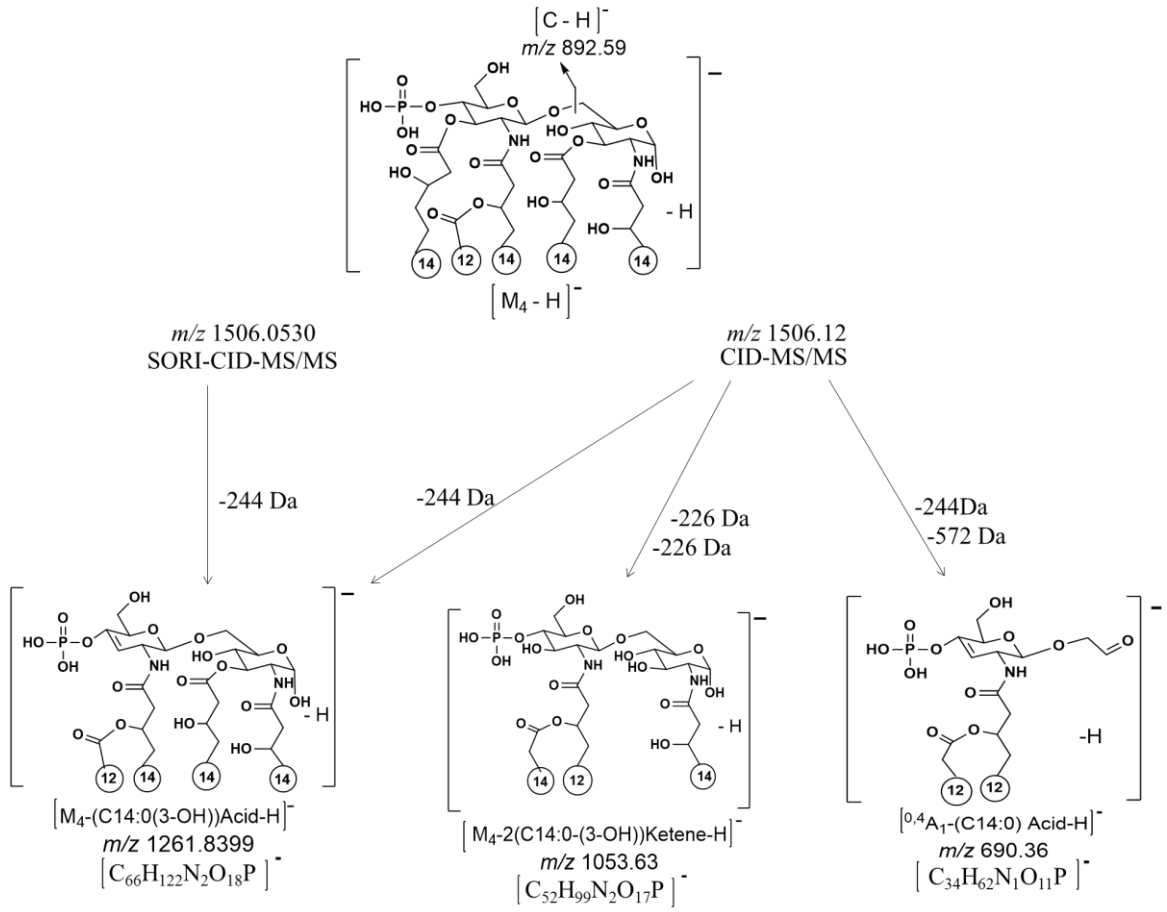

Scheme 4.1.5: Proposed fragmentation pathways obtained by CID-QqQ-MS/MS and SORI-CID-FTICR-MS/MS of the precursor deprotonated $[M_4\text{-}H]^-$ molecules at *m/z* 1506.12.

This indicated that both deprotonated molecules for *m/z* 1506 are indeed isobaric and have completely different structures.

The product ion scan of the deprotonated di-phosphorylated $LipA_5$ molecules $[M_5-H]^-$ at *m/z* 1359.75 gave a series of product ions at *m/z* 1209.75, *m/z* 1085.53, *m/z* 1000.55, *m/z* 953.50, and *m/z* 554.24 (Figure 4.1.6, Table 4.1.6 and Scheme 4.1.6). The product ion at *m/z* 1209.75 was assigned as $[M_5-HPO_3-(C_5H_{10})-H]^-$ ion. It was formed by the elimination of the neutral HPO_3 (-80 Da) moiety and a molecule of C_5H_{10} (-116 Da) as part of the fatty acid chain properly located at N-2′ position. The product ion at *m/z* 1085.53 was assigned as $[M_5-(C_{10}H_{20})-HPO_4-2H_2O-H]^-$ ion. It was formed by consecutive elimination of two molecules of water (-36 Da), a molecule of $C_{10}H_{20}$ (-140 Da) FROM the fatty acid chain located at O-3 position, and the elimination of the neutral H_3PO_4 (-98 Da) moiety. The product ion at *m/z* 1000.55 was assigned as $[M_5-HPO_3-(C14:0)ketene-(C_5H_{10})-H]^-$ ion. It was formed by the consecutive elimination of the neutral HPO_3 (-80 Da) moiety, the alkane (C_5H_{10}) (-70 Da) as part of the fatty acid chain located at O-3 position, and the myristic ketene (-208 Da) from the branched fatty (C12:0(3-*O*-14:0)) acid located on N-2′. The product ion at *m/z* 953.50 was assigned as $[M_5-HPO_3-(C12:0)acid-(C_7H_{16})-H]^-$ ion, and it was formed by consecutive elimination of the neutral HPO_3 (-80 Da) moiety, (C_7H_{16}) (-116 Da) as part of the fatty acid chain properly located at O-3 position, and the myristic acid (-226 Da) from the branched fatty (C12:0(3-*O*-14:0)) acid located on N-2′. The last product ion at *m/z* 554.24 was assigned as the $[C-(C_8H_{16})-H]^-$ ion, and it was formed by the elimination of the (C_8H_{16}) (-112 Da) as part of the fatty acid chain located at N-2 position.

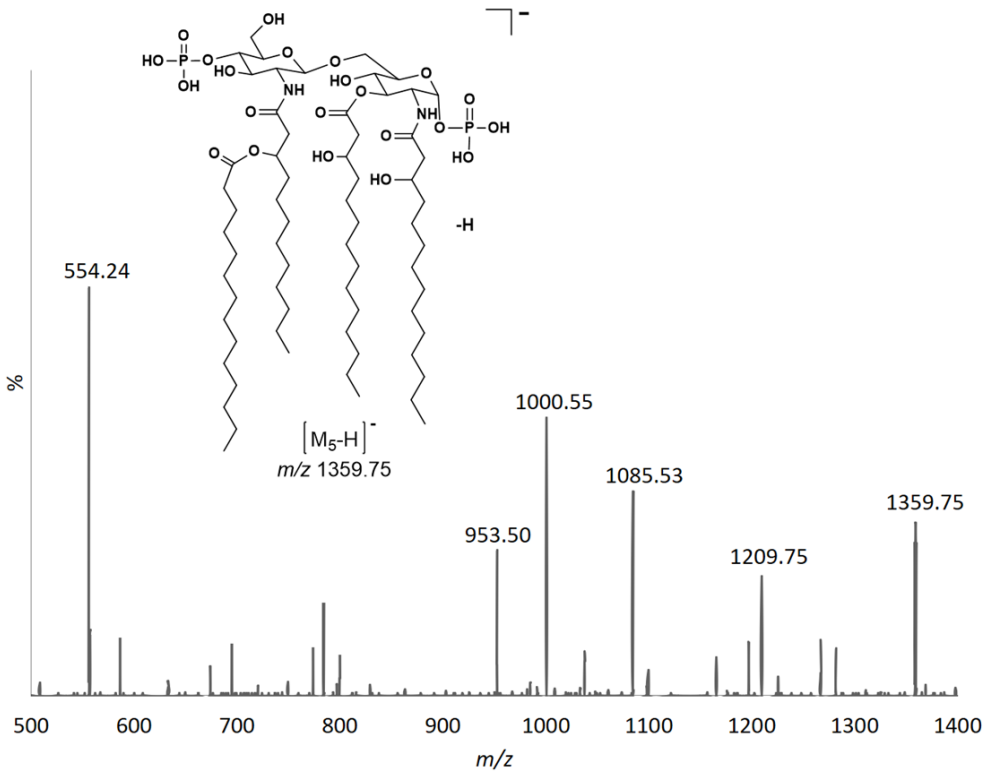

Figure 4.1.6: CID-MS/MS of the precursor deprotonated $[M_5\text{-}H]^-$ molecules at *m/z* 1359.75.⁕

⁕ Please note, that some product ions were not assigned as these were produced by other isobars isolated during the MS/MS analysis

Table 4.1.6: Assignments of the product ions observed from CID-MS/MS of the precursor deprotonated $[M_5\text{-}H]^-$ molecules at *m/z* 1359.75.

Product ions of the deprotonated molecules $[M_5\text{-}H]^-$ at *m/z* 1359.75						
Empirical Formula	**ESI-QqQ-MS/MS**		**ESI-FTICR-MS/MS**		**MALDI-TOF/TOF-MS/MS**	
	m/z **Observed; Calculated (%)**	**δ ppm**	***m/z*** **Observed; Calculated (%)**	**δ ppm**	***m/z*** **Observed; Calculated (%)**	**δ ppm**
$C_{66}H_{122}N_2O_{18}P$	-	-	1261.8027; 1261.8420 (13.1)	-1	1261.8436; 1261.8510 (20)	-5.8
$C_{61}H_{114}N_2O_{19}P$	1209.77; 1209.75 (20.3	-16	1261.8436; 1261.8399 (91)	-2.9	-	-
$C_{52}H_{97}N_2O_{19}P_2$	-	-	1115.6166; 1115.6120 (31)	-4.1	1115.6166; 1115.6097 (45)	-6.1
$C_{52}H_{91}N_2O_{19}P_2$	1085.56; 1085.53 (33.2)	-27.6	-	-	1085.5602; 1085.5630 (19.6)	2.5
$C_{52}H_{96}N_2O_{16}P$	-	-	1035.6681; 1035.6676 (38.2)	-0.4	-	-
$C_{52}H_{94}N_2O_{15}P$	-	-	1017.6397; 1017.6390 (68.5)	-22.9	-	-
$C_{47}H_{89}N_2O_{18}P$	1000.58; 1000.55 (48.9)	-29.9	-	-	-	-
$C_{45}H_{82}N_2O_{17}P$	953.53; 953.50 (25.3)	-31.4	-	-	-	-
$C_{24}H_{45}N_{211}P$	554.27; 554.24 (70.6)	54.1	-	-	-	-

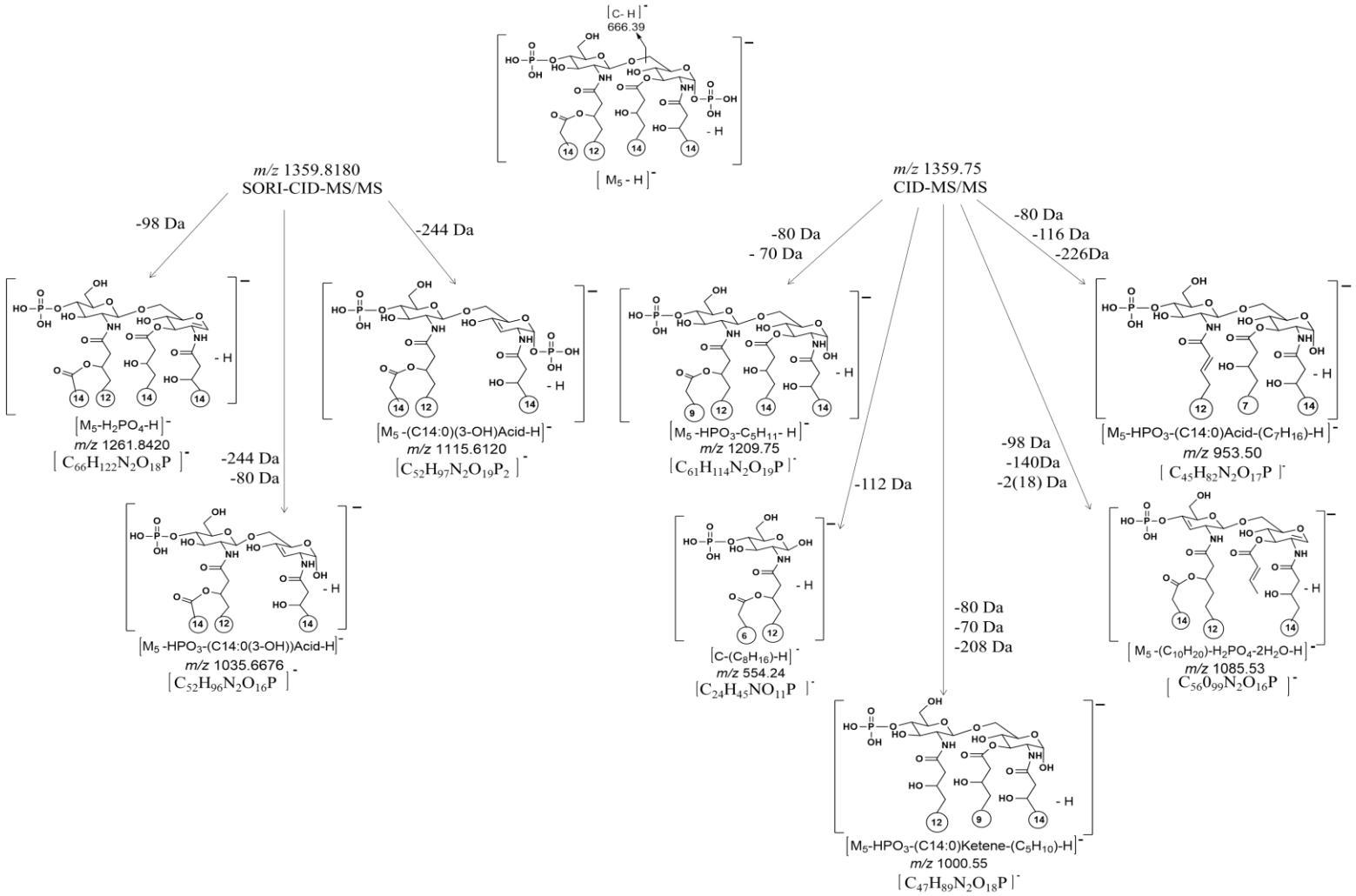

Scheme 4.1.6: Proposed fragmentation pathways obtained by CID-QqQ-MS/MS and SORI-CID-FTICR-MS/MS of the precursor deprotonated $[M_5\text{-}H]^-$ molecules at *m/z* 1359.75.

These findings support that our suggested $LipA_5$ structure contains two H_2PO_3 groups at the O-4′ and O-1 position of lipid A_5 (El-Aneed *et al*., 2006, Lukasiewicz *et al*., 2010, John *et al*., 2014, and Brodbelt *et al*., 2014).

The product ion scan of the deprotonated mono-phosphorylated $LipA_6$ molecules $[M_6\text{-}H]^-$ at *m/z* 1279.87 gave a series of product ions at *m/z* 1147.50 and *m/z* 1035.64. The product ion at *m/z* 1147.5 which was assigned as the $[M_6\text{-}C_8H_{17}\text{-}H_2O\text{-}H]^-$ ion. It was created by the elimination of the (C_8H_{17}) (-113 Da) as part of the fatty acid chain properly located at N-2´ position, and a molecule of water (Figure 4.1.7, Table 4.1.7 and Scheme 4.1.7). The product ion at *m/z* 1035.64 which was assigned as the $[M_6\text{-}(C14{:}0(3\text{-}OH))acid\text{-}H]^-$ ion. It was created by the elimination of 3-hydroxy-myristic acid (C14:0(3-OH)) (-244 Da) located at the position O-3 of the reducing GlcN end (Figure 4.1.7, Table 4.1.7 and Scheme 4.1.7) (El-Aneed *et al*., 2006, Lukasiewicz *et al*., 2010, John *et al*., 2014, and Brodbelt *et al*., 2014).

It is important to note that the obtained product ion scan of the deprotonated mono-phosphorylated $LipA_6$ molecules at *m/z* 1279.87 is completely different from the one obtained for the deprotonated molecule of $LipA_4$ isolated from the lipid A_n SJ-19a (Chapter 3). This indicated that both deprotonated molecules for *m/z* 1279 are indeed isobaric and have completely different structures.

The product ion scan of $LipA_7$ at *m/z* 1097.64 gave a series of product ions at *m/z* 1079.65, *m/z* 1023.59, *m/z* 961.34, and *m/z* 852.47 (Figure 4.1.8, Table 4.1.8, and Scheme 4.1.8). The product ion at *m/z* 1079.65 was created by the loss of a molecule of water. The product ion *m/z* 1023.59 was assigned as the $[M_7\text{-}(C_4H_{18})\text{-}H_2O\text{-}H]^-$ ion.

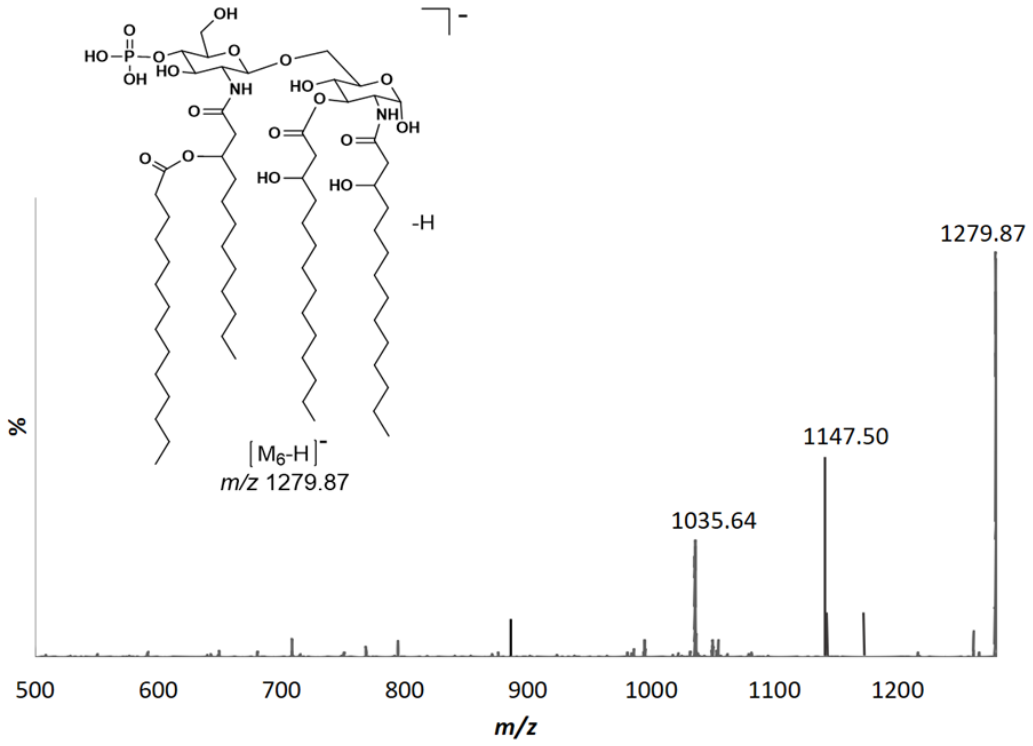

Figure 4.1.7: CID-MS/MS of the precursor deprotonate $[M_6\text{-}H]^-$ molecules at *m/z* 1279.87.⁕

⁕ Please note, that some product ions were not assigned as these were produced by other isobars isolated during the MS/MS analysis.

Table 4.1.7: Assignments of the product ions observed from CID-MS/MS of the precursor deprotonated $[M_6\text{-}H]^-$ molecules at *m/z* 1279.87.

Product ions of the deprotonated molecules $[M_6\text{-}H]^-$ at *m/z* 1279.87						
Empirical Formula	**ESI-QqQ-MS/MS**		**ESI-FTICR-MS/MS**		**MALDI-TOF/TOF-MS/MS**	
	m/z **Observed; Calculated (%)**	**δ ppm**	***m/z*** **Observed; Calculated (%)**	**δ ppm**	***m/z*** **Observed; Calculated (%)**	**δ ppm**
$C_{54}H_{100}N_2O_{17}P$	**1147.50;1147.71 (49.2)**	**-18.2**	**-**	**-**	**-**	**-**
$C_{52}H_{96}N_2O_{16}P$	**1035.66; 1035.64 (37)**	**-19.3**	**1035.6681; 1035.6678 (91.0)**	**-0.2**	**1035.6681; 1035.6598 (35)**	**-8**
$C_{42}H_{78}N_2O_{17}P$	**-**	**-**	**-**	**-**	**913.4989; 913.4996 (79)**	**8.3**
$C_{32}H_{61}NO_{11}P$	**-**	**-**	**-**	**-**	**666.3988; 666.3897 (55)**	**-13**

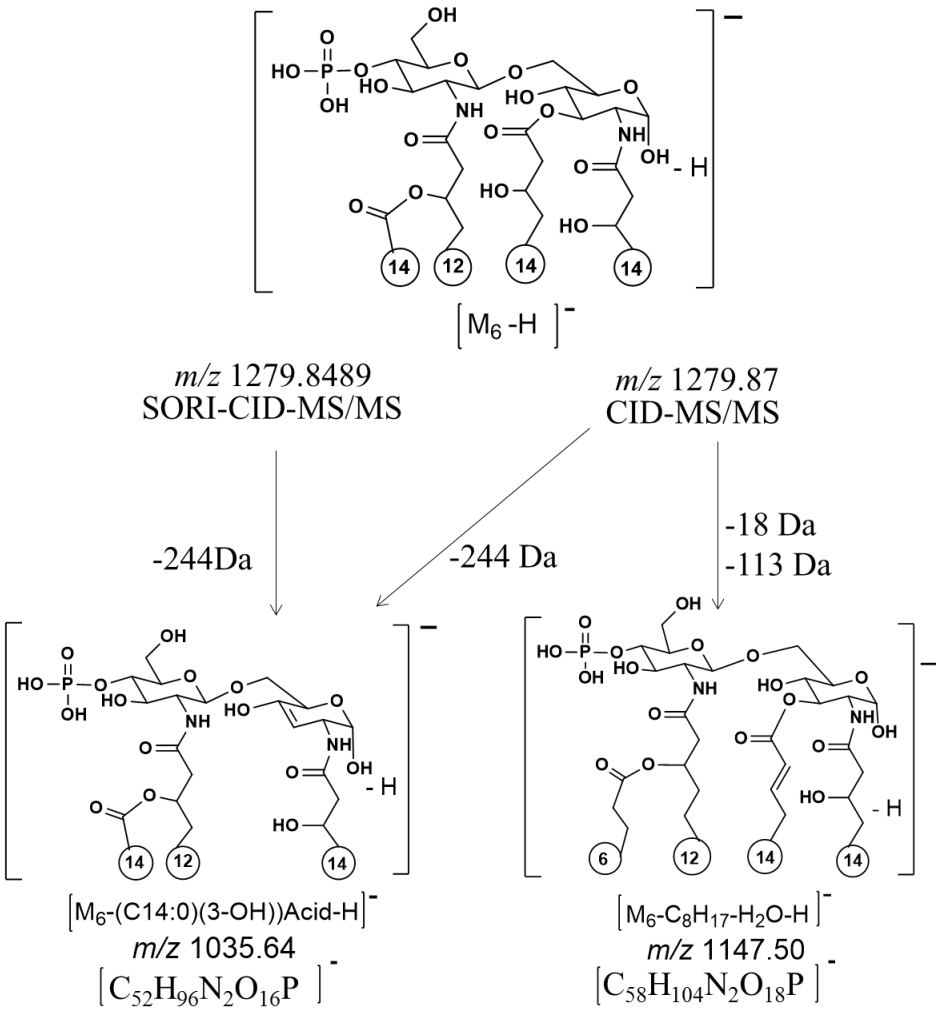

Scheme 4.1.7: Proposed fragmentation pathways obtained by CID-QqQ-MS/MS and SORI-CID-FTICR-MS/MS of the precursor deprotonated $[M_6\text{-H}]^-$ molecules at *m/z* 1279.87.

It was created by the eliminations of nC_4H_8 (-56 Da) as part of the fatty acid chain located at O-3, and a molecule of water (-18 Da). The product ion *m/z* 961.34 was assigned as the $[M_7\text{-}(C_7H_{16})\text{-}2H_2O\text{-}H]^-$ ion. It was created by the eliminations of a molecule of nC_7H_{16} (-100 Da) as part of the fatty acid chain located at O-3, and two molecules of water (-36 Da). The product ion at *m/z* 852.48 was assigned as the $[M_7\text{-}(C14{:}0(3\text{-}OH))\ acid\text{-}H]^-$ ion, which was created by the elimination of a myristic acid (C14:0(3-OH)) (-244 Da) located at the position O-3 of the reducing GlcN end of the $LipA_7$ disaccharide (El-Aneed *et al*., 2006, Lukasiewicz *et al*., 2010, and Brodbelt *et al*., 2014).

It is important to note that the obtained product ion scan of the deprotonated di-phosphorylated $LipA_7$ molecules at *m/z* 1097.64 is completely different from the one obtained for the deprotonated molecule of $LipA_5$ isolated from the lipid A_n SJ-19a (Chapter 3). This indicated that both deprotonated molecules for *m/z* 1097 are indeed isobaric and have completely different structures.

The product ion scan of $LipA_8$ at *m/z* 1053.69 gave a series of product ions at *m/z* 843.45, *m/z* 763.48, and *m/z* 648.36 (Figure 4.1.9, Table 4.1.9, and Scheme 4.1.9). The product ion at *m/z* 843.45 was assigned as the $[M_8\text{-}(C14{:}0))ketene\text{-}H]^-$ ion. It was formed by the elimination of the myristic ketene (-210 Da) from the branch (Cl2:0(3-*O*-C14:0)) fatty acids which was attached to the N-2′ position. The product ion at *m/z* 763.48 was assigned as the $[M_8\text{-}(C14{:}0)keten\text{-}HPO_3\text{-}H]^-$ ion, and it was created by the consecutive losses of myristic ketene molecule (-210 Da) from the branched (C12:0(3-*O*-C14:0)) fatty acid at the N-2´ position, and HPO_3 (-80 Da) released from the O-4′ position of the D-GlcN non-reducing end of $LipA_8$.

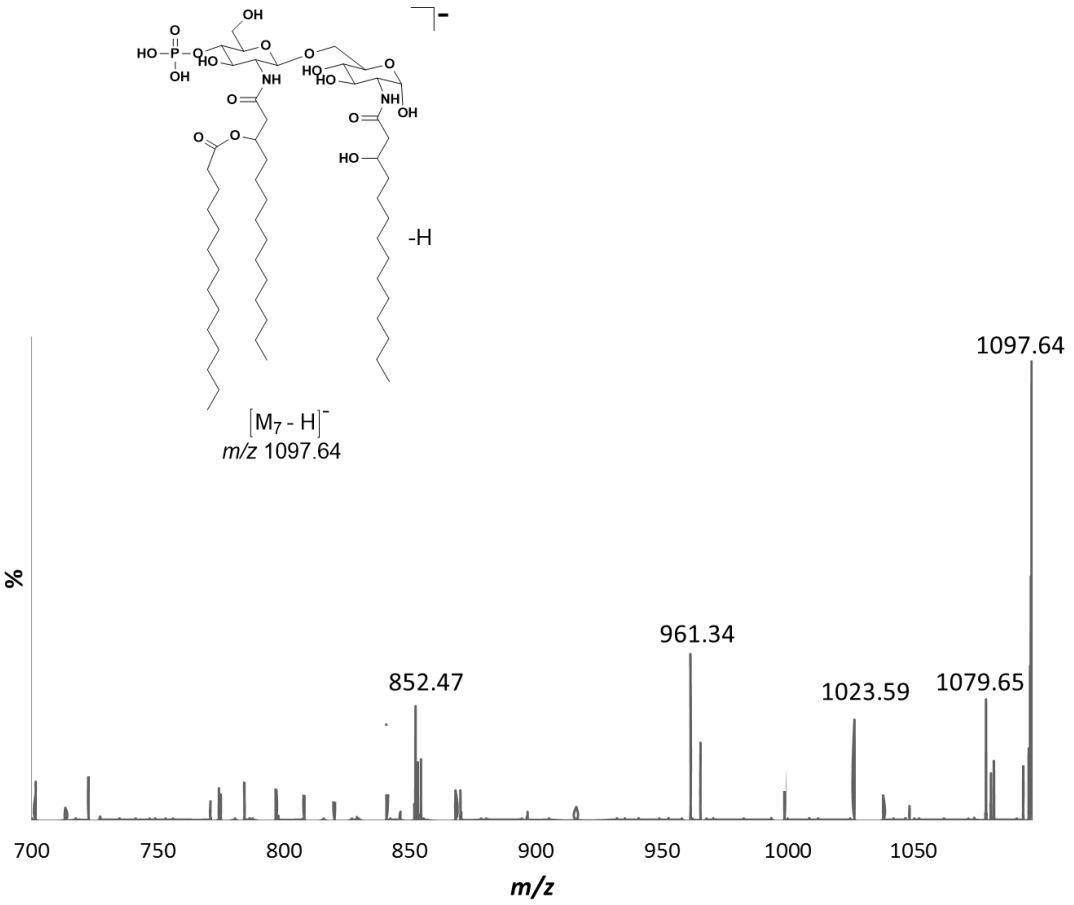

Figure 4.1.8: CID-MS/MS of the precursor deprotonated $[M_7\text{-}H]^-$ molecules at *m/z* 1097.64.*

* Please note, that some product ions were not assigned as these were produced by other isobars isolated during the MS/MS analysis.

Table 4.1.8: Assignments of the product ions observed from CID-MS/MS of the precursor deprotonated $[M_7\text{-}H]^-$ molecules at *m/z* 1097.64.

Product ions of the deprotonated molecules $[M_7\text{-}H]^-$ at *m/z* 1097.64						
Empirical Formula	**ESI-QqQ-MS/MS**		**ESI-FTICR-MS/MS**		**MALDI-TOF/TOF-MS/MS**	
	m/z **Observed; Calculated (%)**	**δ ppm**	***m/z*** **Observed; Calculated (%)**	**δ ppm**	***m/z*** **Observed; Calculated (%)**	**δ ppm**
$C_{50}H_{92}N_2O_{17}P$	**1023.61; 1023.59 (20)**	**-19.5**	**-**	**-**	**-**	**-**
$C_{48}H_{84}N_2O_{15}P$	**961.34; 961.58 (37.5)**	**-41.5**	**-**	**-**	**-**	**-**
$C_{40}H_{74}N_2O_{15}P$	**852.48; 852.47 (29)**	**-11.7**	**852.4832; 852.4835 (79)**	**-0.3**	**852.4832; 852.4797 (21)**	**-4.1**
$C_{38}H_{66}N_2O_9$	**-**	**-**	**-**	**-**	**693.4959; 693.5820 (12.2)**	**4.7**

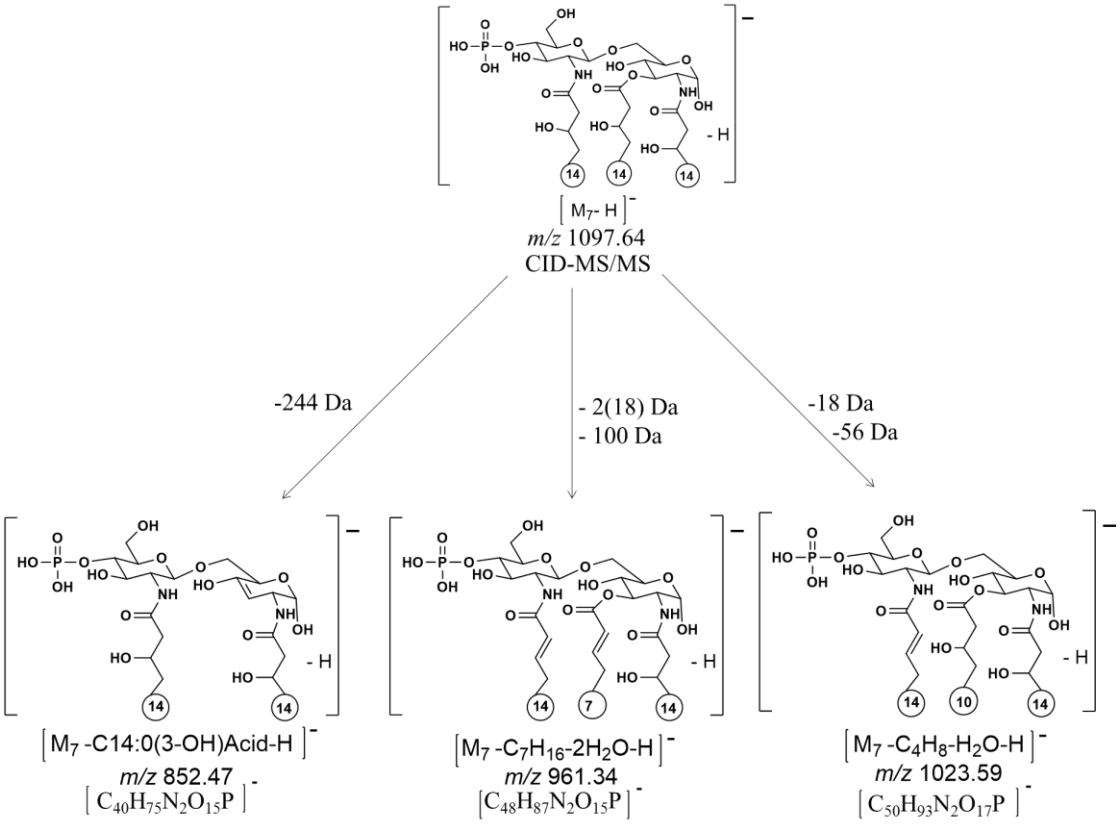

Scheme 4.1.8: Proposed fragmentation pathways obtained by CID-QqQ-MS/MS and SORI-CID-FTICR-MS/MS of the precursor deprotonated $[M_7\text{-}H]^-$ molecules at *m/z* 1097.64.∗

∗ Please note, that some product ions were not assigned as these were produced by other isobars isolated during the MS/MS analysis.

Table 4.1.9: Assignments of the product ions observed from CID-MS/MS of the precursor deprotonated $[M_8\text{-}H]^-$ molecules at *m/z m/z* 1053.69.

	Product ions of the deprotonated molecules $[M_8\text{-}H]^-$ at *m/z* 1053.69			
	CID-QqQ-MS/MS		SORI-CID-FTICR-MS/MS	
Empirical formula	Product ion *m/z* Calculated; Observed (%)	δ ppm	Product ion *m/z* Calculated; Observed (%)	δ ppm
$C_{38}H_{72}N_2O_{16}P$	843.48; 843.45 (26.7)	23	843.4832; 843.4829 (100)	-0.3
$C_{38}H_{71}N_2O_{13}P$	763.50; 763.48 (26.4)	-26.4	-	-
$C_{32}H_{59}N_2O_{10}P$	648.38; 648.36 (26.1)	34	-	-

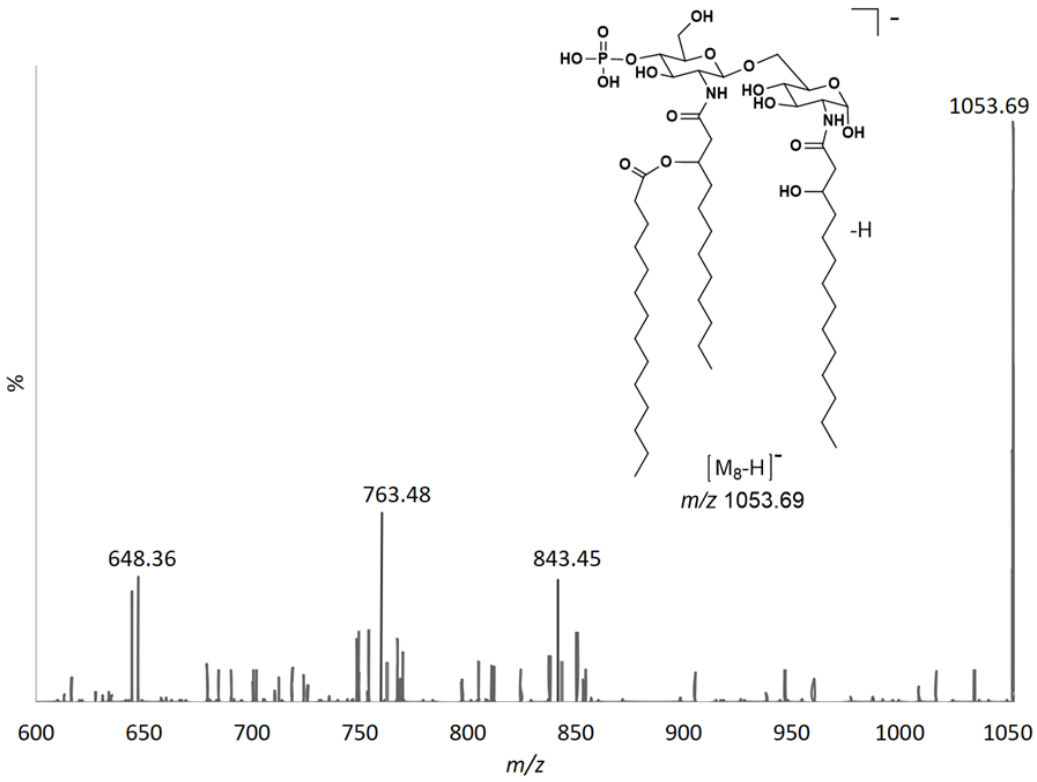

Figure 4.1.9: CID-MS/MS of the precursor deprotonated $[M_8\text{-}H]^-$ molecules at *m/z* 1053.69.∗

∗ Please note, that some product ions were not assigned as these were produced by other isobars isolated during the MS/MS analysis.

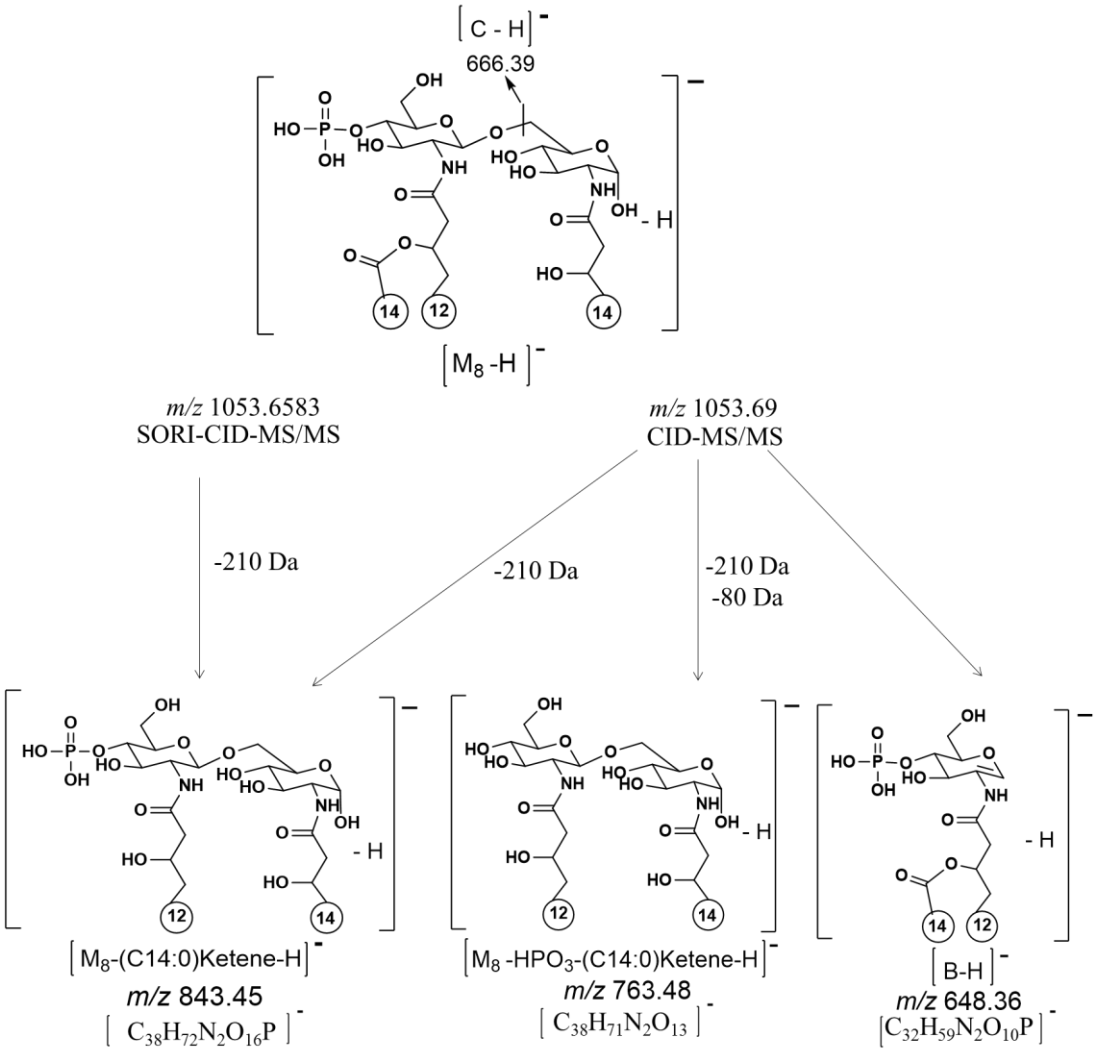

Scheme 4.1.9: Proposed fragmentation pathways obtained by CID-QqQ-MS/MS and SORI-CID-FTICR-MS/MS of the precursor deprotonated $[M_8\text{-}H]^-$ molecules at *m/z* 1035.69.

The last product ion at *m/z* 648.36 was assigned to be formed by the $[B-H]^-$ cleavage of the reducing D-Glucosamine end (Domon and Costello, 1988).

Lastly, we also investigated the nature of the deprotonated molecules at *m/z* 892.55, *m/z* 710.40 and *m/z* 666.37 observed in the ESI-MS of this lipid A_n mixture. We have previously assigned these deprotonated molecules as being created by the $[C-H]^-$ and $[Y-H]^-$ ion series whose presence are probably an indication of the incomplete biosynthesis of the lipid A_{1-8} series of the LPS *A. hydrophilla* SJ-55a.

The product ion scan of the deprotonated $[C-(C14:0)ketene-H]^-$ molecule at *m/z* 892.56 gave a series of product ions at *m/z* 791.45, *m/z* 682.38, and *m/z* 648.40 (Figure 4.1.10, Scheme 4.1.10, and Table 4.1.10). The product ion at *m/z* 791.45 was assigned as $[C-(C14:0)ketene-C_6H_{11}-H_2O-H]^-$ ion, and it was generated by the consecutive eliminations of n-hexane as a part of the fatty acid (-83 Da) probably located at N-2 or O-3, and a molecule of water. It is important to note that the obtained product ion scan of the deprotonated mono-phosphorylated molecules at *m/z* 892.56 is completely different from the one obtained for the deprotonated molecule that was isolated from the lipid A_n SJ-19a and was assigned as $[C-(C14:0)ketene-H]^-$ (Chapter 3). This indicated that both deprotonated molecules for *m/z* 892 are indeed isobaric and have completely different structures.

Similarly, the product ion at *m/z* 682.39 was assigned as the $[C-2(C14:0)ketene-H]^-$ ion, and it was created by losses of the myristic ketene molecule (-210 Da) from the branched fatty acids (C14:0(3-*O*-C12:0)) at the N-2 position.

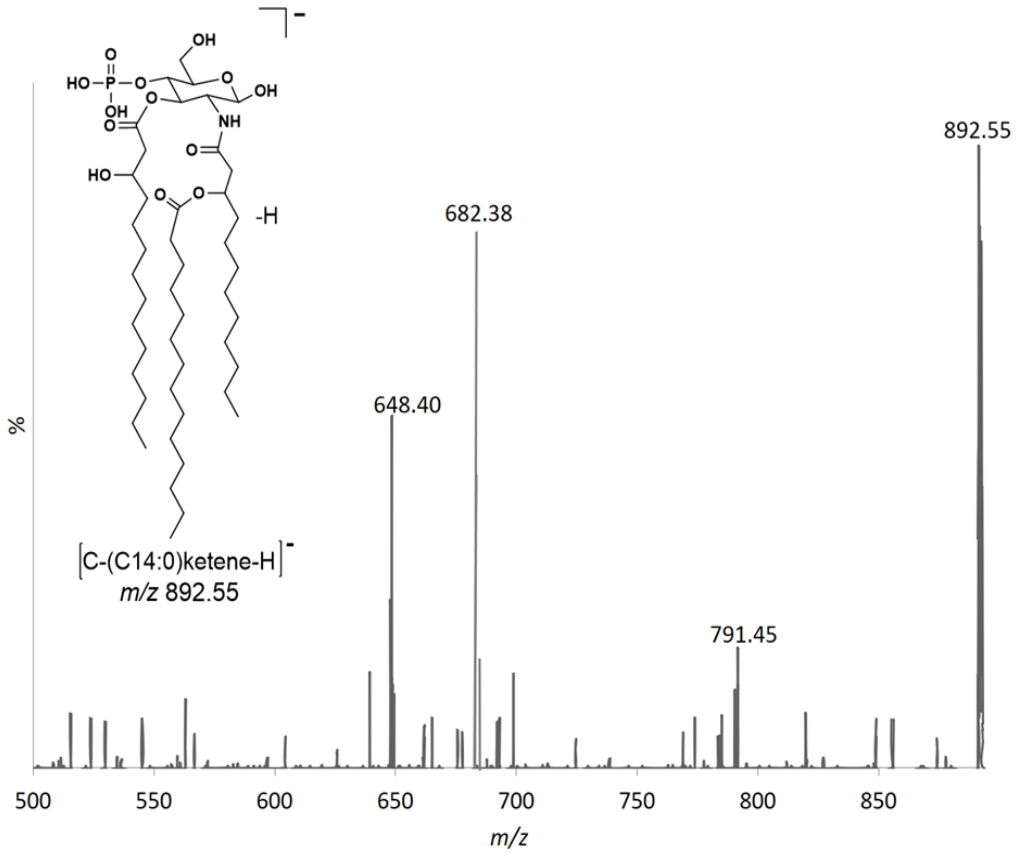

Figure 4.1.10: CID-MS/MS of the precursor deprotonated [C-(C14:0)ketene-H]$^-$ molecules at *m/z* 892.55.*

* Please note, that some product ions were not assigned as these were produced by other isobars isolated during the MS/MS analysis.

Table 4.1.10: Assignments of the product ions observed from the SORI-MS/MS and CID-MS/MS analysis of the precursor deprotonated [C-(C14:0)ketene-H]$^-$ molecules at *m/z* 892.55.

	Product ions of the deprotonated molecules [C-(C14:0)ketene-H]$^-$ at *m/z* 892.55			
	CID-QqQ-MS/MS		SORI-FTICR-MS/MS	
Empirical formula	Product ion *m/z* Calculated; Observed (%)	δ ppm	Product ion *m/z* Calculated; Observed (%)	δ ppm
$C_{40}H_{73}NO_{12}P$	790.48; 790.45 (20)	-37.9	-	-
$C_{32}H_{62}NO_{12}P$	682.40; 682.38 (46)	-29.3	-	-
$C_{32}H_{54}NO_{10}P$	648.39; 648.40 (55.4)	15	648.3955; 648.3949 (89)	-0.9

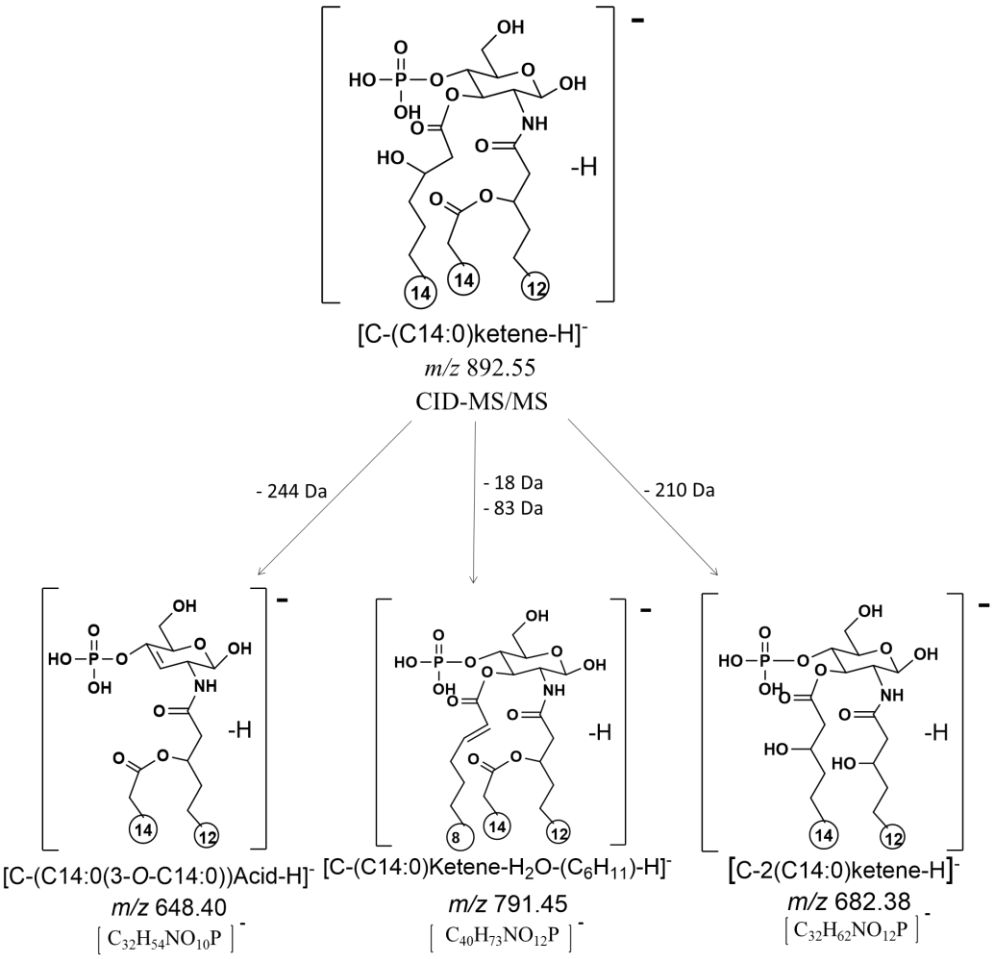

Scheme 4.1.10: Proposed fragmentation pathways obtained by CID-QqQ-MS/MS and SORI-CID- FTICR MS/MS analysis of the precursor deprotonated [C-(C14:0)ketene-H]$^-$ molecules at *m/z* 892.55.

The product ions at *m/z* 648.40 was assigned as [C-(C14:0)ketene-(C14:0(3-OH))acid-H]$^-$ ion and it was formed by the loss of the 3-hydroxy-myristic acid (-244 Da) at O-3 position.

Once more, we have again a strong support indicating that the lipid A_1, lipid A_5, and lipid A_7 only knows, and lipid a have structures containing two H_2PO_3 group at O-4′ of the D-GlcN non-reducing end, and at O-1 at the reducing end of the D-GlcN. These deprotonated molecules also contain a primary myristic ester located at N-2, O-3, and O-3′ position, and a primary lauric esters located at the N-2′ position of this lipid GlcN disaccaride backbone. It also means that the myristic acid ester is located on the branched fatty acids (C14:0(3-*O*-C12:0)) acyl group located at N-2´. Whereas the branched fatty ester (C14:0(3-*O*-C14:0)) is located at O-3´ position of the reducing GlcN residue present in the β-D-Glc*p*N-(1→6)-α-D-Glc*p*N disaccharide backbone. Whereas the structures of the deprotonated molecules Lip A_2, Lip A_3, Lip A_4, Lip A_6, and Lip A_8 are identical to that of the di-phosphorylated Lip A_1, Lip A_5, and Lip A_7 with the absence of one phosphate group located on O-1.

The product ion scan of the deprotonated [Y-H]$^-$ molecule at *m/z* 710.40 gave a series of product ions at *m/z* 664.36, and *m/z* 466.20 (Figure 4.1.11, Table 4.1.11 and Scheme 4.1.11). The product ion at *m/z* 664.36 was assigned as [Y-C_2H_4-H_2O-H]$^-$ ion and it was generated by consecutive eliminations of n-C_2H_4 as a part of the fatty acid (-28 Da) probably located at O-3 and a molecule of water. Similarly, the product ion at *m/z* 466.20 was assigned as the [Y-(C14:0(3-OH))acid-H]$^-$ ion and it was created by loss the 3-hydroxy-myristic acid (C14:0(3-OH)) (-244 Da) located at the position O-3.

Table 4.1.11: Assignments of the product ions observed from CID-MS/MS and SORI-MS/MS of the precursor ion at *m/z* 710.40.

	Product ions of the deprotonated molecules $[Y\text{-}H]^-$ at *m/z* 710.40			
	CID-QqQ-MS/MS		SORI-FTICR-MS/MS	
Empirical formula	Product ion *m/z* Calculated; Observed (%)	δ ppm	Product ion *m/z* Calculated; Observed (%)	δ ppm
$C_{32}H_{60}NO_{11}P$	664.38; 664.36 (26.9)	-30	-	-
$C_{20}H_{37}NO_9P$	466.22; 466.20 (20.1)	-42.8	466.2211; 466.2219 (91)	1.7

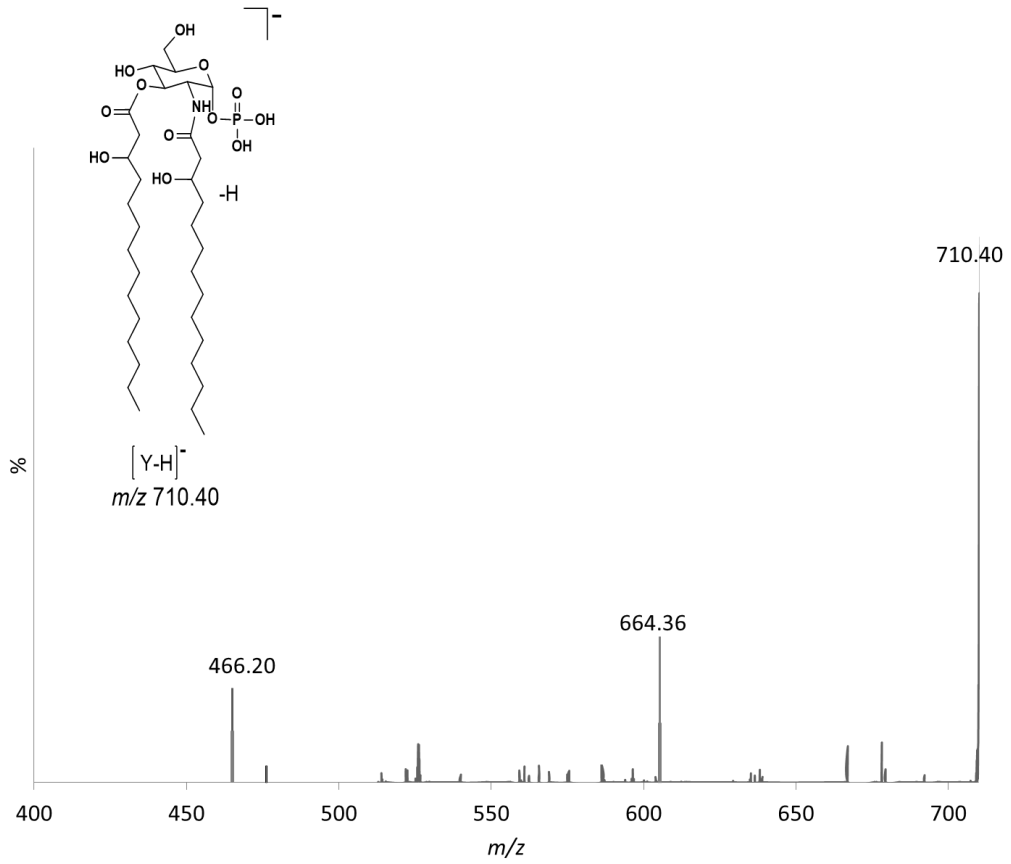

Figure 4.1.11: CID-MS/MS of the precursor deprotonated $[Y\text{-}H]^-$ molecules a *m/z* 710.40.*

* Please note, that some product ions were not assigned as these were produced by other isobars isolated during the MS/MS analysis.

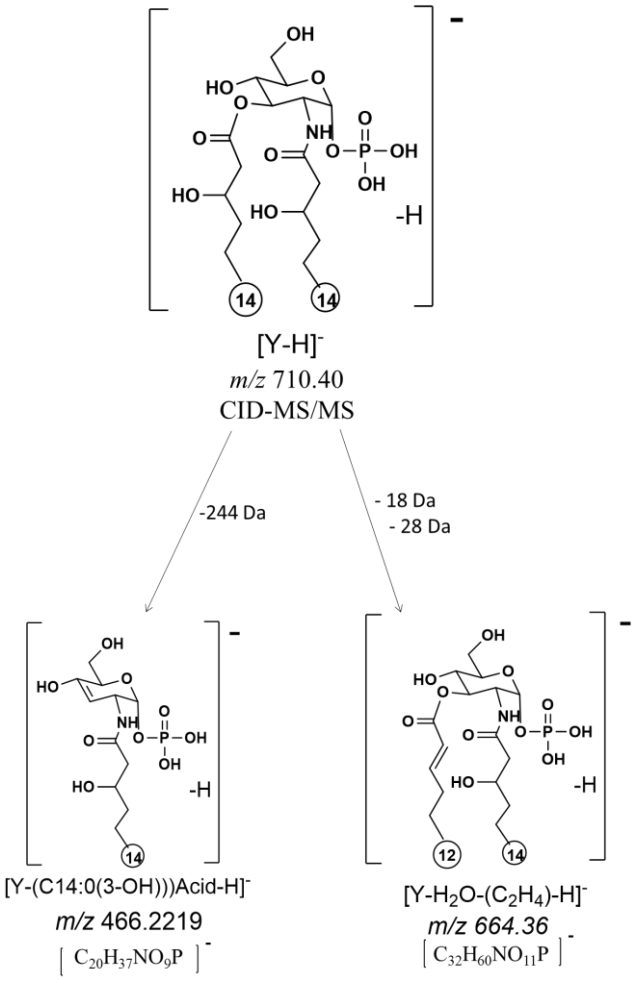

Scheme 4.1.11: Proposed fragmentation pathways obtained by CID-QqQ-MS/MS and SORI-CID-FTICR-MS/MS of the precursor mono-phosphorylated ion $[Y\text{-}H]^-$ *m/z* 710.40.

Finally, the CID-MS/MS affords the precursor deprotonated mono-phosphorylated molecules at *m/z* 666.37 assigned as [C-(C14:0(3-*O*-C14:0))ketene-H]$^-$ gave the following series of product ions at *m/z* 648.30, *m/z* 563.29, *m/z* 520.25, and *m/z* 438.20 (Figure 4.1.12, Table 4.1.12, and Scheme 4.1.12). The product ion at *m/z* 648.30 was formed by the loss of a molecule of water. The product ion at *m/z* 563.29 was assigned as [C-(C14:0(3-*O*-C14:0))acid-(C_6H_{14})-H_2O-H]$^-$ ion, and it was formed by the consecutive eliminations of n-C_6H_{14} as a part of the fatty acid (-86 Da) located at N-2, and a molecule of water. The product ion at *m/z* 520.25 was assigned as [C-(C14:0(3-*O*-C14:0))ketene-(C_9H_{20})-H_2O-H]$^-$ ion, and it was formed by the consecutive eliminations of n-C_9H_{20} as a part of the fatty acid (-128 Da) probably located at N-2, and a molecule of water. The product ion at *m/z* 438.20 was assigned as [C-(C14:0(3-*O*-C14:0))ketene-(C14:0)acid-H]$^-$ ion, and it was formed by the elimination of a molecule of myristic acid (-228 Da) from the branched (C12:0(3-*O*-C14:0)) ester at the N-2 position. It is important to note that the obtained product ion scan of the deprotonated mono-phosphorylated molecules at *m/z* 666.37 is completely different from the one obtained for the deprotonated molecule that was isolated from the lipid A_n SJ-19a, which was assigned as [C-(C14:0(3-*O*-C14:0))ketene-H]$^-$ (Chapter 3). This indicated that both deprotonated molecules for *m/z* 666 are indeed isobaric and have completely different structures.

It should be noticed that the CID-MS/MS analysis of the deprotonated molecules [M_{1-8}-H]$^-$ at *m/z* 1796.30 ($LipA_1$), *m/z* 1716.15 ($LipA_2$), *m/z* 1688.26 ($LipA_3$), *m/z* 1506.12 ($LipA_4$), *m/z* 1359.75 ($LipA_5$), *m/z* 1279.87 ($LipA_6$), *m/z* 1097.64 ($LipA_7$), and *m/z* 1053.69 ($LipA_8$) afford distinctive series of product ions. Additionally, it is important to

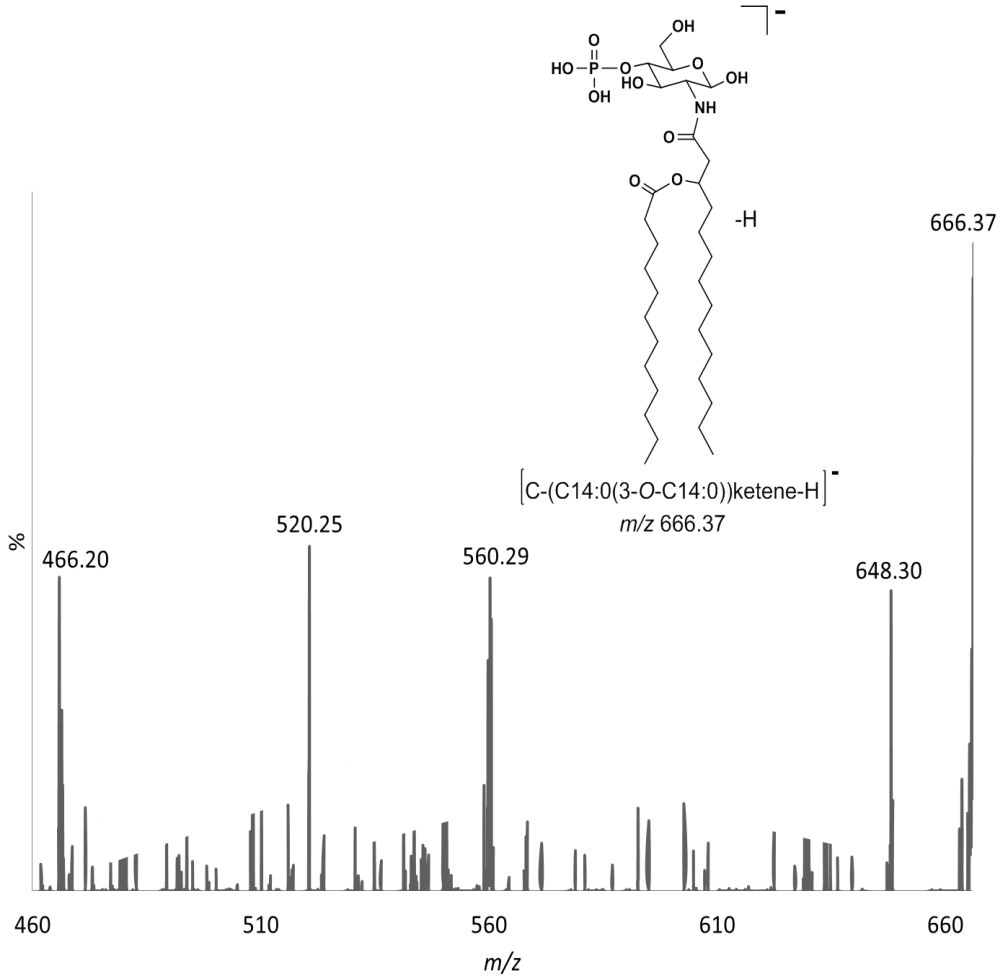

Figure 4.1.12: CID-MS/MS of the precursor deprotonated [C-(C14:0(3-*O*-C14:0))ketene-H]$^-$ molecules at *m/z* 666.37.∗

∗ Please note, that some product ions were not assigned as these were produced by other isobars isolated during the MS/MS analysis.

Table 4.1.12: Assignments of the product ions observed from CID-MS/MS and SORI-MS/MS of the precursor ion at *m/z* 666.37.

	Product ions of the deprotonated molecules [C-(C14:0(3-*O*-C14:0))ketene-H]$^-$ at *m/z* 666.37			
	CID-QqQ-MS/MS		SORI-FTICR-MS/MS	
Empirical formula	Product ion *m/z* Calculated; Observed (%)	δ ppm	Product ion *m/z* Calculated; Observed (%)	δ ppm
$C_{32}H_{59}NO_{10}P$	648.38; 648.30 (48.3)	-30.8	648.3282; 648.3239 (20.9)	-0.4
$C_{26}H_{46}NO_{10}P$	563.31; 563.29 (47.9)	-35.6	-	-
$C_{23}H_{40}NO_{10}P$	520.23; 520.25 (55)	-38.4	-	-
$C_{18}H_{34}NO_9P$	438.22; 438.20 (49)	-42	438.2211; 438.2216 (94)	-1

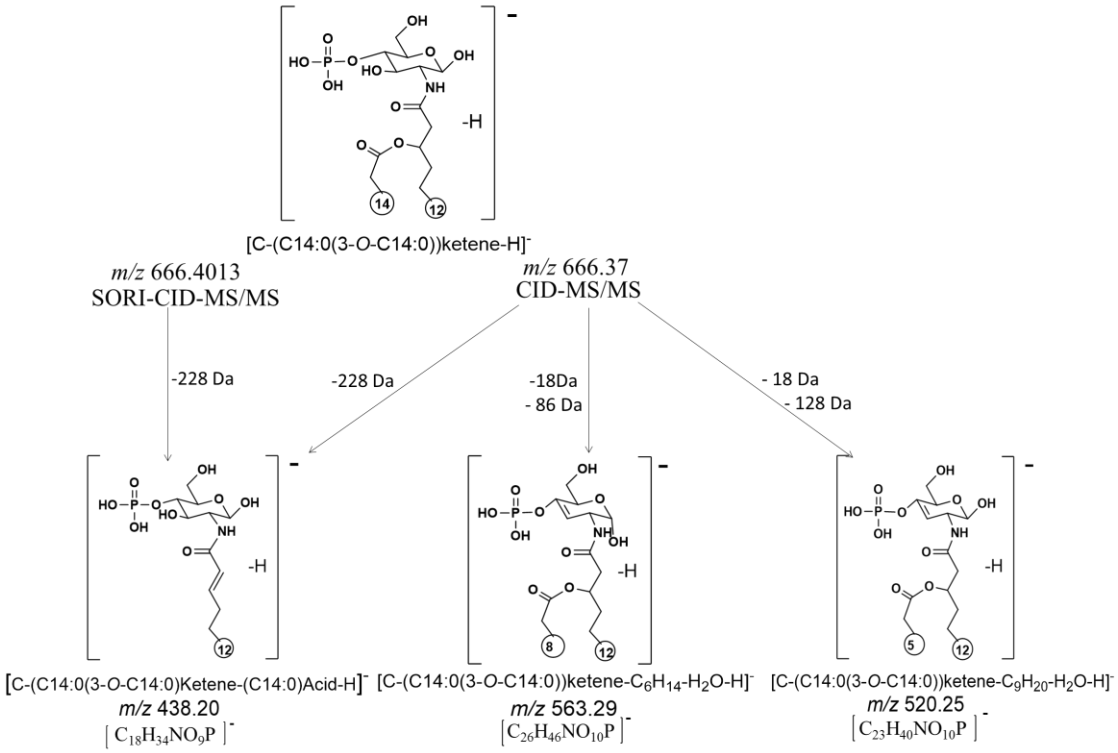

Scheme 4.1.12: Proposed fragmentation pathways obtained by CID-QqQ-MS/MS and SORI-CID-FTICR MS/MS of the precursor mono-phosphorylated ion [C-(C14:0(3-*O*-C14:0))ketene-H]$^-$ *m/z* 666.37.

reference that there was no cross connectivity between the different precursor deprotonated molecules. These findings indicate that each one of these species was individual and created specific product ions.

In conclusion, the MS/MS finding described herewith confirm that the origins and presence of this series of precursor ions was caused by an incomplete biosynthesis of the LPS. Also, it is important to note that during the low-energy CID-MS/MS analyses conducted with the QqQ-tandem instrument on these series of deprotonated molecules, we were able to confirm that the formation of each deprotonated molecule recorded in single stage ESI-QqQ-MS instrument, were indeed single unique diagnostic molecules that were not produced by further fragmentation from contiguous higher masses deprotonated molecules. In addition, these product ion scans created series of product ions, that excluded the possibility, that they could be related to each other.

Finally, precursor ion scans of these deprotonated molecules formed during the ESI-QqQ-MS showed that there were no connectivities and/or genesi relations between these different deprotonated molecules (see Appendix).

4.3. ESI-FTICR-MS analysis of heterogeneous lipid A_n mixture isolated from the LPS of *A. hydrophilla* SJ-55a

The ESI-FTICR-mass spectrometer analysis was also applied to the mixture of lipid A_n (where n=1-8), in order to produce spectrum as a time depending technique with its high resolving power and mass accuracy currently available, which allows to determine the elemental conformation of the analyzed produced ions (Marshall, *et al*., 1998, Marshall, *et al*., 1999, Palumbo *et al*., 2011, and van Agthoven *et al*., 2015).

Unsurprisingly, this ESI-MS (- ion mode) obtained for lipid A of *A. hydrophilla* SJ-55a displayed an incomplete biosynthesis as demonstrated by the multiple deprotonated molecules.

Similarly, to the ESI-QqQ-MS, the ESI-FTICR-MS (- ion mode) showed the presence of *inter-alia* eight fragment ions, three of which were assigned to different $[M-H]^-$ deprotonated di-phosphorylated molecules $LipA_1$ at *m/z* 1796.2228, $LipA_5$ at *m/z* 1359.8180, and $LipA_7$ at *m/z* 1097.6930, and five deprotonated mono-phosphorylated molecules $LipA_2$ at *m/z* 1716.2610, $LipA_3$ at *m/z* 1688.2253, $LipA_4$ at *m/z* 1506.0530, $LipA_6$ at *m/z* 1279.8489, and $LipA_8$ *m/z* 1053.6583. Also, the last deprotonated molecules at *m/z* 892.5979, *m/z* 710.4258, and *m/z* 666.4013 were assigned as belonging to the $[Y-H]^-$ and $[C-H]^-$, indicating the presence of a heterogeneous mixture of lipid A_n (Figure 4.2.1, Scheme 4.1,1 and Table 4.1.1).

It should be noted that the ESI-FTICR-mass spectrum gives the same deprotonated molecules of the $LipA_{1-8}$ mixture as ESI-QqQ-MS with different abundances. In the ESI-

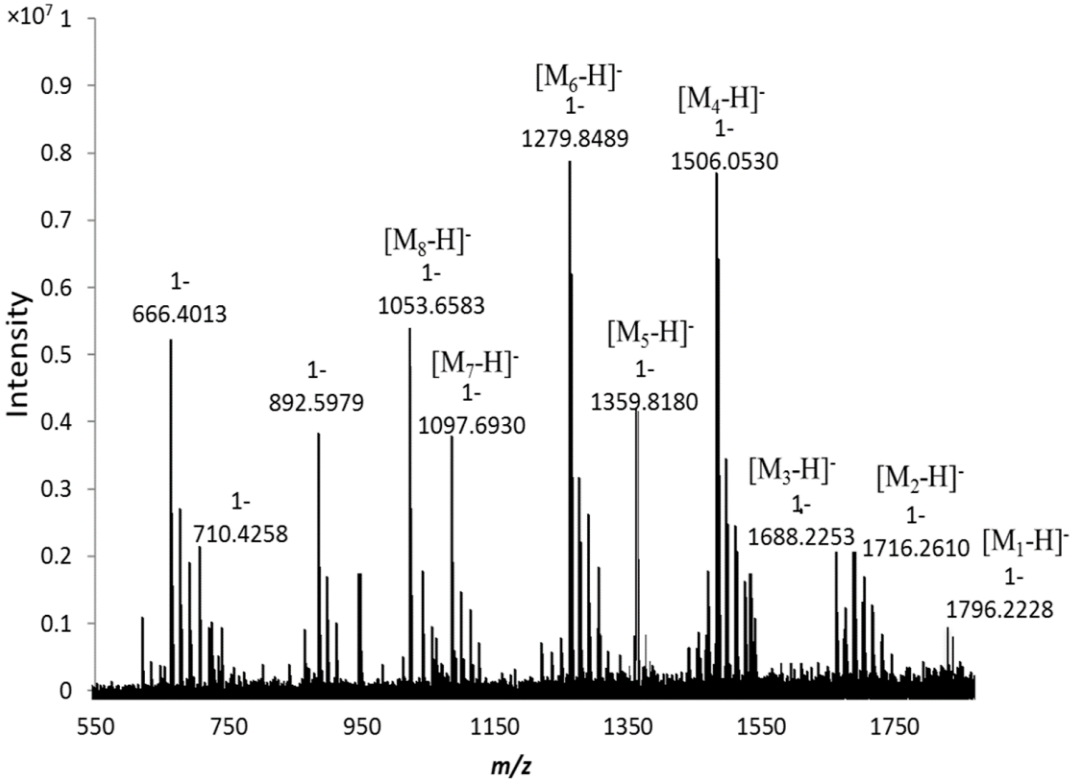

Figure 4.2.1: ESI-FTICR-MS (- ion mode) of the native lipid A_n mixture extracted from *A. hydrophilla* SJ-55a.

FTICR-mass spectrum, we noticed that the deprotonated molecule assigned to the $LipA_6$ at *m/z* 1279.8489 was the most abundant.

4.3.1. Measurement of the FT-ICR-MS isotopic distributions of the deprotonated molecules of lipid A_n isolated from the LPS of *A. hydrophilla* SJ-55a

The influence of spectral accuracy of the deprotonated molecular ions on elemental composition calculations was investigated by high-resolution mass spectrometer. The isotopic distribution of this series of deprotonated lipid A_n (where n=1-8), namely: $LipA_1$ at *m/z* 1796.2228, $LipA_2$ at *m/z* 1716.2610, $LipA_3$ at *m/z* 1688.2253, $LipA_4$ at *m/z* 1506.0530, $LipA_5$ at *m/z* 1359.8180, $LipA_6$ at *m/z* 1279.8489, $LipA_7$ at *m/z* 1097.6930, *m/z* 1053.6583, and $LipA_8$ at *m/z* 1053.69, and in addition to the two deprotonated molecules at *m/z* 892.5979, *m/z* 710.4258, and *m/z* 666.4013, is indicated in (Figure 4.2.2, Figure 4.2.3, and Figure 4.2.4) (Kind *et al*., 2010, and Jaitly *et al*., 2009). Therefore, the calculated elemental compositions of the deprotonated molecule $[M_1\text{-}H]^-$, $[M_2\text{-}H]^-$, $[M_3\text{-}H]^-$, $[M_4\text{-}H]^-$, $[M_5\text{-}H]^-$, $[M_6\text{-}H]^-$, $[M_7\text{-}H]^-$, and $[M_8\text{-}H]^-$, matched their experimental isotopic abundances using the algorithm “Gaussian 09 software package”, which allowed us to calculate the isotopic fine structures and allow the modeling of Gaussian peak shapes according to the selected resolving power of the instrument (Kind *et al*., 2010, and Jaitly *et al*., 2009).

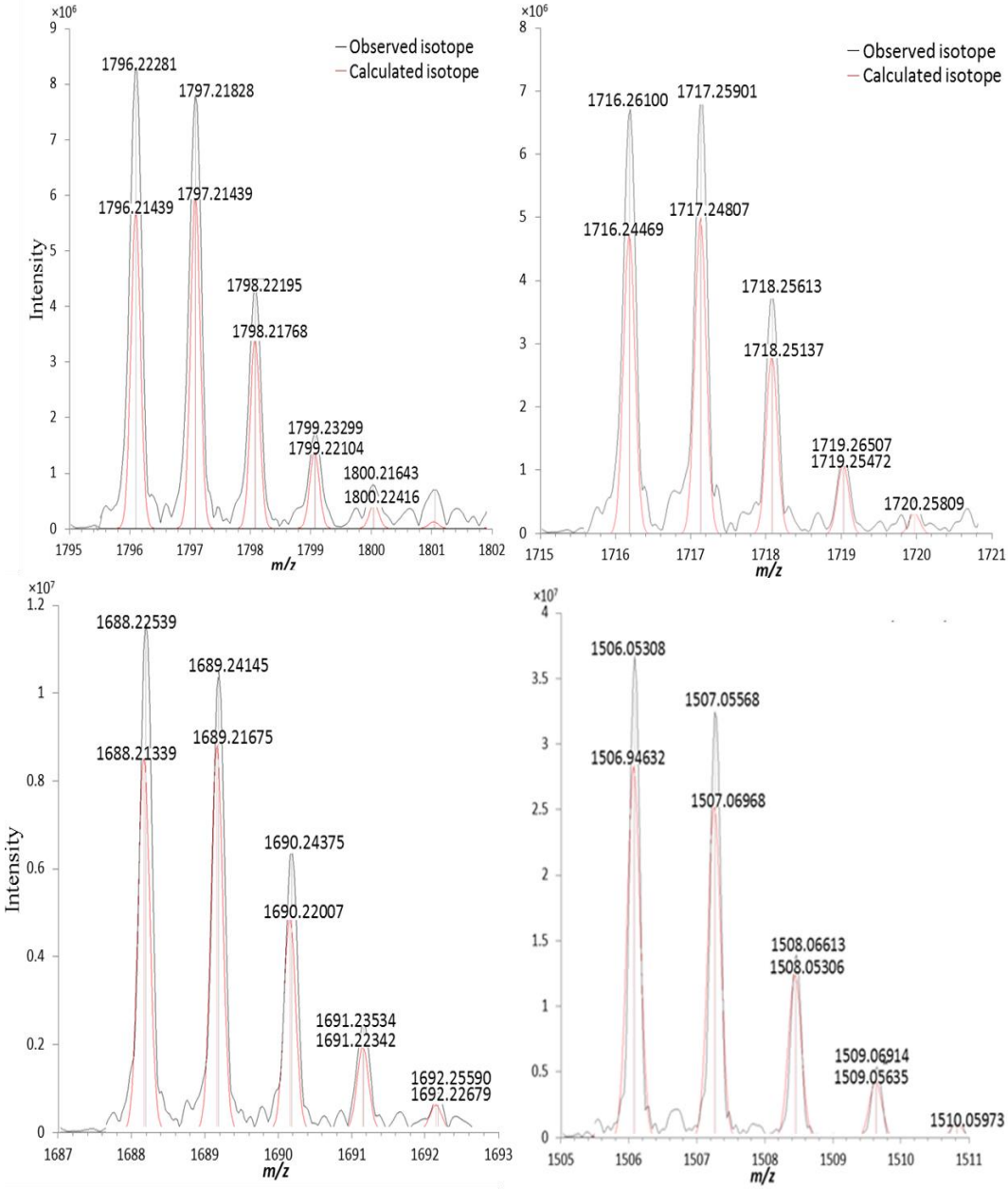

Figure 4.2.2: Theoretical isotope distribution overlapped on top of the observed pattern of the lipid A_n extract from the LPS of *A. hydrophilla* SJ-55a.

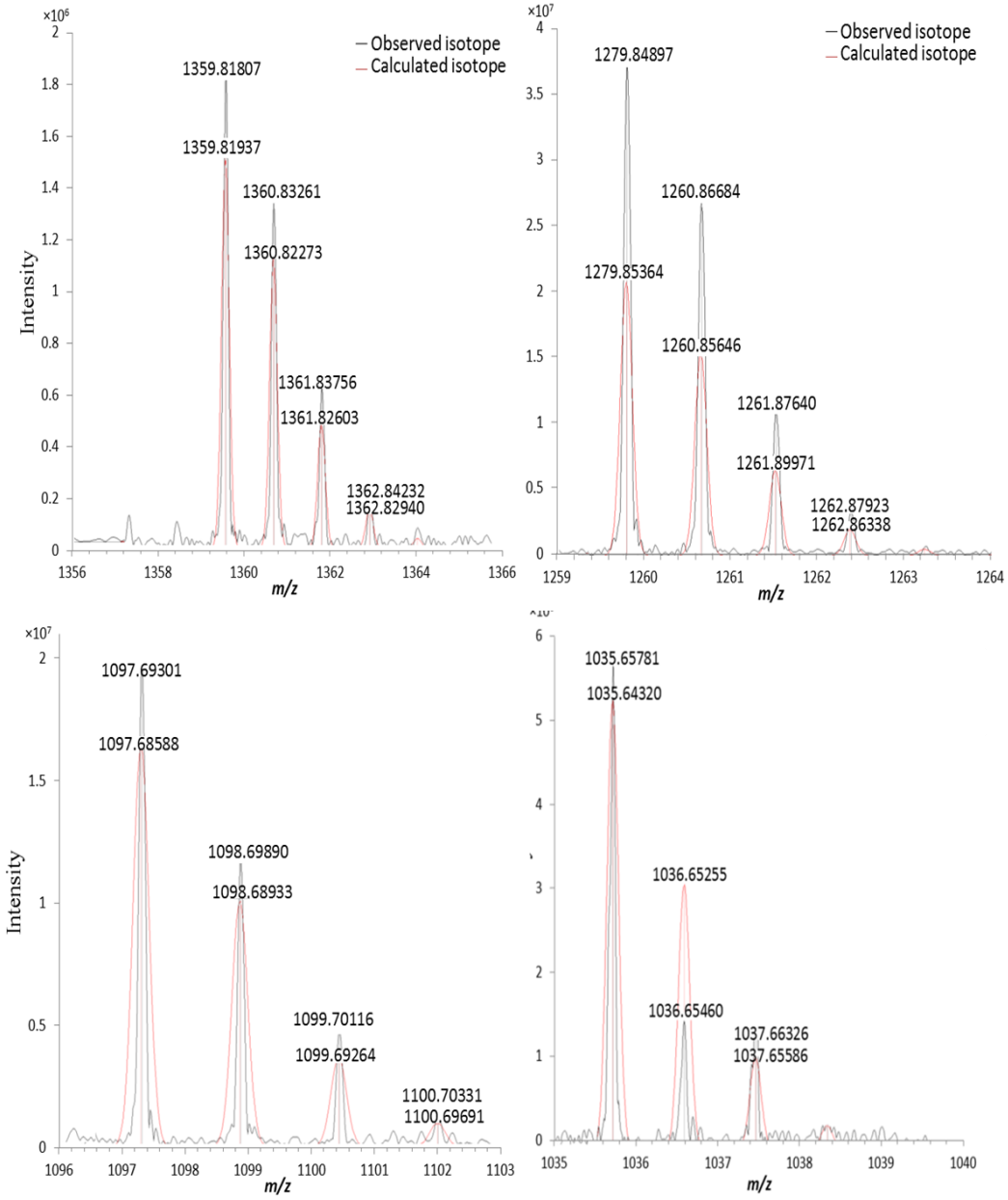

Figure 4.2.3: Theoretical isotope distribution overlapped on top of the observed pattern of the lipid A_n extract from the LPS of *A. hydrophilla* SJ-55a.

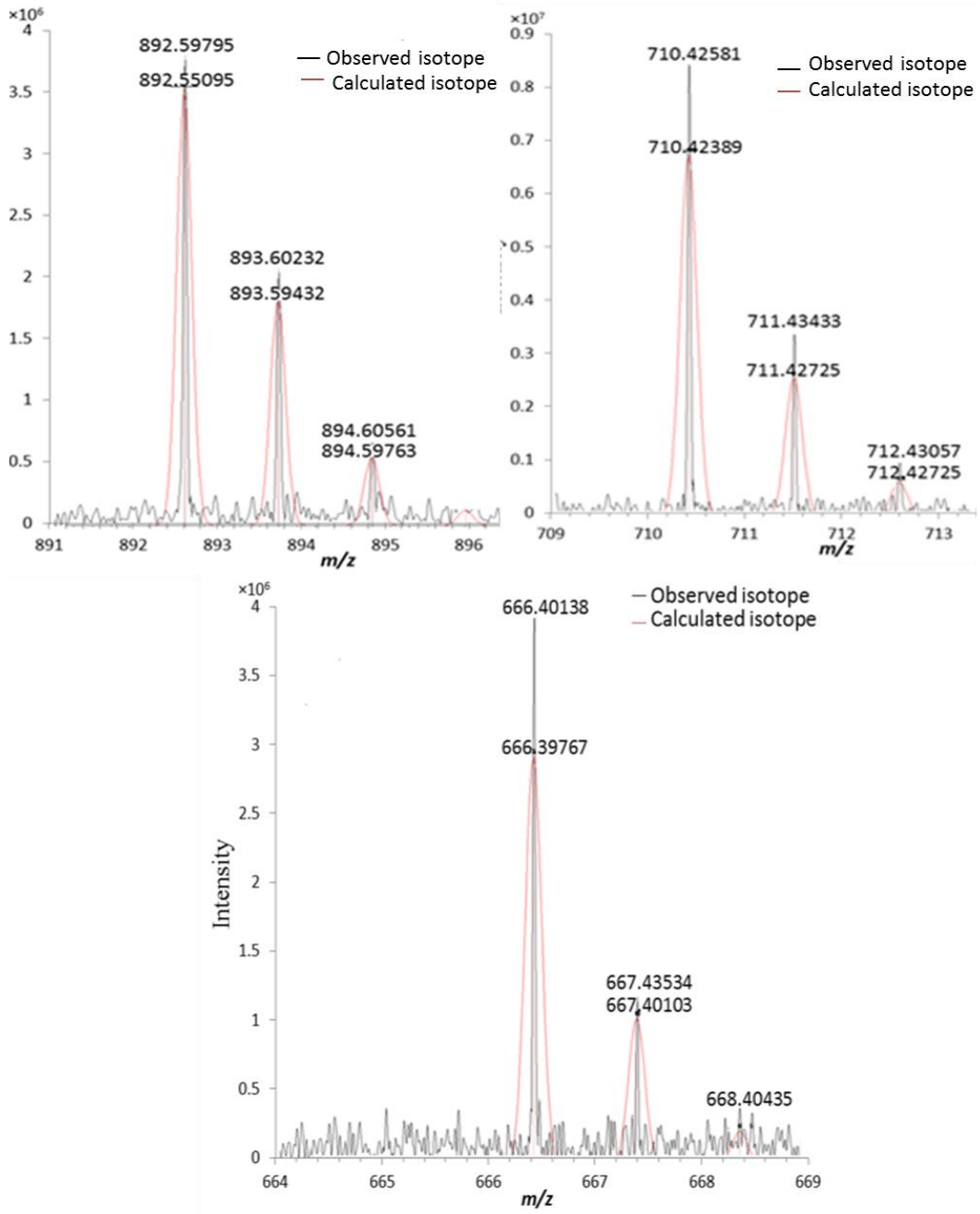

Figure 4.2.4: Theoretical isotope distribution overlapped on top of the observed pattern of the lipid A_n extract from the LPS of *A. hydrophilla* SJ-55a.

4.3.2. SORI-CID-FTICR-MS/MS analysis of lipid A_n mixture isolated from the LPS of *A. hydrophilla* SJ-55a

In this study, like in chapter 3, we have used SORI-CID-FTICR-MS/MS experiments for the CID-analysis of these series of deprotonated molecules, in order to further confirm their exact structures.

It is important to note that the SORI product ion scan of the precursor deprotonated molecules of $LipA_1$ at *m/z* 1796.2228 was not successful, as regrettably this was due to the low count abundance of species which deceptively refused to MS/MS fragment. The product ion scan of the deprotonated $LipA_2$ molecules at *m/z* 1716.2610 gave the product ions at *m/z* 1488.0460, *m/z* 1243.8380, and *m/z* 1035.6578. The product ion at *m/z* 1488.08 was assigned as the $[M_2$-(C14:0)acid-H$]^-$ ion, which was created by elimination of myristic acid form the branched fatty (C14:0(3-*O*-C14:0)) acid acyl group located at O-3′ (-228 Da). The product ion at *m/z* 1243.8380 was assigned as the $[M_2$-(C14:0(3-*O*-C14:0))acid-H_2O-H$]^-$ ion, which was created by elimination of the branched fatty (C14:0(3-*O*-C14:0)) acid acyl group located at O-3′ (-454 Da) and a molecule of water. The product ion at *m/z* 1035.6578 was assigned as the $[M_2$-(C14:0(3-*O*-C14:0))ketene-(C14:0)(3-OH)acid-H$]^-$ ion, which was created by the elimination of the branched fatty (C14:0(3-*O*-C14:0)) acid acyl group located at O-3′ (-436 Da) and 3-hydroxy-myristic acid (C14:0(3-OH)) (-244 Da) located at the position O-3 (Figure 4.2.5, Scheme 4.1.3 and Table 4.1.3) (El-Aneed *et al*., 2006, Shaffer *et al*., 2007, Lukasiewicz *et al*., 2010, John *et al*., 2014, and Brodbelt *et al*., 2014).

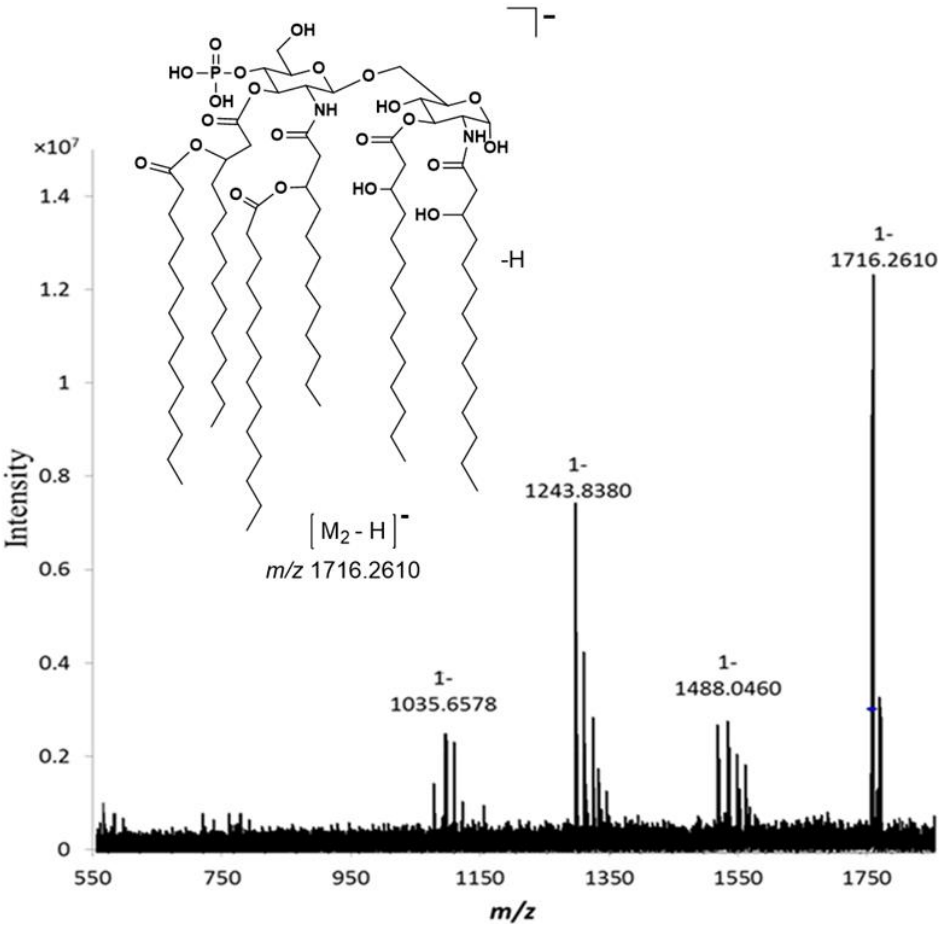

Figure 4.2.5: SORI-CID-MS/MS of the precursor deprotonated $[M_2\text{-}H]^-$ molecules at *m/z* 1716.2610.

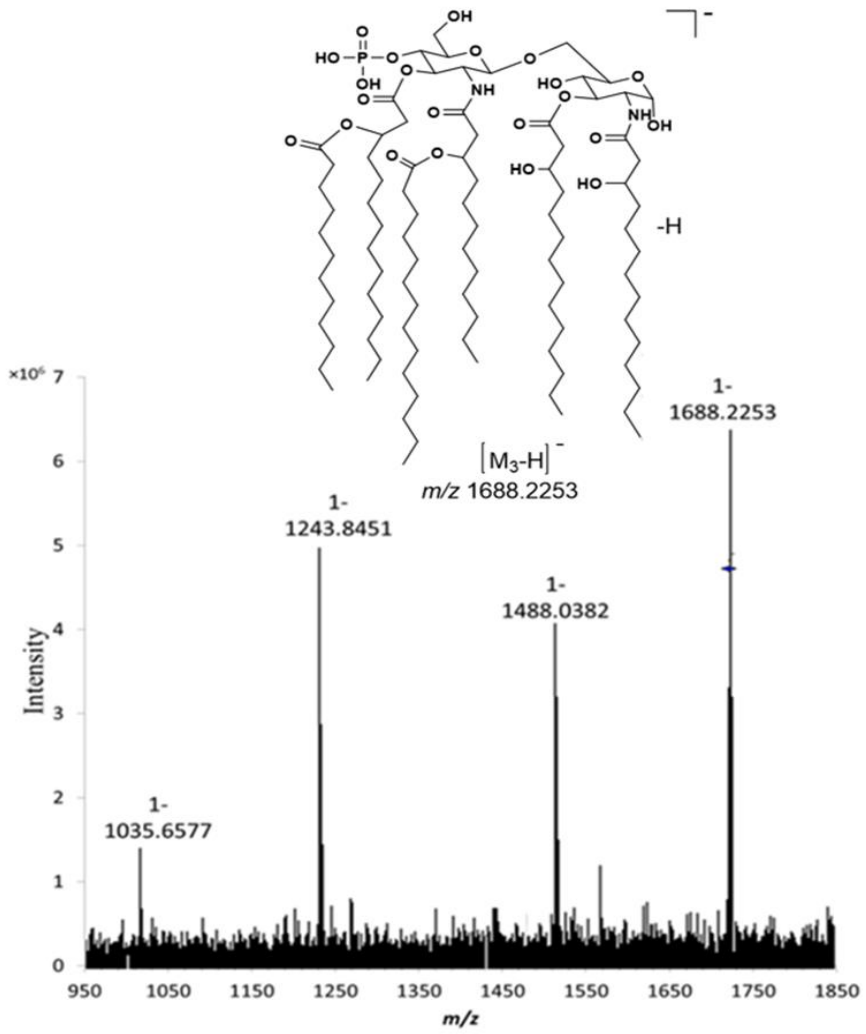

Figure 4.2.6: SORI-CID-MS/MS of the precursor deprotonated $[M_3\text{-}H]^-$ molecules at *m/z* 1688.2253.

The product ion scan of the deprotonated $LipA_3$ molecules at *m/z* 1688.2253 gave the product ions at *m/z* 1488.0382, *m/z* 1243.8451 and *m/z* 1035.6577 (Figure 4.2.6, Table 4.1.4, and Scheme 4.1.4). The product ion at *m/z* 1488.0382 was assigned as the $[M_3$-(C12:0)acid-H$]^-$ ion, which was created by the elimination of the lauryl acid (-200 Da) from the branched fatty (C14:0(3-*O*-C12:0)) acid located on N-2′. The product ion at *m/z* 1243.8451 was assigned as the $[M_3$-(C14:0(3-*O*-C12:0)acid)acid-H_2O-H$]^-$ ion, which was created by the elimination of the branched fatty (C14:0(3-*O*-C12:0)) acid acyl group located at O-3′ (-426 Da) and a molecule of water. The product ion at *m/z* 1035.6577 was assigned as the $[M_3$-(C14:0(3-*O*-C12:0))ketene-(C14:0)(3-OH)acid-H$]^-$ ion, which was created by elimination the branched fatty (C14:0(3-*O*-C12:0)) acyl group located at O-3′ (-408 Da) and 3-hydroxy-myristic acid (C14:0(3-OH)) (-244 Da) located at the position O-3.

The product ion scan of the precursor deprotonated molecules of $LipA_4$ *m/z* 1506.0530 gave the major product ion at *m/z* 1261.8399. This product ion was assigned as $[M_4$-(C14:0(3-OH)acid-H$]^-$ ion, which was formed by the elimination of 3-hydroxy-myristic acid (-244 Da) from the precursor ion located either at the O-3 and O-3′ positions located respectively in the reducing end or non-reducing end of the lipid A (Figure 4.2.7, Table 4.1.5 and Scheme 4.1.5) (El-Aneed *et al*., 2006, Shaffer *et al*., 2007, Lukasiewicz *et al*., 2010, John *et al*., 2014, and Brodbelt *et al*., 2014).

The product ion scan of the deprotonated $LipA_5$ molecules at *m/z* 1359.8180 gave the product ions at *m/z* 1261.8420, *m/z* 1115.6120, *m/z* 1035.6676, and *m/z* 1017.6390 (Figure 4.2.8, Table 4.1.6, and Scheme 4.1.6).

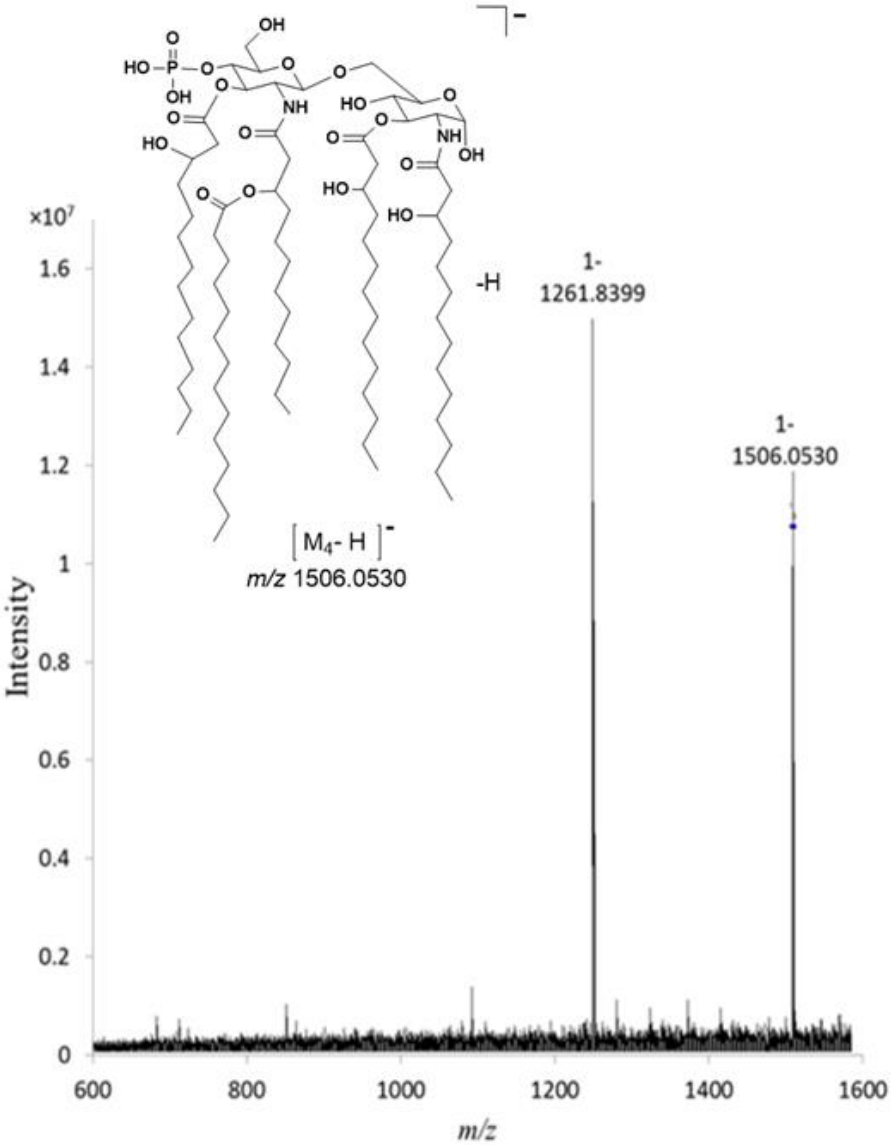

Figure 4.2.7: SORI-CID-MS/MS of the precursor deprotonated $[M_4\text{-}H]^-$ molecules at *m/z* 1506.0530.

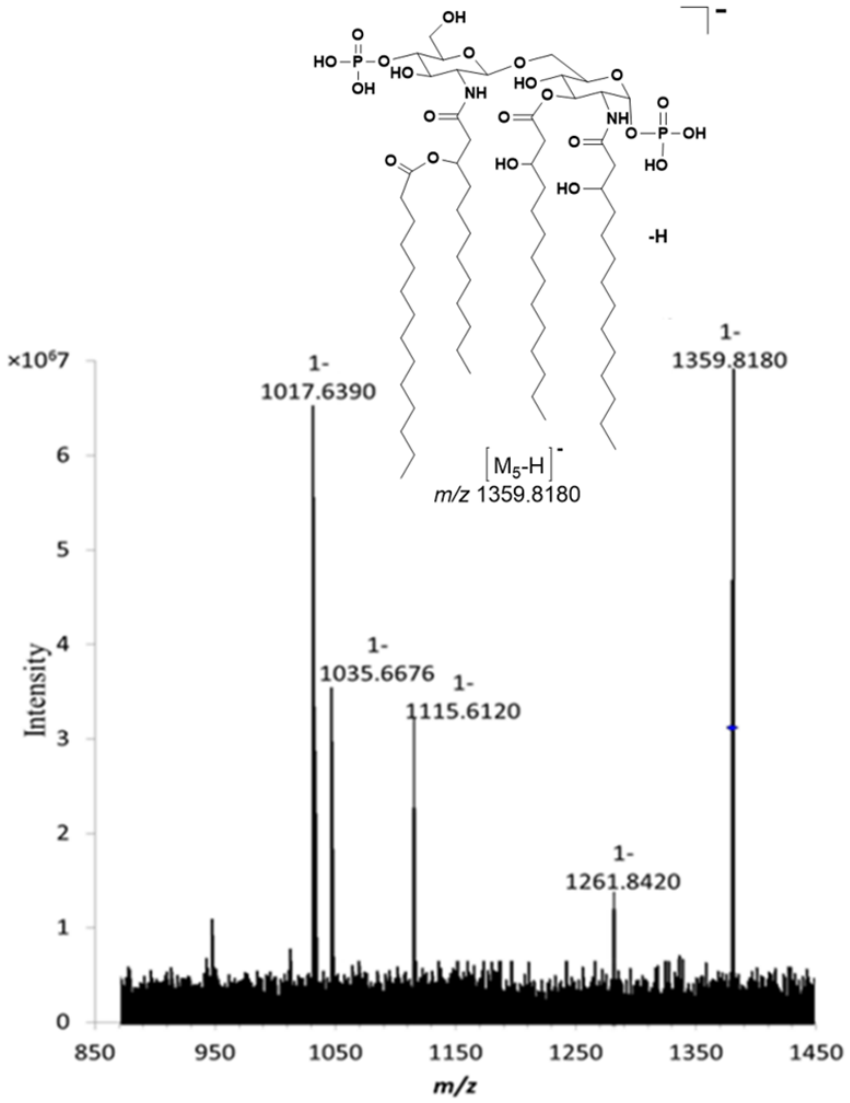

Figure 4.2.8: SORI-CID-MS/MS of the precursor deprotonated $[M_5\text{-}H]^-$ molecules at *m/z* 1359.8180.

The product ions at *m/z* 1261.8349 was assigned as $[M_5\text{-}H_2PO_4\text{-}H]^-$ ion, and it was formed by the elimination of the neutral H_3PO_4 (-98 Da) moiety. The product ion at *m/z* 1115.6120 was assigned as $[M_5\text{-}(C14:0)(3\text{-}OH)acid\text{-}H]^-$ ion, and it was formed by the elimination of 3-hydroxy-myristic acid (-244 Da) from the precursor ion located either at the O-3. The product ion *m/z* 1035.6676 was assigned as $[M_5\text{-}(C14:0)(3\text{-}OH)acid\text{-}HPO_3\text{-}H]^-$ ion. It was formed by the elimination of 3-hydroxy-myristic acid (-244 Da) from the precursor ion located either at the O-3, and the neutral HPO_3 (-80 Da) moiety. The product ion at *m/z* 1017.6390 created by the loss of a molecule of water from the product ion at *m/z* 1035.6676 (El-Aneed *et al*., 2006, Shaffer *et al*., 2007, Lukasiewicz *et al*., 2010, John *et al*., 2014, and Brodbelt *et al*., 2014).

Additionally, the product ion scan of $LipA_6$ at *m/z* 1279.8489 afforded the product ion at *m/z* 1035.6678. The product ion at *m/z* 1035.6678 was assigned as $[M_6\text{-}(C14:0)(3\text{-}OH)acid\text{-}H]^-$ ion. It was formed by the elimination of 3-hydroxy-myristic acid (-244 Da) from the precursor ion located either at the O-3 (Figure 4.2.9, Table 4.1.7 and Scheme 4.1.7) (El-Aneed *et al*., 2006, Shaffer *et al*., 2007, Lukasiewicz *et al*., 2006, John *et al*., 2014, and Brodbelt *et al*., 2014).

The product ion scan of deprotonated molecules of $LipA_7$ at *m/z* 1097.6930 gave the product ion at *m/z* 853.4835 which was assigned as the $[M_7\text{-}(C14:0)acid\text{-}H]^-$ ion. It was created by the elimination of 3-hydroxy-myristic acid (C14:0(3-OH)) (-244Da) located at the position O-3 of the reducing GlcN end of the $lipidA_7$ disaccharide (Figure 4.2.10, Table 4.1.8 and Scheme 4.1.8).

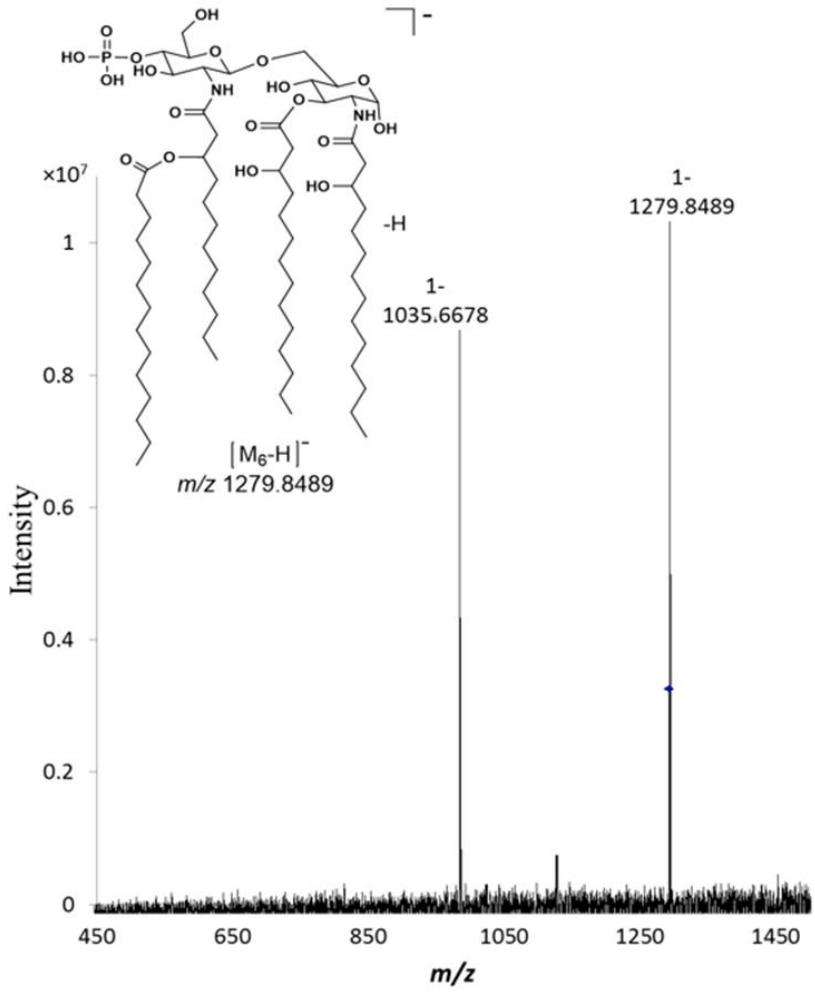

Figure 4.2.9: SORI-CID-MS/MS of the precursor deprotonated $[M_6\text{-}H]^-$ molecules at *m/z* 1279.8489.

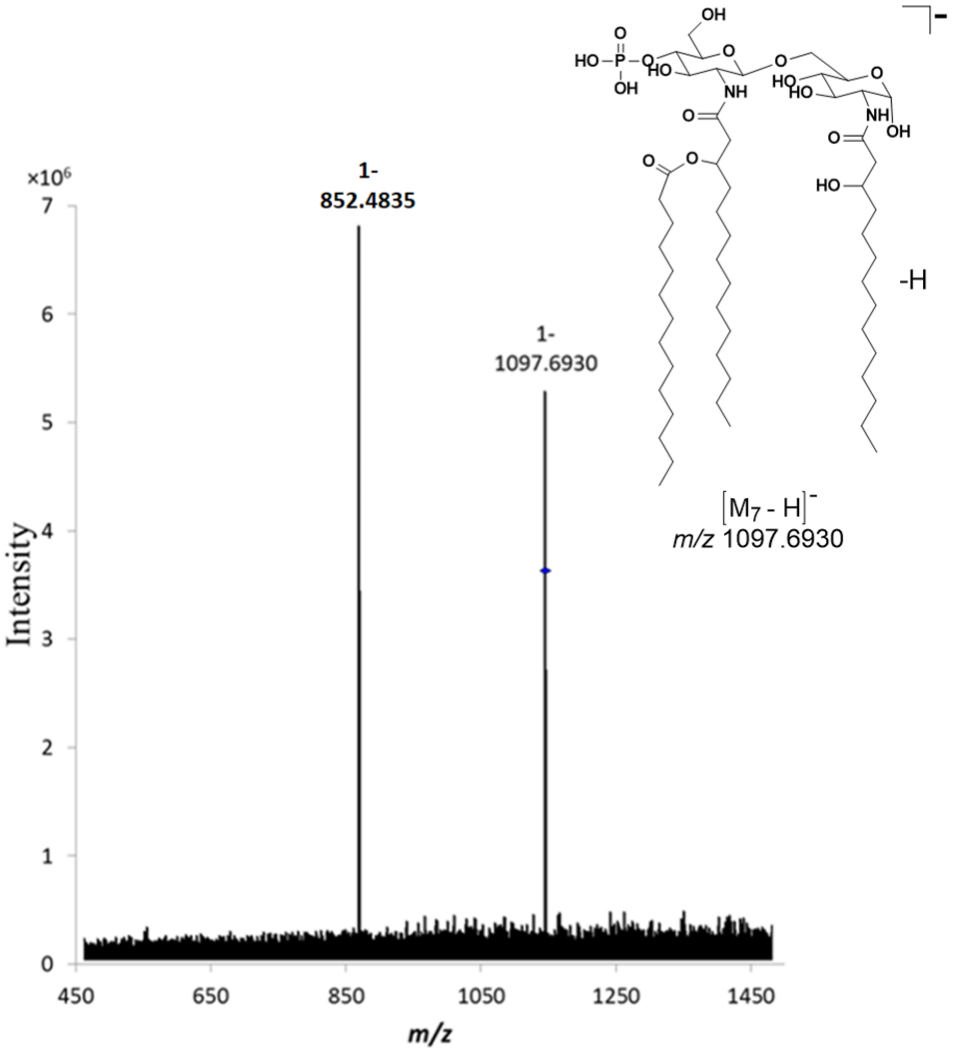

Figure 4.2.10: SORI-CID-MS/MS of the precursor deprotonated $[M_7\text{-}H]^-$ molecules at *m/z* 1097.6930.

Similarly, the product ion scan of deprotonated molecules of $LipA_8$ at *m/z* 1053.6583 gave the product ion at *m/z* 843.4829 which was assigned as $[M_8$-(C14:0)keten-H$]^-$ ion. It was formed by the elimination of the myristic acid (-210 Da) from the branch (Cl2:0(3-*O*-C14:0)) fatty acids which was attached to the N-2′ position (Figure 4.2.11, Table 4.1.9 and Scheme 4.1.9) (El-Aneed *et al*., 2006, Shaffer *et al*., 2007, Lukasiewicz *et al*., 2010, John *et al*., 2014, and Brodbelt *et al*., 2014).

SORI-CID-MS/MS of the deprotonated molecules at *m/z* 892.5979, which was assigned previously as [C-(C14:0)ketene-H]$^-$, gave the product ion at *m/z* 648.3949 (Figure 4.2.12, Table 4.1.10, Scheme 4.10). The product ion at *m/z* 648.3949 was assigned as the [C-(C14:0)ketene-(C14:0(3-OH))acid-H]$^-$ ion and it was formed by the elimination of the 3-hydroxy-myristic acid (C14:0(3-OH)) (-244 Da) from the O-3 of the precursor ion.

The deprotonated molecules at *m/z* 710.4259, which were assigned previously as [Y-H]$^-$, gave the product ion at *m/z* 466.2219 which was assigned as [Y-(C14:0(3-OH))acid-H]$^-$ ion, and it was formed by the elimination of the 3-hydroxy-myristic acid (C14:0(3-OH)) (-244 Da) from the O-3 position of the precursor ion (Figure 4.2.13, Table 4.1.11 and Scheme 4.1.11) (El-Aneed *et al*., 2006, Shaffer *et al*., 2007, Lukasiewicz *et al*., 2010, John *et al*., 2014, and Brodbelt *et al*., 2014).

The SORI-CID-MS/MS of the precursor deprotonated [C-(C14:0(3-*O*-C14:0))ketene-H]$^-$ molecule at *m/z* 666.4013 gave the product ions at *m/z* 648.3239 and *m/z* 438.2216 (Figure 4.2.11, Table 4.1.12 and Scheme 4.1.12). The product ions *m/z* 648.3239 was described previously as just a loss of a molecule of water.

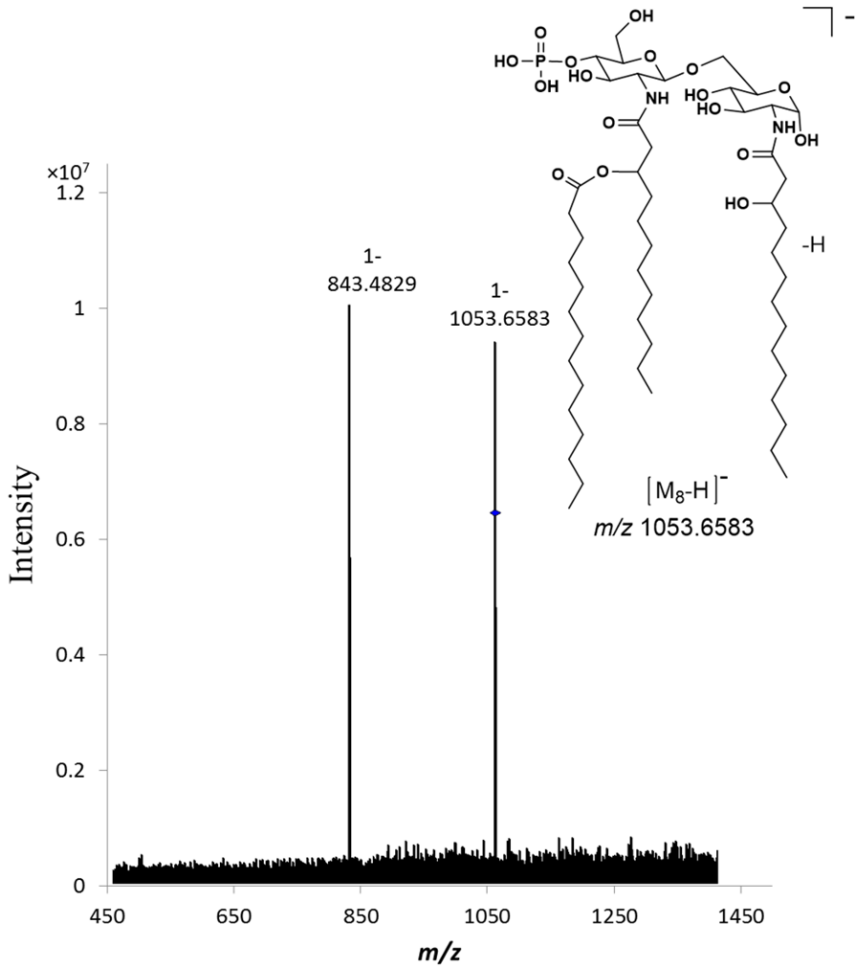

Figure 4.2.11: SORI-CID-MS/MS of the precursor deprotonated $[M_8\text{-}H]^-$ molecules at *m/z* 1053.6583.

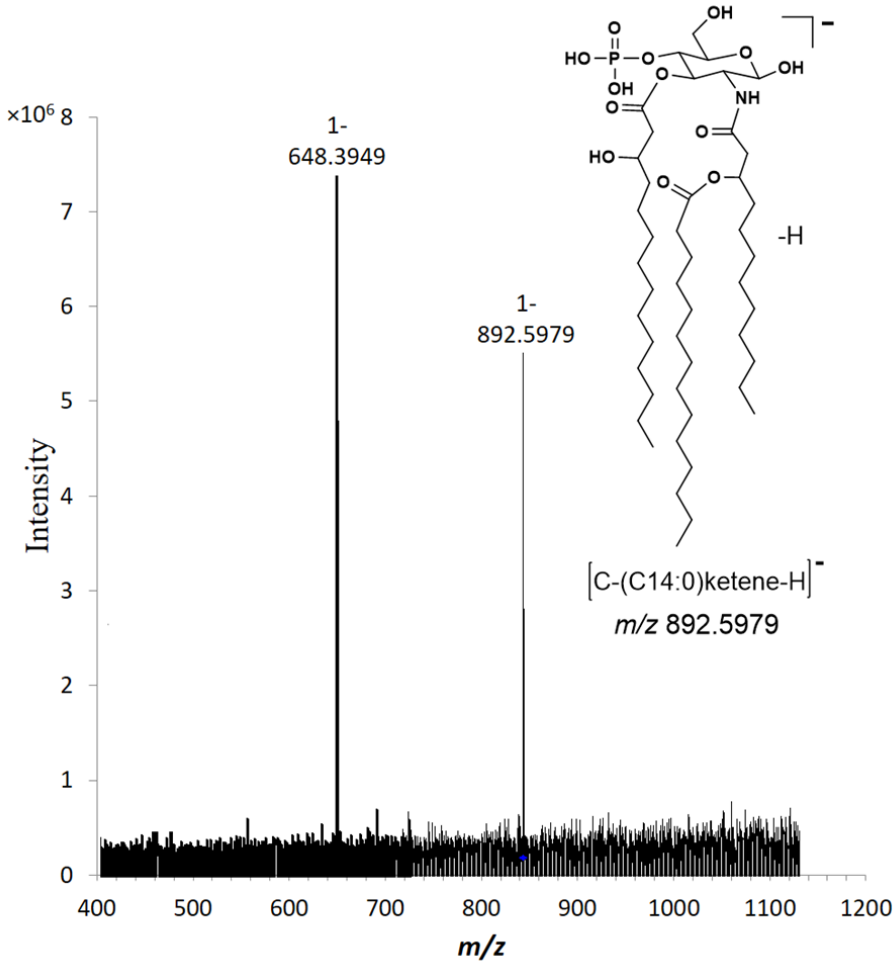

Figure 4.2.12: SORI-CID-MS/MS of the precursor deprotonated [C-(C14:0)ketene-H]$^-$ molecules at *m/z* 892.5979.

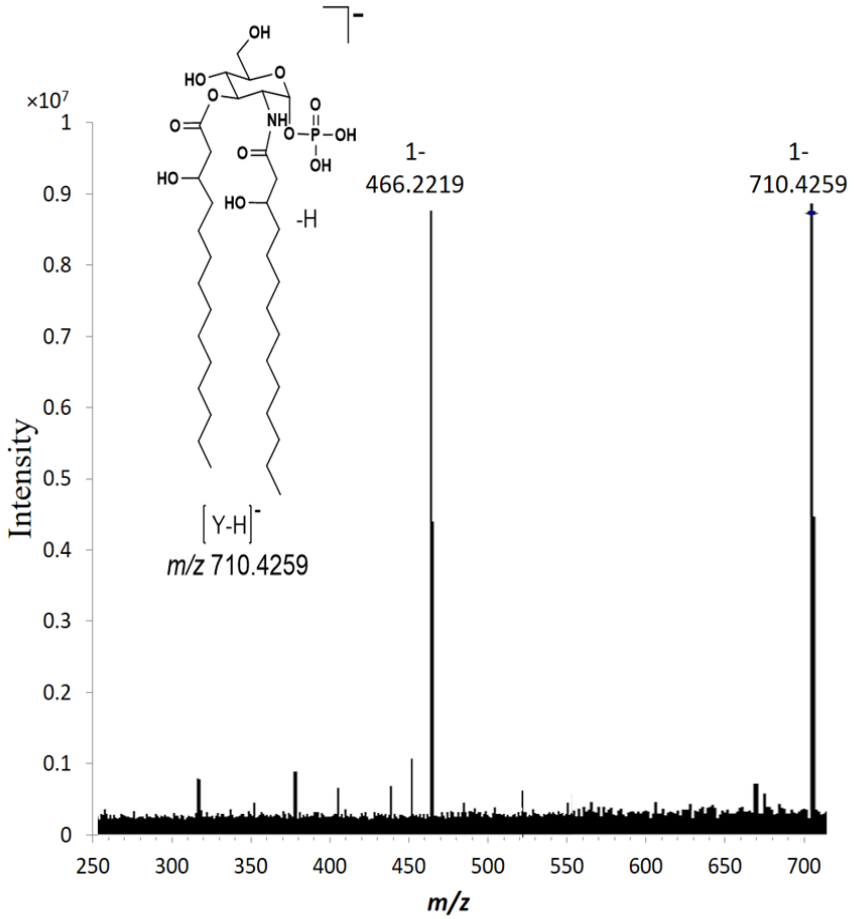

Figure 4.2.13: SORI-CID-MS/MS of the precursor deprotonated [C-(C14:0)ketene-(C12:0)Ketene-H]$^-$ molecules at *m/z* 710.4259.

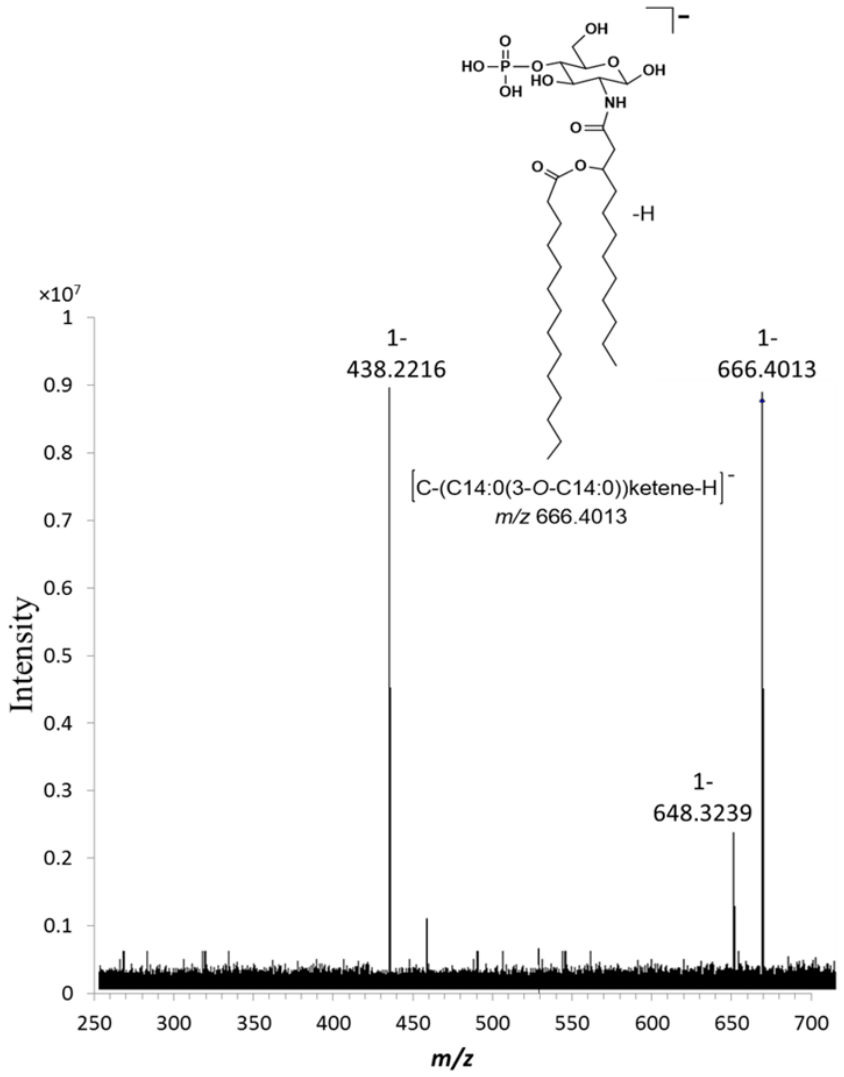

Figure 4.2.14: SORI-CID-MS/MS of the precursor deprotonated [C-(C14:0(3-*O*-C14:0))ketene-H]$^-$ molecules at *m/z* 666.4013.

The product ion at *m/z* 438.2216 was assigned as [C-(C14:0(3-*O*-C14:0))ketene-(C14:0)acid-H]$^-$ ion. It was formed by the elimination of a myristic acid (-228 Da), which was located at N-2 position of the precursor ion.

The SORI-MS/MS of the precursor ion at *m/z* 666.4013 and its associated product ions strongly confirm our suggested structures of the $LipA_{1-8}$ (El-Aneed *et al*., 2006, Shaffer *et al*., 2007, Lukasiewicz *et al*., 2010, John *et al*., 2014, and Brodbelt *et al*., 2014).

4.3.3. Comparison between low-energy CID-QqQ-MS/MS and SORI-CID-MS/MS of the deprotonated molecules obtained from the mixture of lipid A_n isolated from the LPS of *A. hydrophilla* SJ-55a

As discussed in the chapter 3 sections 3.3.3, we have made a comparison between the CID-MS/MS analyses with the QqQ-MS/MS and SORI-MS/MS. We have noticed that the number of distinctive product ions decreased with SORI-MS/MS analyses, when compared to CID-MS/MS analyses with the QqQ-mass spectrometer instrument. As in all of the previous schemes (4.1.2 – 4.1.8), we have noticed that all of the product ions obtained from SORI-CID-MS/MS were produced by the primary fatty acid fragmentation only. There were no CID-fragmentation from the branched fatty acyl groups and it was noted that most eliminations occurred from the O-3 and O-3´ positions. The reasons for the obtained differences in product ions formation are the same as these presented in section 3.3.3.

4.4. High-energy MALDI-TOF-MS analysis of the extracted mixture of lipid A_n isolated from the LPS of *A. hydrophilla* SJ-55a

The MALDI-TOF-MS (- ion mode) of the lipid A obtained from *A. Hydrophilla* SJ-55a was measured in the reflector mode with the TOF/TOF instrument and high laser power. Similarly, MALDI-MS shows similar spectra to the ones measured with the ESI-QqQ-MS and FTICR-MS instruments. Accordingly, we have assigned for this lipid A mixture, the original seven common structures of the lipid A as suggested previously in sections: 4.2 and 4.3. They were assigned to different $[M-H]^-$ deprotonated di-phosphorylated molecules $LipA_1$ at *m/z* 1796.2088 and $LipA_5$ at *m/z* 1359.8615, and mono-phosphorylated molecules $LipA_2$ at *m/z* 1716.2569, $LipA_3$ at *m/z* 1688.2145, $LipA_4$ at *m/z* 1506.0499, $LipA_6$ at *m/z* 1279.8615, and $LipA_7$ at *m/z* 1097.6426 (Figure 4.3.1, Scheme 4.1.1 and Table 4.1.1) (Kussak *et al.*, 2002, El-Aneed *et al*., 2006, Shaffer *et al*., 2007, Lukasiewicz *et al*., 2010, and Brodbelt *et al*., 2014).

In MALDI-TOF-mass spectrum, we noticed that the deprotonated molecules assigned to the $LipA_6$ at *m/z* 1279.8432 were the most abundant in the mass spectrum. It is important to note that there was no observation of the deprotonated molecules as being created by the$[C-H]^-$ or $[Y-H]^-$ ion in the MALDI-TOF-MS, as illustrated in (Figure 4.3.1). In order to examine the difference in CID-gas-phase fragmentations between the low-energy-CID-QqQ-MS/MS and the SORI-CID-FTICR-MS/MS analysis, we subjected this series of deprotonated molecules to a detailed analysis of the high energy CID-TOF/TOF-MS/MS analysis.

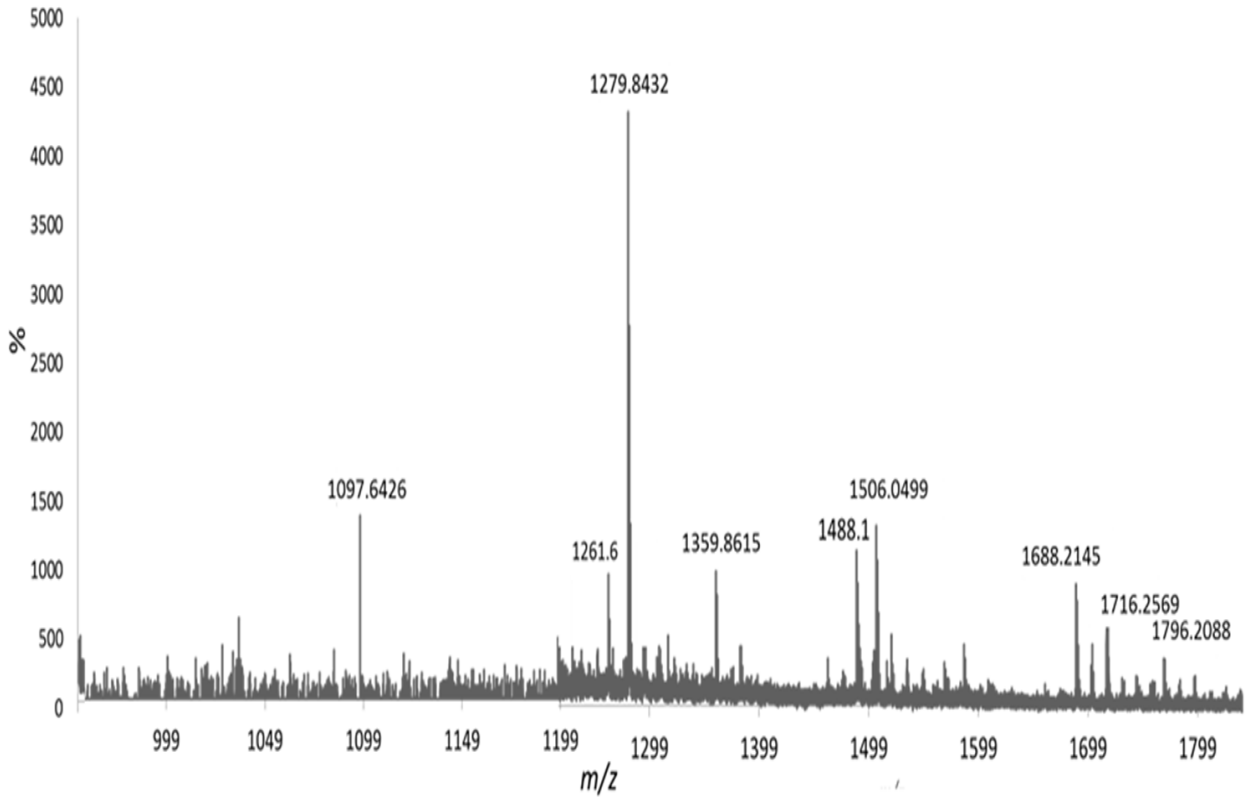

Figure 4.3.1: MALDI-TOF-MS (- ion mode) of the native lipid A_n mixture extracted from *A. hydrophilla* SJ-55a**.**

4.4.1. High-energy MALDI-CID-TOF/TOF-MS/MS analysis of the extracted mixture of lipid A_n isolated from the LPS of *A. hydrophilla* SJ-55a

These series of deprotonated molecules were subjected to high-energy CID-TOF/TOF-MS/MS, and the structures of the obtained product ions were deduced as previously described in the low-energy CID-QqQ-MS/MS and SORI-CID-FTICR-MS/MS described in section 4.2 and 4.3.

High-energy CID-TOF/TOF-MS/MS of the deprotonated molecules $LipA_1$ at *m/z* 1796.2088 is illustrated in (Figure 4.3.2, Tables 4.1.2, and Scheme 4.1.2). This product ion scan of $LipA_1$ produced the product ions at *m/z* 1506.0529, *m/z* 1488.0465, and *m/z* 1279.8498. The product ion at *m/z* 1506.0529 was assigned as $[M_1$-(C14:0)ketene-HPO_3-$H]^-$ ion. It was created by the loss of a myristic ketene (-210 Da) from the branched fatty (C14:0(3-*O*-C14:0)) located at O-3′ positions and neutral HPO_3 (-80 Da) located at O-1. The product ion at *m/z* 1488.0465 was created by extra losses of a molecule of water from the product ion at *m/z* 1506.0529. The last product ion at *m/z* 1279.8498 was assigned as $[M_1$-(C14:0(3-*O*-C14:0))ketene-HPO_3-$H]^-$. It was formed by the elimination of the consecutive losses of the branched fatty (C14:0(3-*O*-C14:0)) located on position O-3′ (-436 Da) and by the elimination of the neutral HPO_3 (-80 Da) moiety located at O-1 (Kussak *et al.*, 2002, El-Aneed *et al*., 2006, Shaffer *et al*., 2007, Lukasiewicz *et al*., 2010, and Brodbelt *et al*., 2014).

High-energy CID-TOF/TOF-MS/MS of the deprotonated molecules $LipA_2$ at *m/z* 1716.2569 is illustrated in (Figure 4.3.3, Tables 4.1.3, and Scheme 4.1.3).

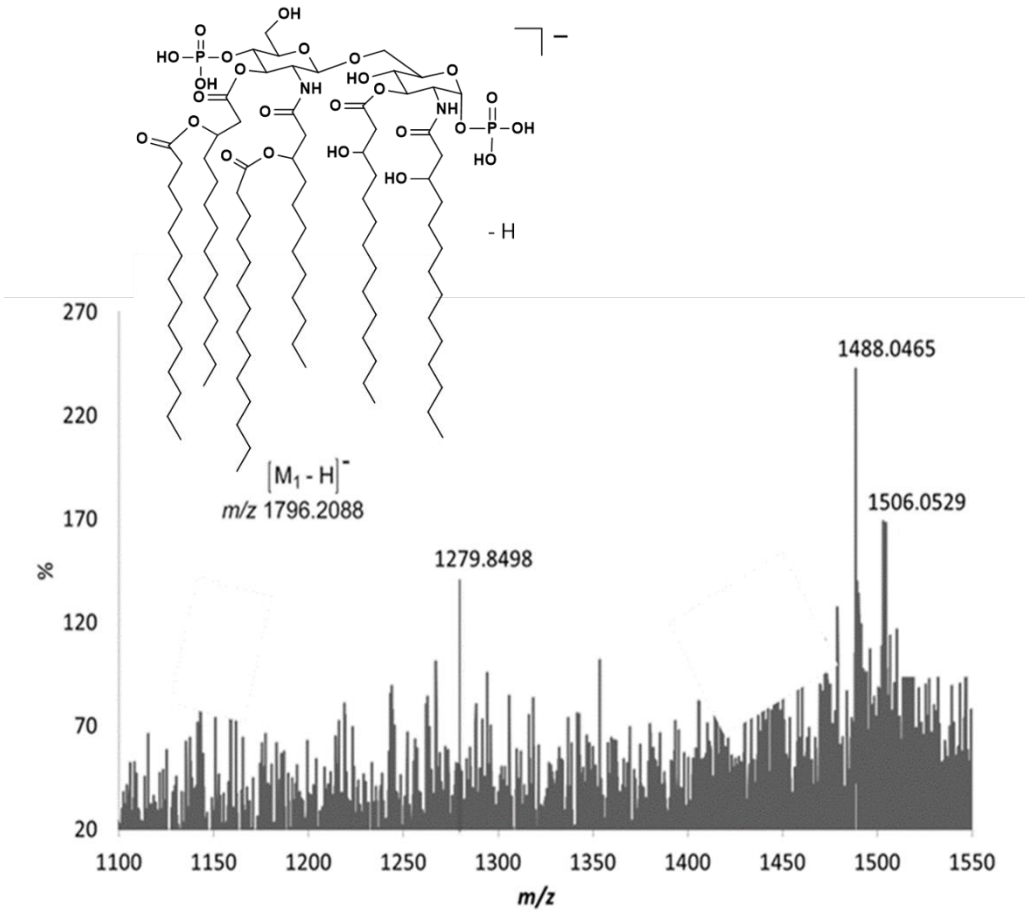

Figure 4.3.2: High-energy CID-TOF/TOF-MS/MS of the precursor ion $[M_1\text{-}H]^-$ ion at *m/z* 1796.2088.

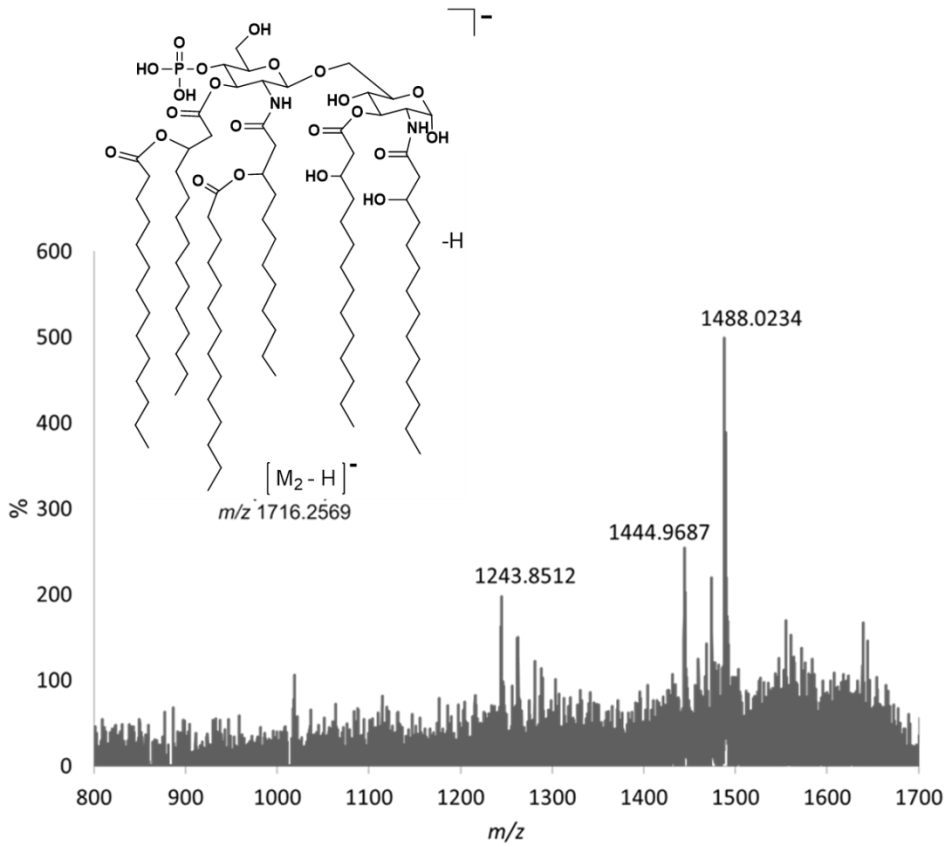

Figure 4.3.3: High-energy CID-TOF/TOF-MS/MS of the precursor ion $[M_2\text{-}H]^-$ ion at *m/z* 1716.2569.

The product ion scan of the deprotonated $LipA_2$ molecules gave the product ions at *m/z* 1488.0234, *m/z* 1444.9687, and *m/z* 1243.8512. The product ion at *m/z* 1488.0234 was assigned as the $[M_2$-(C14:0)acid-H$]^-$ ion, which was created by the elimination of myristic acid form the branched fatty (C14:0(3-*O*-14:0)) acid acyl group located at O-3′ (-228 Da). The product ions at *m/z* 1444.9687 is created by extra losses of n-propane (-44 Da) from the alkyl chain (C14:0) located at N-2′.The product ion at *m/z* 1243.8512 was assigned as was assigned as $[M_2$-(C14:0)acid-(C14:0(3-OH))acid-H$]^-$ ion. It was formed by consecutive losses of a 3-hydroxyl myristic acid (-244 Da), which was located at O-3 position, and a myristic acid form the branched fatty (C14:0(3-*O*-C14:0)) acid acyl group located at O-3′ (-228 Da) from the precursor ion at *m/z* 1716.2569 (Kussak *et al.*, 2002, El-Aneed *et al*., 2006, Shaffer *et al*., 2007, Lukasiewicz *et al*., 2010, and Brodbelt *et al*., 2014).

High-energy CID-TOF/TOF-MS/MS of the deprotonated molecules $LipA_3$ at *m/z* 1688.2145 is illustrated in (Figure 4.3.4, Tables 4.1.4, and Scheme 4.1.4). The production scan of the deprotonated $LipA_3$ molecules gave the product ions at *m/z* 1488.0403 *m/z* 1444.9765, and *m/z* 1243.8520. The product ion at *m/z* 1488.0403 was assigned as the $[M_2$-(C12:0)acid-H$]^-$ ion, which was created by the elimination of the lauryl acid (-200 Da) from the branched fatty (C14:0(3-*O*-12:0)) acid located on N-2′.The product ions at *m/z* 1444.9765 was assigned as $[M_3$-(C14:0(3-OH)acid-H$]^-$ ion. It was created by the loss of a 3-hydroxyl myristic acid (-244 Da), which was located at O-3 position of the $LipA_3$.

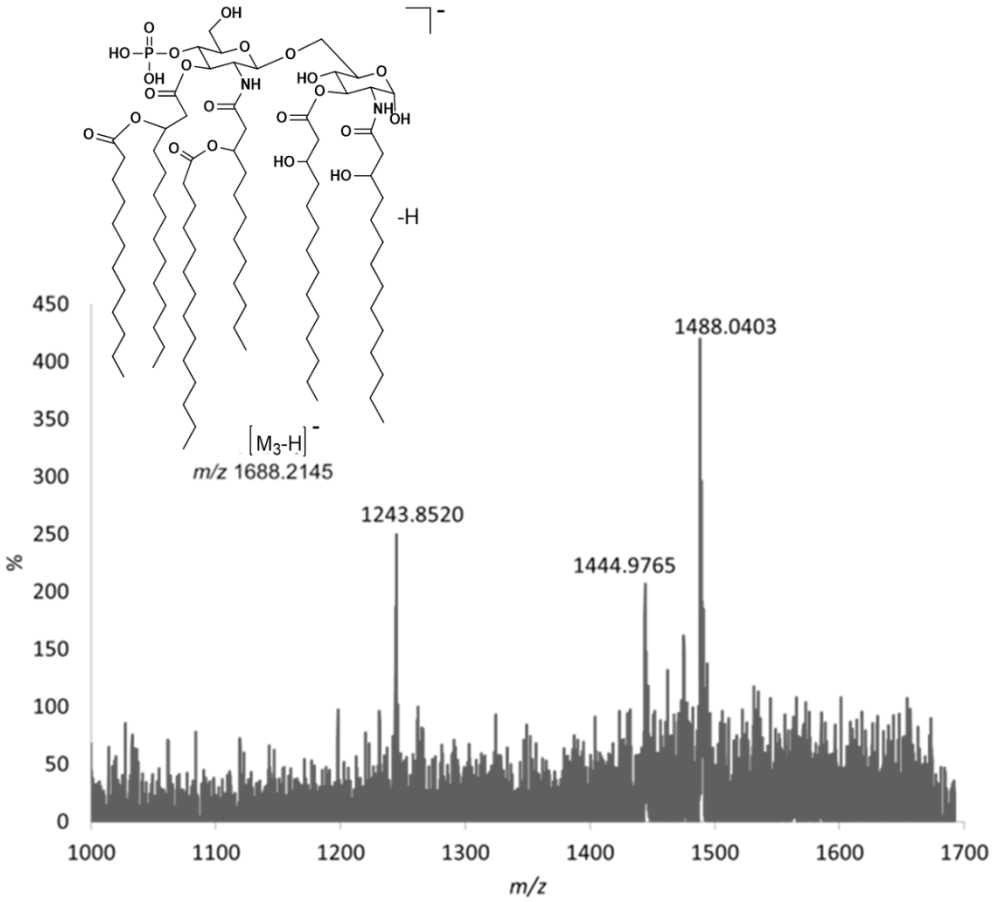

Figure 4.3.4: High-energy CID-TOF/TOF-MS/MS of the precursor ion $[M_3\text{-}H]^-$ ion at *m/z* 1688.2145.

The product ion at *m/z* 1243.8520 was assigned as [M_3-(C14:0(3-*O*-12:0))acid-H_2O-H]$^-$ ion, and it was formed by the consecutive losses of the branched fatty (C14:0(3-*O*-C12:0)) acid (-426 Da) located on position O-3′ and a molecule of water from the precursor ion at *m/z* 1688.2145 (Kussak *et al.*, 2002, El-Aneed *et al*., 2006, Shaffer *et al*., 2007, Lukasiewicz *et al*., 2010, and Brodbelt *et al*., 2014).

High-energy CID-TOF/TOF-MS/MS of the deprotonated molecules $LipA_4$ at *m/z* 1506.0499 is illustrated in (Figure 4.3.5, Tables 4.1.5, and Scheme 4.1.5). The product ion scan of the deprotonated $LipA_4$ molecules gave the product ions at *m/z* 1488.0420, *m/z* 1261.8501, *m/z* 1243.8511, and *m/z* 1035.6614. The product ion at *m/z* 1488.0420 was obtained by the loss of a molecule of water from the precursor ion. The product ions at *m/z* 1261.8501 was assigned as [M_4-(C14:0(3-OH)acid-H]$^-$ ion. It was formed by the elimination of 3-hydroxy-myristic acid (-244 Da) from the precursor ion. This elimination could in fact occur from either at the O-3 and O-3′ positions; located respectively in the reducing end or non-reducing end of the lipid A disaccharide backbone. The product ion at *m/z* 1243.8511 was assigned as [M_4-(C14:0(3-OH))acid-H_2O-H]$^-$ ion, and it was formed by the consecutive losses of a molecule of water and 3-hydroxy-myristic acid (-244 Da). It can in fact occur from either at the O-3 and O-3′ positions located respectively in the reducing end or non-reducing end of the lipid A disaccharide backbone (Kussak *et al.*, 2002, El-Aneed *et al*., 2006, Shaffer *et al*., 2007, Lukasiewicz *et al*., 2010, and Brodbelt *et al*., 2014). The product ion at *m/z* 1035.6614 was assigned as [M_4-(C14:0(3-OH))acid-(C14:0(3-OH))ketene-H]$^-$ ion.

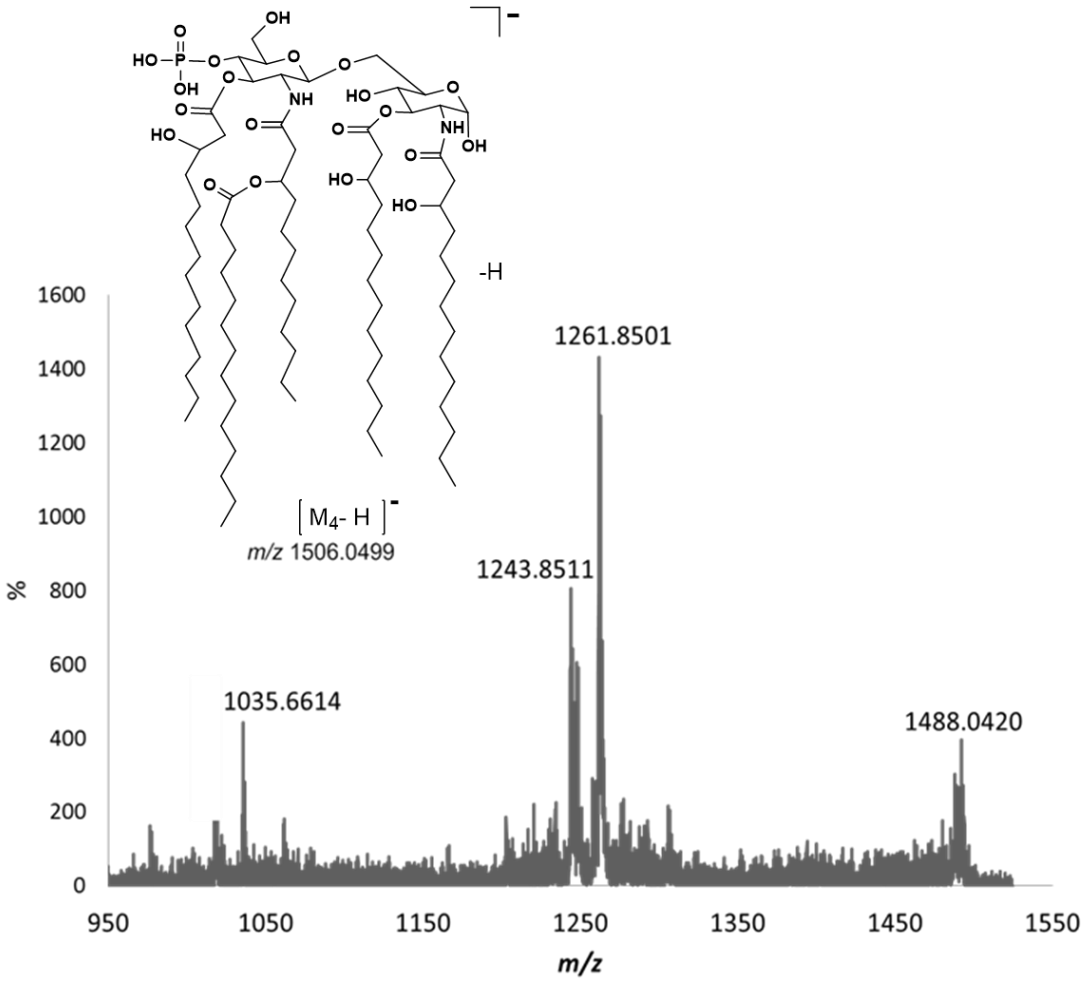

Figure 4.3.5: High-energy CID-TOF/TOF-MS/MS of the precursor ion $[M_4\text{-}H]^-$ ion at *m/z* 1506.0499.

It was formed by the consecutive losses of the 3-hydroxy-myristic acid (-244 Da) and the 3-hydroxy-myristic ketene (-226 Da), which can in fact occur from either at the O-3 and O-3′ positions; located respectively in the reducing end or non-reducing end of the lipid A disaccharide backbone (Kussak *et al.*, 2002, El-Aneed *et al*., 2006, Shaffer *et al*., 2007, Lukasiewicz *et al*., 2010, and Brodbelt *et al*., 2014).

High-energy CID-TOF/TOF-MS/MS of the deprotonated molecule $LipA_5$ at *m/z* 1359.8615 is illustrated in (Figure 4.3.6, Tables 4.1.6, and Scheme 4.1.6). The product ion scan of the deprotonated $LipA_5$ molecules gave the product ions at *m/z* 1262.8510, *m/z* 1115.6097 and *m/z* 1085.5630. The product ion at *m/z* 1261.8510 was assigned as $[M_5-H_2PO_4-H]^-$, which was created by the loss of H_3PO_4 (-98 Da). The product ion at *m/z* 1115.6097 was assigned as $[M_5$-(C14:0)(3-OH)acid-H$]^-$ ion, and it was formed by the elimination of 3-hydroxy-myristic acid (-244 Da) from the precursor ion located at O-3. The product ion at *m/z* 1085.5630 was assigned as $[M_5$-(C12:0)acid-(C_4H_8)-H_2O-H$]^-$ ion. It was formed by the consequent elimination of a water molecule, (C_4H_8) (-56 Da) as part of the fatty acid chain properly located at O-3 position, and the lauryl acid (-200 Da) from the branched fatty (C14:0(3-*O*-12:0)) acid located on N-2′ (Kussak *et al.*, 2002, El-Aneed *et al*., 2006, Shaffer *et al*., 2007, Lukasiewicz *et al*., 2010, and Brodbelt *et al*., 2014).

High-energy CID-TOF/TOF-MS/MS of the deprotonated molecules $LipA_6$ anion at *m/z* 1279.8432 is illustrated in (Figure 4.3.7, Tables 4.1.7, and Scheme 4.1.7). The product ion scan of the deprotonated $LipA_6$ molecules gave the product ions at *m/z* 1035.6598, *m/z* 913.4996, *m/z* 817.4598 and *m/z* 666.3897 (Kussak *et al.*, 2002, El-Aneed *et al*., 2006, Shaffer *et al*., 2007, Lukasiewicz *et al*., 2010, and Brodbelt *et al*., 2014).

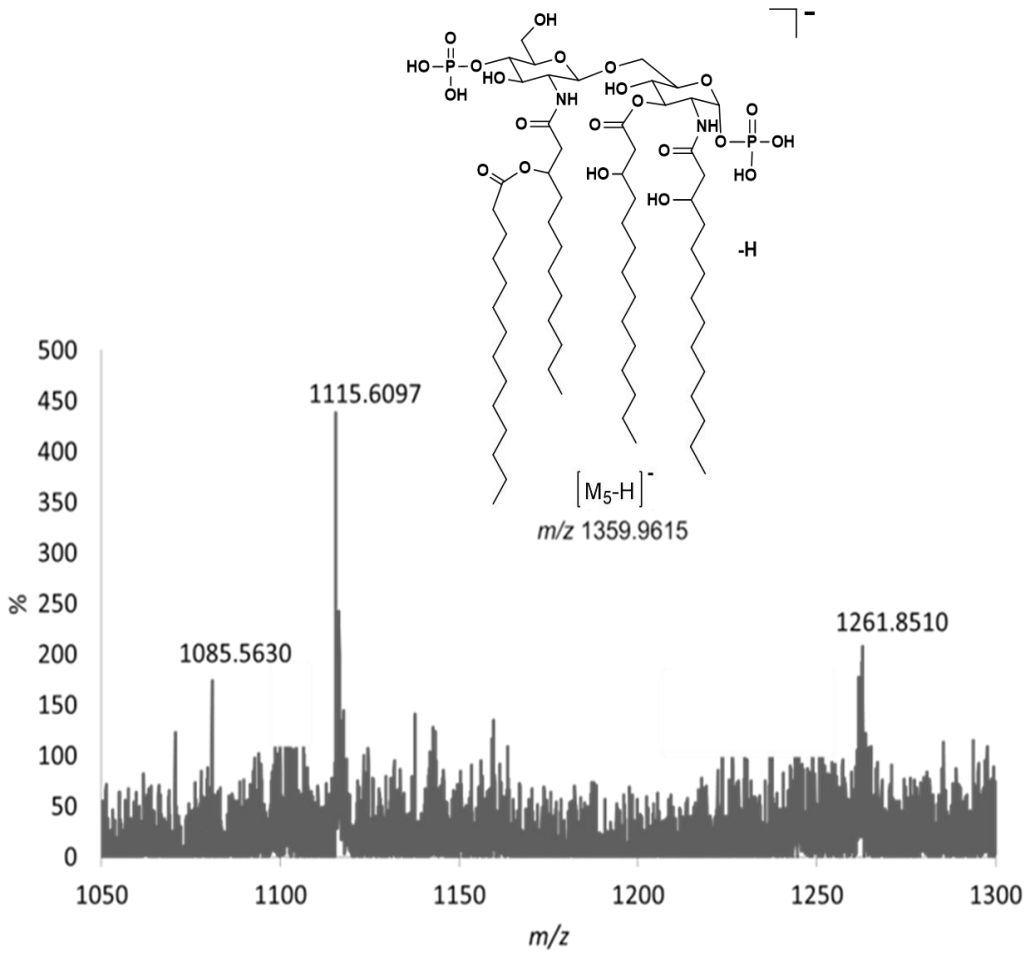

Figure 4.3.6: High-energy CID-TOF/TOF-MS/MS of the precursor ion $[M_5\text{-}H]^-$ ion at *m/z* 1359.8615.

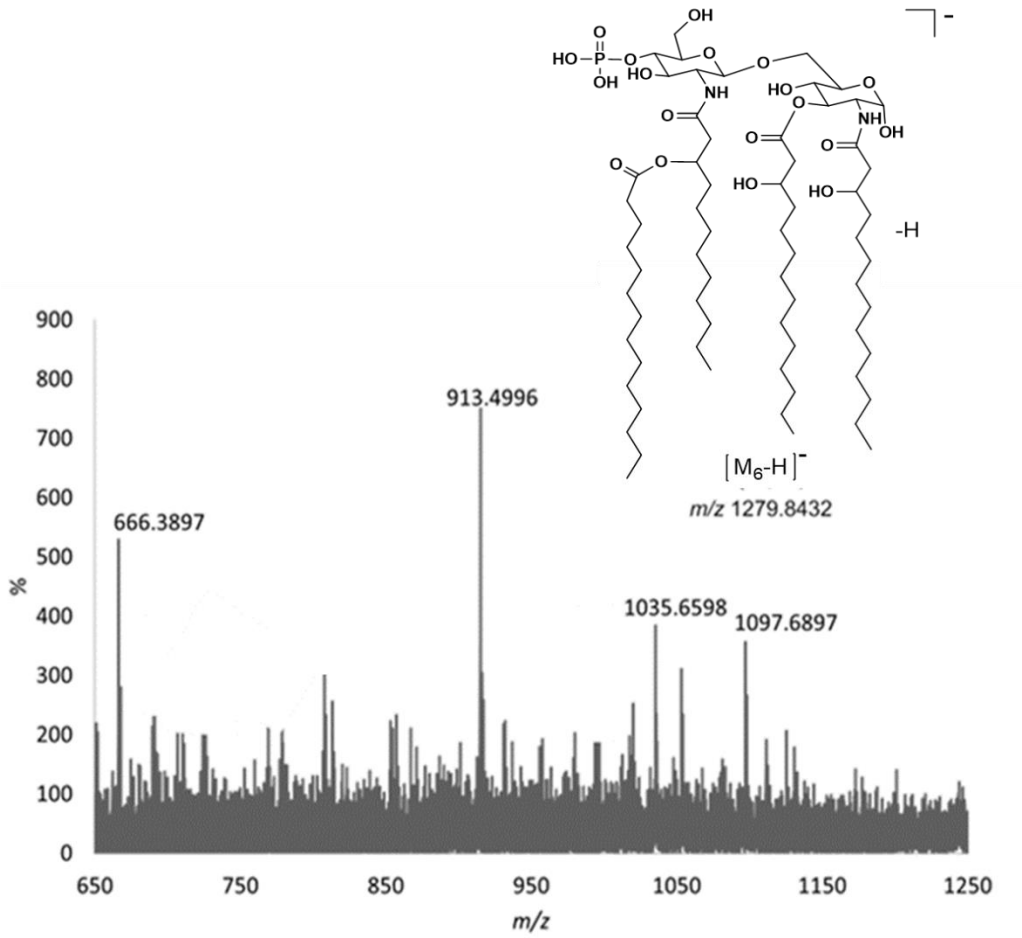

Figure 4.3.7: High-energy CID-TOF/TOF-MS/MS of the precursor ion $[M_6\text{-}H]^-$ ion at *m/z* 1279.8432.

The product ion at *m/z* 1035.6598 was assigned as the [M_6-(C14:0(3-OH))acid-H]$^-$ ion, which was created by the elimination of 3-hydroxy-myristic acid (C14:0(3-OH)) (-244 Da) located at the position O-3 of the reducing GlcN end. The product ion at *m/z* 913.4996 was assigned as [M_6-(C14:0(3-OH))ketene-(C10H20)-H]- ion, which was created by the elimination of 3-hydroxy-myristic ketene (C14:0(3-OH)) (-226 Da) located at the position O-3, and n-($C_{10}H_{20}$) as a part of the fatty acid located in N-2′(-140 Da). The last product ion at *m/z* 666.3897 was assigned as [C-H]$^-$ as the mono-phosphorylated D-GlcN species containing one branched (Cl4:0(3-*O*-C12:0)) fatty acyl group on the N-2 position (Scheme 4.1.1) (Kussak *et al.*, 2002, El-Aneed *et al*., 2006, Shaffer *et al*., 2007, Lukasiewicz *et al*., 2010, and Brodbelt *et al*., 2014).

High-energy CID-TOF/TOF-MS/MS of the deprotonated molecules $LipA_7$ at *m/z* 1097.6426 is illustrated in (Figure 4.3.8, Tables 4.1.8, and Scheme 4.1.8). The product ion scan of the deprotonated $LipA_7$ molecules gave the product ions at *m/z* 852.4797 and *m/z* 527.2520. The product ion at *m/z* 852.4797 was assigned as the [M_7-(C14:0) acid-H_2O-H]$^-$ ion, which was created by the elimination of a myristic acid (C12:0(3-*O*-C14:0)) (-244 Da) located at the position N-2′ of the non-reducing GlcN end of the $LipA_7$ disaccharide, and a molecule of water. The product ion *m/z* 693.4959 was assigned as the [M_7-(C14:0)ketene-$2H_2PO_4$-H]$^-$ ion. It was created by the elimination of a myristic ketene (C12:0(3-*O*-C14:0)) (-208 Da) located at the position N-2′ of the non-reducing GlcN end of the $LipA_7$ disaccharide, and a two neutral H_3PO_4 (-196 Da) moiety (as shown in Figure 4.3.8) (Kussak *et al.*, 2002, El-Aneed *et al*., 2006, Shaffer *et al*., 2007, Lukasiewicz *et al*., 2010, and Brodbelt *et al*., 2014).

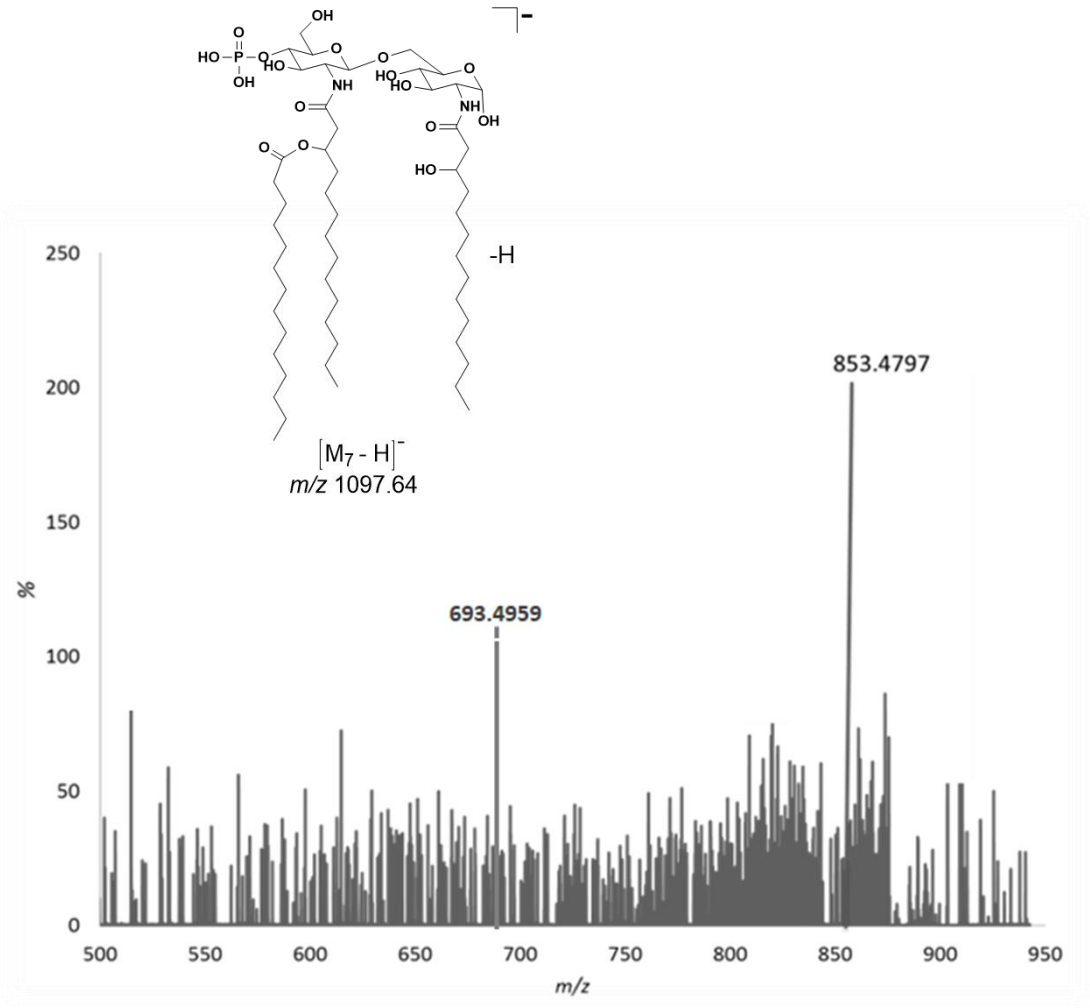

Figure 4.3.8: High-energy CID-TOF/TOF-MS/MS of the precursor ion $[M_7\text{-}H]^-$ ion at *m/z* 1097.6426.

4.4.2. Comparison between low-energy CID-QqQ-MS/MS and high-energy CID-TOF-TOF-MS/MS

Similarly, to Chapter 3 in section 3.4.2, when we compared between the MALDI-CID-TOF/TOF-MS/MS analysis and the ESI-CID-QqQ-MS/MS, we have noticed that the number of distinctive product ions decreased with MALDI-CID-TOF/TOF analysis which was probably due the number of collisions. We have noticed that all the of the product ions which obtained from MALDI-CID-TOF/TOF just like SORI-CID-MS/MS were produced by the primary fatty acid fragmentation not the branched, most of the time the elimination occur at O-3 and O-3´ position (Schemes 4.1.2 - 4.1.8 and Tables 4.1.2 - 4.1.8). Once more, we have attributed this anomaly to the high-energy CID that leads to few collisions of the precursors. Also, the high kinetic energy of the ions leads to shorter time scale for dissociation (few microseconds).

4.5. Summary

The deprotonated molecules obtained from this heterogeneous mixture of lipid A_n were investigated by tandem mass spectrometry using low-energy collision SORI-CID-MS/MS (tandem in time) and CID-MS/MS (tandem in space) instruments. Likewise, The MALDI-CID-TOF/TOF-MS/MS, CID-QqQ, and SORI-FTICR-MS/MS fragmentation studies of the different lipid $A_{1\text{-}6}$ have shown the presence of diagnostic and unique C-C heterolytic fragmentation of the fatty acid chains.

We have noticed that the SORI-MS/MS spectra of the various precursor deprotonated molecules were much simpler than those of the acquired CID-MS/MS with the MALDI-TOF/TOF and QqQ-instrument.

The combined MS/MS studies indicate that all the proposed structures of the lipid A_1 to A_8 contain two phosphate groups at the position O-1 and O-4′. They were built by a β-D-Glc*p*N-(1→6)-α-D-Glc*p*N disaccharide blueprint. the lipid A backbone disaccharide was substituted with (C14:0(3-OH)) at the O-3, O-3´ and N-2 positions, and (C12:0(3-OH)) at N-2´position, which contain different substitution permutations with (C12:0(3-*O*-C14:0)) at the N-2´ position, and (C14:0(3-*O*-C14:0)) at the O-3´ position (Scheme 4.1.1).

The presence of this mixture series of lipid A_n isolated from SJ-55a in the ESI- and MALDI-MS spectra is good indicator to incomplete biosynthesis of lipid A. Also, the presence of the monosaccharide backbone was reported in all of them, such as the deprotonated molecules at *m/z* 892, *m/z* 710,40 and *m/z* 666.55.

In conclusion, the interaction between the bacteria and the bacteriophages lead to some mutation which leads to incomplete lipid A biosynthesis, due to the disruption in core biosynthesis process occurring at different stages. Such structural aberrations could affect bacteriophage adsorption which could increases the resistance of the bacteria to the bacteriophages.

Chapter 5

Mass Spectral analysis of the mixture of Lipid A_n isolated from the LPS of *A. salmonicida* SJ-113

Aeromonas Salmonicida is a genus of Gram-negative, anaerobic homogeneous in cultural and biochemical characteristics. *Aeromonas Salmonicida* is considered as one of the oldest described fish pathogens, and causes the disease known as furunculosis (ex. ulcers and tail rot in fish) in cultured pond-fish and salmonids (Brisson *et al*., 2004). First, its genus was belonged to the Gram-negative of the family *Pseudomonadaceae*. Then, it was transferred to the family of *Vibrionaceae*. Then consequently to its own family which is *Aeromonadaceae* (Austin 2011, and Chart *et al.*, 1984). The LPS of SJ-113a was obtained from the rough mutant Gram-negative bacteria *A. salmonicida* grown in the presence of phage and it was classified as phage resistant.

5.1. Gas chromatography-mass spectrometry (GC-MS) of the fatty methyl ester released from the lipid A_n mixture isolated from the LPS of the *A. salmonicida* SJ-113

The qualitative analysis of fatty acids was carried out by GC-MS to identify separately the amide and the ester-bound fatty acids. The (R)-3-hydroxytetradecanoic acid (C14:0(3-OH)) was identified as an amide-linked fatty acid, whereas the (R)-3-hydroxytetradecanoic acid (C14:0(3-OH)) (3-hydroxymyristic acid) and dodecanoic acid (C12:0) (lauric acid) were identified as amide-linked fatty acids (Perry *et al*., 1979, Rebeil

et al., 2004, and Almostafa *et al*., 2016). In addition to the methyl ester derivative of 3-methoxytetradecanoic acid, the fatty acid methyl esters obtained by trans-esterification with sodium methoxide also showed the presence of the (C14:0(3-OH)) acid, which was substituted by dodecanoic acid (lauric acid) (C12:0) in the native lipid A. The absolute configuration of the GlcN residues in lipid A was determined as D on the deacylated, dephosphorylated lipid A fraction, using (R)-2-butanol (M. Almostafa., *et al* 2016).

5.2. ESI-QqQ-MS analysis of the extracted mixture of lipid A_n isolated from the LPS of *A. salmonicida* SJ-113a

The *A. salmonicida* SJ-113a bacteria dissolved in chloroform and methanol was electrosprayed in the negative ion mode. The ESI-QqQ-ToF-MS is shown in (Figure 5.1.1). The lipid A_n component of the *A. salmonicida* SJ-113a bacteria is not merely composed of a single lipid A entity. In reality, it is a complex mixture of many structurally-related components produced by the incomplete biosynthesis of this lipid A.

The ESI-QqQ-MS (- ion mode) of the lipid A_n (where n=1-6). mixture showed the presence of *inter-alia seven* different fragment ions at *m/z* 1768.20, *m/z* 1688.17, *m/z* 1586.12, *m/z* 1506.09, *m/z* 1359.79, *m/z* 1279.89, and *m/z* 892.55. This indicates the presence of a heterogeneous mixture of lipid A_n assigned by the $[M_n\text{-}H]^-$ molecules (Scheme.5.1.1).

We have assigned these fragment ions as the series of $[M_n\text{-}H]^-$ deprotonated mono-phosphorylated molecules, and assigned as deprotonated di-phosphorylated molecules. The

deprotonated di-phosphorylated molecules are *m/z* 1768.20, *m/z* 1586.12 and *m/z* 1359.79. The rest are assigned as deprotonated mono-phosphorylated molecules *m/z* 1688.17, *m/z* 1506.09, *m/z* 1279.89, and *m/z* 892.50 represented as the following: $LipA_1$ at *m/z* 1768.20, $LipA_2$ *m/z* 1688.17, $LipA_3$ at *m/z* 1586.12, $LipA_4$ at *m/z* 1506.09, $LipA_5$ at *m/z* 1359.79, and $LipA_6$ at *m/z* 1279.89 (Figure 5.1.1, Scheme 5.1.1, and Table 5.1.1). For simplification, we have tied this series of analyzed deprotonated $[C\text{-}H]^-$ ion molecules to previously nomenclature adopted in sections 3.2. and 4.2. It is important to note that our tentative structural assignments of this series of deprotonated molecules have relied on comparison with well know Lipid A structures by a manual and expert-driven process. This was done without help of any software such as LipidView™ Software produced by Sciex.

Based on well-known literature, the structures of the heterogeneous lipid A_n mixture may contain phosphate groups, which can be located on the O-4′ and O-1 positions of the β-D-Glc*p*N-(1→6)-α-D-Glc*p*N disaccharide backbone of lipid A. Also, the 3-hydroxy-myristic acid (C14:0(3-OH)) fatty acid chains that acylate the various free positions of the β-D-Glc*p*N-(1→6)-α-D-Glc*p*N backbone of the fully biosynthesized lipid A_n. These fatty acid chains were certainly attached to the O-3, O-3′, N-2 and N-2′ positions of this lipid A. Also, it is proposed that the two of these (C14:0(3-OH)) fatty acyl groups are substituted with a lauric acid (Cl4:0(3-*O*-C12:0)) fatty acyl groups, which are probably located on the O-3 position at the reducing end, and N-2′ positions of the non-reducing end group of the β-D-Glc*p*N-(1→6)-α-D-Glc*p*N disaccharide backbone of this lipid A_n mixture (Scheme 5.1.1) (Lukasiewicz *et al*., 2010, Banoub *et al*., 2010, Kilár *et al*., 2013, Brodbelt *et al*., 2014, and Almostafa *et al*., 2016).

The deprotonated molecule $[M_1\text{-}H]^-$ $LipA_1$ at *m/z* 1768.20 was assigned as the di-phosphorylated hexa-acylated forms carrying four primary 3-hydroxy-myristic acid (C14:0(3-OH)) fatty acids, in which two of them were substituted by lauric acids forming the branched fatty acids (Cl4:0(3-*O*-C12:0)). This series of fatty acyl groups can be distributed on the O-3, O-3′, N-2, and N-2′ position, not necessarily in that order (Scheme 5.1.1).

The deprotonated molecule $[M_2\text{-}H]^-$ of $LipA_2$ at *m/z* 1688.17 was attributed to the mono-phosphorylated hexa-acylated molecules. Accordingly, we presume that this molecule was formed by four (C14:0(3-OH)) 3-hydroxy-myristic acids in which two of these fatty acids were esterified with two separate molecules of lauric acid (C12:0) at the 3-hydroxyl position of (C14:0(3-OH)) myristic acids. Once more, by comparing with other known structures of lipid A these two branched (Cl4:0(3-*O*-C12:0)) fatty acids are probably located on the O-3 position of the reducing end, and N-2′ positions of the non-reducing end group of the $LipA_2$ disaccharide backbone (Scheme 5.1.1).

The deprotonated molecules $LipA_3$ at *m/z* 1586.12 was assigned as the di-phosphorylated penta-acylated form of the β-D-(1→6)-Glucosamine disaccharide carrying four primary 3-hydroxy-myristic acid (C14:0(3-OH)) fatty acids, in which one of them was substituted by lauric acids forming the branched fatty acids (Cl4:0(3-*O*-C12:0)), which we tentatively assigned to be located at N-2′ of the non-reducing end residue of β-D-GlcpN-(1→6)-α-D-GlcpN disaccharide of $LipA_3$.

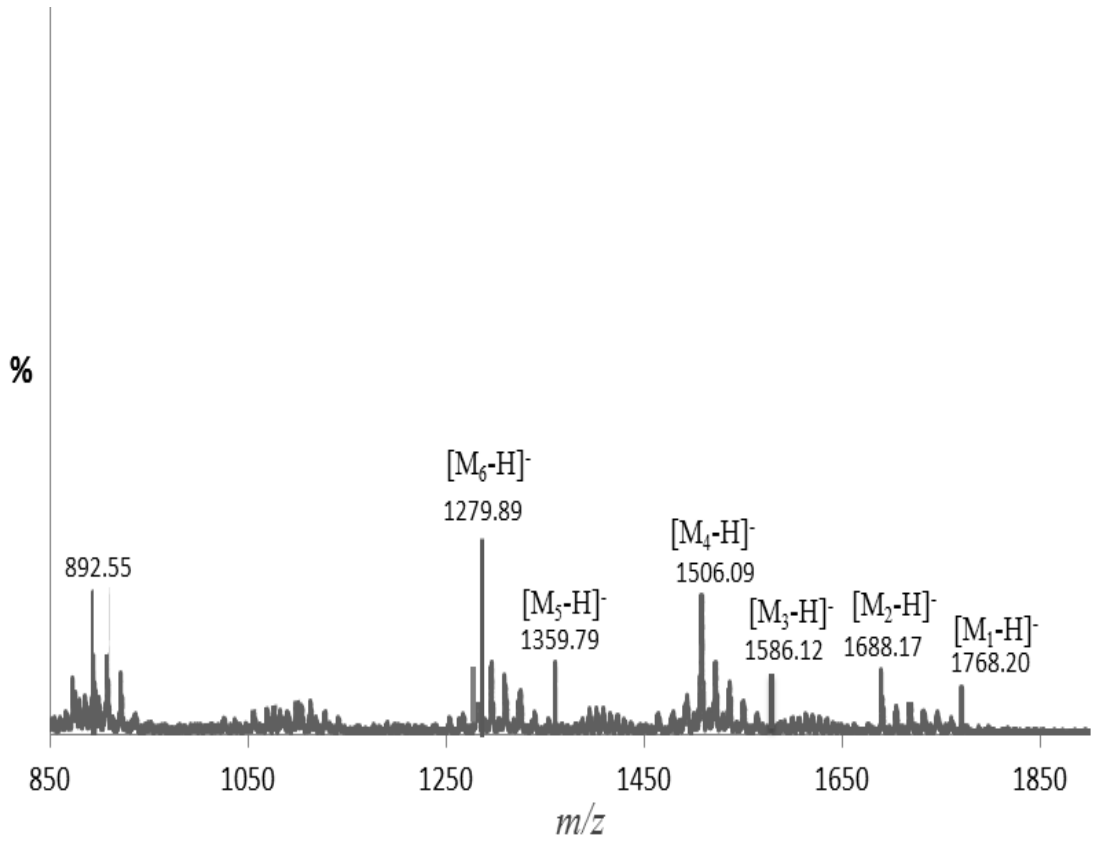

Figure 5.1.1: ESI-QqQ-MS of the native lipid A_n extract from the LPS of *A. salmonicida* SJ-113a.

The deprotonated molecules $LipA_4$ at *m/z* 1506.09 was assigned as the mono-phosphorylated penta-acylated form of the β-D-(1→6)-Glucosamine disaccharide carrying four primary 3-hydroxy-myristic acid (C14:0(3-OH)) fatty acids, in which one of them was substituted by lauric acids forming the branched fatty acids (Cl4:0(3-*O*-C12:0)), which we tentatively assigned to be located at N-2′ of the non-reducing end residue of β-D-GlcpN-(1→6)-α-D-GlcpN disaccharide of $LipA_4$.

The deprotonated molecule of $LipA_5$ $[M_5\text{-H}]^-$ at *m/z* 1359.79 was assigned as containing a di-phosphorylated tri-acylated form of the β-D-Glc*p*N-(1→6)-α-D-Glc*p*N disaccharide carrying three primary 3-hydroxy-myristic acid (C14:0(3-OH)) fatty acids, in which one of them was substituted by lauric acids forming the branched fatty acids (Cl4:0(3-*O*-C12:0)), probably located at the N-2′ position of this lipid A.

The deprotonated molecule of $LipA_6$ $[M_6\text{-H}]^-$ at *m/z* 1279.89 was assigned as containing a mono-phosphorylated tri-acylated form of the β-D-Glc*p*N-(1→6)-α-D-Glc*p*N disaccharide carrying three primary 3-hydroxy-myristic acid (C14:0(3-OH)) fatty acids, and the other one was substituted by lauric acids forming the branched fatty acids (Cl4:0(3-*O*-C12:0)), probably located at the N-2′ position of this lipid A.

In addition, we have also observed the deprotonated molecule at *m/z* 892.55 which was tentatively assigned as $[\text{C-(C14:0)ketene-H}]^-$. This latter deprotonated molecule was attributed to the deprotonated molecule mono-phosphorylated D-GlcN species containing a 3-hydroxy-myristic (C14:0(3-OH)) fatty and a branched (Cl4:0(3-*O*-C12:0)) fatty acid group located on N-2 (Scheme 5.1.1).

Table 5.1.1: Assignments of the deprotonated molecules observed in ESI-QqQ-MS and ESI-FTICR-MS (- ion mode) of native mixture of lipid A_{1-6} extracted from the LPS of *A. salmonicida* SJ-113a.

Deprotonated Molecules	Empirical Formula	ESI-QqQ-MS		ESI-FTICR-MS		MALDI-TOF/TOF-MS	
		m/z Observed; Calculated (%)	δ ppm	*m/z* Observed; Calculated (%)	δ ppm	*m/z* Observed; Calculated (%)	δ ppm
$[M_1 -H]^-$	$C_{92}H_{174}N_2O_{25}P_2$	1796.30; 1796.21 (18.2)	11	1768.1817; 1768.1808 (1.19)	0.5	1768.1798; 1768.1808 (44)	-1
$[M_2 -H]^-$	$C_{92}H_{172}N_2O_{21}P_2$	1688.26; 1688.21 (20.3)	-23	1688.2115; 1688.2145 (1.23)	-1.7	1688.2123; 1688.2145 (33.7)	-1.3
$[M_3 -H]^-$	$C_{80}H_{152}N_2O_{24}P_2$	1586.12; 1586.02 (8)	56	1586.0254; 1586.0210 (3.2)	2.7	1586.0210; 1586.0246 (65)	2.2
$[M_4 -H]^-$	$C_{80}H_{150}N_2O_{21}P$	1506.09; 1506.05 (35.2)	-26.5	1506.0580; 1506.0574 (4.1)	0.3	1506.0466; 1506.0574 (100)	-7.1
$[M_5 -H]^-$	$C_{66}H_{125}N_2O_{22}P_2$	1359.79; 1359.82 (30.9)	-44	1359.8166; 1359.8205 (1.8)	-2.8	1359.8259; 1359.8205 (47)	3.7
$[M_6 -H]^-$	$C_{66}H_{124}N_2O_{19}P$	1279.89; 1279.85 (41)	31.2	1279.8496; 1279.8541 (3.15)	-3.5	1279.8510; 1279.8541 (100)	-2.4
$[C -H]^-$	$C_{46}H_{87}NO_{13}P$	892.55; 892.59 (55.8)	-56	892.5979; 892.5993 (39.2)	-1.5	892.5961; 892.5993 (77)	-3.5

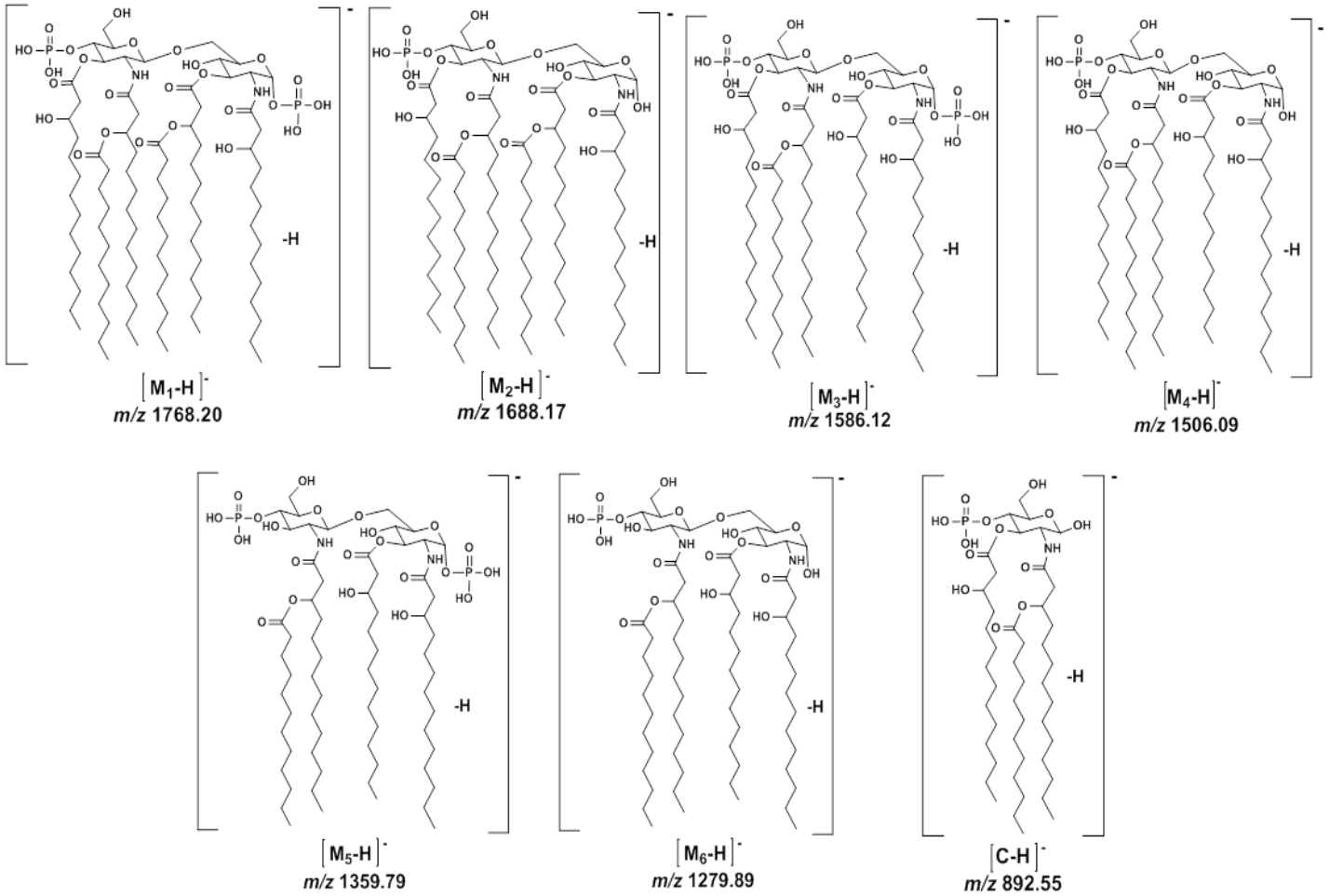

Scheme 5.1.1: Schematic representation of suggested structures of the deprotonated molecules of the lipid A_n mixture extracted from *A. salmonicida* SJ-113a.

At this stage, we have tentatively identified a series of complete and incomplete O-3, O-3′, N-2 and N-2′ acylated the β-D-Glc*p*N-(1→6)-α-D-Glc*p*N disaccharide backbone of the lipid A_{1-8} structures sharing common properties. We have identified the presence of two primary hydroxytetradecanoic acids (14:0(3-OH)) at N-2 and O-3 positions present on the β-D-Glc*p*N-(1→6)-α-D-Glc*p*N disaccharide backbone of this mixture of lipidA_{1-8}. In addition, we have also proposed the presence of branched fatty acid (Cl4:0(3-*O*-C12:0)) at the positions O-3 and N-2′.

The use of the low-energy collision dissociation tandem mass spectrometry analysis confirms our tentative assignments and the putative structures for the six deprotonated molecules $LipA_1$ to $LipA_6$ and the other various fragment ions. Domon and Costello carbohydrate nomenclature was used to define and characterize all the deprotonated molecules, which were produced by their gas-phase fragmentation in the ESI-MS and CID-MS/MS analysis (Domon and Costello, 1988).

The glycosidic cleavage provides useful structural information and defends the sugar sequencing of the lipid A backbone (Domon and Costello., 1988, Banoub *et al*., 2010, Kilár *et al*., 2013, and Almostafa *et al*., 2016).

5.2.1. Low-energy CID-MS/MS analysis of the extracted mixture of lipid A_n isolated from the LPS OF *A. salmonicida* SJ-113a using the QqQ-MS/MS instrument

The triple quadrupole (QqQ) instrument was used in this investigation using the low-energy CID-MS/MS (tandem-in-space) analysis, which conducted on the eight

different precursor $[M-H]^-$ deprotonated molecules at *m/z* 1768.20 ($LipA_1$), *m/z* 1688.17 ($LipA_2$), *m/z* 1586.12 ($LipA_3$), *m/z* 1506.09 ($LipA_4$), *m/z* 1359.79 ($LipA_5$), and *m/z* 1279.89 ($LipA_6$) (Figure 5.1.1). These precursor molecules afforded series of distinct and diagnostic product ions which produced by competitive hydrolysis of the primary and/or secondary fatty esters located on β-D-Glc*p*N-(1→6)-α-D-Glc*p*N disaccharide backbone of lipid A. It is well known that the ester-linked fatty groups at O-3 and O-3′ are more readily hydrolysable than the fatty acyl amide groups at N-2 and N-2′ (Banoub *et al*., 2010, Kilár *et al*., 2013). Also, the cleavages arising from the glycosidic bond followed by inter-ring bond cleavages (Domon and Costello., 1988).

The product ion scan of the deprotonated di-phosphorylated $LipA_1$ molecules at *m/z* 1768.20 allowed us to investigate the fatty acyl group distributions detected in ESI-QqQ-MS analysis of $LipA_1$ as shown in (Figure 5.1.2). The CID-MS/MS of the deprotonated molecules at *m/z* 1768.20 produced the following series of product ions at *m/z* 1532.95, *m/z* 1279.81, *m/z* 1097.63, and *m/z* 803.49 (Figure 5.1.2, Scheme 5.1.2 and Table 5.1.2) (Lukasiewicz *et al*., 2010). The product ion at *m/z* 1532.95 was assigned as the $[M_1-2(H_2O)-(C14:0)acid-H]^-$ ion, and it was created by the elimination of two molecules of water and myristic acid form the branched fatty (C14:0(3-*O*-C14:0) acid acyl group located at O-3 (-228 Da).

The product ion at *m/z* 1279.81 was formed by the consecutive losses of the branched fatty (C14:0(3-*O*-C12:0)) located on position O-3 (-408 Da), and by the elimination of the neutral HPO_3 (-80 Da) moiety located at O-1 position. This product ion was assigned as $[M_1-(C14:0(3-O-C12:0))ketene-HPO_3-H]^-$ ion (-488 Da).

The product ion at *m/z* 1097.63 was formed by the elimination of a molecule of the branched fatty (C14:0(3-*O*-C12:0)) ketene (-408 Da) from the O-3 position, lauryl ketene molecule (-182 Da) from the branched fatty acids (C14:0(3-*O*-C12:0)) located on the N-2′ position, and by the elimination of the neutral HPO_3 (-80 Da) located at O-1 position. This product ion was assigned as $[M_1$-(C14:0(3-*O*-C12:0))ketene-(C12:0)ketene-HPO_3-H$]^-$ ion (as shown in Figure 5.1.2, Table 5.1.2, and Scheme 5.1.2).

The product ion at *m/z* 804.49 was formed by the glycosidic cleavages of the β-D-Glc*p*N-(1→6)-α-D-Glc*p*N disaccharide backbone to afford the reducing D-GlcN-OH species. It was obtained by the consecutive losses of myristic (-228 Da) located at O-3 position and a molecule of C_5H_{10} (-70 Da), as part of the fatty acid chain properly located at N-2. This product ion was assigned as [C-(C14:0)acid-(C_5H_{10})-H$]^-$ ion.

This MS/MS studies supports our suggested structural assignments of the deprotonated molecule ($LipA_1$), and indicates that the two H_2PO_3 groups are located at the O-1 and O-4′ position of the disaccharide backbone. It also confirms the presence of the two molecules of 3-hydroxyl myristic acids at the positions O-3, and N-2 of the reducing end of the disaccharide backbone, whereas the branched (C14:0(3-*O*-C12:0) fatty acids were located on O-3 positions of the reducing end, and N-2′ positions of the non-reducing end of the β-D-Glc*p*N-(1→6)-α-D-Glc*p*N disaccharide backbone of this lipid A_1 (El-Aneed *et al*., 2006, Lukasiewicz *et al*., 2010, John *et al*., 2014, and Brodbelt *et al*., 2014).

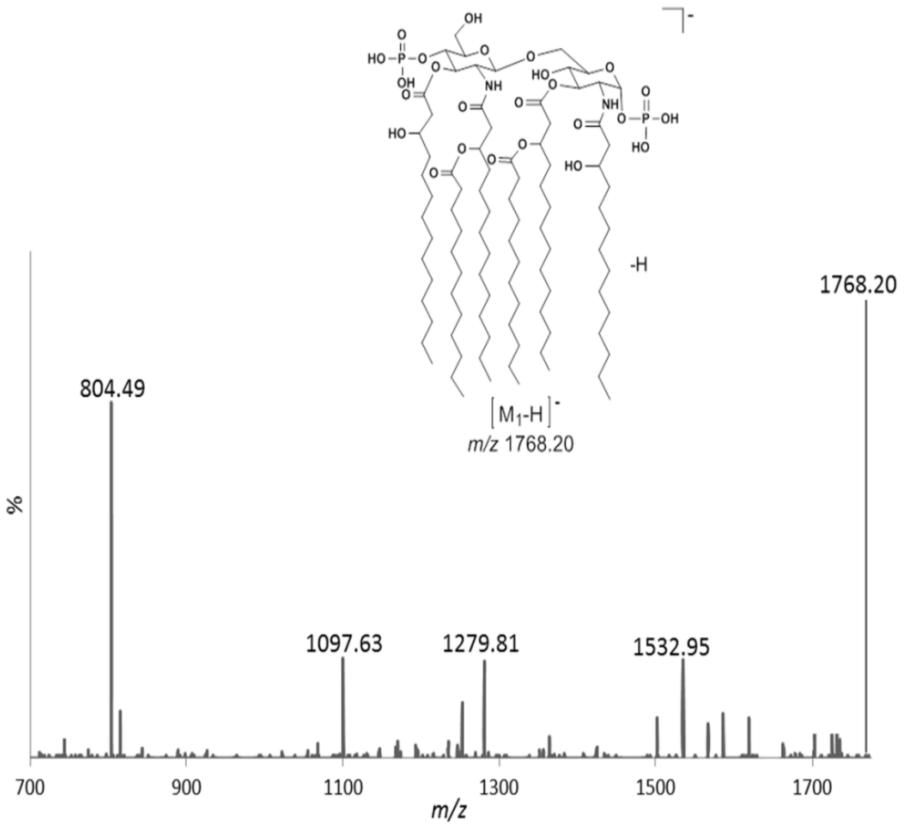

Figure 5.1.2: CID-MS/MS of the precursor deprotonated $[M_1\text{-}H]^-$ molecules at *m/z* 1768.20.∗

∗ Please note, that some product ions were not assigned as these were produced by other isobars isolated during the MS/MS analysis.

Table 5.1.2: Assignments of the product ions observed from CID-MS/MS of the precursor deprotonated $[M_1\text{-}H]^-$ molecules at *m/z* 1768.20.

Product ions of the deprotonated molecules $[M_1\text{-}H]^-$ at *m/z* 1768.20						
Empirical Formula	**ESI-QqQ-MS**		**ESI-FTICR-MS**		**MALDI-TOF/TOF-MS**	
	m/z **Observed; Calculated (%)**	**δ ppm**	***m/z*** **Observed; Calculated (%)**	**δ ppm**	***m/z*** **Observed; Calculated (%)**	**δ ppm**
$C_{80}H_{145}N_2O_{21}P_2$	1532.98; 1532.95 (20.9)	-19.5	-	-	-	-
$C_{80}H_{148}N_2O_{20}P$	-	-	-	-	1488.0465; 1488.0412 (100)	3.5
$C_{66}H_{124}N_2O_{19}P$	1279.87; 1279.81 (25)	-46.8	-	-	-	-
$C_{66}H_{120}N_2O_{17}P$	-	-	1243.8403; 1243.8450 (46)	3.7	1243.8403; 1243.8512 (49)	-8.7
$C_{54}H_{102}N_2O_{18}P$	1097.68; 1097.63 (26)	-45.3	-	-	1359.8615; 1359.8205 (14.5)	3
$C_{52}H_{96}N_2O_{16}P$	-	-	1035.6581; 1035.6578 (38)	-0.2	1279.8432; 1279.8541 (45)	-3
$C_{52}H_{94}N_2O_{15}P$	-	-	1017.6397; 1017.6378 (40)	-1.8	1017.6397; 1017.6320 (35)	-7.5
$C_{41}H_{76}NO_{12}P$	804.51; 804.49 (78)	-24.8	-	-	-	-
$C_{32}H_{59}NO_{10}P$	-	-	648.3955; 648.3945 (31)	1.5	-	-

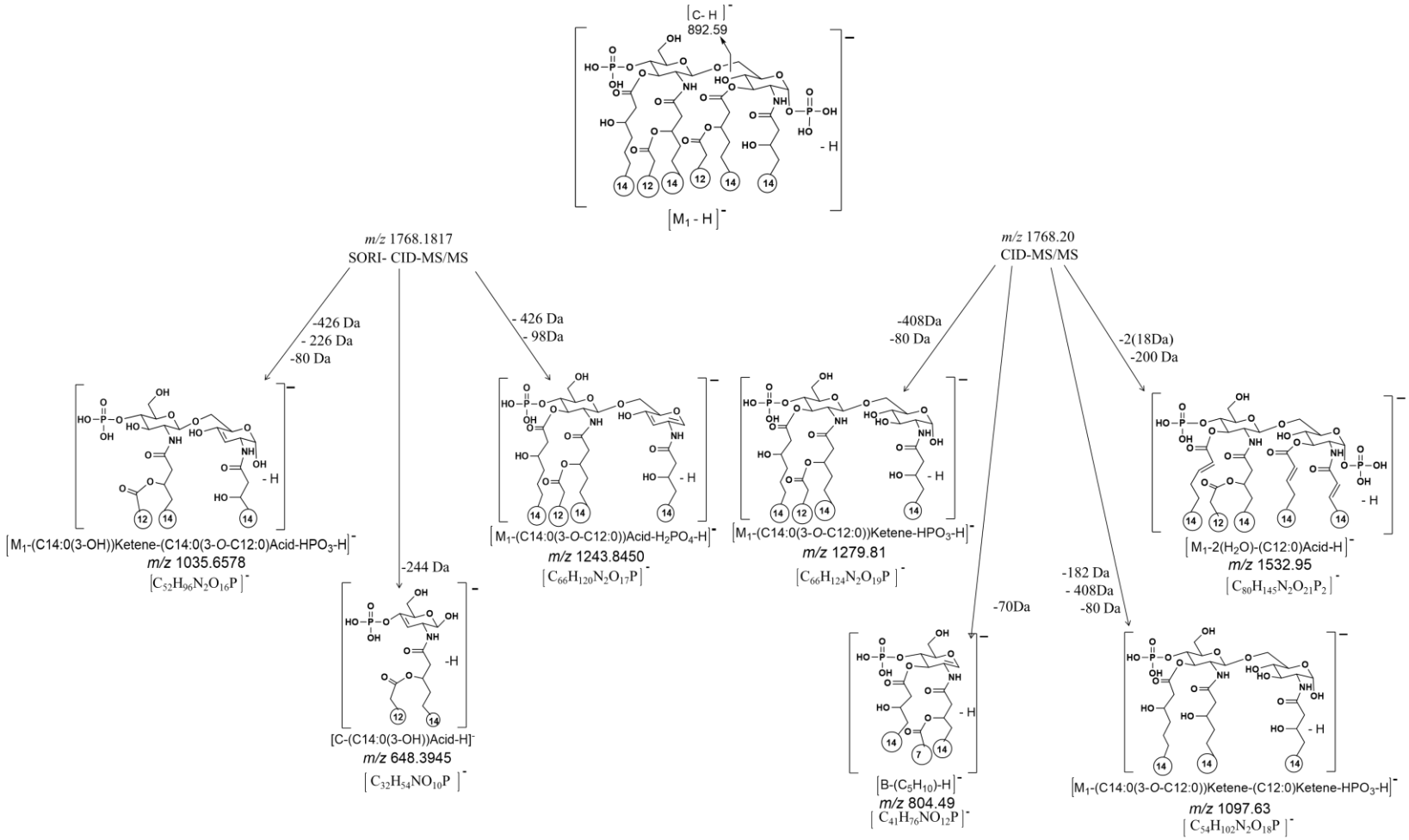

Scheme 5.1.2: Proposed fragmentation pathways obtained by CID-QqQ-MS/MS and SORI-CID-FTICR-MS/MS of the precursor deprotonated $[M_1–H]^-$ molecules at *m/z* 1768.20.

The product ion scan of the deprotonated mono-phosphorylated $LipA_2$ molecules at *m/z* 1688.17 afforded the product ions at *m/z* 1305.83, *m/z* 1243.79, *m/z* 1035.62 and *m/z* 710.43 (Figure 5.1.3, Table 5.1.3 and Scheme 5.1.3). The product ion at *m/z* 1305.83 was assigned as the $[M_2$-(C12:0)acid-(C12:0)ketene-H$]^-$ ion, and it was generated by both eliminations of lauric acid (-200 Da) and lauryl ketene (-182 Da) from the precursor ion at *m/z* 1688.17. These two losses originated from both the branched fatty acids (C14:0(3-*O*-C12:0)) and (C14:0(3-*O*-C12:0)) fatty acyl groups located respectively O-3 positions of the reducing end, and N-2′ of the non-reducing of the disaccharide backbone of lipid A (Figure 5.1.3). Similarly, the product ion at *m/z* 1243.79 was assigned as $[M_2$-(C14:0(3-*O*-12:0)))acid-H_2O-H$]^-$ ion, and it was formed by the consecutive losses of the branched fatty (C14:0(3-*O*-C12:0)) acid (-426 Da) located on position O-3 and a molecule of water from the precursor ion at *m/z* 1688.17.

The product ion of at *m/z* 1035.62 was assigned as $[M_2$-(C14:0(3-*O*-12:0)))acid-(C14:0(3-OH))ketene-H$]^-$ ion, and it was formed by the consecutive losses of the branched fatty (C14:0(3-*O*-C12:0)) acid (-426 Da) located at the O-3 position, and the 3-hydroxy-myristic ketene (C14:0(3-OH)) (-226 Da) located at the position O-3′.

The last product ion at *m/z* 710.43 was assigned as the [C-(C12:0)ketene-H$]^-$ ion, which was created by the elimination of a molecule of a lauryl ketene (-182 Da) from the branched fatty acids (C14:0(3-*O*-C12:0) which is located at N-2 (Figure 5.1.3, Table 5.1.3 and Scheme 5.1.3). The structure of this product ion confirms the presence of the branched (C14:0(3-*O*-C12:0)) fatty acid ester group on the N-2′ position (El-Aneed *et al*., 2006, Lukasiewicz *et al*., 2010, John *et al*., 2014, and Brodbelt *et al*., 2014).

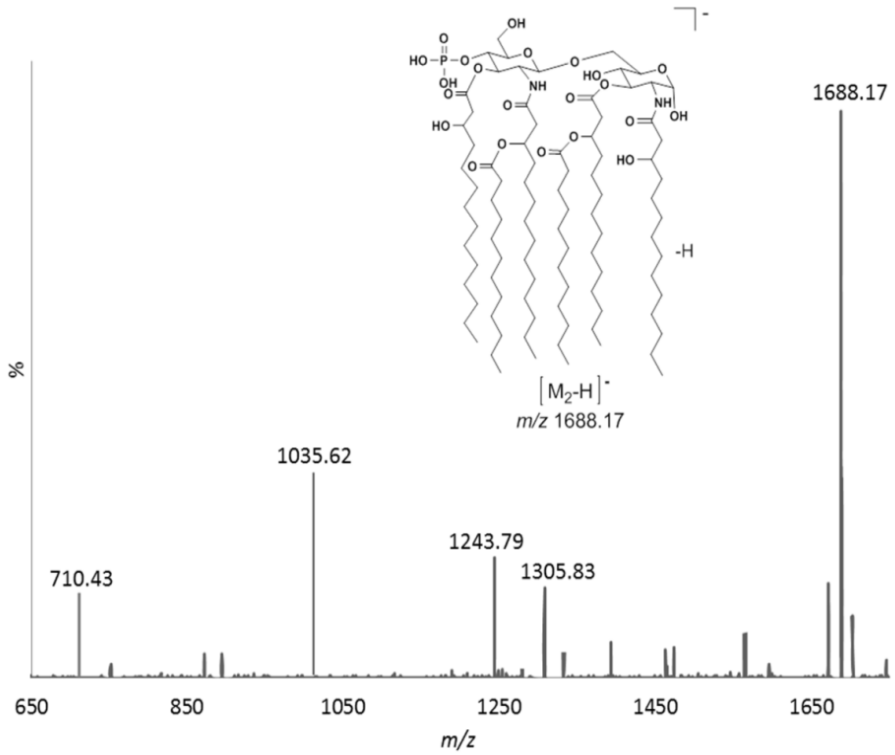

Figure 5.1.3: CID-MS/MS of the precursor deprotonated $[M_2\text{-}H]^-$ molecules at *m/z* 1688.17.*

* Please note, that some product ions were not assigned as these were produced by other isobars isolated during the MS/MS analysis.

Table 5.1.3: Assignments of the product ions observed from CID-MS/MS of the precursor deprotonated $[M_2\text{-}H]^-$ molecules at *m/z* 1688.17.

Product ions of the deprotonated molecules $[M_2\text{-}H]^-$ at *m/z* 1688.17						
Empirical Formula	**ESI-QqQ-MS/MS**		**ESI-FTICR-MS/MS**		**MALDI-TOF/TOF-MS/MS**	
	m/z **Observed; Calculated (%)**	**δ ppm**	***m/z*** **Observed; Calculated (%)**	**δ ppm**	***m/z*** **Observed; Calculated (%)**	**δ ppm**
$C_{86}H_{148}N_2O_{20}P$	-	-	1488.0379; 1488.0359 (82)	-1.3	1488.0379; 1488.0315 (100)	-4.3
$C_{78}H_{145}N_2O_{19}P$	-	-	1444.9815; 1444.9820 (44)	0.3	-	-
$C_{68}H_{126}N_2O_{19}P$	1305.86; 1305.83 (23)	-22.9	-	-	-	-
$C_{66}H_{122}N_2O_{18}P$	-	-	-	-	1261.8436; 1261.8497 (70)	-4.8
$C_{66}H_{120}N_2O_{17}P$	1243.84; 1243.79 (31)	-40.1	-	-	1359.8615; 1359.8205 (14.5)	3
$C_{52}H_{96}N_2O_{16}P$	1035.65; 1035.62 (35)	-28.9	1035.6581; 1035.6591 (95)	0.9	1035.6581; 1035.6520 (45)	-5.8
$C_{52}H_{94}N_2O_{15}P$	-	-	1017.6397; 1017.6381 (42)	-1.5	-	-
$C_{34}H_{66}NO_{12}P$	710.40; 710.43 (21)	-42.2	-	-	-	-

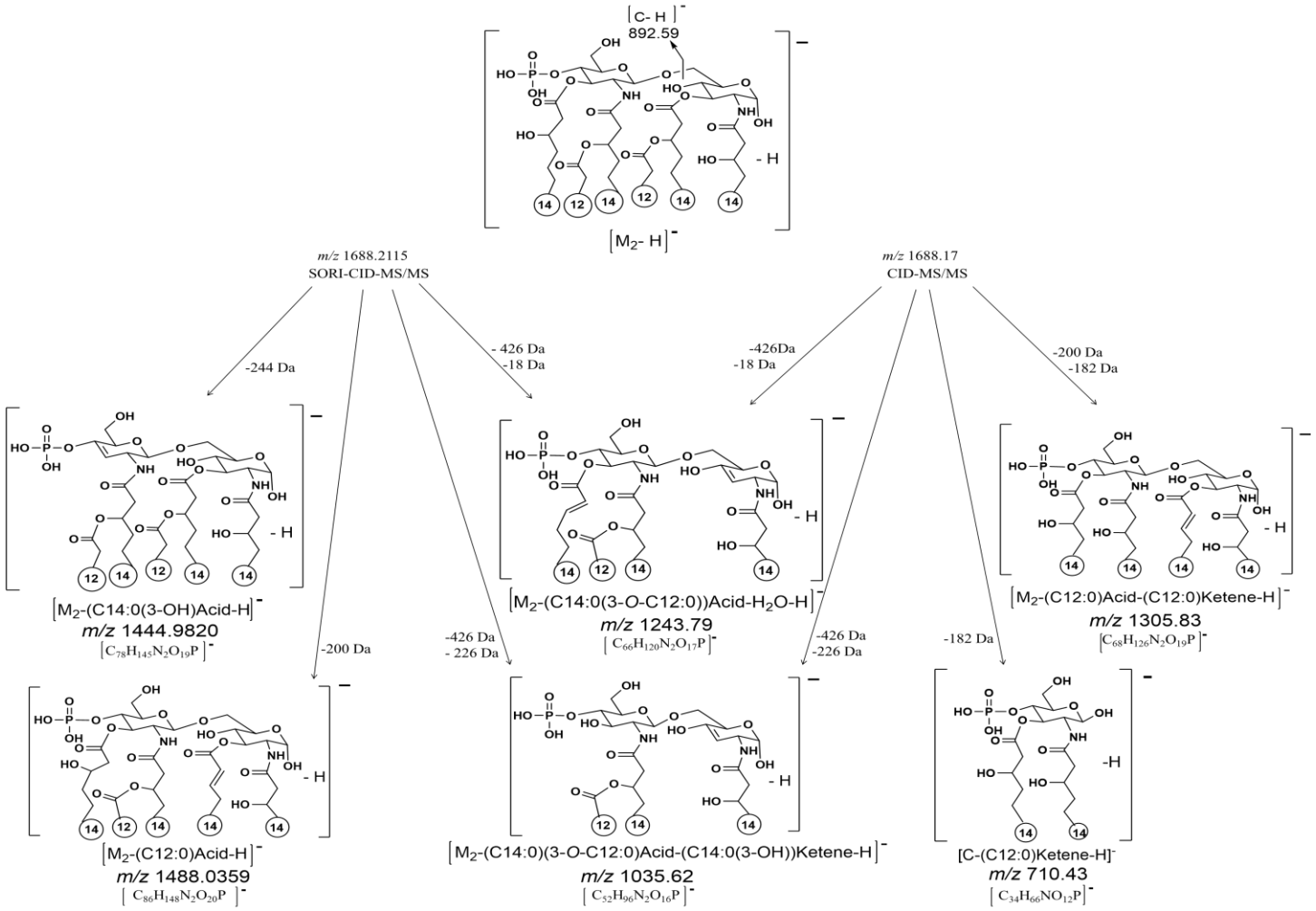

Scheme 5.1.3: Proposed fragmentation pathways obtained by CID-QqQ-MS/MS and SORI-CID-FTICR-MS/MS of the precursor deprotonated $[M_2\text{-}H]^-$ molecules at *m/z* 1688.17.

It is important to note that the obtained product ion scan of the deprotonated mono-phosphorylated $LipA_2$ molecules at *m/z* 1688.17 is completely different from the one obtained for the deprotonated molecule of $LipA_2$ and $LipA_3$ that were isolated from the lipid A_n SJ-19a (Chapter 3) and SJ-55a (Chapter 4). This indicated that the deprotonated molecules for *m/z* 1688 are indeed isobaric and have completely different structures.

The product ion scan of the deprotonated $LipA_3$ molecules at *m/z* 1586.12 gave the series of product ions at *m/z* 1341.85, *m/z* 1261.81, *m/z* 1053.62, *m/z* 690.35 and *m/z* 630.49 (Figure 5.1.4, Table 5.1.4, and Scheme 5.1.4). The product ion at *m/z* 1341.85 was assigned as the $[M_3$-(C14:0(3-OH))acid-H$]^-$, and it was formed by the elimination of the 3-hydroxy-myristic acid (C14:0(3-OH)) (-244 Da) located either at the position O-3 or O-3′. The product ion at *m/z* 1261.81 was assigned as the $[M_3$-(C14:0(3-OH))acid-HPO_3-H$]^-$ ion and was formed by elimination of the neutral HPO_3 (-80 Da) moiety located at O-1 position, and the 3-hydroxy-myristic acid (C14:0(3-OH)) (-244 Da) located either at the position O-3 or O-3′.

The product ion *m/z* 1053.62 was assigned as the $[M_3$-2(C14:0(3-OH))ketene-HPO_3-H$]^-$. It was formed by the elimination of the neutral HPO_3 (-80 Da) moiety located at O-1 position, and two of the 3-hydroxy-myristic ketene (C14:0(3-OH)) (-226 Da) located at the position O-3 and O-3′. The product ion at *m/z* 690.35 was assigned as $[^{0,4}A$-(C14:0(3-OH))acid-H$]^-$ produced by the cleavage of the non-reducing mono-phosphorylated D-Glucose residue, and it was formed by the loss of a 3-hydroxy-myristic ketene molecule (-244 Da) from the O-3 position. The product ion at *m/z* 630.49 was formed by the by consecutive elimination of neutral HPO_3 (-80 Da) moiety located at O-4 position,

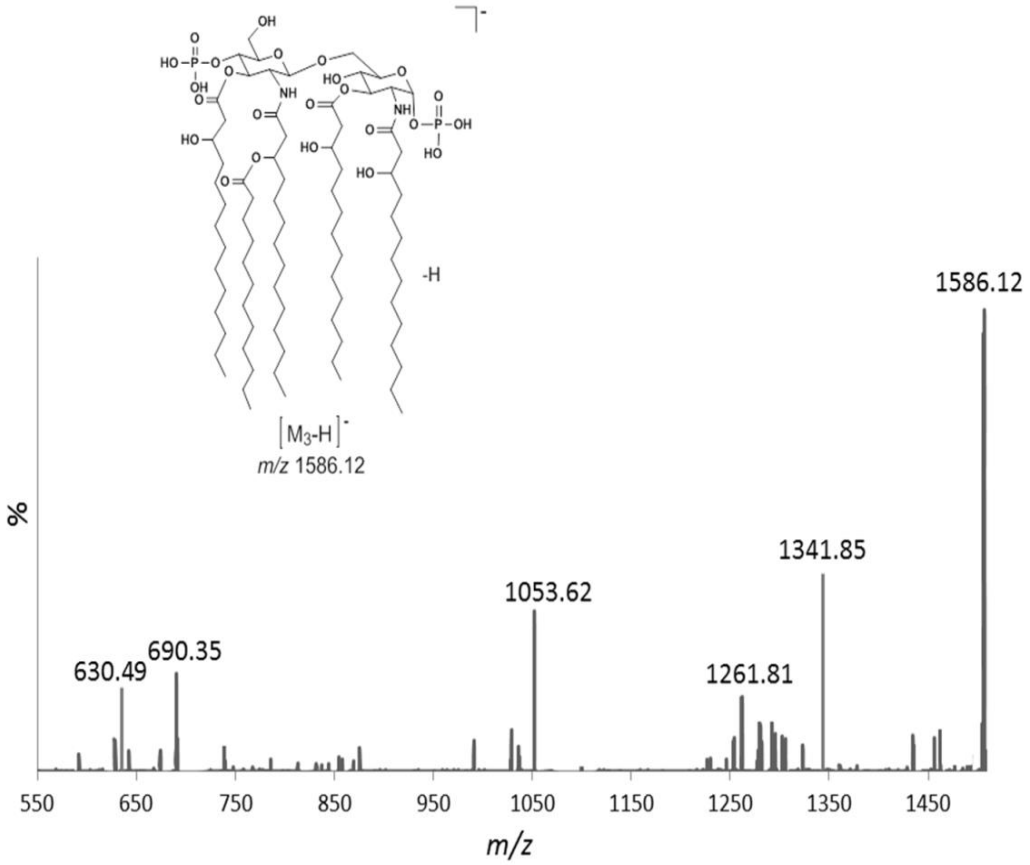

Figure 5.1.4: CID-MS/MS of the precursor deprotonated $[M_3\text{-H}]^-$ molecules at *m/z* 1586.12. ⁕

⁕ Please note, that some product ions were not assigned as these were produced by other isobars isolated during the MS/MS analysis.

Table 5.1.4: Assignments of the product ions observed from CID-MS/MS of the precursor deprotonated $[M_3\text{-}H]^-$ molecules at *m/z* 1586.12.

Product ions of the deprotonated molecules $[M_3\text{-}H]^-$ at *m/z* 1586.12						
Empirical Formula	**ESI-QqQ-MS/MS**		**ESI-FTICR-MS/MS**		**MALDI-TOF/TOF-MS/MS**	
	m/z **Observed; Calculated (%)**	**δ ppm**	***m/z*** **Observed; Calculated (%)**	**δ ppm**	***m/z*** **Observed; Calculated (%)**	**δ ppm**
$C_{86}H_{148}N_2O_{20}P$	-	-	1488.0465; 1488.0499 (66)	2.2	1488.0465; 1488.0423 (41)	-2.8
$C_{66}H_{123}N_2O_{21}P_2$	1341.80; 1341.85 (41)	37.2	1341.8099; 1341.8083 (21)	-1.1	1341.8099; 1341.8041 (100)	-4.3
$C_{66}H_{122}N_2O_{18}P$	1261.84; 1261.81 (19)	-23.7	-	-	-	-
$C_{66}H_{120}N_2O_{17}P$	-	-	1243.8430; 1243.8425 (30)	-0.4	1243.8430; 1243.8495 (39)	5.2
$C_{52}H_{99}N_2O_{17}P$	1053.66.; 1053.63 (35)	-28.6	-	-	-	-
$C_{34}H_{62}NO_{11}P$	690.39; 690.35 (22)	56	-	-	-	-
$C_{34}H_{64}NO_9$	630.45; 630.49 (20)	63	-	-	-	-

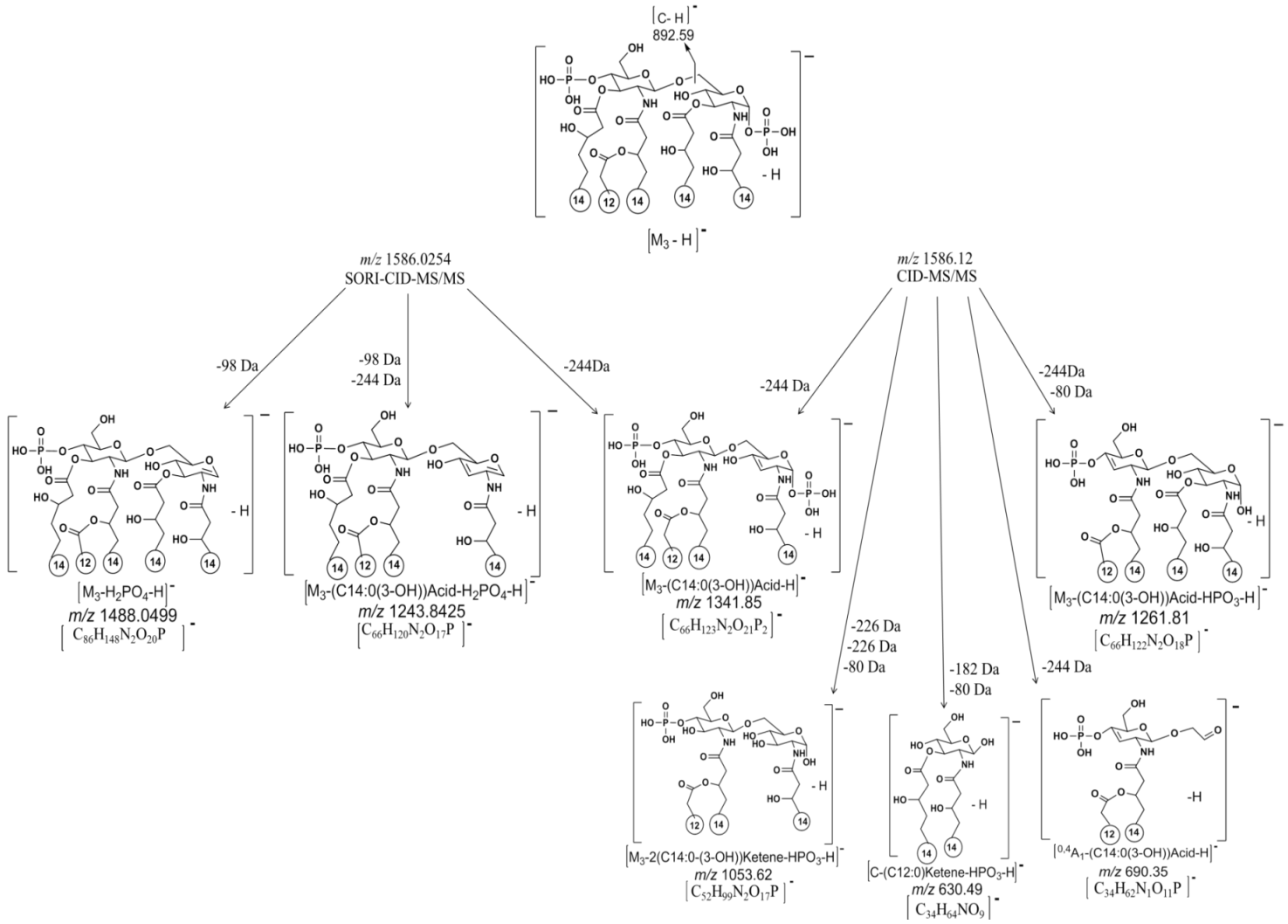

Scheme 5.1.4: Proposed fragmentation pathways obtained by CID-QqQ-MS/MS and SORI-CID-FTICR-MS/MS of the precursor deprotonated $[M_3\text{-}H]^-$ molecules at *m/z* 1586.12.

and a lauryl ketene (-182 Da) from the branched fatty acids (C14:0(3-*O*-C12:0)) located on the N-2′ position. It was assigned as[C-(C12:0)ketene-HPO_3-H]$^-$ ion (El-Aneed *et al*., 2006, Lukasiewicz *et al*., 2010, John *et al*., 2014, and Brodbelt *et al*., 2014).

These latter product ions were indeed produced from the C-fragmentation routes described by Domon and Costello. It is initiated by the glycosidic cleavages of the β-D-(l→6)-GlcN disaccharide (Domon and Costello., 1988).

The product ion scan of the deprotonated $LipA_4$ molecules at *m/z* 1506.09 gave the series of product ion at *m/z* 1261.82, *m/z* 1035.62, *m/z* 690.36, and *m/z* 630.41 (Figure 5.1.5, Table 5.1.5, and Scheme 5.1.5). The product ion at *m/z* 1261.82 was assigned as the [M_4-(C14:0(3-OH))acid-H]$^-$ ion, and it was created by the elimination of 3-hydroxy-myristic acid (C14:0(3-OH)) (-244 Da) located either at the position O-3 or O-3′. The product ion *m/z* 1035.62 was assigned as the [M_4-(C14:0(3-OH))ketene-(C14:0(3-OH))acid-H]$^-$. It was formed by the elimination of the 3-hydroxy-myristic ketene (C14:0(3-OH)) (-226 Da) and 3-hydroxy-myristic acid (C14:0(3-OH)) (-244 Da) located at the position O-3 and O-3′. The product ion at *m/z* 690.36 was assigned as [^{0,4}A-(C14:0(3-OH))acid-H]$^-$. It was produced by the cleavage of the non-reducing mono-phosphorylated D-Glucose residue, and it was formed by the losses of a 3-hydroxy-myristic ketene molecule (-244 Da) from the O-3 position. The product ion at *m/z* 630.41 was by the consecutive elimination of neutral HPO_3 (-80 Da) moiety and a lauryl ketene (-182 Da) from the branched fatty acids (C14:0(3-*O*-C12:0)) located on the N-2′ position.

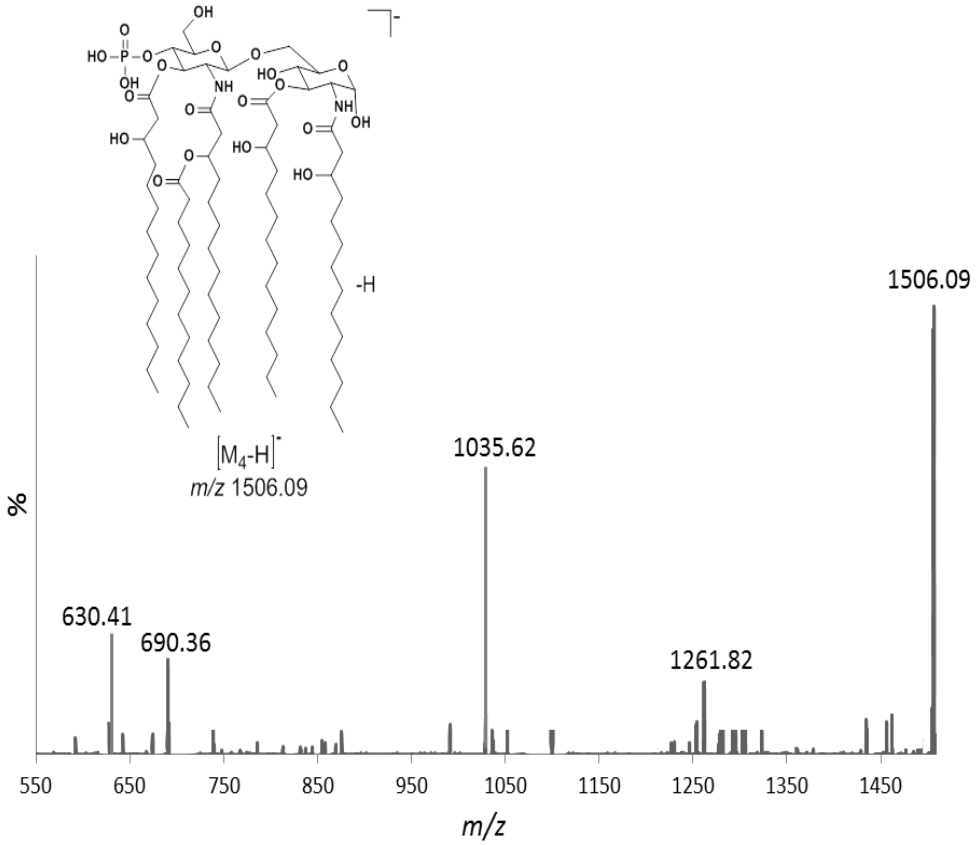

Figure 5.1.5: CID-MS/MS of the precursor deprotonated $[M_4\text{-}H]^-$ molecules at *m/z* 1506.09.∗

∗ Please note, that some product ions were not assigned as these were produced by other isobars isolated during the MS/MS analysis.

Table 5.1.5: Assignments of the product ions observed from CID-MS/MS of the precursor deprotonated $[M_4\text{-}H]^-$ molecules at *m/z* 1505.09.

Product ions of the deprotonated molecules $[M_4\text{-}H]^-$ at *m/z* 1506.09						
Empirical Formula	**ESI-QqQ-MS/MS**		**ESI-FTICR-MS/MS**		**MALDI-TOF/TOF-MS/MS**	
	m/z **Observed; Calculated (%)**	**δ ppm**	***m/z*** **Observed; Calculated (%)**	**δ ppm**	***m/z*** **Observed; Calculated (%)**	**δ ppm**
$C_{68}H_{126}N_2O_{19}P$	-	-	1305.8671; 1305.8680 (18)	0.6	-	-
$C_{66}H_{122}N_2O_{18}P$	1261.84; 1261.82 (23)	-23.7	1261.8436; 1261.8399 (41)	-2.9	1261.8436; 1261.8485 (79)	-3.8
$C_{52}H_{99}N_2O_{17}P$	1035.66; 1035.62 (65.3)	-38.6	1035.6681; 1035.6692 (15)	1	1035.6681; 1035.6621 (46)	-5.7
$C_{34}H_{62}NO_{11}P$	690.39; 690.36 (26)	-43.4	-	-	-	-
$C_{34}H_{64}NO_9$	630.45; 630.41 (28)	40	-	-	-	-

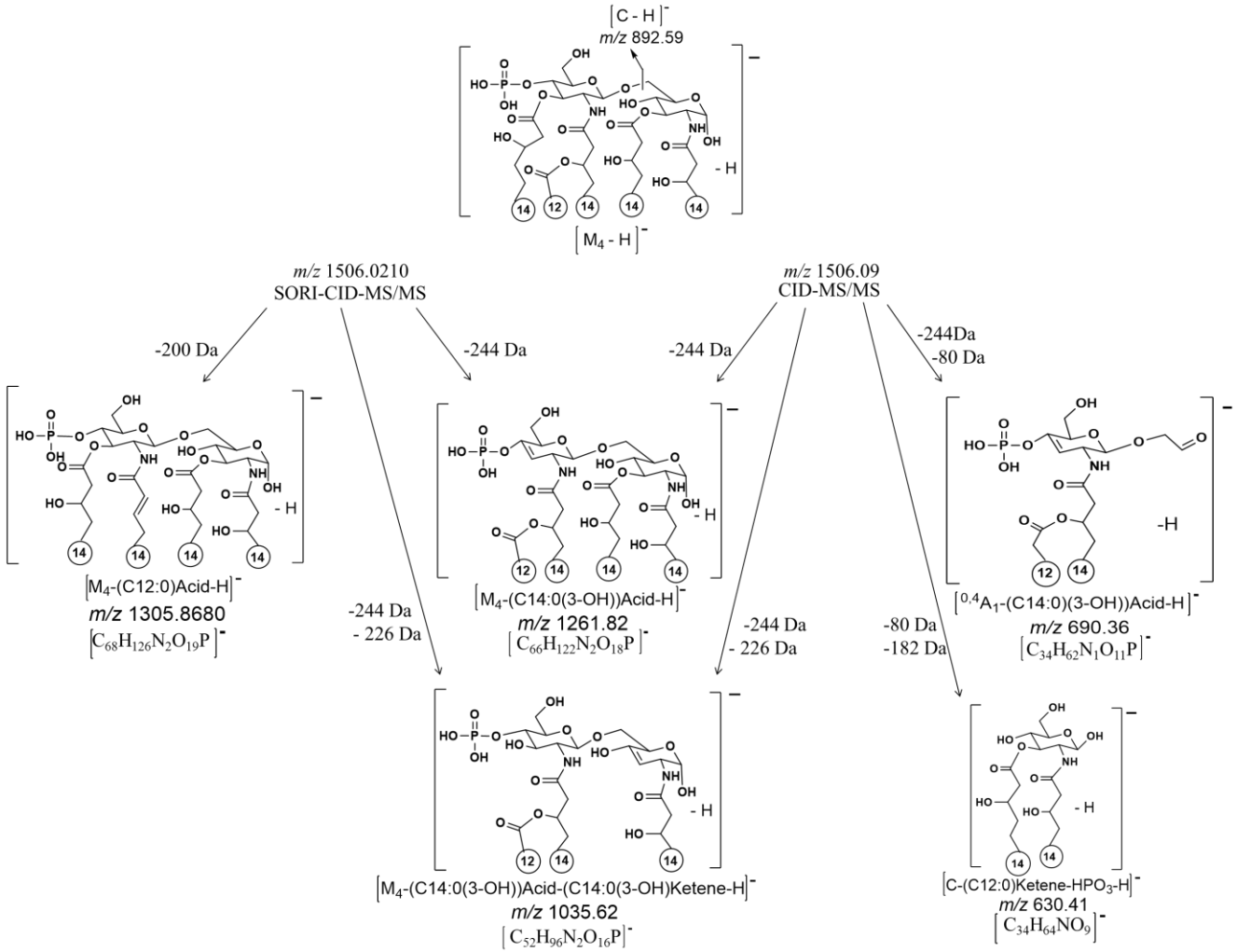

Scheme 5.1.5: Proposed fragmentation pathways obtained by CID-QqQ-MS/MS and SORI-CID-FTICR-MS/MS of the precursor deprotonated $[M_4\text{-}H]^-$ molecules at *m/z* 1506.09.

It was assigned as [C-(C12:0)ketene-HPO_3-H]$^-$ ion (El-Aneed *et al*., 2006, Lukasiewicz *et al*., 2010, John *et al*., 2014, and Brodbelt *et al*., 2014).

These latter product ions were indeed, produced from the C-fragmentation routes described by Domon and Costello. It is initiated by the glycosidic cleavages of the β-D-(l→6)-GlcN disaccharide (Domon and Costello, 1988).

It is important to note that the obtained product ion scan of the deprotonated mono-phosphorylated $LipA_4$ molecules at *m/z* 1506.09 is completely different from the one obtained for the deprotonated molecule of $LipA_1$ and $LipA_4$ isolated from the lipid A_n SJ-19a (Chapter 3) and SJ-55a (Chapter 4). This indicated that the deprotonated molecules for *m/z* 1506 are indeed isobaric and have completely different structures.

The product ion scan of the deprotonated di-phosphorylated $LipA_5$ molecules [M_5-H]$^-$ at *m/z* 1359.79 gave a series of product ions at *m/z* 1279.90, *m/z* 1209.74, *m/z* 1035.64, and *m/z* 690.36 (Figure 5.1.6, Table 5.1.6 and Scheme 5.1.6). The product ion at *m/z* 1279.90 was assigned as [M_5-HPO_3-H]$^-$ ion, and it was formed by the elimination of the neutral HPO_3 (-80 Da) moiety properly located at O-1 position. The product ion at *m/z* 1209.74 was assigned as [M_5-HPO_3-(C_5H_{10})-H]$^-$ ion. It was formed by the elimination of the neutral HPO_3 (-80 Da) moiety located at O-1 position, and a molecule of C_5H_{10} (-70 Da) as part of the fatty acid chain properly located at N-2′ position. The product ion at *m/z* 1035.64 was assigned as [M_5-HPO_3-(C14:0)(3-OH))acid-H]$^-$ ion, and it was formed by the consequent elimination of the neutral HPO_3 (-80 Da) moiety located at O-1 position, and the 3-hydroxy-myristic acid (C14:0(3-OH)) (-244 Da) located at the position O-3. The product ion at *m/z* 690.36 was assigned as [^{0,4}A-H]$^-$.

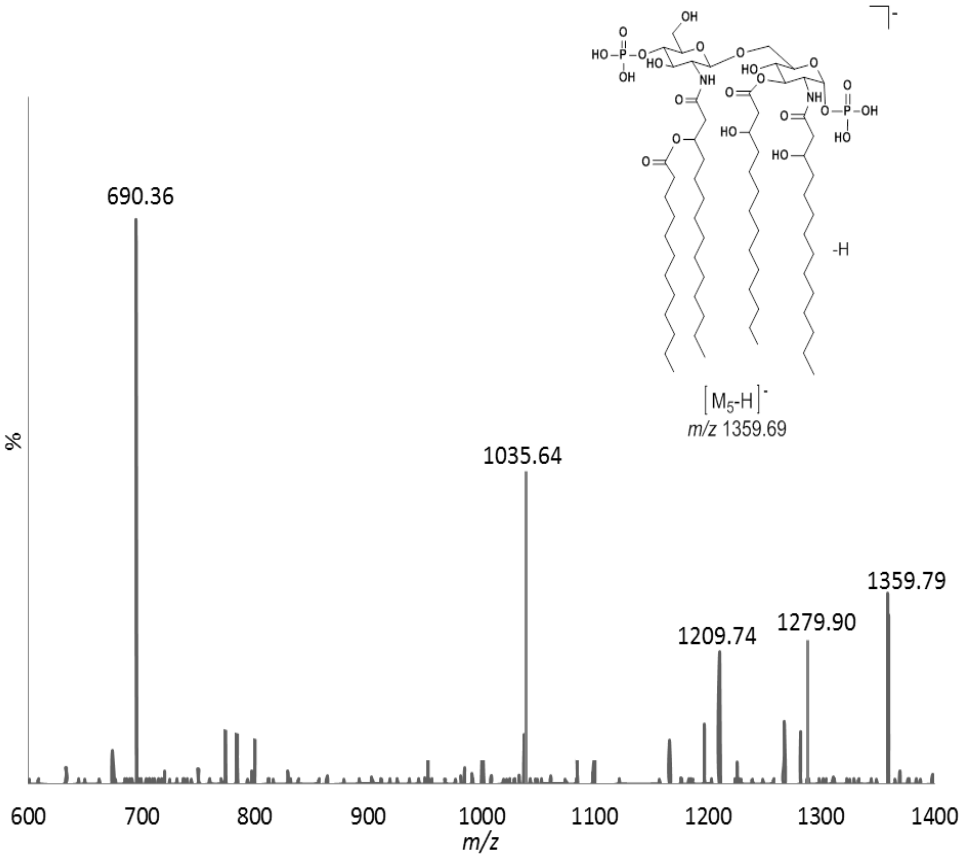

Figure 5.1.6: CID-MS/MS of the precursor deprotonated $[M_5\text{-}H]^-$ molecules at *m/z* 1359.79.*

* Please note, that some product ions were not assigned as these were produced by other isobars isolated during the MS/MS analysis.

Table 5.1.6: Assignments of the product ions observed from CID-MS/MS of the precursor deprotonated $[M_5\text{-}H]^-$ molecules at *m/z* 1359.79.

Product ions of the deprotonated molecules $[M_5\text{-}H]^-$ at *m/z* 1359.79						
Empirical Formula	**ESI-QqQ-MS/MS**		**ESI-FTICR-MS/MS**		**MALDI-TOF/TOF-MS/MS**	
	m/z **Observed; Calculated (%)**	**δ ppm**	***m/z*** **Observed; Calculated (%)**	**δ ppm**	***m/z*** **Observed; Calculated (%)**	**δ ppm**
$C_{66}H_{124}N_2O_{19}P$	1279.87; 1279.90 (27)	-23.4	1305.8671; 1305.8680 (18)	0.6	-	-
$C_{66}H_{122}N_2O_{18}P$	-	-	1261.8436; 1261.8379 (17)	-2.5	1261.8436; 1261.8476 (28)	3.1
$C_{61}H_{114}N_2O_{19}P$	1209.77; 1209.74 (25.3)	57	-	-	-	-
$C_{52}H_{97}N_2O_{19}P_2$	-	-	1115.6166; 1115.6125 (25)	-3.5	1115.6166; 1115.6120 (45)	-4.1
$C_{52}H_{96}N_2O_{16}P$	1035.66; 1035.64 (47)	20	1035.6681; 1035.6669 (17.2)	-1.1	-	-
$C_{52}H_{94}N_2O_{15}P$	-	-	1017.6397; 1017.6377 (35)	-1.9	-	-
$C_{34}H_{62}NO_{11}P$	690.39; 690.36 (79.4)	-43.4	-	-	-	-

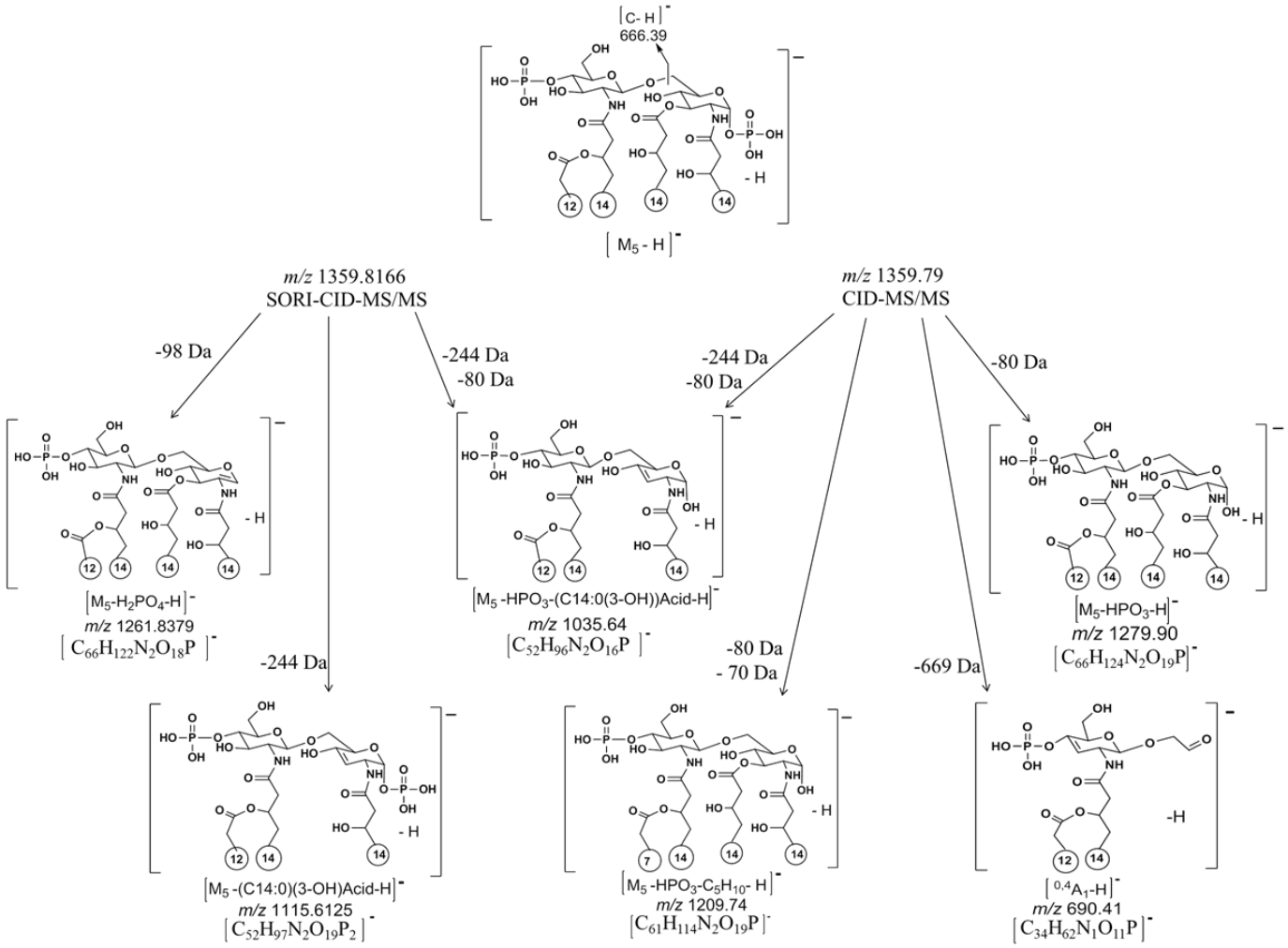

Scheme 5.1.6: Proposed fragmentation pathways obtained by CID-QqQ-MS/MS and SORI-CID-FTICR-MS/MS of the precursor deprotonated $[M_5\text{-}H]^-$ molecules at *m/z* 1359.79.

It is produced by the cleavage of the non-reducing mono-phosphorylated D-Glucose residue (Scheme 5.1.6) (El-Aneed *et al*., 2006, Lukasiewicz *et al*., 2010, John *et al*., 2014, and Brodbelt *et al*., 2014).

It is important to note that the obtained product ion scan of the deprotonated mono-phosphorylated $LipA_5$ molecules at *m/z* 1359.79 is completely different from the one obtained for the deprotonated molecule of $LipA_5$ isolated from the lipid A_n SJ-55a (Chapter 4). This indicated that both deprotonated molecules for *m/z* 1359 are indeed isobaric and have completely different structures.

The product ion scan of the deprotonated mono-phosphorylated $LipA_6$ molecules $[M_6\text{-H}]^-$ at *m/z* 1279.89 gave a series of product ion at *m/z* 1035., *m/z* 853.46, and *m/z* 648.40 (Figure 5.1.7, Table 5.1.7 and Scheme 5.1.7). The ion at *m/z* 1035.68 was assigned as the $[M_6\text{-(C14:0(3-OH))acid-H}]^-$ ion, which was created by the elimination of 3-hydroxy-myristic acid (C14:0(3-OH)) (-244 Da) located at the position O-3 of the reducing GlcN end. The product ion at *m/z* 853.46 which was assigned as the $[M_6\text{-(C12:0)ketene-(C14:0(3-OH))acid-H}]^-$ ion, which was created by the elimination of a lauryl ketene molecule (-182 Da) from the branched fatty acids (C14:0(3-*O*-C12:0)), located on the N-2′ position, and 3-hydroxy-myristic acid (C14:0(3-OH)) (-244 Da) located at the position O-3 of the reducing GlcN end. The product ion at *m/z* 648.40 was assigned as $[\text{B-H}]^-$, and it is produced by the cleavage of the non-reducing mono-phosphorylated D-Glucose residue (as shown in Scheme 5.1.7) (El-Aneed *et al*., 2006, Lukasiewicz *et al*., 2010, John *et al*., 2014, and Brodbelt *et al*., 2014).

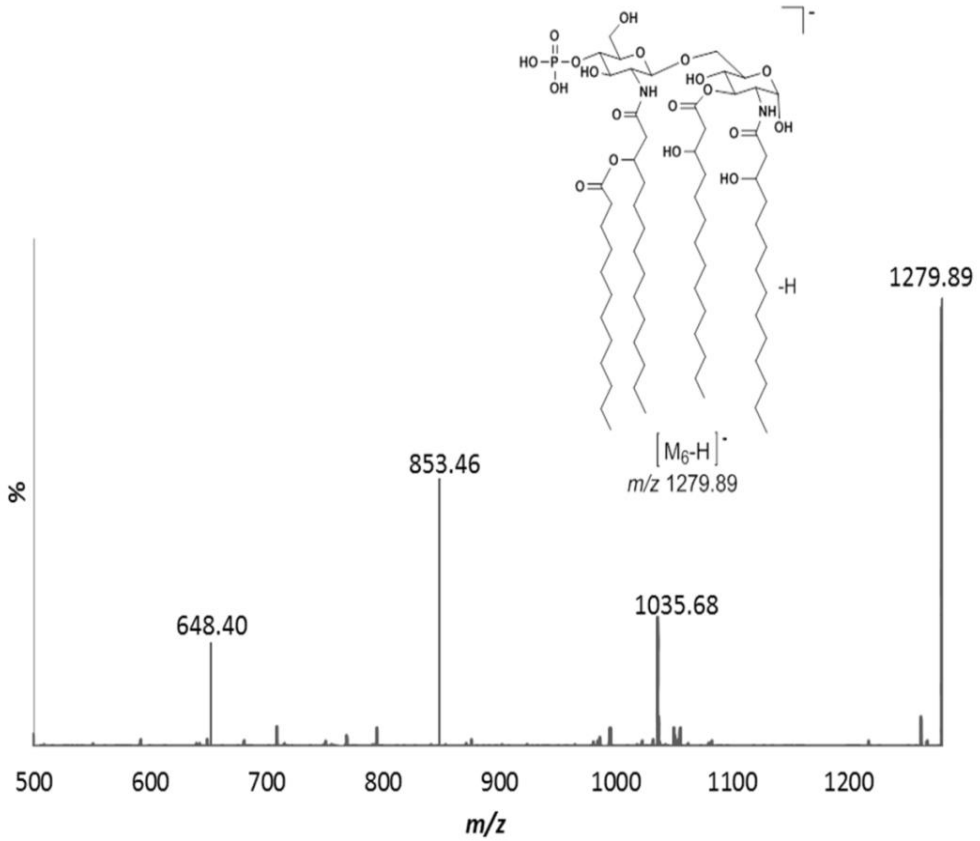

Figure 5.1.7: CID-MS/MS of the precursor deprotonate $[M_6\text{-}H]^-$ molecules at *m/z* 1279.89.⁕

⁕ Please note, that some product ions were not assigned as these were produced by other isobars isolated during the MS/MS analysis

Table 5.1.7: Assignments of the product ions observed from CID-MS/MS of the precursor deprotonated $[M_6\text{-}H]^-$ molecules at *m/z* 1279.89.

Product ions of the deprotonated molecules $[M_6\text{-}H]^-$ at *m/z* 1279.89						
Empirical Formula	**ESI-QqQ-MS/MS**		**ESI-FTICR-MS/MS**		**MALDI-TOF/TOF-MS/MS**	
	m/z **Observed; Calculated (%)**	**δ ppm**	***m/z*** **Observed; Calculated (%)**	**δ ppm**	***m/z*** **Observed; Calculated (%)**	**δ ppm**
$C_{54}H_{100}N_2O_{17}P$	-	-	1079.6765; 1079.6750 (9)	-1.3	1079.6765; 1079.6711 (30)	5
$C_{52}H_{96}N_2O_{16}P$	1035.66; 1035.68 (38)	19.4	1035.6681; 1035.6667 (30)	-1	1035.6681; 1035.6619 (100)	-5.9
$C_{49}H_{91}N_2O_{16}P$	-	-	-	-	994.6106; 994.6175 (40)	6.9
$C_{40}H_{74}N_2O_{15}P$	853.48; 853.46 (53)	-23.4	853.4832; 853.4846 (5)	-1.6	-	-
$C_{32}H_{59}NO_{10}P$	648.38; 648.40 (24)	30.7	-	-	-	-

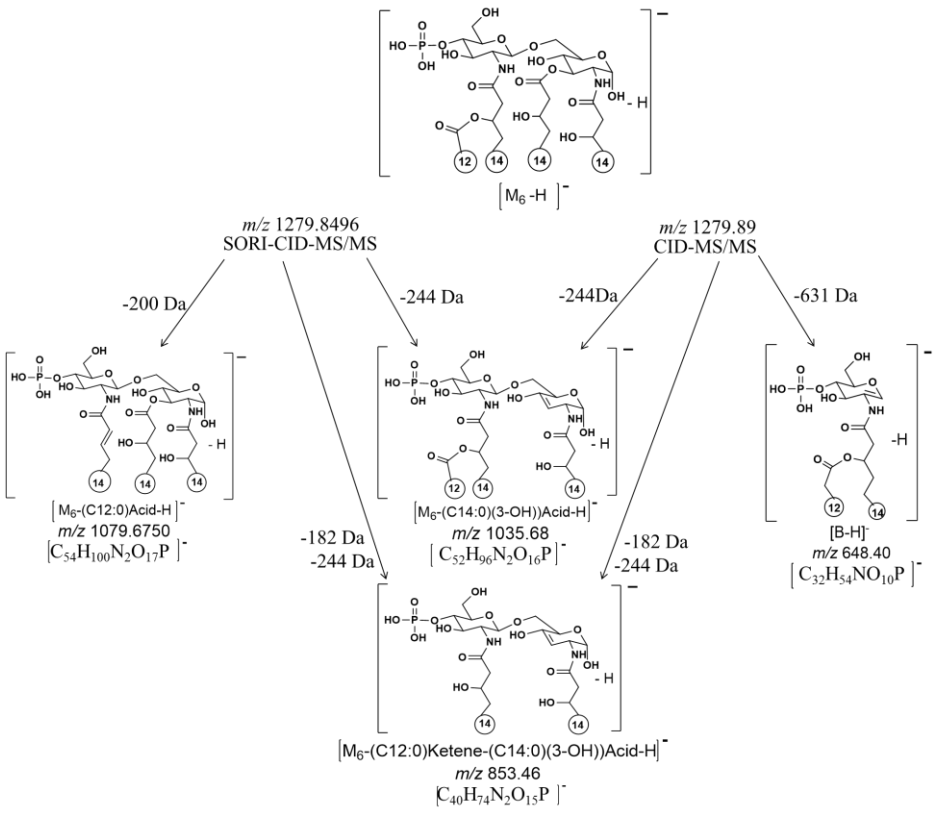

Scheme 5.1.7: Proposed fragmentation pathways obtained by CID-QqQ-MS/MS and SORI-CID-FTICR-MS/MS of the precursor deprotonated $[M_6\text{-H}]^-$ molecules at *m/z* 1279.89.

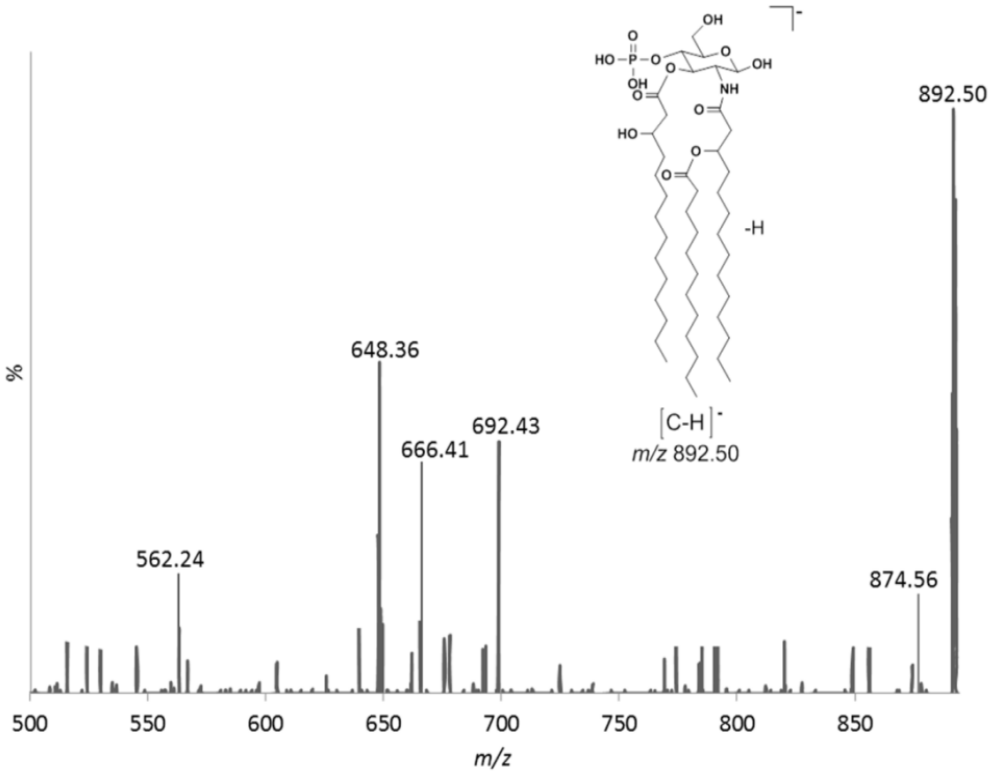

Figure 5.1.8: CID-MS/MS of the precursor deprotonated $[C\text{-}H]^-$ molecules at *m/z* 892.55. ⁕

⁕ Please note, that some product ions were not assigned as these were produced by other isobars isolated during the MS/MS analysis.

Table 5.1.8: Assignments of the product ions observed from the SORI-MS/MS and CID-MS/MS analysis of the precursor deprotonated $[C\text{-}H]^-$ molecules at *m/z* 892.55.

Product ions of the deprotonated molecules [C-(C14:0)ketene-H]$^-$ molecules at *m/z* 892.55						
Empirical Formula	**ESI-QqQ-MS/MS**		**ESI-FTICR-MS/MS**		**MALDI-TOF/TOF-MS/MS**	
	m/z **Observed; Calculated (%)**	**δ ppm**	***m/z*** **Observed; Calculated (%)**	**δ ppm**	***m/z*** **Observed; Calculated (%)**	**δ ppm**
$C_{46}H_{85}NO_{12}P$	874.58; 874.56 (19.3)	-22.8	-	-	-	-
$C_{34}H_{63}NO_{11}P$	692.41; 692.43 (46	-28.8	-	-	-	-
$C_{32}H_{61}NO_{11}P$	666.39; 666.41 (32.2)	-45	-	-	666.3988; 666.3922 (24)	9.9
$C_{32}H_{59}NO_{10}P$	648.38; 648.36 (53.2)	-30.8	648.3955; 648.3961 (45)	0.9	648.3955; 648.3897 (48)	-8.9
$C_{20}H_{38}NO_9P$	562.27; 562.24 (21)	-53.3	-	-	-	-
$C_{20}H_{35}NO_8P$	-	-	448.2106; 448.2117(13)	2.4	-	-

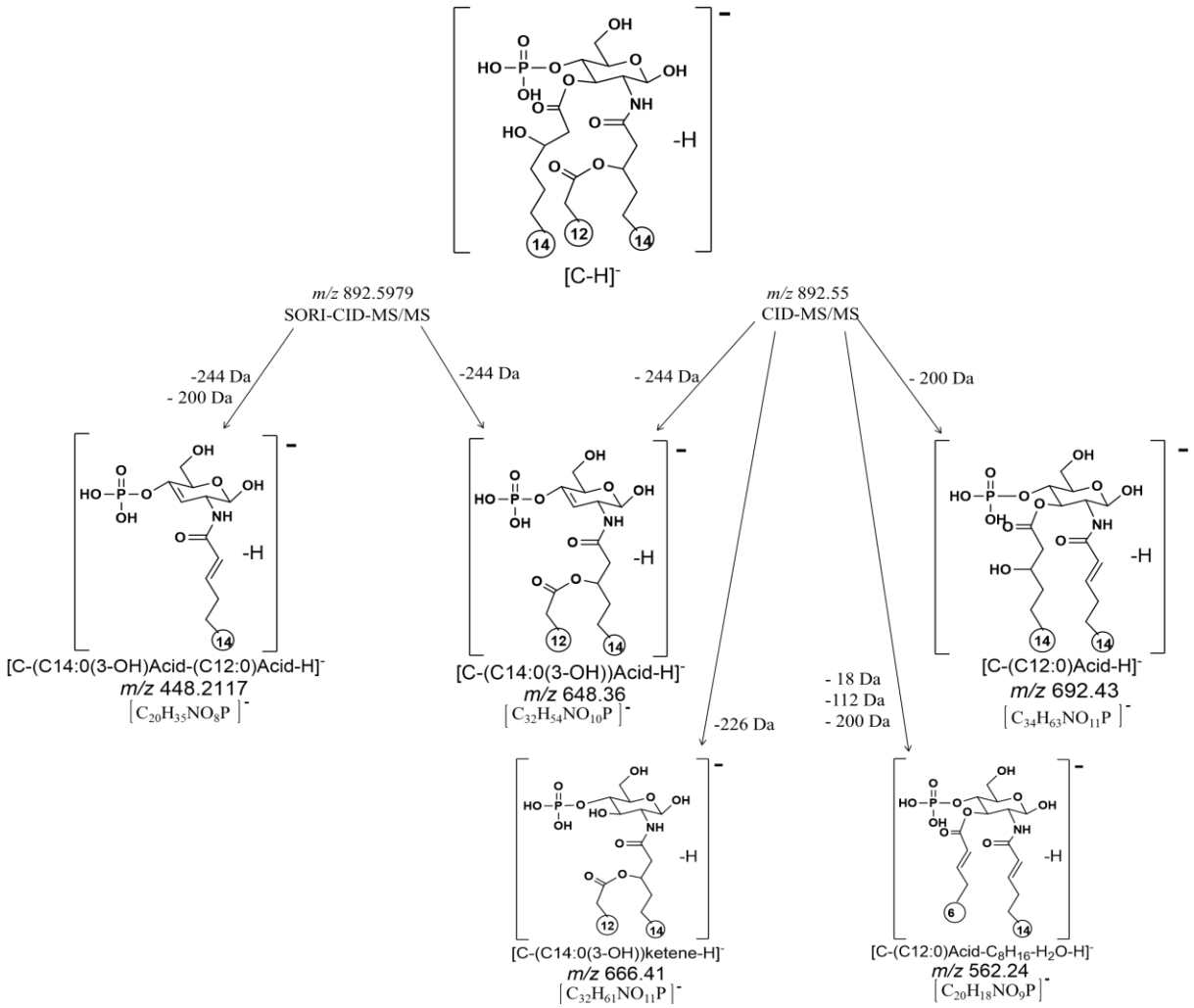

Scheme 5.1.8: Proposed fragmentation pathways obtained by CID-QqQ-MS/MS and SORI-CID- FTICR MS/MS analysis of the precursor deprotonated $[C\text{-}H]^-$ molecules at *m/z* 892.55.

It is important to note that the obtained product ion scan of the deprotonated mono-phosphorylated $LipA_6$ molecules at *m/z* 1279.89 is completely different from the one obtained for the deprotonated molecule of $LipA_4$ and $LipA_6$ isolated from the lipid A_n SJ-19a (Chapter 3) and SJ-55a (Chapter 4). This indicated that the deprotonated molecules for *m/z* 1279 are indeed isobaric and have completely different structures.

Lastly, we also investigated the nature of the deprotonated molecules at *m/z* 892.55 observed in the ESI-MS of this lipid A_n mixture. The deprotonated molecule was assigned as being created by the $[C\text{-}H]^-$ ion series; whose presence are probably an indication of the incomplete biosynthesis of the lipid $A_{1\text{-}6}$ series of the LPS *A. Hydrophilla* SJ-55a.

For simplification, we have tied these deprotonated molecules to the $[M\text{-}H_{1\text{-}6}]^-$ molecules and adopted a similar nomenclature. Hence, the product ion scan of the deprotonated $[C\text{-}H]^-$ molecule at *m/z* 892.55 gave a series of product ions at *m/z* 874.56, *m/z* 692.43, *m/z* 666.41, *m/z* 648.40, and *m/z* 562.24 (Figure 5.1.8, Scheme 5.1.8, and Table 5.1.8). The product ion at *m/z* 874.56 was created by the loss of water molecule from the precursor ion at *m/z* 892.55. The product ion at *m/z* 692.43 which was assigned as $[C\text{-}(C12{:}0)acid\text{-}H]^-$ ion, and it was generated by the loss of the lauric acid molecule (-200 Da) from the branched fatty acids (C14:0(3-*O*-C12:0)) at the N-2 position. The product ions at *m/z* 648.36 was assigned as $[C\text{-}(C14{:}0(3\text{-}OH))acid\text{-}H]^-$ ion, and it was generated by the loss the 3-hydroxy-myristic acid (-244 Da) at O-3 position. The product ion at *m/z* 666.41 was assigned as $[C\text{-}(C14{:}0(3\text{-}OH))ketene\text{-}H]^-$ ion, and it was generated by the loss the 3-hydroxy-myristic ketene (-226 Da) at O-3 position. The last product ion at *m/z* 562.24 was assigned as $[C\text{-}(C12{:}0)acid\text{-}(C_8H_{16})\text{-}H_2O\text{-}H]^-$ ion, and it was created by the consecutive

elimination of a molecule of water, a (C_8H_{16}) (-112 Da) as part of the fatty acid chain properly located at O-3 position, and the lauryl acid (-200 Da) from the branched fatty (C14:0(3-*O*-12:0)) acid located on N-2′.

These product ions strongly support that the lipid $A_{1\text{-}6}$ structures contain two H_2PO_3 group at O-4′ of the D-GlcN at the non-reducing end, and the other H_2PO_3 group is located at O-1 of the reducing end residue of the β-D-Glc*p*N-(1→6)-α-D-Glc*p*N disaccharide backbone.

It is important to note that the obtained product ion scan of the deprotonated mono-phosphorylated molecules at *m/z* 892.55 is completely different from the one obtained for the deprotonated molecule that were isolated from the lipid A_n SJ-19a (Chapter 3) and SJ-55a (Chapter 4). This indicated that the deprotonated molecules for *m/z* 892.55 are indeed isobaric and have completely different structures.

Also, it indicates the presence of primary myristic esters located at both the O-3′ and N-2′ positions of this lipid $A_{1\text{-}6}$ mixture. It also means that the position of the branched lauric acids ester are located on the O-3 and N-2′ position of the reducing GlcN residue present in the β-D-Glc*p*N-(1→6)-α-D-Glc*p*N disaccharide backbone (El-Aneed *et al*., 2006, Lukasiewicz *et al*., 2006, John *et al*., 2014, and Brodbelt *et al*., 2014).

It should be noticed that the CID-MS/MS analysis of the deprotonated molecules $[M_{1\text{-}6}\text{-H}]^-$ at *m/z* 1768.20 ($LipA_1$), *m/z* 1688.17 ($LipA_2$), *m/z* 1586.12 ($LipA_3$), *m/z* 1506.09 ($LipA_4$), *m/z* 1359.76 ($LipA_5$), and *m/z* 1279.89 ($LipA_6$) afforded distinctive series of product ions.

Furthermore, it is important to mention that there was no cross connectivity between the different precursor deprotonated molecules. This indicates that the genesis of each of these species of precursor ions was individual, and creates its specific product ions. This confirms that the origins of the precursor ions were indeed caused by an incomplete biosynthesis of the LPS (El-Aneed *et al*., 2006, and Lukasiewicz *et al*., 2010).

In general, it is important to note that during the low-energy MS/MS analyses conducted with the QqQ-tandem instrument on these series of deprotonated molecules, we were able to confirm that the formation of each deprotonated molecule recorded in single stage ESI-QqQ-MS instrument, were indeed single unique diagnostic molecules that were not produced by further fragmentation from contiguous higher masses deprotonated molecules. In addition, these product ion scans created series of product ions that excluded the possibility, that they could be related to each other.

Finally, precursor ion scans of these deprotonated molecules formed during the ESI-QqQ-MS showed that there were no connectivities and/or genesi relations between these different deprotonated molecules (see Appendix).

5.3. ESI-FTICR-MS analysis of heterogeneous lipid A_n mixture isolated from the LPS of *A. salmonicida* SJ-113a

The ESI-FTICR-mass spectrometer analysis was also applied to the mixture of lipid A_n (where n=1-8), in order to produce spectrum as a time depending technique with its high resolving power and mass accuracy currently available, which allowed us to determine the elemental conformation of the analyzed produced ions (Marshall *et al*., 1998, Marshall *et al*., 1999, Palumbo *et al.*, 2011, van Agthoven *et al*., 2015, and Almostafa *et al*., 2016). The ESI-MS (- ion mode) obtained for lipid A of *A. salmonicida* SJ-113a displayed an incomplete biosynthesis as demonstrated by the multiple deprotonated molecules. Likewise, to the ESI-QqQ-MS, the ESI-FTICR-MS (- ion mode) showed the presence of inter-alia six fragment ions, which were assigned to different $[M-H]^-$ deprotonated di-phosphorylated molecules $LipA_1$ at *m/z* 1768.1817, $LipA_3$ at *m/z* 1586.0210, and $LipA_5$ at *m/z* 1359.8166, and deprotonated mono-phosphorylated molecules $LipA_2$ at *m/z* 1688.2115, $LipA_4$ at *m/z* 1506.0580, and $LipA_6$ at *m/z* 1279.8496. Also, the last deprotonated molecule at *m/z* 892.5979, which was assigned as it belongs to the $[C-H]^-$ indicating the presence of a heterogeneous mixture of lipid As (Figure 5.2.1, Scheme 5.1.1 and Table 5.1.1). ESI-FTICR-MS spectrum gives the same deprotonated molecules of the $LipA_{1-6}$ mixture as ESI-QqQ-MS with different abundances. In the ESI-FTICR-mass spectrum, we noticed that the deprotonated molecule assigned to the $LipA_4$ at *m/z* 1506.0580 was the most abundant ion (as shown in Figure 5.2.1) (John *et al*., 2014, and Brodbelt *et al*., 2014).

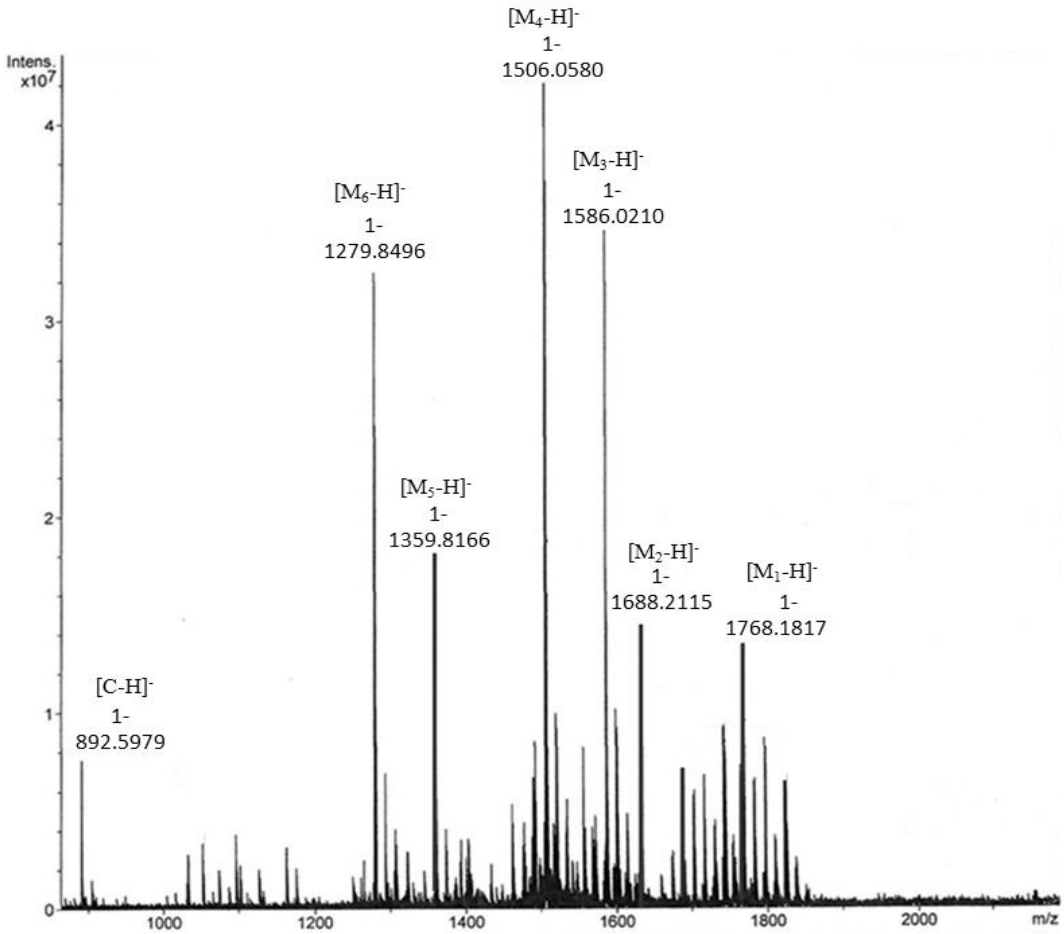

Figure 5.2.1: ESI-FTICR-MS (- ion mode) of the native lipid A_n mixture extracted from *A. salmonicida* SJ-113a.

5.3.1. Measurement of the FT-ICR-MS isotopic distributions of the deprotonated molecules of lipid A_n isolated from the LPS of *A. salmonicida* SJ-113a.

As discussed before in chapter 3 section 3.3.1 and chapter 4 section 4.3.1 we investigated the obtained FTICR-MS spectral accuracy of the deprotonated molecular ions measured by high-resolution FT-ICR-MS. For that reason, we determined the high isotopic abundance accuracy. This latter, allowed us to calculate the excat molecular formula candidates from these accurate mass measurements. The isotopic distribution of this series of deprotonated lipid A_n, (where n=1-6) namely: $LipA_1$ at *m/z* 1768.1817, $LipA_3$ at *m/z* 1586.0210, and $LipA_5$ at *m/z* 1359.8166, and at *m/z* 892.5979, is indicated in the (Figure5.2.2 and Figure 5.2.3) (Kind *et al*., 2010, and Jaitly *et al*., 2009).

Therefore, the calculated elemental compositions of the deprotonated molecule $[M_1\text{-}H]^-$, $[M_2\text{-}H]^-$, $[M_3\text{-}H]^-$, $[M_4\text{-}H]^-$, $[M_5\text{-}H]^-$, and $[M_6\text{-}H]^-$, matched their experimental isotopic abundances using the algorithm “Gaussian 09 software package”, which allowed us to calculate the isotopic fine structures and allow the modeling of Gaussian peak shapes according to the selected resolving power of the instrument (Kind *et al*., 2010, and Jaitly *et al*., 2009). In order to examine the difference in CID-gas-phase fragmentations between the QqQ and the FTICR-instruments, we subjected this series of deprotonated molecules to SORI-CID-FTICR-MS/MS analysis in order to confirm their exact structures.

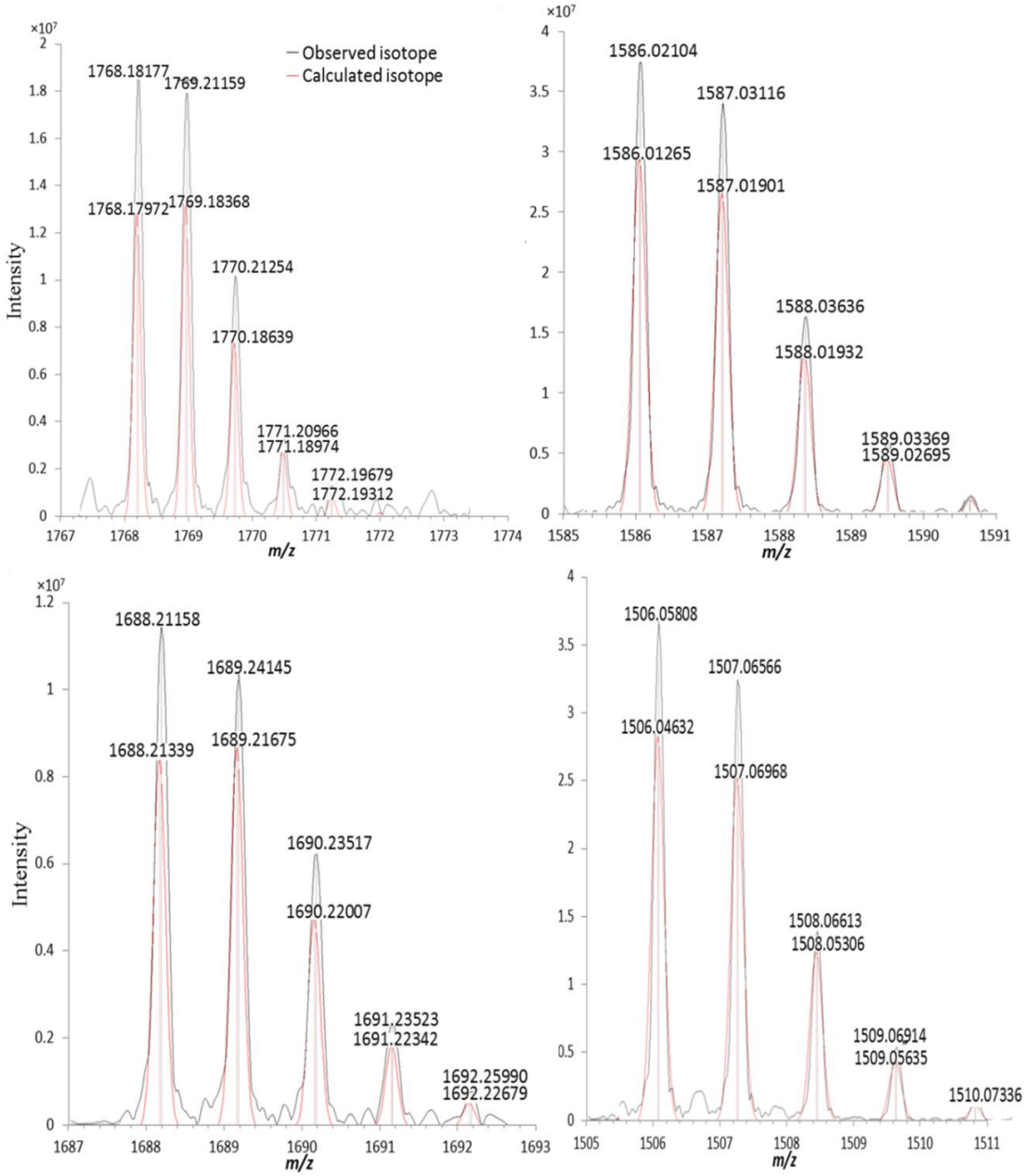

Figure 5.2.2: Theoretical isotope distribution overlapped on top of the observed pattern of the lipid A_n extract from the LPS of *A. salmonicida* SJ-113a.

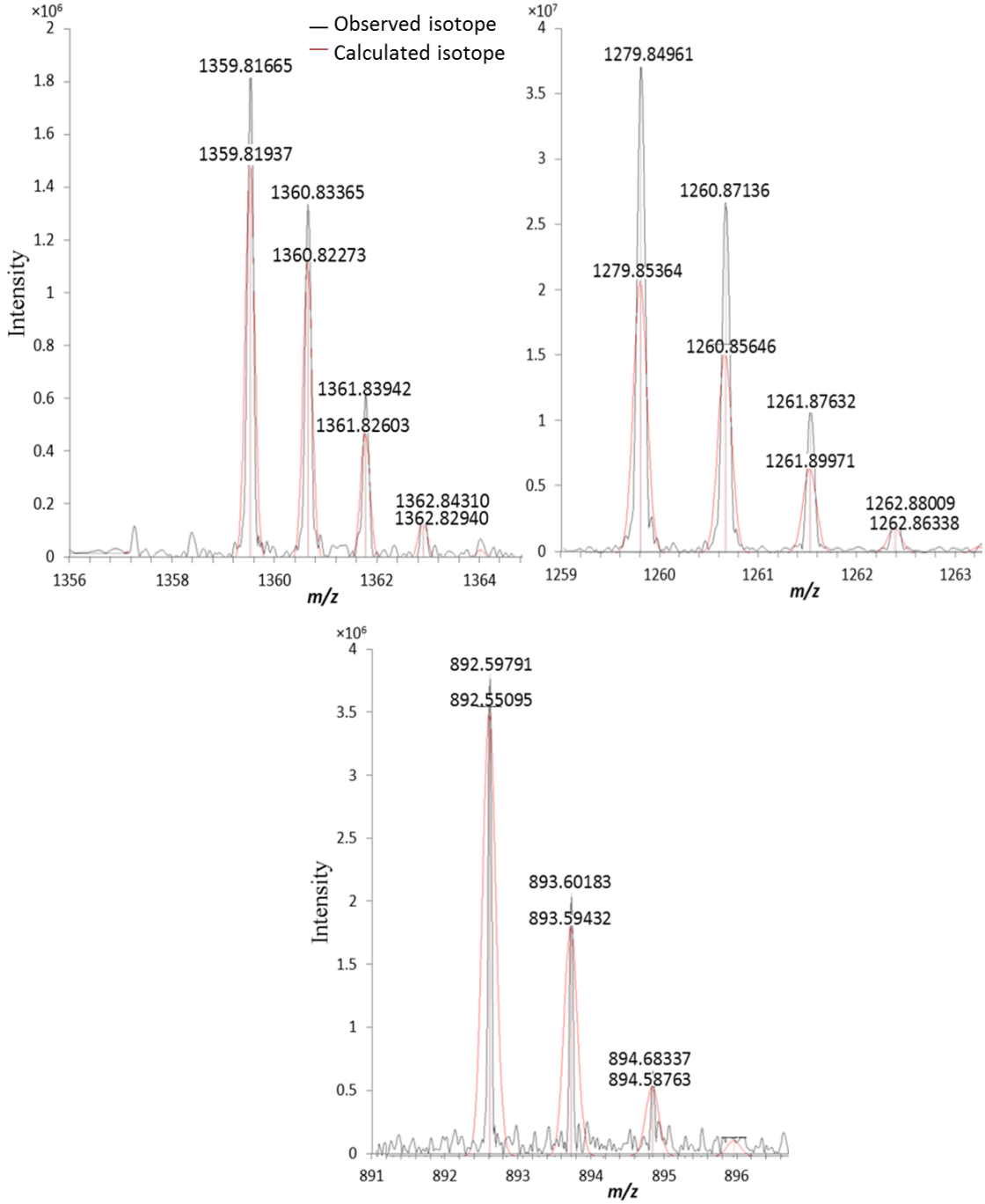

Figure 5.2.3: Theoretical isotope distribution overlapped on top of the observed pattern of the lipid A_n extract from the LPS of *A. salmonicida* SJ-113a.

5.3.2. SORI-CID-FTICR-MS/MS analysis of lipid A isolated from the LPS OF *A. salmonicida* SJ-113a

The MS/MS analysis have provided researchers with information about Lipid A structures including the number and location of phosphoryl groups. The fatty acids on the lipid A backbone (lengths and location), and by defining the nature of the ion charges (singly and doubly charged ions).

The low-energy collision induced dissociation mass spectrometry (SORI-CID-MS/MS) with a Fourier transform ion cyclotron resonance mass spectrometer instrument was used to establish the MS/MS fragmentation routes.

Unfortunately, the SORI product ion scan of the deprotonated molecules of $LipA_1$ at *m/z* 1768.1817 gave the product ions at *m/z* 1243.8450, *m/z* 1035.6578, *m/z* 1017.6378, and *m/z* 648.3945 (Figure 5.2.4, Scheme 5.1.2, and Table 5.1.2). The product ion at *m/z* 1243.8450 was assigned as the $[M_1$-(C14:0(3-*O*-C12:0))acid-H_2PO_4-H$]^-$ ion. It was created by the elimination of the branched fatty (C14:0(3-*O*-C12:0)) acids located at O-3 (-426 Da), and the neutral H_3PO_4 (-98 Da) moiety which located at O-1 position. The product ion at *m/z* 1035.6578 was assigned as $[M_1$-(C14:0(3-*O*-C12:0))acid-(C14:0(3-OH))ketene-HPO_3-H$]^-$ ion, and it was created by the elimination of the branched fatty (C14:0(3-*O*-C12:0)) acids located at O-3 (-426 Da), the 3-hydroxy-myristic ketene (-226 Da) located at O-3′, and the neutral HPO_3 (-80 Da) moiety which located at O-1 position. The product ion at *m/z* 1017.6378 was created by the loss of a molecule of water from the product ion at *m/z* 1035.6578. The product ion at *m/z* 648.3945 was assigned as the [C-(C14:0(3-

OH))acid-H]$^-$ ion, and it was formed by the elimination of the 3-hydroxy-myristic acid (C14:0(3-OH)) (-244 Da) from the O-3 of the precursor deprotonated molecule at *m/z* 1768.1817 (Shaffer *et al*., 2007, John *et al*., 2014, and Brodbelt *et al*., 2014).

The product ion scan of the deprotonated $LipA_2$ molecules at *m/z* 1688.2115 gave the product ions at *m/z* 1488.0382, *m/z* 1444.9820, *m/z* 1243.8446, *m/z* 1035.6591 and *m/z* 1017.6381 (Figure 5.2.5, Table 5.1.3, and Scheme 5.1.3). The product ion at *m/z* 1488.0382 was assigned as the [M_2-(C12:0)acid-H]$^-$ ion, which was created by the elimination of the lauryl acid (-200 Da) from the branched fatty (C14:0(3-*O*-12:0)) acid located either on N-2′or O-3. The product ion at *m/z* 1444.9820 was assigned as the [M_2-(C14:0(3-OH))acid-H]$^-$ ion, which was created by the elimination of the 3-hydroxy-myristic acid (C14:0(3-OH)) (-244 Da) from the O-3′. The product ion at *m/z* 1243.8446 was assigned as the [M_2-(C14:0(3-*O*-C12:0)acid)acid-H_2O-H]$^-$ ion, which was created by the elimination of the branched fatty (C14:0(3-*O*-C12:0)) acid acyl group located at O-3′ (-426 Da) and a molecule of water. The product ion at *m/z* 1035.6591 was assigned as the [M_2-(C14:0(3-*O*-C12:0))acid-(C14:0)(3-OH)ketene-H]$^-$ ion, which was created by the elimination of the branched fatty (C14:0(3-*O*-C12:0)) acyl group located at O-3′ (-426 Da) and 3-hydroxy-myristic ketene (C14:0(3-OH)) (-226 Da) located at the position O-3′. The product ion at *m/z* 1017.6381 was created by the loss of a molecule of water from the product ion at *m/z* 1035.6591 (Shaffer *et al*., 2007, Lukasiewicz *et al*., 2010).

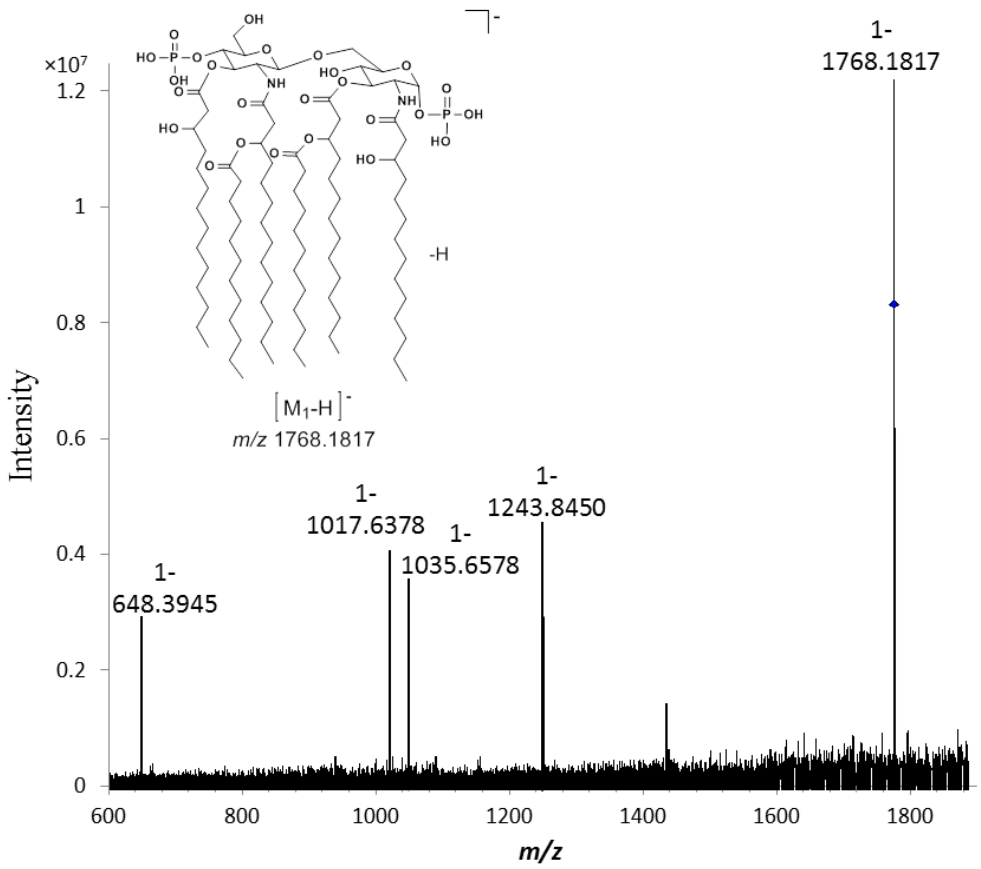

Figure 5.2.4: SORI-CID-MS/MS of the precursor deprotonated $[M_1\text{-}H]^-$ molecules at *m/z* 1768.1817.

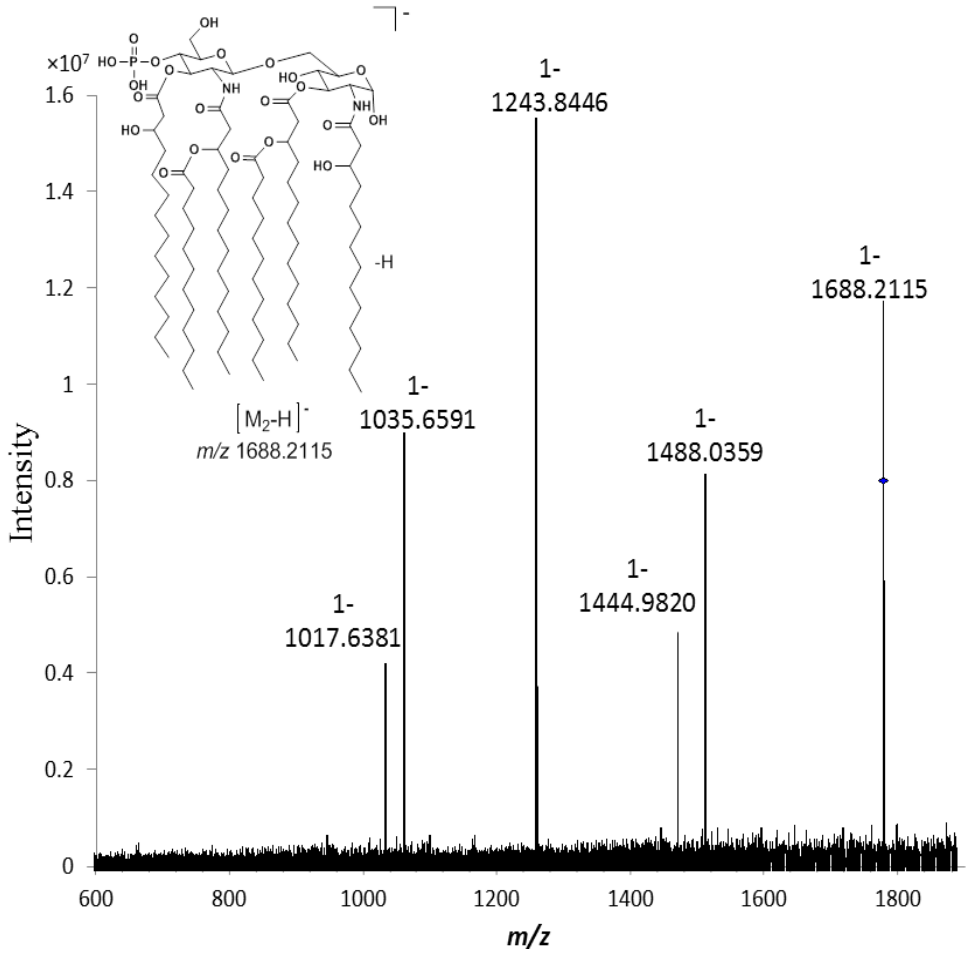

Figure 5.2.5: SORI-CID-MS/MS of the precursor deprotonated $[M_2\text{-}H]^-$ molecules at *m/z* 1688.2115.

The product ion scan of the deprotonated $LipA_3$ molecules at *m/z* 1586.0254 gave the product ions at *m/z* 1488.0499, *m/z* 1341.8083 and *m/z* 1243.8425 (Figure 5.2.6, Table 5.1.4, and Scheme 5.1.4). The product ion at *m/z*1488.0499 was assigned as the $[M_3\text{-}H_2PO_4\text{-}H]^-$ ion, which was created by the elimination of the H_3PO_4 (-98 Da) located at O-1. The product ion at *m/z* 1341.8083 was assigned as $[M_3\text{-(C14:0(3-OH))acid-H}]^-$ ion, which was created by the elimination of the 3-hydroxy-myristic acid (C14:0(3-OH)) (-244 Da) located either at the position O-3 or O-3′. The product ion at *m/z* 1243.8425 $[M_3\text{-(C14:0(3-OH))acid-}HPO_3\text{-H}]^-$ ion, which was created by the elimination of the H_3PO_4 (-98 Da) located at O-1, and the 3-hydroxy-myristic acid (C14:0(3-OH)) (-244 Da) located either at the position O-3 or O-3′ (El-Aneed *et al*., 2006, Shaffer *et al*., 2007, Lukasiewicz *et al*., 2006, John *et al*., 2014, and Brodbelt *et al*., 2014).

The product ion scan of the precursor deprotonated molecules of $LipA_4$ *m/z* 1506.0580 gave the major product ion at *m/z* 1305.8680, *m/z* 1261.8399, and *m/z* 1035.6692. The product ion at *m/z* 1305.8680 was assigned as the $[M_4\text{-(C12:0)acid-H}]^-$ ion, and it was formed by the loss of a molecule of lauric acid (-200 Da) from the branched (C14:0(3-*O*-C12:0)) fatty acyl group located at the N-2′ position of $LipA_4$. The product ion at *m/z* 1261.8399 was assigned as $[M_4\text{-(C14:0(3-OH))acid-H}]^-$ ion, which was created by the elimination of the 3-hydroxy-myristic acid (C14:0(3-OH)) (-244 Da) located either at the position O-3 or O-3′. The product ion at *m/z* 1035.6692 was assigned as $[M_4\text{-(C14:0(3-OH))acid-(C14:0(3-OH))ketene-H}]^-$ ion, which was formed by the elimination of 3-hydroxy-myristic acid (-244 Da) and of 3-hydroxy-myristic ketene (-226 Da) from the

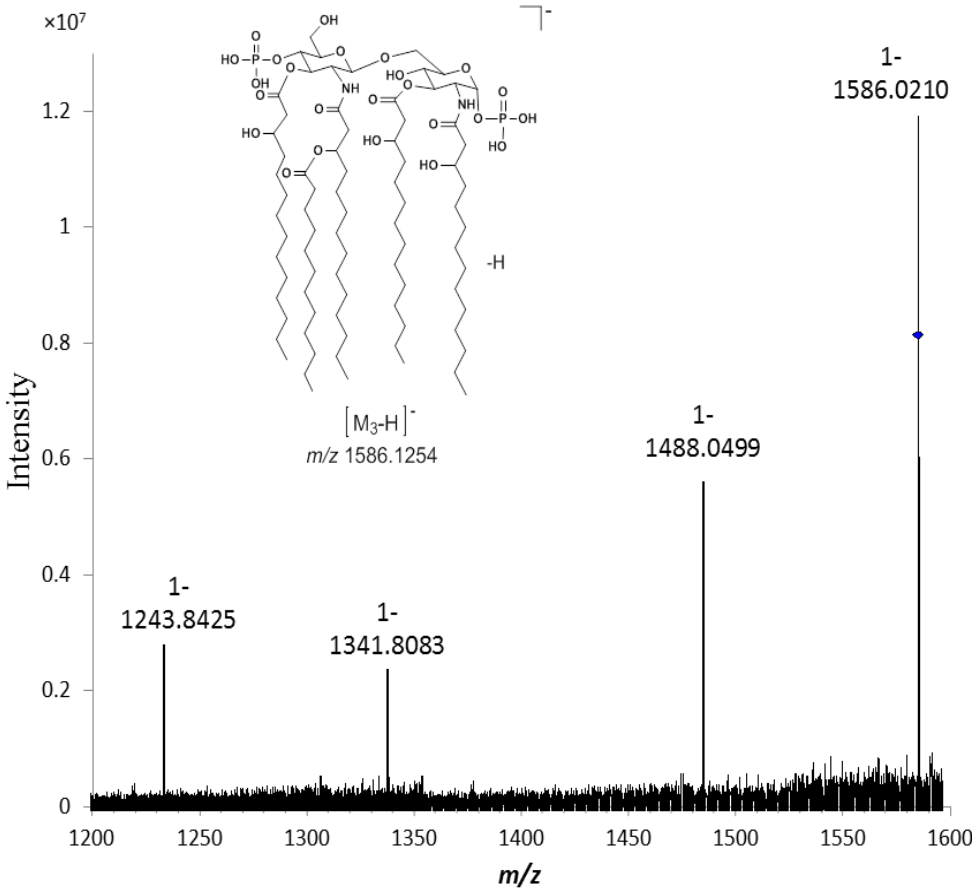

Figure 5.2.6: SORI-CID-MS/MS of the precursor deprotonated $[M_3\text{-}H]^-$ molecules at *m/z* 1586.0210.

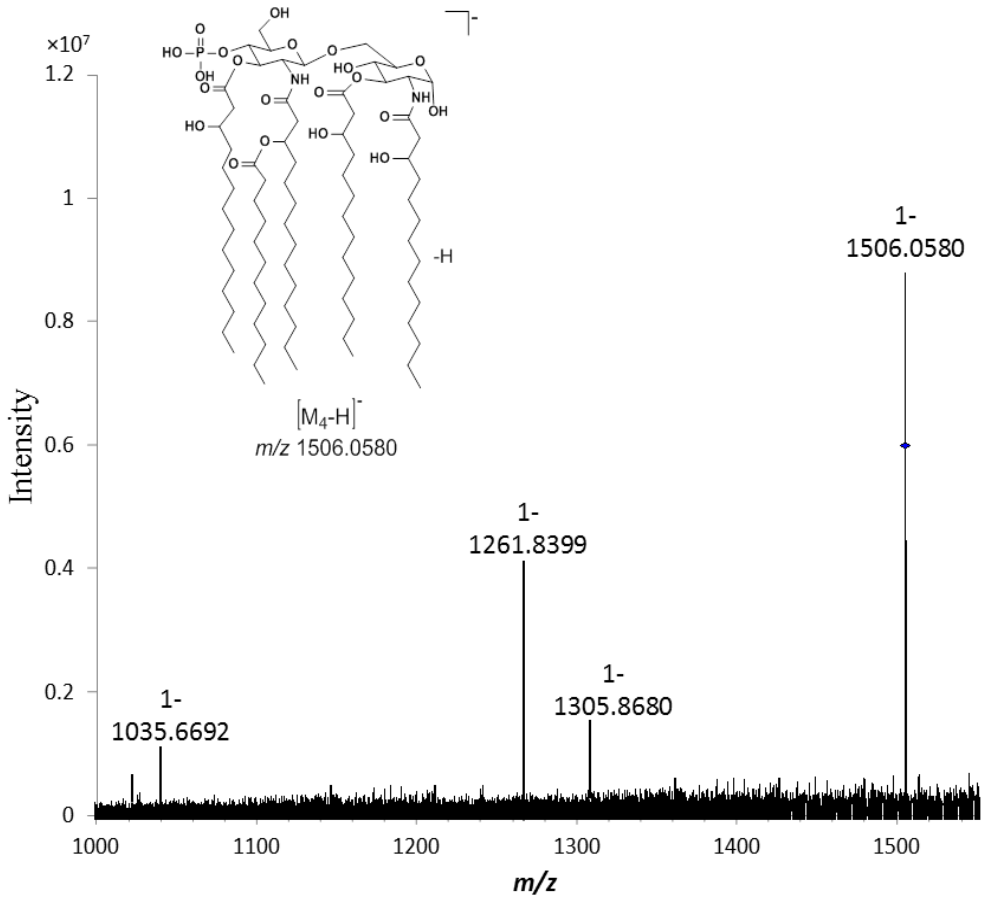

Figure 5.2.7: SORI-CID-MS/MS of the precursor deprotonated $[M_4\text{-}H]^-$ molecules at *m/z* 1506.0580.

precursor ion located either at the O-3 and O-3′ positions (Figure 5.2.7, Table 5.1.5 and Scheme 5.1.5) (Shaffer *et al*., 2007, John *et al*., 2014, and Brodbelt *et al*., 2014).

The product ion scan of the deprotonated $LipA_5$ molecules at *m/z* 1359.8180 gave the product ions at *m/z* 1261.8379, *m/z* 1115.6120, *m/z* 1035.6669, and *m/z* 1017.6377 (Figure 5.2.8, Table 5.1.6, and Scheme 5.1.6). The product ions at *m/z* 1261.8379 was assigned as $[M_5\text{-}H_2PO_4\text{-}H]^-$ ion, and it was formed by the elimination of the neutral H_3PO_4 (-98 Da) moiety. The product ion at *m/z* 1115.6125 was assigned as $[M_5\text{-}(C14:0)(3\text{-}OH)acid\text{-}H]^-$ ion, and it was formed by the elimination of 3-hydroxy-myristic acid (-244 Da) from the precursor ion located at the O-3.The product ion *m/z* 1035.6669 was assigned as $[M_5\text{-}(C14:0)(3\text{-}OH)acid\text{-}HPO_3\text{-}H]^-$ ion, and it was formed by the elimination of 3-hydroxy-myristic acid (-244 Da) from the precursor ion located at the O-3, and the neutral HPO_3 (-80 Da) moiety. The product ion at *m/z* 1017.6377 created by the loss of a molecule of water from the product ion at *m/z* 1035.6669 (El-Aneed *et al*., 2006, Shaffer *et al*., 2007, Lukasiewicz *et al*., 2010, John *et al*., 2014, and Brodbelt *et al*., 2014).

Additionally, the product ion scan of $LipA_6$ at *m/z* 1279.8496 afforded the product ion at *m/z* 1079.6750 *m/z* 1035.6678, and *m/z* 835.4846. The product ion at *m/z* 1079.6750 was assigned as $[M_6\text{-}(C12:0)acid\text{-}H]^-$ ion, and it was formed by the elimination of the lauric acid (-200 Da) from the branch (Cl4:0(3-*O*-12:0)) fatty acids, which was attached to the N-2′ position. The product ion at *m/z* 1035.6667 was assigned as $[M_6\text{-}(C14:0)(3\text{-}OH)acid\text{-}H]^-$ ion, and it was formed by the elimination of 3-hydroxy-myristic acid(-244 Da) from the

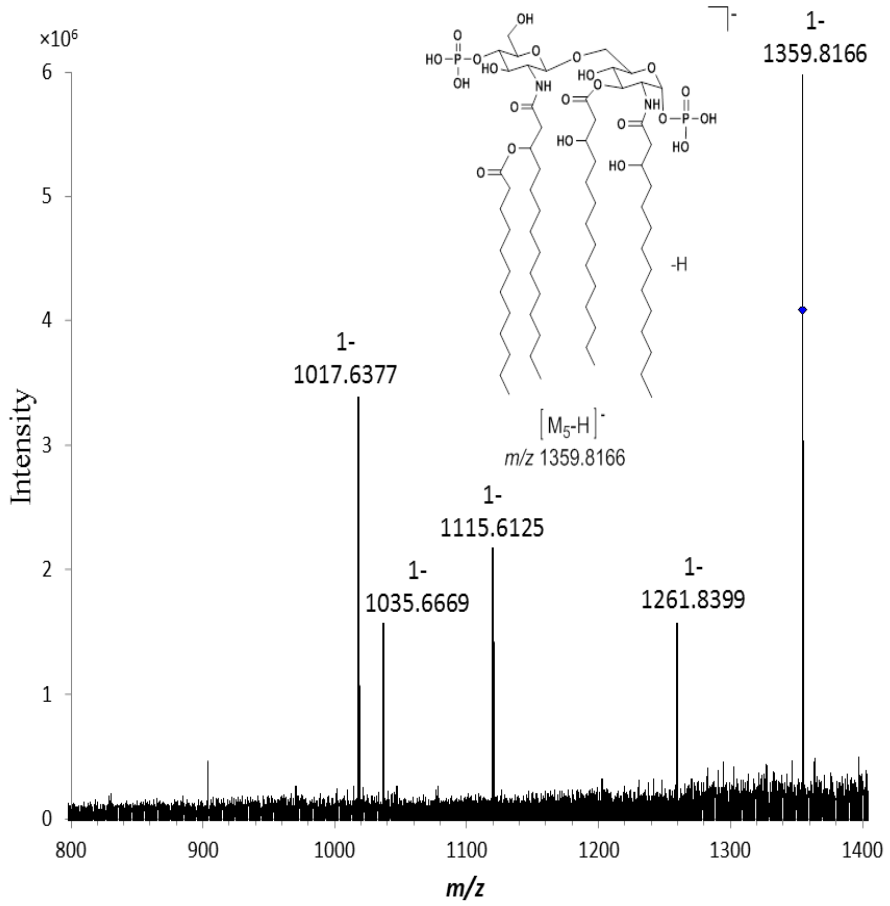

Figure 5.2.8: SORI-CID-MS/MS of the precursor deprotonated $[M_5\text{-}H]^-$ molecules at *m/z* 1359.8180.

precursor ion located either at the O-3.The last product ion at *m/z* 835.4846 was assigned as the [M_6-(C12:0)ketene-(C14:0(3-OH))acid-H]$^-$ ion, which was created by elimination of the lauryl ketene molecule (-182 Da) from the branched fatty acids (C14:0(3-*O*-C12:0)) located on the N-2′ position, and the 3-hydroxy-myristic acid (C14:0(3-OH)) (-244Da) located at the position O-3 of the reducing GlcN end of the lipidA_6 disaccharide (Figure 5.2.9, Table 5.1.7 and Scheme 5.1.7) (El-Aneed *et al*., 2006, Shaffer *et al*., 2007, Lukasiewicz *et al*., 2010, John *et al*., 2014, and Brodbelt *et al*., 2014).

In the same way to the MS/MS experiments described with the QqQ-MS spectrometer, the lower diagnostic deprotonated molecules were also selected, and subjected to SORI-CID-MS/MS measurements with the FTICR-mass spectrometer instrument. This was achieved to confirm the putative structures of these precursors' deprotonated molecules, and also to confirm the location of the phosphate group.

Consequently, the SORI-CID-MS/MS of the deprotonated molecules at *m/z* 892.5979, previously assigned as [C-H]$^-$ gave the product ions at *m/z* 648.3961 and *m/z* 466.2117 (Figure 5.2.10, Table 5.1.8, Scheme 5.1.8). The product ion at *m/z* 648.3949 was assigned as the [C-(C14:0(3-OH))acid-H]$^-$ ion, and it was formed by the elimination of the 3-hydroxy-myristic acid (C14:0(3-OH)) (-244 Da) from the O-3 of the precursor deprotonated molecule. The product ions at *m/z* 466.2117 was attributed as the [C-(C14:0(3-OH))acid-(C12:0)ketene-H]$^-$, which was formed by the consecutive elimination of the 3-hydroxy-myristic acid (C14:0(3-OH)) (-244 Da), from the O-3 position, and the lauric acid (-200 Da) from the branch (Cl4:0(3-*O*-12:0)) fatty acids, which was attached to the N-2 position of the non-reducing GlcN residue of the precursor ion at *m/z* 892.5979.

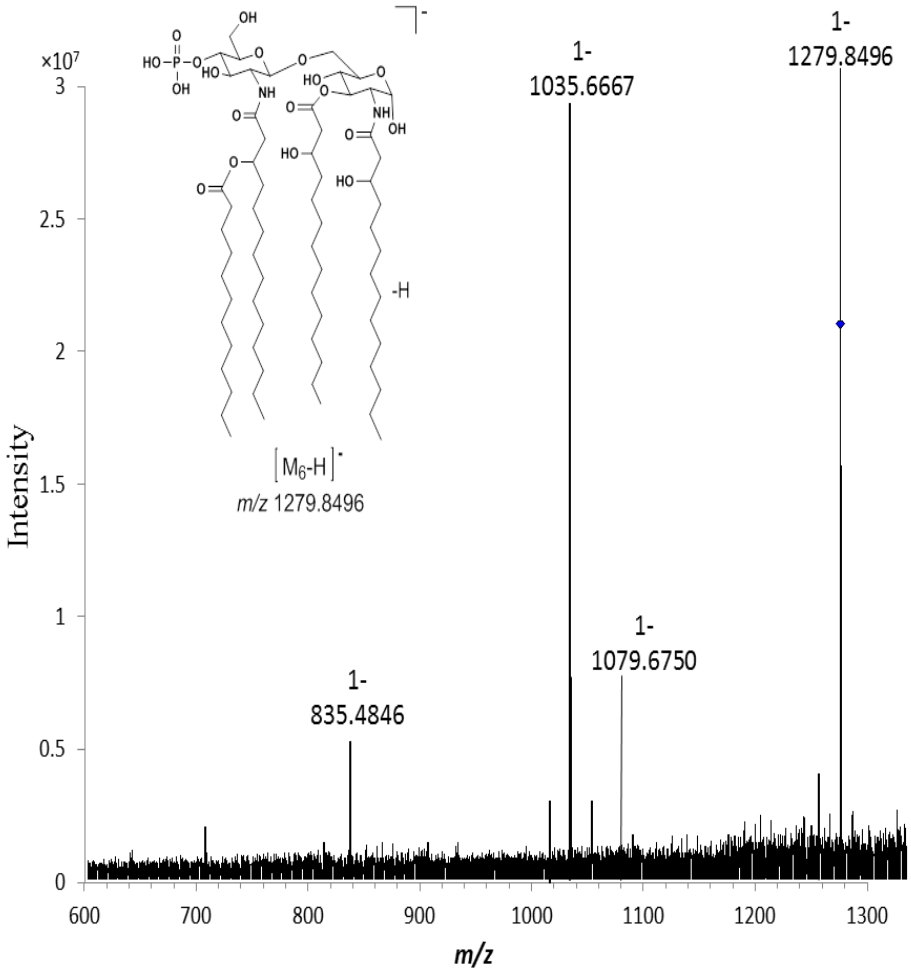

Figure 5.2.9: SORI-CID-MS/MS of the precursor deprotonated $[M_6\text{-}H]^-$ molecules at *m/z* 1279.8489.

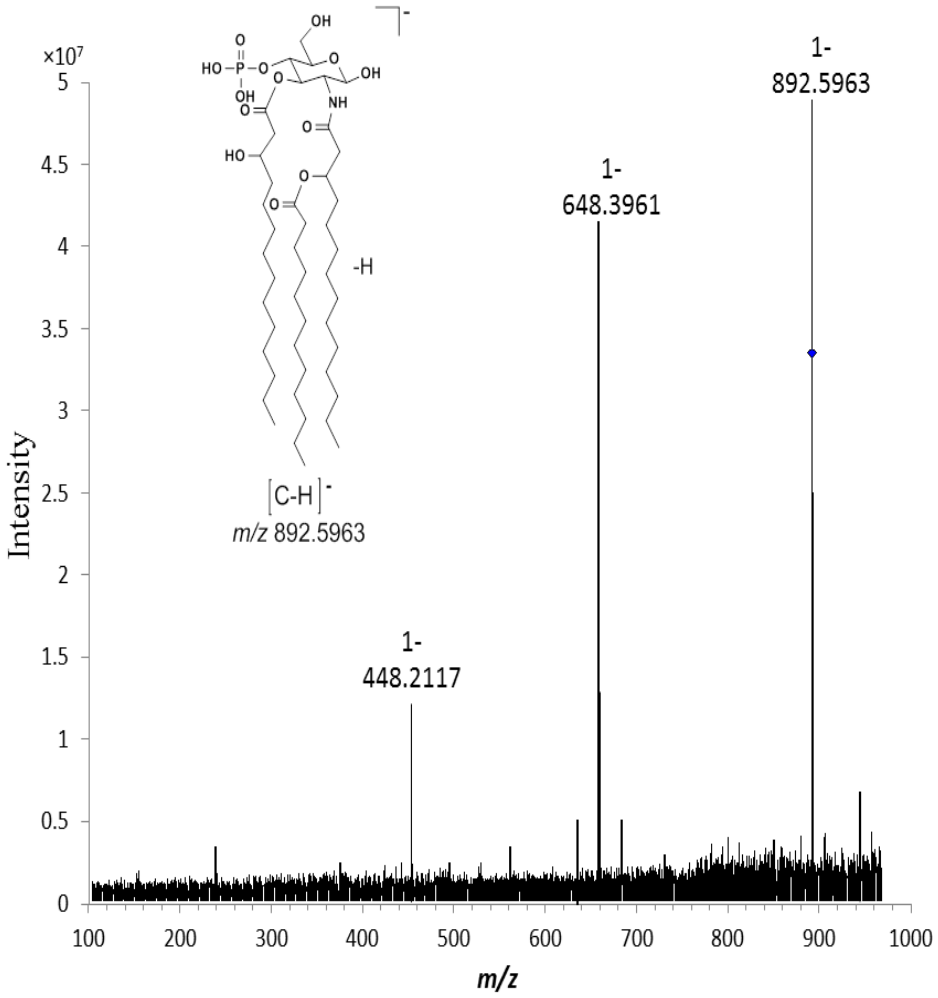

Figure 5.2.10: SORI-CID-MS/MS of the precursor deprotonated [C-H]$^-$ molecules at *m/z* 892.5979.

5.3.3. Comparison between low-energy CID-QqQ-MS/MS and SORI-CID-MS/MS of the deprotonated molecules obtained from the mixture of lipid As isolated from the LPS of the *A. salmonicida* SJ-113a

As discussed in the chapter 3 and 4 sections 3.3.3 and 4.3.3 we have made a comparison between the CID-MS/MS analyses with the QqQ-MS/MS and SORI-MS/MS. We have noticed that the number of distinctive product ions decreased with SORI-MS/MS analyses, when compared to CID-MS/MS analyses with the QqQ-mass spectrometer instrument. As in all of the previous schemes (5.1.2 – 5.1.8), we have noticed that all of the product ions obtained from SORI-CID-MS/MS were produced by the primary fatty acid fragmentation only. There were no CID-fragmenttaion from the branched fatty acyl groups and it was noted that most eliminations occurred from the O-3 and O-3´ positions. The reasons for the obtained differences in product ions formation are the same as these presented in section 3.3.3.

5.4. High-energy MALDI-TOF-MS analysis of the extracted mixture of lipid As isolated from the LPS of *A. salmonicida* SJ-113a

The MALDI-TOF-MS (-ion mode) of the lipid A obtained from *A. salmonicida* SJ-113a was measured in the reflector mode with the TOF/TOF instrument and high laser power. Similarly, the MALDI-MS showed comparable spectra to the ones measured with the ESI-QqQ-MS and FTICR-MS instruments.

Again, the MALDI-TOF-MS indicated that the biosynthesis of lipid A was incomplete. Accordingly, we have assigned for this lipid A mixture, the original seven common structures of the lipid A as suggested previously in sections: 5.2 and 5.3. They were assigned to different $[M-H]^-$ deprotonated di-phosphorylated molecules $LipA_1$ at *m/z* 1768.1798, $LipA_3$ at *m/z* 1586.0210, $LipA_5$ at *m/z* 1359.8259, and mono-phosphorylated molecules $LipA_2$ at *m/z* 1688.2123, $LipA_4$ at *m/z* 1506.0466, and $LipA_6$ at *m/z* 1279.8510 (Figure 5.3.1, Scheme 5.1.1 and Table 5.1.1). In the MALDI-TOF-mass spectrum, we noticed that the deprotonated molecules assigned to the $LipA_6$ at *m/z* 1279.8510 was the most abundant in the mass spectrum. Also, the last deprotonated molecule at *m/z* 892.5961, which was assigned as belonging to the $[C-H]^-$ indicating the presence of a heterogeneous mixture of lipid A_n (as shown in Figure 5.3.1).

In order to examine the difference in high-energy collision MS/MS dissociation with that of the low-energy collision MS/MS recorded with the QqQ and the FTICR-instruments, we measured this series of product ion scans of these deprotonated molecules with the high energy CID-TOF/TOF-MS/MS instrument.

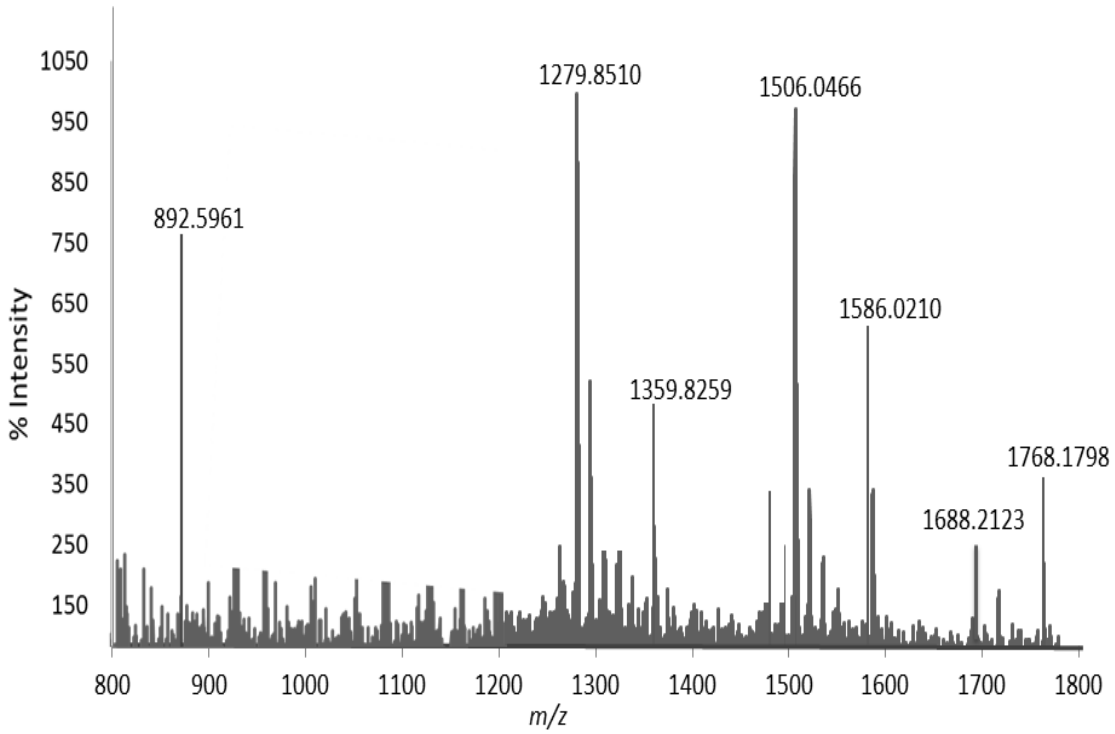

Figure 5.3.1: High-energy MALDI-TOF-MS (- ion mode) of the native lipid A_n mixture extracted from *A. salmonicida* SJ-113a.

5.4.1 High-energy MALDI-CID-TOF/TOF-MS/MS analysis of the extracted mixture of lipid As isolated from the LPS of *A. salmonicida* SJ-113a

The lipid A_{1-6} mixture isolated from *A. salmonicida* SJ-113a was subjected to high-energy CID-TOF/TOF-MS/MS. The structures of the detected product ions were deduced as previously described in the ESI-CID-MS/MS studies of this lipid A_n mixture.

High-energy CID-TOF/TOF-MS/MS of the deprotonated molecules $LipA_1$ at *m/z* 1768.1798 is illustrated in (Figure 5.3.2, Tables 5.1.2, and Scheme 5.1.2). $LipA_1$ produced the product ions at *m/z* 1488.0412, *m/z* 1243.8512, and *m/z* 1017.6320. The product ion at *m/z* 1488.0412 was assigned as $[M_1\text{-(C12:0)acid-}HPO_3\text{-H}]^-$ ion, and it was created by the loss of the lauryl acid (-200 Da) from the branched (C14:0(3-*O*-C12:0)) located at N-2′ positions and neutral HPO_3 (-80 Da) located at O-1. The product ion at *m/z* 1243.8512 was assigned as the $[M_1\text{-(C14:0(3-}O\text{-C12:0))acid-}H_2PO_4\text{-H}]^-$ ion, which was created by the elimination of the branched fatty (C14:0(3-*O*-C12:0)) acids located at O-3 (-426 Da), and the neutral H_3PO_4 (-98 Da) moiety which is located at O-1 position.

The product ion at *m/z* 1017.6320 was assigned as $[M_1\text{-(C14:0(3-}O\text{-C12:0))acid-(C14:0(3-OH))acid-}HPO_3\text{-H}]^-$ ion, which was created by the elimination of the branched fatty (C14:0(3-*O*-C12:0)) acids located at O-3 (-426 Da), the 3-hydroxy-myristic ketene (-226 Da) located at O-3′, and the neutral HPO_3 (-80 Da) moiety which located at O-1 position (Kussak *et al.*, 2002, Shaffer *et al*., 2007, Lukasiewicz *et al*., 2010, and Brodbelt *et al*., 2014).

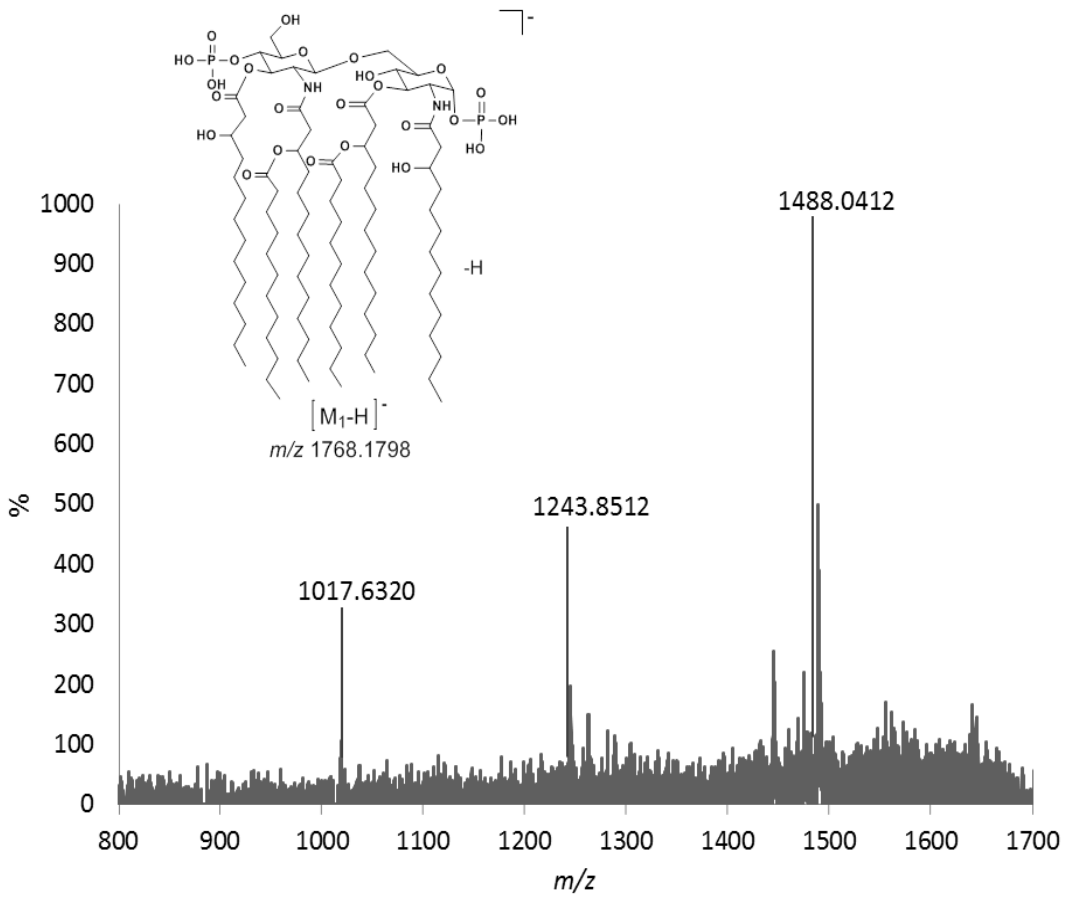

Figure 5.3.2: High-energy CID-TOF/TOF-MS/MS of the precursor ion $[M_1\text{-}H]^-$ ion at *m/z* 1768.1798.

High-energy CID-TOF/TOF-MS/MS of the anion at *m/z* 1688.2123 $LipA_2$ is illustrated in (Figure 5.3.3, Tables 5.1.3, and Scheme 5.1.3). A product ion scan of the deprotonated $LipA_2$ molecules gave the product ions at *m/z* 1488.0315, *m/z* 1261.8497, and *m/z* 1035.6520. The product ion at *m/z* 1488.0315 was assigned as the $[M_2$-(C12:0)acid-H$]^-$ ion, which was created by the elimination of the lauryl acid (-200 Da) from the branched (C14:0(3-*O*-C12:0)) located at N-2′ positions. The product ions at *m/z* 1261.8497 was assigned as $[M_2$-(C14:0(3-*O*-12:0))acid-H$]^-$ ion, and it was formed by the consecutive loss of the branched fatty (C14:0(3-*O*-C12:0)) acid (-426 Da) located on position O-3. The product ion at *m/z* 1035.6520 which was assigned as $[M_1$-(C14:0(3-*O*-C12:0))acid-(C14:0(3-OH))ketene-H$]^-$ ion, which was created by the elimination of the branched fatty (C14:0(3-*O*-C12:0)) acids located at O-3 (-426 Da), the 3-hydroxy-myristic ketene (-226 Da) located at O-3′.

High-energy CID-TOF/TOF-MS/MS of the anion at *m/z* 1586.0210 $LipA_3$ is illustrated in (Figure 5.3.4, Tables 5.1.4, and Scheme 5.1.4). The product ion scan of the deprotonated $LipA_3$ molecules gave the product ions at *m/z* 1488.0423, *m/z* 1341.8041, and *m/z* 1243.8495. The product ion at *m/z* 1488.0423 was obtained by the loss of a H_3PO_4 (-98 Da) released from the O-1 position of the D-GlcN non-reducing end of $LipA_3$. The product ion at *m/z* 1341.85 was assigned as the $[M_3$-(C14:0(3-OH))acid-H$]^-$, and it was formed by the elimination of the 3-hydroxy-myristic acid (C14:0(3-OH)) (-244 Da) located either at the position O-3 or O-3′. The product ion at *m/z* 1243.8495 was assigned as the $[M_3$-(C14:0(3-OH))acid-HPO_3-H$]^-$ ion, and it was formed by the elimination of the neutral

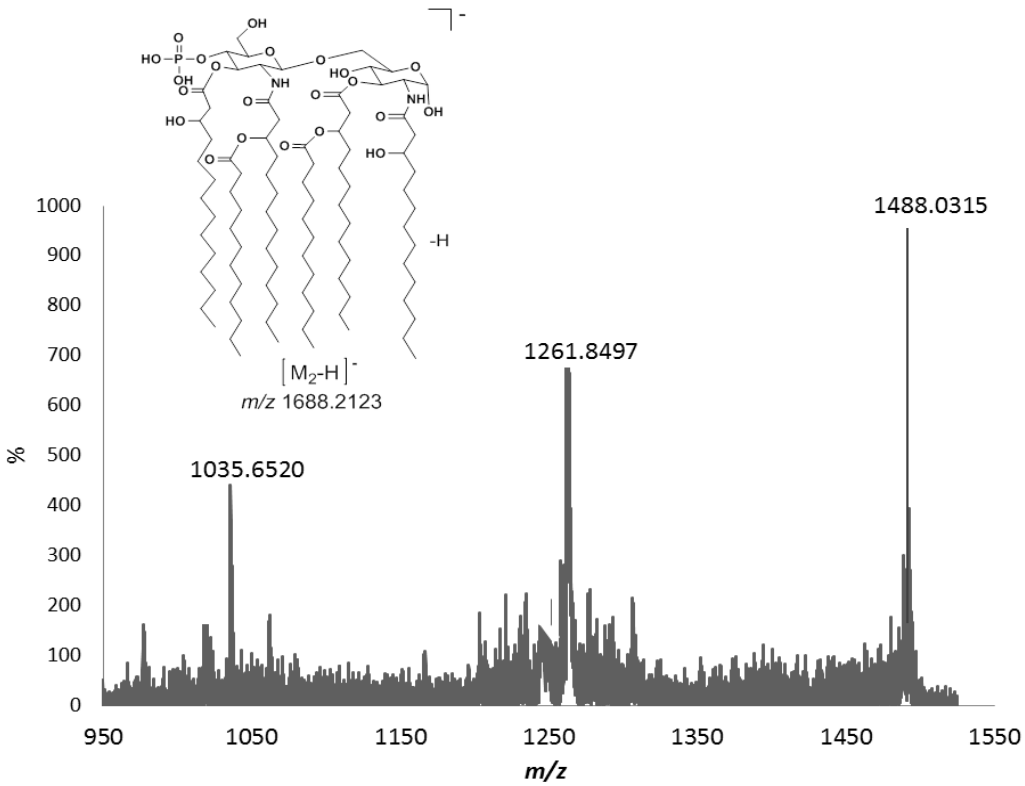

Figure 5.3.3: High-energy CID-TOF/TOF-MS/MS of the precursor ion $[M_2\text{-}H]^-$ ion at *m/z* 1688.2126.

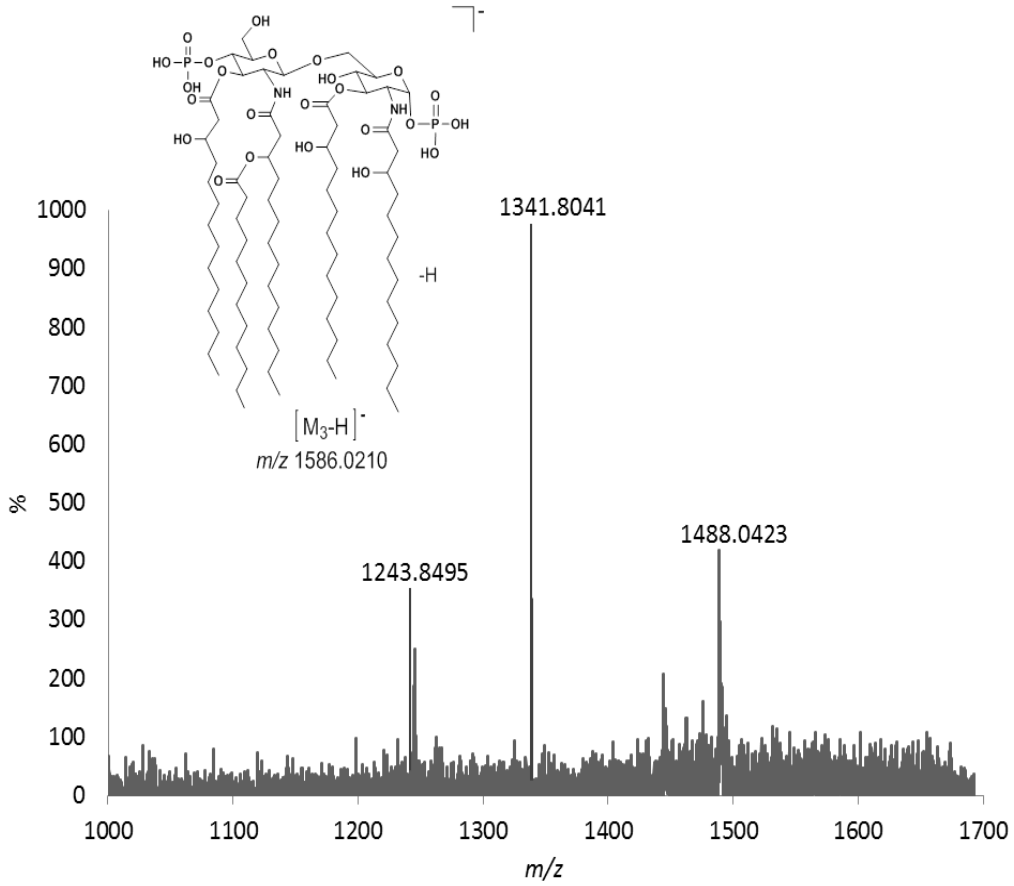

Figure 5.3.4: High-energy CID-TOF/TOF-MS/MS of the precursor ion $[M_3\text{-}H]^-$ ion at *m/z* 1586.0210.

H_3PO_4 (-98 Da) moiety located at O-1 position, and the 3-hydroxy-myristic acid (C14:0(3-OH)) (-244 Da) located either at the position O-3 or O-3′ (Kussak *et al.*, 2002, El-Aneed *et al*., 2006, Shaffer *et al*., 2007, Lukasiewicz *et al*., 2010, and Brodbelt *et al*., 2014).

High-energy CID-TOF/TOF-MS/MS of the anion at *m/z* 1506.0466 $LipA_4$ is illustrated in (Figure 5.3.5, Tables 5.1.5, and Scheme 5.1.5). The product ion scan of the deprotonated $LipA_4$ molecules gave the product ions at *m/z* 1261.8485 and *m/z* 1035.6621. The product ions at *m/z* 1261.8485 was formed by the elimination of 3-hydroxy-myristic acid (-244 Da) located either at O-3 or O-3′ from the precursor ion. This product ion was assigned as $[M_4$-(C14:0(3-OH)acid-H$]^-$ ion. The product ion at *m/z* 1035.6621 was assigned as $[M_4$-(C14:0(3-OH))acid-(C14:0(3-OH))ketene-H$]^-$ ion, and it was formed by the consecutive losses of the 3-hydroxy-myristic acid (-244 Da) and the 3-hydroxy-myristic ketene (-226 Da) which can be in fact occur from either at the O-3 and O-3′ positions located respectively in the reducing end or non-reducing end of the lipid A disaccharide backbone (Kussak *et al.*, 2002, El-Aneed *et al*., 2006, Shaffer *et al*., 2007, Lukasiewicz *et al*., 2010, and Brodbelt *et al*., 2014).

High-energy CID-TOF/TOF-MS/MS of the anion at *m/z* 1359.8259 $LipA_5$ is illustrated in (Figure 5.3.6, Tables 5.1.6, and Scheme 5.1.6). The product ion scan of the deprotonated $LipA_5$ molecules gave the product ions at *m/z* 1261.8476 and *m/z* 1115.6120. The product ion at *m/z* 1261.8476 was obtained by the loss of a H_3PO_4 (-98 Da) released from the O-1 position of the D-GlcN non-reducing end of $LipA_5$.The product ion at *m/z* 1115.6120 was assigned as $[M_5$-(C14:0)(3-OH)acid-H$]^-$ ion, and it was formed by the

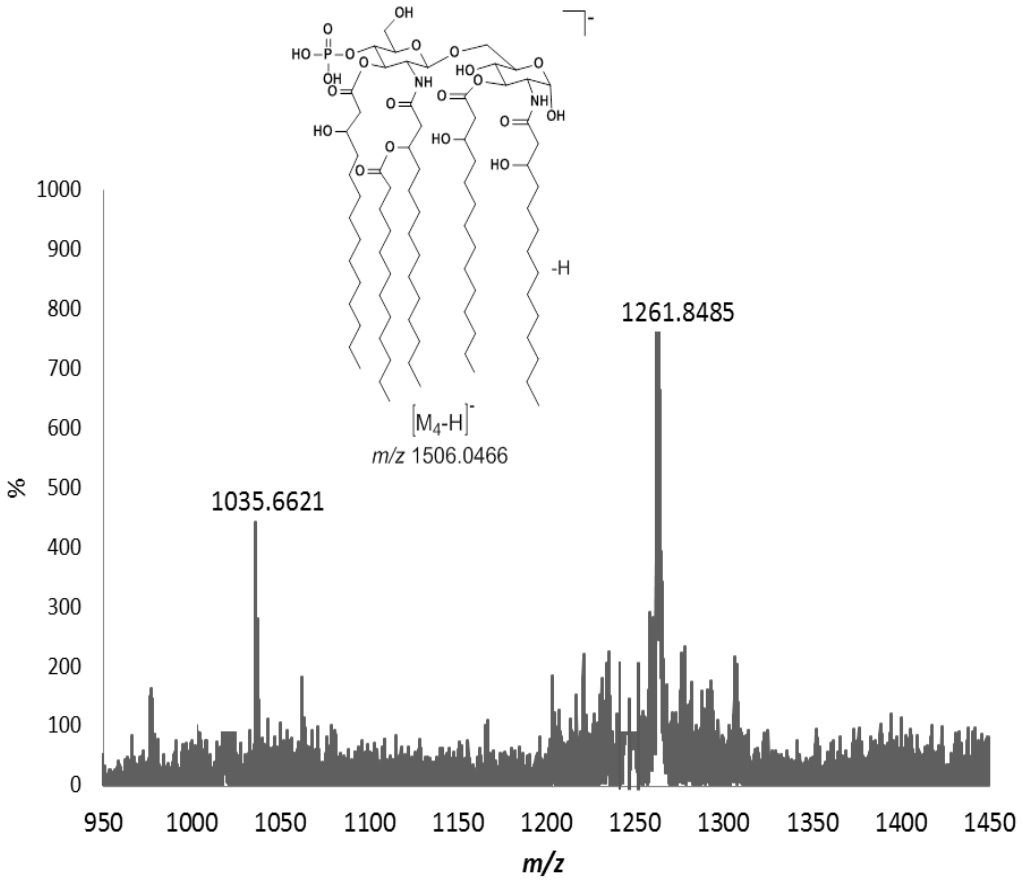

Figure 5.3.5: High-energy CID-TOF/TOF-MS/MS of the precursor ion $[M_4\text{-}H]^-$ ion at *m/z* 1506.1466.

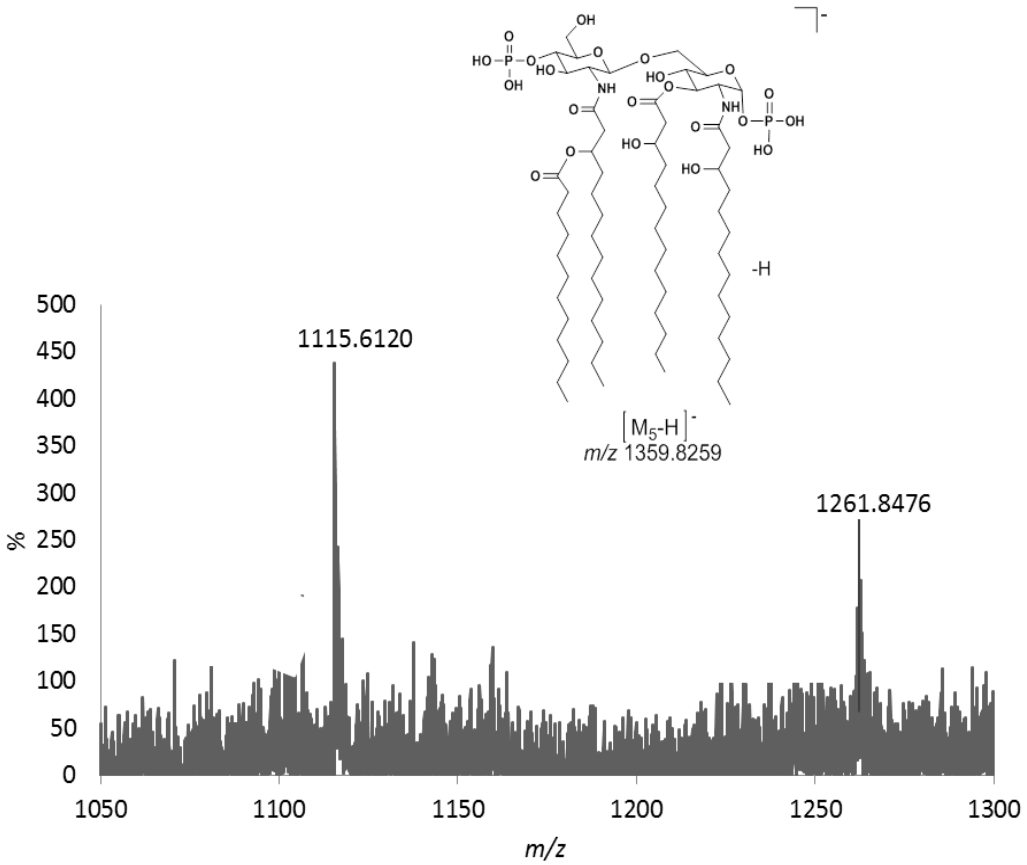

Figure 5.3.6: High-energy CID-TOF/TOF-MS/MS of the precursor ion $[M_5\text{-H}]^-$ ion at *m/z* 1359.8259.

elimination of 3-hydroxy-myristic acid (-244 Da) from the precursor ion located either at the O-3′. High-energy CID-TOF/TOF-MS/MS of the anion at *m/z* 1279.8510 $LipA_6$ is illustrated in (Figure 5.3.7, Tables 5.1.7, and Scheme 5.1.7). The product ion scan of the deprotonated $LipA_6$ molecules gave the product ions at *m/z* 1079.6711, *m/z* 1035.6619, and *m/z* 994.6175. The product ion at *m/z* 1079.6711 was assigned as $[M_6\text{-(C12:0)acid-H}]^-$ ion, which was formed by the elimination of the lauric acid (-200 Da) form the branched fatty acids (C14(3-*O*-C12:0)) at the N-2′ position of the non–reducing GlcN residue obtained from the precursor ion. The product ion at *m/z* 1035.6619 was assigned as the $[M_6\text{-(C14:0(3-OH))acid-H}]^-$ ion, which was created by the elimination of 3-hydroxy-myristics acid (C14:0(3-OH)) (-244 Da) located at the position O-3 of the reducing GlcN end. The product ion at *m/z* 994.6175 was assigned as $[M_6\text{-(C14:0(3-OH))acid-}(C_3H_6)\text{-H}]^-$ ion, which was created by the elimination of 3-hydroxy-myristic acid (C14:0(3-OH)) (-244 Da) located at the position O-3, and n-(C_3H_6) as a part of the fatty acid located in N-2′(-41 Da). High-energy CID-TOF/TOF-MS/MS of the anion at *m/z* 892.5961, which was assigned previously as $[\text{C-H}]^-$, gave the product ions at *m/z* 666.3922 and *m/z* 648.3897. The product ion at *m/z* 666.3922 was assigned as the $[\text{C-(C14:0(3-OH))ketene-H}]^-$ ion, and it was formed by the elimination of the 3-hydroxy-myristic ketene (C14:0(3-OH)) (-226 Da) from the O-3 of the precursor ion. The product ion at *m/z* 648.3931 was assigned as the $[\text{C-(C14:0(3-OH))acid-H}]^-$ ion , and it was formed by the elimination of the 3-hydroxy-myristic acid (C14:0(3-OH)) (-244 Da) from the O-3 of the precursor ion (Kussak *et al.*, 2002, El-Aneed *et al*., 2006, Shaffer *et al*., 2007, Lukasiewicz *et al*., 2010, and Brodbelt *et al*., 2014).

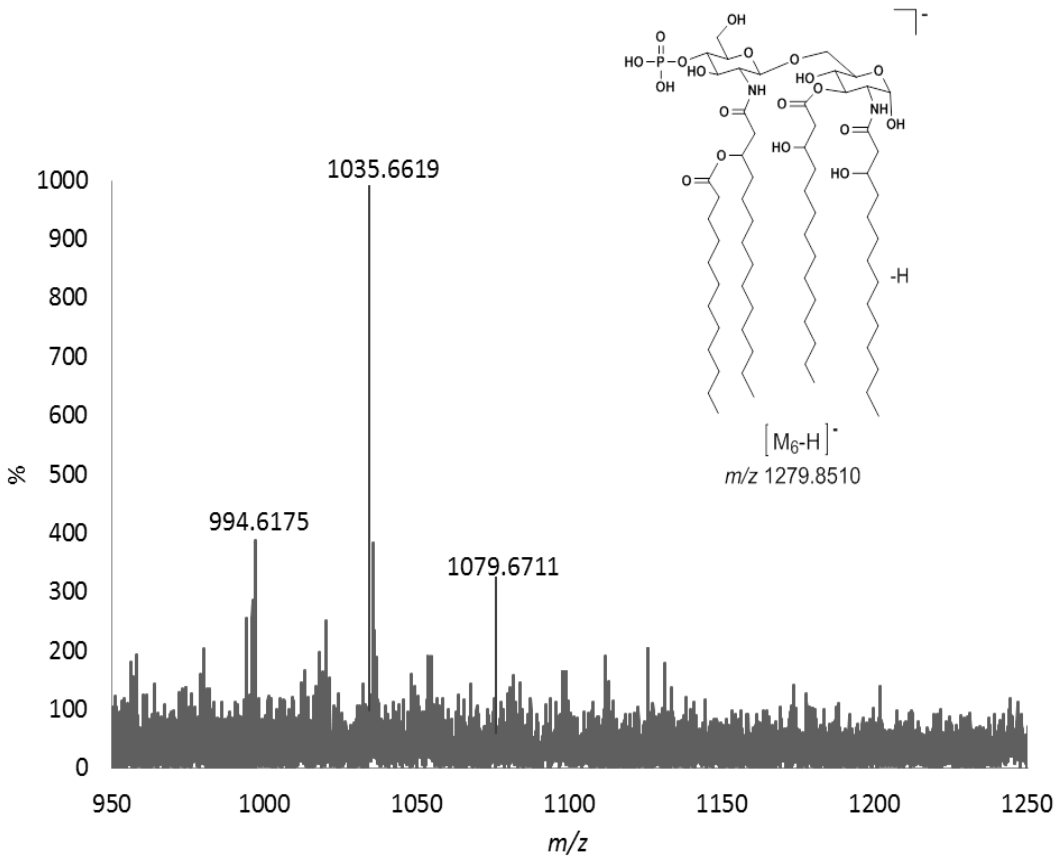

Figure 5.3.7: High-energy CID-TOF/TOF-MS/MS of the precursor ion $[M_6\text{-}H]^-$ ion at *m/z* 1279.8510.

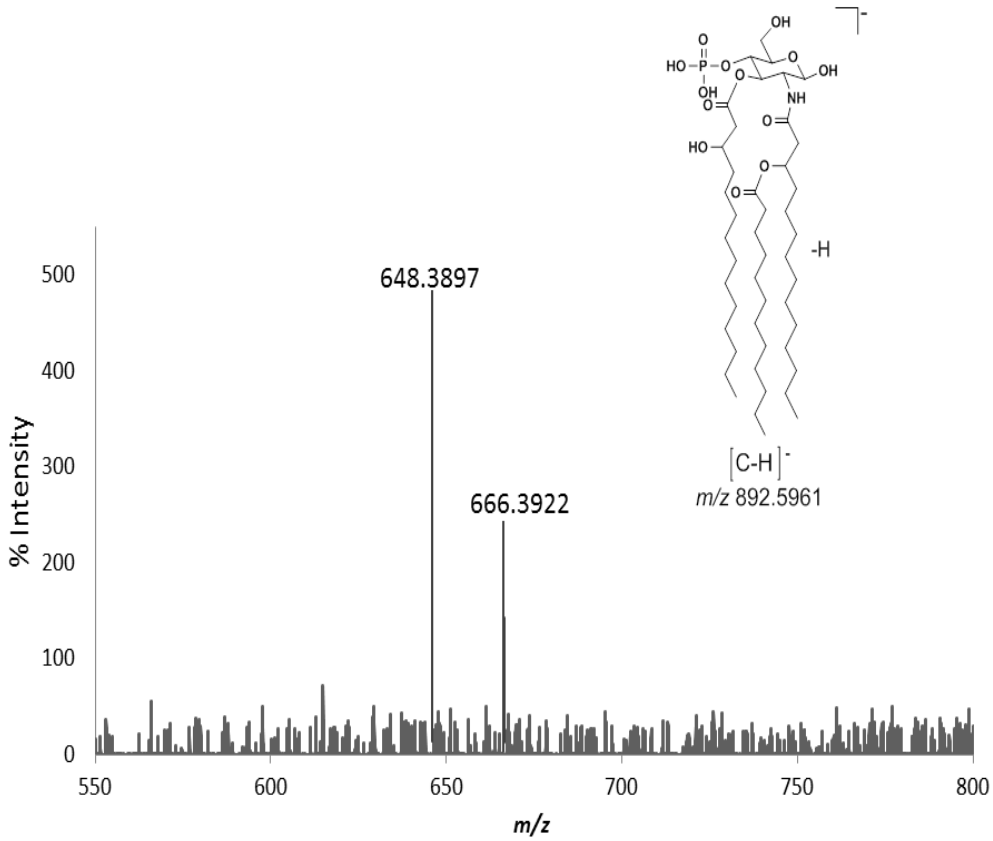

Figure 5.3.8: High-energy CID-TOF/TOF-MS/MS of the precursor ion $[C\text{-}H]^-$ ion at *m/z* 892.5961.

5.4.2. Comparison between low-energy CID-QqQ-MS/MS and high-energy CID-TOF/TOF-MS/MS

The comparison between the MALDI-CID-TOF/TOF-MS/MS analysis and the ESI-CID-QqQ-MS/MS, indicated that the number of distinctive product ions obatined with MALDI-CID-TOF/TOF analysis decreased. This was attributed to the same reasons given in chapeter 3 and 4 (section 3.4.2 and 4.4.2). We have noticed that all the of the product ions which obtained from MALDI-CID-TOF/TOF just like SORI-CID-MS/MS were produced by the primary fatty acid fragmentation not the branched, most of the time the elimination occur at O-3 and O-3´ position (Schemes 5.1.2-5.1.8 and Tables 5.1.2 - 5.1.8).

5.5. Summary

The LPS extracted from the Gram-negative bacteria *A. salmonicida* SJ-113a exhibited a series of incomplete biosynthesized lipid A_{1-6}. The series of structures of lipid A_1 to A_6 and the fragment ions, observed in ESI-QqQ-MS, ESI-FTICR-MS, and MALDI-TOF/TOF-MS spectra obtained from LPS of the *A. salmonicida* SJ-113a (phage resistant) were never reported before. Accordingly, we have assigned these fragment ions as the series of $[M_n\text{-}H]^-$ deprotonated molecules, represented as the following: $LipA_1$ *m/z* 1768.20, $LipA_2$ *m/z* 1688.17, $LipA_3$ *m/z* 1586.12, $LipA_4$ *m/z* 1506.09, $LipA_5$ *m/z* 1359.79, $LipA_6$ *m/z* 1279.89, and *m/z* 892.55.

The deprotonated molecules obtained from this heterogeneous mixture of lipid A_n were investigated by tandem mass spectrometry using low-energy collision SORI-CID-MS/MS (tandem in time) and CID-MS/MS (tandem in space) instruments. Likewise, The MALDI-CID-TOF/TOF-MS/MS, CID-QqQ, and SORI-FTICR-MS/MS fragmentation studies of the different lipid A_{1-6} have shown the presence of diagnostic and unique C-C heterolytic fragmentation of the fatty acid chains.

We have noticed that the SORI-MS/MS spectra of the various precursor deprotonated molecules were much simpler than those of the acquired CID-MS/MS with the MALDI-TOF/TOF and QqQ-instrument.

The combined MS/MS studies indicate that all the proposed structures of the lipid A_1 to A_6 contain two phosphate groups at the position O-1 and O-4′. They were built by a β-D-Glc*p*N-(1→6)-α-D-Glc*p*N disaccharide blueprint, which is substituted with (C14:0(3-

OH)) at the N-2 and O-3 and contain different substitution permutations with (C14:0(3-*O*-12:0)) at the N-2´, and the O-3 positions (Scheme 5.1.1).

The presence of this mixture series of lipid A_n isolated from SJ-113a in the ESI- and MALDI-MS spectra is good indicator to incomplete biosynthesis of lipid A. Also, the presence of the monosaccharide backbone was reported in all of them, such as the deprotonated molecules at *m/z* 892.

In conclusion, the interaction between the bacteria and the bacteriophages lead to some mutation which leads to incomplete lipid A biosynthesis, due to the disruption in core biosynthesis process occurring at different stages. Such structural aberrations could affect bacteriophage adsorption which could increases the resistance of the bacteria to the bacteriophages.

Chapter 6

Summary and Conclusions

Biological mass spectrometry advancements have made significant strides over the past few decades, driven by its capacity to help with identification of novel complex biological compounds (Raetz *et al.*, 2002, and li *et al.*, 2006). Bacteria are well known to causes many serious human and animal diseases. Lipid A obtained from the LPS of such bacteria, and is considered the most toxic part within the LPS biomolecule.

The biosynthesis of LPS is completely altered by infection with bacteriophages which are viruses that infect and duplicate within the host bacteria (Viertel *et al*., 2014). Lately, the physical interactions between tailed phages and Gram-negative bacterial pathogens have been used as models in the development of a phage therapeutic strategy for treatment of bacteria infections. For these reasons, the investigation of the effect of tailed bacteriophages was on the marine pathogen Gram-negative bacteria *Aeromonas Liquefaciens* SJ-19, *hydrophilla* SJ-55, and *Salmonicidia* SJ-113.

In these studies, the investigation was on the structures of lipid As extracted from different lipopolysaccharides (LPSs) of the *Vibrionacaceae* family. This investigation was specific to the molecular structures of the released lipid A portions of these LPSs, and the data presented here will help understanding the phages bio-mechanisms of action that govern the biosynthesis of cellular membrane of the bacteria. It is well known that LPS obtained from Gram-bacteria which are resistant to phage infections afford incomplete specific *O*-antigen and rough core oligosaccharides (Rakhuba *et al*., 2010, and Viertel *et*

al., 2014). No studies were ever undertaken to assess if the LPS biosynthesis deregulation by the phage affected the lipid A part of these LPSs. This structural investigation is an important task for the development of potential phage therapeutic strategy against marine bacterial infections.

The investegation started by recording the ESI- and MALDI-MS (- ion mode) on the lipid A obtained from the LPS of the Gram-negative bacteria *A. liquefactions* SJ-19a (phage resistant). The recorded MS exhibited a series of deprotonated lipid As molecules which were assigned as lipid A_n (where n=1-5). The presence of the series of deprotonated molecules were tentatively assigned as being produced by an incomplete biosynthesis of their LPS. The various MS analyses were conducted with ESI-QqQ-MS, ESI-FTICR-MS, and MALDI-TOF/TOF-MS hybrid instruments using the negative ion mode. Similar studies were also used to investigate the structure of lipid A_n mixture extracted from the LPS of the Gram-negative bacteria *A. hydrophilla* SJ-55a (phage resistant), which once more exhibited an incomplete biosynthesized lipid A_n (where n=1-8). Finally, by using the same methodology described before, we investigated the lipid A_n (where n=1-6) mixture extracted from the LPS of the Gram-negative bacteria *A. salmonicida* SJ-113a (phage resistant). As tentatively proposed before, this lipid A_n mixture exhibited a series of incomplete biosynthesized lipid A_{1-6}. The combined ESI- and MALDI-MS and MS/MS techinques allowed us to propose tentative structures for the lipid A_n extracted from LPSs of *A. salmonicida* SJ-113a, *A. liquefactions* SJ-19a and *A. hydrophilla* SJ-55a. These studies can be summarized as the following:

The major deprotonated molecule obtained from $LipA_n$ mixture of the LPSs was assigned as $LipA_1$ as follows: *A. salmonicida* SJ-113a at *m/z* 1768.20 ($LipA_1$) and for the LPS of *A. hydrophilla* SJ-55a at *m/z* 1796.30 ($LipA_1$) containing two phosphate groups at the position O-1 and O-4′. This assignment was different for the $LipA_1$ obtained from the LPS of *A. liquefactions* SJ-19a which appeared at *m/z* 1716.30 which was shown to contain one phosphate group located at O-4´ position. All of the individual members of the Lipid A_n isolated from these different LPSs were built on a β-D-Glc*p*N-(1→6)-α-D-Glc*p*N disaccharide backbone.

The lipid A_n obtained from the LPS of *A. liquefactions* SJ-19a contains a β-D-Glc*p*N-(1→6)-α-D-Glc*p*N disaccharide which was substituted by (C14:0(3-OH)) at the N-2, N-2´, O-3 and O-3´ and contained different substitution permutations by (C14:0(3-*O*-12:0)) at the N-2´, and (C14:0(3-*O*-14:0)) at the O-3´ positions (Scheme 6.1.1).

Whereas, the lipid A_n obtained from the LPS of *A. hydrophilla* SJ-55a contains a β-D-Glc*p*N-(1→6)-α-D-Glc*p*N disaccharide substituted by (C14:0(3-OH)) at the N-2, O-3´ and O-3 position, and substituted by (C12:0(3-OH)) at N-2´ position. Also, these fatty acids contained substitution permutations by (C14:0(3-*O*-14:0)) at the N-2´ and O-3´ positions (Scheme 6.1.1).

Finally, the lipid A_n obtained from the LPS of *A. salmonicida* SJ-113a contains β-D-Glc*p*N-(1→6)-α-D-Glc*p*N disaccharide substituted by (C14:0(3-OH)) at the N-2, N-2´, O-3, and O-3´ and contained different substitution permutations by (C14:0(3-*O*-12:0)) at the N-2´, and O-3 positions (Scheme 6.1.1).

Confirmation of all proposed molecular structures of these series of heterogeneous mixture of lipid A_n of *A. salmonicida* SJ-113a, A. *liquefactions* SJ-19a and *A. hydrophilla* SJ-55a were investigated using low-energy collision SORI-CID-MS/MS (tandem in time) and CID-MS/MS (tandem in space) tandem mass spectrometry. In general, it was observed that SORI-MS/MS spectra obtained with the FTICR-MS instrument gave simpler gas-phase fragmentation than those of the acquired the low-energy CID-MS/MS (QqQ) and with the high collision CID-MS/MS analyses obtained with the MALDI-TOF/TOF instruments. It should be noticed that we have obtained the most characeristic prodcut ions using CID-QqQ-MS/MS techniques, however, the ESI-FTICR-MS and MS/MS gave the most accuate results in term of resolution and sensitivities.

It important to mention that for the various mixtures of $LipA_n$ isolated from the LPSs SJ-19a, SJ-55a, and SJ-113a (lipid A_{1-5}, lipid A_{1-8}, and lipid A_{1-6}), we noticed that their MS contained some deprotonated molecules sharing the same exact molecular weights. These identical masses deprotonated molecules turned out to be diastereomers and isobars.

The origins of all the deprotonated molecules and fragment ions observed during single stage ESI- and MALDI-MS recording were also explored, to prove whether these were related or were unique individual structures. Indeed, MS/MS studies conducted on these series of deprotonated molecules confirmed that these ions were single unique diagnostic molecules that were not produced by further fragmentation from contiguous higher masses deprotonated molecules. For these reasons, each deprotonated molecule extracted form the LipAn mixtures were examined by performing their precursor ion scan

using only the ESI-QqQ-MS/MS instrument. Therefore, the obtained series of product ions excluded the possibility that they could be related to other examined precursor deprotonated molecules of the same lipid A_n mixture. These results were also confirmed by recording the parent ion scans of the different series of deprotonated molecules obtained from the various lipid A_n.

In general, we surmise that the fatty acid distributions of the primary fatty acids on the β-D-Glc*p*N-(1→6)-α-D-Glc*p*N disaccharide of this entire lipid A_n mixtures are different with respect to their length and to their acylation positions on the GlcN disaccharide.

In conclusion, we have shown that these series of gram negative bacteria, which were phage treated, exhibited an incomplete biosynthesized of the lipid A portion of the LPS, affording lipid A_n mixtures, that included various number of different acylation sites with either myristic acid and/or lauric acid on the main GLcN disaccharide backbone.

In addition, the phages treatment of these bacteria appeared to change the various phosphorylation degrees of these different lipids A_n mixtures. This far-reaching study showed that the various mass spectrometry instruments were used resourcefully to distinguish between the main lipid A_n components of these series of complex lipid A_n mixtures, and allowed us to locate the fatty acid and the phosphate groups on their proper positions on the D-GlcN disaccharide.

Finally, for comparison sake only, the following scheme 6.1.1 indicate the structures of the major deprotonated molecules obtained from the LPS of the bacteria SJ-19a, SJ-55a, and SJ-113a. It also indicates the differences in their fatty acid acylation patterns. In addition, table 6.1.1 shows the various diastereomeric and isobaric

deprotonated molecules measured on the three-different lipid A_n mixtures with the ESI-QqQ-MS hybrid instrument.

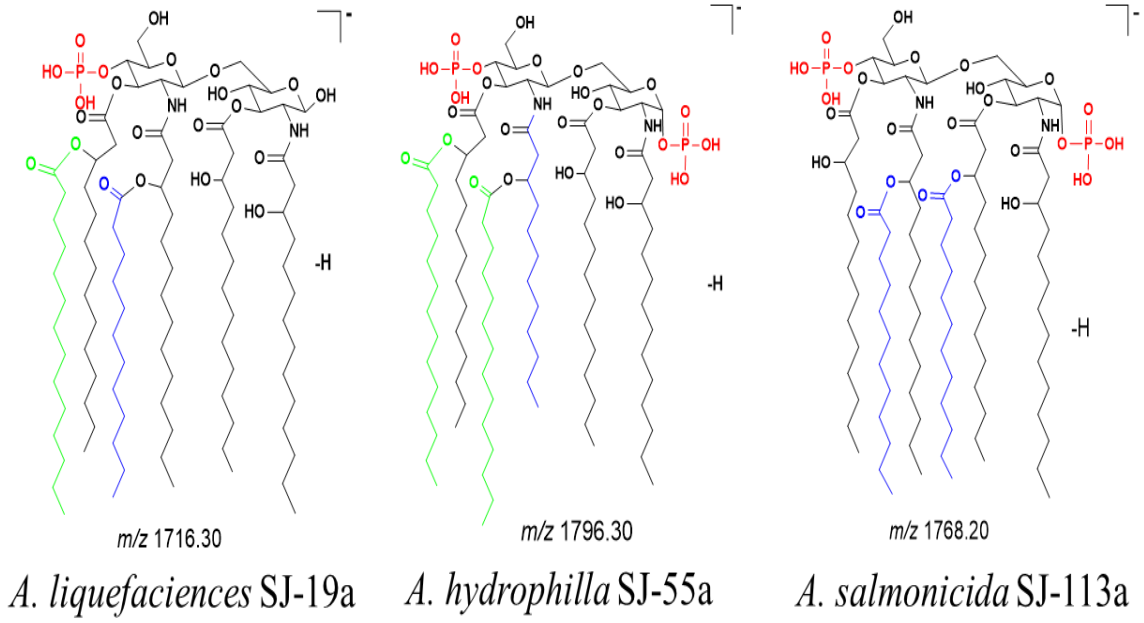

Scheme 6.1.1: Schematic representation of suggested structures of the highest masses for the deprotonated molecules of the lipid A_n mixture extracted from bacteria A. *liquefactions* SJ-19a, *A. hydrophilla* SJ-55a, and *A. salmonicida* SJ-113a.

Table 6.1.1: Assignments of the deprotonated molecules observed in ESI-QqQ-MS (- ion mode) of native mixture of lipid A_n extracted from the LPS of A. *liquefactions* SJ-19a, *A. hydrophilla* SJ-55a, and *A. salmonicida* SJ-113a.

	CID-QqQ-MS of *A. liquefaciences* SJ-19a		CID-QqQ-MS of *A. hydrophilla* SJ-55a		CID-QqQ-MS of *A. salmonicida* SJ-113a	
Empirical formula	Product ion *m/z* Calculated; Observed (%)	δ ppm	Product ion *m/z* Calculated; Observed (%)	δ ppm	Product ion *m/z* Calculated; Observed (%)	δ ppm
$C_{94}H_{177}N_2O_{25}P_2$	-	-	1796.30; 1796.21 (18.2)	50.8	-	-
$C_{92}H_{174}N_2O_{25}P_2$	-	-	-	-	1768.20; 1768.18 (18.2)	11
$C_{94}H_{176}N_2O_{22}P$	1716.30; 1716.24 (27.5)	-10	1716.15; 1716.24 (27.5)	52.4	-	-
$C_{92}H_{172}N_2O_{21}P_2$	1688.19; 1688.21 (30.7)	-11.8	1688.26; 1688.21 (20.3)	29.6	1688.26; 1688.21 (20.3)	-23
$C_{80}H_{152}N_2O_{24}P_2$	-	-	-	-	1586.12; 1586.02 (18)	56
$C_{80}H_{150}N_2O_{21}P$	1506.10; 1506.05 (93.5)	-33.1	1506.12; 1506.05 (35.2)	53.1	1506.09; 1506.05 (35.2)	-26.5
$C_{66}H_{125}N_2O_{22}P_2$	-	-	1359.75; 1359.82 (30.9)	51.4	1359.79; 1359.82 (30.9)	-44
$C_{66}H_{124}N_2O_{19}P$	1279.73; 1279.85 (97.3)	-15.6	1279.87; 1279.85 (41)	51.6	1279.89; 1279.85 (41)	31.2
$C_{52}H_{96}N_2O_{18}P_2$	1097.63; 1097.68 (36.4)	45.5	1097.64; 1097.69 (28)	45	-	-
$C_{52}H_{99}N_2O_{17}P$	-	-	1053.69; 1053.66 (29.4)	28.4	-	-
$C_{46}H_{87}NO_{13}P$	892.56; 892.59 (46.8)	-33.6	892.55; 892.59 (55.8)	44.5	892.55; 892.59 (55.8)	-56
$C_{34}H_{65}NO_{12}P$	-	-	710.40; 710.42 (54.7)-	28.1	-	-
$C_{32}H_{61}NO_{11}P$	666.06; 666.43 (100)	55	666.37; 666.39 (54.7)	-30	-	-

References:

- Abeyrathne, P. D.; Daniels, C.; Poon, K. K.; Matewish, M. J.; and Lam, J. S. Functional characterization of WaaL, a ligase associated with linking *O*-antigen polysaccharide to the core of Pseudomonas aeruginosa lipopolysaccharide. *J. Bacteriol.* **2005**, *187*:3002-12.
- Alberici, R.; Simas, R.; Sanvido, G.; Romão, W.; Benassi, M.; Cunha, I.; Eberlin, M. Ambient mass spectrometry: bringing MS into the "real world". *Ana. Bio. Chem*. **2010**, *398*(1), 265-294.
- Almostafa, M.; Allehyane, B.; Egli, S.; Bottaro., C; Fridgen, T.; and Banoub, J. Tandem mass spectrometry determination of the putative structure of a heterogeneous mixture of Lipid A_s isolated from the lipopolysaccharide of the Gram-negative bacteria Aeromonas liquefaciens SJ-19a. *Rapid Commun. Mass Spe*ctrom. **2016**, *30*: 1043-1058.
- Aoki, T.; Egusa, S.; Kimura, T.; and Watanabe, T. Detection of resistance factors in fish pathogen *Aeromonas liquefaciens. J. Gen. Microbiol.* **1971**, *65*: 343.
- Arpino, P. Combined liquid chromatography mass spectrometry. Part I. Coupling by means of a moving belt interface. *Mass Spectrom. Rev*. **1989**, *8*: 35-55.
- Aston, F.W. *Mass Spectra and Isotopes*, 2nd edn, Edward Arnold, London. **1942**.
- Austin, B. Taxonomy of bacterial fish pathogens. *Veterinary Research*. **2011**, 42: 20.
- Azargun, M.; and Fridgen, T. Guanine tetrads: an IRMPD spectroscopy, energy resolved SORI-CID, and computational study of M(9-ethylguanine)$^{4+}$ (M = Li, Na, K, Rb, Cs) in the gas phase. *Phys. Chem. Chem. Phys*. **2015**, *17*: 25778-25785.
- Banoub, J. H.; Choy, Y. M.; Michon, F.; and Shaw, D. H. Structural investigations on the core oligosaccharide of *Aeromonas hydrophila* (chemotype II) lipopolysaccharide. *Carbohydrate Res*. **1983**. *114*: 267-276.
- Banoub, J.; Aneed, A.; Cohen, A.; and Joly, N. Structural investigation of bacterial lipopolysaccharides by mass spectrometry and tandem mass spectrometry. *Mass Spectrom. Rev*. **2010**, *29*: 606-650.

- Barber, M.; Bordoli, R. S.; Garner, G. V.; Gordon, D. B.; Sedgwick, R. D.; Tetler, L. W.; and Tyler, A. N. Fast-atom-bombardment mass spectra of enkephalins. *Biochem. J.* **1981**, *197*: 401-404.
- Beavis, R. C.; Chait, B. T.; and Fales, H. M. Cinnamic acid derivatives as matrices for ultraviolet laser desorption mass spectrometry of proteins. *Rapid Communications in Mass Spectrometry*.**1989**, *3*(12): 432-435.
- Beavis, R. C.; Chaudhary, T.; and Chait, B. T. α-Cyano-4-hydroxycinnamic acid as a matrix for matrix assisted laser desorption mass spectrometry. *Organic Mass Spectrometry*, **1992**, *27*(2): 156-158.
- Brisson, E.; Dacanay, J.; Greenwell, A.; Brown, M.; Li, L.; and Altman, E. Structural studies of the capsular polysaccharide and lipopolysaccharide *O*-antigen of *Aeromonas salmonicida* strain 80204-1 produced under in *vitro* and in *vivo* growth conditions. *Eur. J. Biochem*. **2004**, *271*: 4507-4516.
- Brodbelt, J. S. Photodissociation mass spectrometry: new tools for characterization of biological molecules**.** *Chem. Soc. Rev***. 2014,** *43***:** 2757-2783**.**
- Burgoyne, T.W.; and Hieftje, G.M. An introduction to ion optics for the mass spectrograph. *Mass Spectrom. Rev*. **1996**. *15*(4), 241-59.
- Burlingame, P. H.; Boyd, R. K.; and Gaskell, S. J. Mass spectrometry. *Anal.Chem*. **1996**, *68*: 599R.
- Busch, K.L.; Glish, G.L.; and McLuckey, S. A. Mass spectrometry/mass spectrometry: techniques and applications of tandem mass spectrometry, VCH, New York. **1988.**
- Carillo, S., Pieretti, G., Lindner, B., Romano, I., Nicolaus, B., Lanzetta, R., Corsaro, M. M. The Lipid A from the Haloalkaliphilic Bacterium *Salinivibrio sharmensis* Strain BAG. *Marine Drugs*, **2013**, *11*(1): 184-193.
- Carillo, S.; Pieretti, G.; Lindner, B.; Romano, I.; Nicolaus, B.; Lanzetta, R.; Parrilli, M.; Corsaro, M. The lipid A form the *haloalkaliphilic* bacterium *Salinivibrio sharmensis* strain BAGT. *Mar Drugs*. **2013**, 11: 184-193.

- Caroff, M.; Karibian, D. Structure of bacterial lipopolysaccharides. *Carbohydr Res.* **2003**, *338*(23):2431-2447.
- Carroll, D. I.; Dzidic, I.; Stillwell, R. N.; Horning, M. G.; Horning, E. C. Subpicogram detection system for gas phase analysis based upon atmospheric pressure ionization (API) mass spectrometry. *Anal. Chem*. **1974**, *46*(6): 706-710.
- Chanishvili, N. Phage therapy-history from Twort and d'Herelle through Soviet experience to current approaches. *Adv. Virus Res*. **2012**, *83*: 3-40.
- Chart, H.; Shaw, D. H.; Ishiguro, E.; and Trust, T. Structural and immunochemical homogeneity of *Aeromonas salmonicida* Lipopolysaccharide. *J.Bacteriology*. **1984**, *158*: 16-22.
- Chen, F.; Gülbakan, B.; Weidmann, S.; Fagerer, S. R.; Ibáñez, A.; and Zenobi, R. Applying mass spectrometry to study non-covalent biomolecule complexes. *Mass Spectrom. Rev*. **2016**, *35*: 48-70.

  Chen, H., A. Venter, and R.G. Cooks, Extractive electrospray ionization for direct analysis of undiluted urine, milk and other complex mixtures without sample preparation. *Chem Commun*, 2006,19: 2042-2044.

- Chen, H.; Talaty, N. N.; Takats, Z.; Cooks, R. G. Desorption electrospray ionization mass spectrometry for high-throughput analysis of pharmaceutical samples in the ambient environment. *Anal. Chem*. **2005**, *77*(21): 6915-6927.
- Chernetsova, E. S.; Morlock, G. E. Ambient desorption ionization mass spectrometry (DART, DESI) and its bioanalytical applications. *Bioanal. Rev*, **2011**, *3*(1): 1-9.
- Clauser, K. R.; Baker, P. R.; Burlingame, A. L. The role of accurate mass measurement (+ /– 10 ppm) in protein identification strategies employing MS or MS/MS and database searching. *Anal Chem*. **1999**, *71*: 2871-2882.
- Cody, R. B.; Freiser, B. S. *Int. J. Mass Spectrom*. Ion Phys. **1982**, 41: 199.
- Cody, R.B.; Laramée. J. A.; Durst, H. D. Versatile new ion source for the analysis of materials in open air under ambient conditions. *Anal. Chem*. **2005**, *77*(8): 2297-2302.

- Colorado, A.; Shen, J. X.; Vartanian, V. H.; Brodbelt, J. Use of infrared multiphoton photodissociation with SWIFT for electrospray ionization and laser desorption applications in a quadrupole ion trap mass spectrometer. *Anal. Chem*. **1996**, *68*: 4033.
- Comisarow, M.B.; and Marshall, A.G. Fourier transform ion cyclotron resonance spectroscopy. *Chem. Phys. Lett*.**1974**, 25: 282.
- Cooks, R. G.; Ast, T.; Pradeep, T.; and Wysocki, V. H. Reactions of ions with organic surfaces**.** *Acc.Chem. Res.***1994**, 27: 321.
- Cooks, R. G.; Patrick, J. S.; Kotiaho, T.; and McLuckey, S. A. *Mass Spectrom. Rev*. **1994**, *13*: 287.
- Corsaro, M. M.; Piaz, F. D.; Lanzetta, R.; and Parrilli, M. Lipid A structure of Pseudoalteromonas haloplanktis TAC 125: use of electrospray ionization tandem mass spectrometry for the determination of fatty acid distribution. *J.Mass Spectrom*. **2002**, *37*: 48, 1-8.
- Corsaro, M. M.; Piaz, F. D.; Lanzetta, R.; Naldi, T.; and Parrilli, M. Structure of Lipid A from Pseudomonas corrugate by electrospray ionization quadrupole time-off light tandem mass spectrometry. *Rapid Commun Mass Spectrom*. **2004b**, *18*: 853-8.
- Cotter, R. J. Time-of-flight mass spectrometry for the structural analysis of biological molecules. *Anal Chem*. **1992**, *64*(21): 1027A-1039A.
- Cotter. R. The new time-of-flight mass spectrometry. *Anal. Chem*. **1999**, 71, 445A.
- Dass, C. Dimerization of the ketene cation radical in the gas phase. *Rapid Commun. Mass Spe*ctrom. **1993**, *7*(1): 95-98.
- Declercq, A.; Haesebrouck, F.; Van den Broeck, W.; Bossier, P.; and Decostere, A. Columnaris disease in fish: a review with emphasis on bacterium-host interactions. *Veterinary Research*. **2013**, *44*(1): 27.
- Dempster, A. J. A new method of positive ray analysis. *Physical Review*, **1918**, *11*(4): 316-325.
- Dietmar, G.; Schmid, P. G.; Holger, B.; Gu¨ nther, J. FTICR-mass spectrometry for high-resolution analysis in combinatorial chemistry. *Biotechnol. Bioeng*, **2000**, 71: 149-161.

- Downard, K. M. Francis William Aston: the man behind the mass spectrograph. *European Journal of Mass Spectrometry*. **2007**, *13*(3): 177-190.
- Downard, K. Mass spectrometry: a foundation course. TJ International Ltd, Cornwall. **2004**.
- Elaneed, A.; and Banoub, J. Elucidation of the molecular structure of lipid A isolated from both a rough mutant and a wild strain of *Aeromonas salmonicida* lipopolysaccharides using electrospray ionization quadrupole time-of-flight tandem mass spectrometry. *Rapid Commun*. *Mass Spectrom*. **2005**, *19*:1683-1695.
- Es-Safi, N. E.; Kerhoas. L.; and Ducrot, P. H. Application of positive and negative electrospray ionization, collision-induced dissociation and tandem mass spectrometry to a study of the fragmentation of 6-hydroxyluteolin 7-*O*-glucoside and 7-*O*-glucosyl-(l -3)-glucoside. *Rapid Commun Mass Spectrom*. **2005**, *19*: 2734-42.
- Fenn, J. B.; Mann, M.; Meng, C. K.; Wong, S. F.; and Whitehouse, C. M. Electrospray ionization for mass spectrometry of large biomolecules. *Science.* **1989**, *246*(4926): 64-71.
- Fenn, J. Electrospray wings for molecular elephants (Nobel lecture). *Angew Chem, Int*. **2003**, *42*: 3871-3894.
- Gaskell, S. J. Electrospray: principles and practice. *J. Mass Spectrom.* **1997**, *32*: 677- 688.
- Gauthier, J. W.; Trautman, T. R.; and Jacobson, D. B. Sustained off-resonance irradiation for collision-activated dissociation involving Fourier transform mass spectrometry. Collision-activated dissociation technique that emulates infrared multiphoton dissociation. *Anal. Chim. Acta.* **1991**, 246: 211-225.
- Golkar, Z.; and Bagasra, O. Donald Gene Pace. Bacteriophage therapy: a potential solution for the antibiotic resistance crisis. *J Infect Dev Ctries.* **2014**, *8*(2):129-136.
- Griffiths, J. A Brief history of mass spectrometry. *Anal. Chem.* **2008**, *80*: 5678-5683.
- Hakansson, K.; Chambers, M. J.; Quinn, J. P.; McFarland, M. A.; Hendrickson, C. L; and Marshall, A. G. Combined electron capture multiphoton dissociation of multistep MS/MS in a Fourier-transform ion cyclotron resonance mass spectrometer, *Anal.Chem*. **2003**, *75*: 3256-3262.

- Harper, J.D.; Charipar, N.A.; Mulligan, C.C.; Zhang, R. X .; Cooks, G.; Ouyang Z.. Low-temperature plasma probe for ambient desorption ionization. *Anal Chem*. **2008**, *80*(23): 9097–9104.
- Harrison, A. G. Energy-resolved mass spectrometry: a comparison of quadrupole cell and cone-voltage collision-induced dissociation. *Mass Spectrom.* **1999**, *13*:1663-1670.
- Hart-Smith, Gene. A review of electron-capture and electron-transfer dissociation tandem mass spectrometry in polymer chemistry. *Analytica Chimica Acta*. *Polymer Mass Spectrometry*. **2004**. 808: 44-55.
- Hendrickson, C. L.; and Emmett, R. M. Electrospray ionization fourier transform ion cyclotron resonance mass spectrometry. *Phys.Chem*.**1999**, *50*: 517-536.
- Hilton, G. R.; and Benesch, J. L. Two decades of studying non-covalent biomolecular assemblies by means of electrospray ionization mass spectrometry. *J. R. Soc. Interface*. **2012**, *9*: 80-816.
- Hittle, L.; Jones, J. W.; Hajjar, A.; Ernst, R.K.; Prestond, *A. Bordetella parapertussis PagP* mediates the addition of two palmitates to the lipopolysaccharide lipid A. *J. Bacteriol*. **2015**, *197*:572-580.
- Hoai, T. D.; and Yoshida, T. Induction and characterization of a lysogenic bacteriophage of Lactococcus garvieae isolated from marine fish species. *J. Fish Diseases*.**2016**, *39*:799-808.
- Hoffmann, E.; and Stroobant, V. Mass spectrometry: Principles and applications. Chichester, West Sussex, England: J. Wiley. **2007**.
- Janda, J. M.; and Abbott, S. L. The Genus Aeromonas: Taxonomy, Pathogenicity, and Infection. *Clin. Microbiol. Rev*. **2010**, *23*: 35.
- Jennings, K. R. Collision-induced decompositions of aromatic molecular ions. *Int. J. Mass Spectrom. Ion Phys.* **1968**, *1*: 227.

- John, P.; Needham, B.; Henderson, H.; Nowicki, E.; Trent, E.; and Brodbelt, S. 193 nm ultraviolet photodissociation mass spectrometry for the structural elucidation of lipid A compounds in complex mixtures. *Anal. Chem*. **2014,** 86: 2138-2145.
- Junot, C.; Madalinski, G.; Tabet, G. C.; and Ezan, E. Fourier transform mass spectrometry for metabolome analysis. *Analyst*, **2010**, *135*: 2203-2219.
- Karas, M.; Bahr, U.; Ingendoh, A.; Nordhoff, E.; Stahl, B.; Strupat, K.; and Hillenkamp, F. Principles and applications of matrix-assisted UV-laser desorption/ionization mass spectrometry. *Analytica Chimica Acta*. **1990**, *241*(2):175-185.
- Kebarle, P. A brief overview of the present status of the mechanisms involved in electrospray mass spectrometry. *J. Mass Spectrom*. **2000**, *35*(7): 804-817.
- Kebarle, P.; Verkerk, U. H. Electrospray: From ions in solutions to ions in the gas phase, what we know now. *Mass Spectrom. Rev*. **2009**, *28*: 898-917.
- Kilár, A.; Dörnyei, Á.; and Kocsis, B. Structural characterization of bacterial lipopolysaccharides with mass spectrometry and on- and off-line separation techniques. *Mass Spectrom. Rev*. **2013**, *32*: 90-117.
- Kitson, F. G.; Larsen, B. S.; and McEwen, C. N. Gas chromatography and mass spectrometry: a practical guide. *Academic Press*. San Diego, **1996**. pp. 381.
- Klein, G.; Lindner, B.; Brabetz, W.; Brade, H.; and Raina, S. Escherichia coli K-12 suppressor-free mutants lacking early glycosyltransferases and late acyltransferases: minimal lipopolysaccharide structure and induction of envelope stress response. *J Biol Chem*. **2009**, *284*:15369-89.
- Kondakova, A. N.; Vinogradov, E. V.; Knirel, Y. A.; and Lindner, B. Application of electrospray ionization with Fourier transform ion cyclotron resonance mass spectrometry for structural screening of core oligosaccharides from lipopolysaccharides of the bacteria Proteus. *Rapid Commun Mass Spectrom*. **2005**, *19*: 2343-9.
- Konermann, L.; McAllister, R. G.; and Metwally, H. Molecular dynamics simulations of the electrospray process: formation of NaCl clusters via the charged residue mechanism. *J. Phys. Chem. B.* **2014**, *118*: 12025-12033.

- Kussak, A.; Weintraub, A. Quadrupole ion-trap mass spectrometry to locate fatty acids on lipid A form Gram-negative bacteria. *Anal. Biochem.* **2002**, 1, *307*(1):131-7.
- Laskin, J.; and Futrell, J. H. Collisional activation of peptide ions in FT-ICR mass spectrometry. *Mass Spectrom. Rev*. **2003**, *22*: 158-181.
- Li, R.; Zhou, Y.; Wu, Z.; and Ding, L. ESI-QqTOF-MS/MS and APCI-IT-MS/MS analysis of steroid saponins from the rhizomes of Dioscorea panthaica. *J Mass Spectrom.* **2006**. *41*:1-22.
- Lin, S-Y.; Hsu, W. H.; Lin, C. C.; Chen, C. J. Mass spectrometry-based proteomics in Chest Medicine, Gerontology, and Nephrology: subgroups omics for personalized medicine. *BioMedicine*. **2014,** *4*(4):25.
- Liu, Q.; Li, Y.; Zhao, X.; Yang, X.; Liu, Q.; and Kong, Q. Construction of *Escherichia coli* mutant with decreased endotoxic activity by modifying lipid A structure. Molinaro A, ed. *Marine Drugs*. **2015**, *13*(6): 3388-3406.
- Luffer, D. R.; Schram, K. H. Electron ionization mass spectrometry of synthetic C60. *Rapid Communications in Mass Spectrometry*. **1990**. *4*(12): 552–556
- Lukasiewicz, J.; Niedziela, T.; Jachymek, W.; Kenne, L.; and Lugowski, C. Structure of the lipid A-inner core region and biological activity of Plesiomonas shigelloides O54 (strain CNCTC 113/92) lipopolysaccharide. *Glycobiology*. **2006**, *16*(6): 538-550.
- Makarov, A. Electrostatic axially harmonic orbital trapping: a high performance technique of mass analysis. *Anal. Chem.* **2000**, *72*: 1156-62.
- Makarov. A. Electrostatic axially harmonic orbital trapping: A high-performance technique of mass analysis. *Analy. Chem*. **2000**, *72*(6): 1156-62.
- Mamyrin, B. A.; Karataev, V. I.; Schmikk, D. V.; and Zagulin, V. A. The mass-reflectron, a new nonmagnetic time-of-flight mass spectrometer with high resolution. *Sov. Phys. JETP*, **1973**, *37*, 4.
- March, R. E.; Todd, J. F. J (eds). Practical aspects of ion trap mass spectrometry, vols 1, 2 and 3. Eds, CRC Press: Boca Raton, FL, **1995**.

- March, R. E; and Hughes., R. J. Quadrupole storage mass spectrometry. John Wiley & Sons, Inc, New York. **1989**.
- March, R.E. An introduction to quadrupole ion trap mass spectrometry. *J. Mass Spectro*. 1997. 32, 351- 369.
- March, R.E.; and Hughes, R.J., Quadrupole storage mass spectrometry, Wiley, New York, 1989.
- Marshall, A. G. Fourier transform ion cyclotron resonance mass spectrometry. *Acc.Chem. Res.* **1985**, *18*: 316-322.
- Marshall, A. G.; and Hendrickson, C. L. Fourier transform ion cyclotron resonance detection: Principles and experimental configurations. *Int. J. Mass Spectrom*. **2002**, *215*: 59-75.
- Marshall, A. G.; Hendrickson, C. L.; and Jackson, G. S. Fourier transform ion cyclotron resonance mass spectrometry: A primer. *Mass Spectrom. Rev***. 1998**, *17*: 1-35.
- Martin, R.L.; Paine, P. J.; Barker, S. J.; Blanksby.S. Ambient ionisation mass spectrometry for the characterisation of polymers and polymer additives: A review. *Anal. Chem. Acta*. **2014**, 808, 15: 70-82.
- Matsuura, M. Structural modifications of bacterial lipopolysaccharide that facilitate Gram-negative bacteria evasion of host innate immunity. *Frontiers in Immunology*. **2013**, *4*:109.
- McLafferty, F. W. Mass Spectrometry in Chemical Research and Production, *Appl. Spectrosc*. **1957**, *11*, 148.
- McLafferty, F. W. Tandem mass spectrometry. *Science*. **1981.** *214*(4518): 280-7.
- McLafferty, F. W.; and Bryce, T. A. Metastable Ion Characteristics: characterization of isomeric molecules. *Chem. Commun*. **1967**: 12-15.
- McLafferty, F. W.; Todd, P. J.; McGilvery, D. C.; and Baldwin, M. A. Collisional activation and metastable ion characteristics.73. High-resolution tandem mass spectrometer (MS/MS) of increased sensitivity and mass range. *J. Am. Chem. Soc*. **1980**, *102*: 3360.
- McLafferty, F.W. Tandem mass spectrometry, JohnWiley & Sons, Inc. NewYork. **1983**.

- McLuckey, S. A.; and Goeringer, D. E. Slow heating methods in tandem mass spectrometry. *J. Mass Spectrom*. **1997**, 32: 461- 474.
- McLuckey, S. A.; Goeringer, D. E.; and Glish, G. L. Collisional activation with random noise in ion trap mass spectrometry. *Anal.Chem*. **1992**, *64*: 1455-1460.
- Mehmood, S; Allison, T.; Robinson. C. Mass spectrometry of protein complexes: from origins to applications. Annu Rev Phys Chem. 2015, 66: 453-474.
- Melvin, B.; Comisarow, A.; and Marshall, G. Fourier transforms ion cyclotron resonance spectroscopy. *Chemical Physics Letters*. **1974**. *25, 2*, 15: 282-283.
- Metwally, H.; McAllister, R.; Popa, V.; and Konermann, L. Mechanism of Protein Supercharging by Sulfolane and m-Nitrobenzyl Alcohol: Molecular Dynamics Simulations of the Electrospray Process. *Anal.Chem*. **2016**, *88*(10): 5345-5354.
- Michon, F.; Shaw, D. H.; and Banoub, J. Structure of the lipopolysaccharide core isolated from a human strain of *Aeromonas hydrophila. Eur. J. Biochem*. **1984**, *145*: 107.
- Mistou, M.; Sutcliffe, I.; and Van Sorge, N. Bacterial glycobiology: rhamnose-containing cell wall polysaccharides in Gram-positive bacteria. Bitter W, ed. *FEMS Microbiology Reviews*. **2016**, *40*(4): 464-479.
- Molinaro, A.; Holst, O.; Di Lorenzo, F.; Callaghan, M.; Nurisso, A.; D'Errico, G.; Zamyatina, A.; Peri, F.; Berisio, R.; Jerala, R.; Jiménez-Barbero, J.; Silipo. A.; and Martín-Santamaría, S. Chemistry of Lipid A: At the Heart of Innate Immunity. *Chem. Eur. J*. **2015**, *21*: 500-519. Whitfield., C; Trent., S. M. *Annu Rev Biochem*. **2014**, *83*: 99-128.
- Morris, H. R.; Panico, M.; Barber, M.; Bordoli, R. S.; Sedgwick, R. D.; Tyler, A. Fast atom bombardment: a new mass spectrometric method for peptide sequence analysis. *Biochem. Biophys. Res. Commun*. **1981**. *101*(2): 623-31.
- Munson, M. S.; Field, F. H. Chemical ionization mass spectrometry. I. general introduction. *J. Am.Chem.Soc.* **1966**, *88*: 2621-2630.
- Nikolaev, E. N.; Kostyukevich, Y. I.; and Vladimirov, G. N. Fourier transform ion cyclotron resonance (FT ICR) mass spectrometry: Theory and simulations. *Mass Spec Rev*. **2014**: 219-258.

- Paul, W.; Steinwedel, H.; and Einneues, E. Mass enspektrometer Ohne magnetfeld. *Zeitschrift für Naturforschung A.* **1953**, *8* (7): 448-450.
- Peltz, C.; Drahos, L.; Vékey, K. SORI excitation: collisional and radiative processes. *J. Am. Soc. Mass Spectrom*. **2007**, *18*: 2119-2126.
- Perera, M. N.; Abuladze, T.; Li, M.; Woolston, J.; and Sulakvelidze, A. Bacteriophage cocktail significantly reduces or eliminates Listeria monocytogenes contamination on lettuce, apples, cheese, smoked salmon and frozen foods. *Food Microbiology.* **2015**, *52*: 42-48.
- Pittenauer, E.; and Allmaier, G. High-energy collision induced dissociation of biomolecules: MALDI-TOF/RTOF mass spectrometry in comparison to tandem sector mass spectrometry. *Comb.Chem. High Throughput Screen*. **2009**, *12*(2):137-55.
- Portolés, T.; Pitarch, E.; López, F. J.; Hernández, F.; and Niessen, W. M. Use of soft and hard ionization techniques for elucidation of unknown compounds by gas chromatography/time-of-flight mass spectrometry. *Rapid Commun Mass Spectrom.* **2011**, 15, *25*(11):1589-99.
- Price, W. D, Schnier, P. D; Williams, E. R. Tandem mass spectrometry of large biomolecule ions by blackbody infrared radiative dissociation. *Anal. Chem*. **1996**, *68*: 859.
- Putker, F.; Martine, P.; and Tommassen, B. J. Transport of lipopolysaccharide to the Gram-negative bacterial cell surface. *FEMS Microbiology Reviews.* **2015**, *39* (6): 985-1002.
- Raetz, C. R.; Reynolds, C. M.; Trent, M. S.; and Bishop, R. E. Lipid A modification systems in gram-negative bacteria. *Annual Review of Biochemistry*. **2007**. 76: 295-329.
- Raetz, C.R.; and Whitfield, C. Lipopolysaccharide endotoxins. *Annu Rev Biochem*. **2002**, *71*: 635-700.
- Rakhuba, D. V.; Kolomiets, E. I.; Dey, E.; Novik, G. I. Bacteriophage Receptors, Mechanisms of Phage Adsorption and Penetration into Host Cell. *Polish. J. Microbio,* **2010.** *59*(3):145-155.
- Rietschel, E.; and Westphal, O. Endotoxin in Health and Disease (Eds.: H. Brade, S. M. Opal, S. N. Vogel, D. C. Morrisson), Marcel Dekker, New York, **1999**,1-30.

- Robb, D.; Covey, T.; Bruins, A. Atmospheric pressure photoionization: an ionization method for liquid chromatography-mass spectrometry. *Anal Chem*. **2000**; *72*(15): 3653-3659.
- Schiller, J.; Süß, R.; Fuchs, B.; Müller, M.; Petković, M.; Zschörnig, O.; and Waschipky, H. The suitability of different DHB isomers as matrices for the MALDI-TOF MS analysis of phospholipids: which isomer for what purpose? *Europ Biophysics. J*. **2007**, *36*, 517: 4-5.
- Schmid, D. G.; Grosche, P.; Bandel, H.; and Jung, G. FTICR-mass spectrometry for high-resolution analysis in combinatorial chemistry. *Biotechnol. Bioeng*. **2000**, *71*: 149-161.
- Schmid, D. G.; Grosche, P.; Bandel, H.; and Jung, G. FTICR-mass spectrometry for high resolution analysis in combinatorial chemistry. *Biotechnol. Bioeng*. **2000**. *71*: 149–161.
- Schwartz, J. C.; Wade, A. P.; Enke, C. G.; and Cooks, R. G. Systematic delineation of scan modes in multidimensional mass spectrometry. *Anal.Chem*. **1990**, *62*: 1809-18.
- Schwechheimer, C.; and Kuehn, M.J. Outer-membrane vesicles from Gram-negative bacteria: biogenesis and functions. *Nat Rev Microbiol*. **2015**, *13*(10): 605-619.
- Scigelova, M.; Hornshaw, M.; Giannakopulos, A.; Makarov, A. Fourier Transform Mass Spectrometry. *Molecular & Cellular Proteomics: MCP*. **2011**,*10*(7): M111.009431.
- Shaffer, S.; Harvey, M.; Goodlett, D.; Ernst, R. Structural heterogeneity and environmentally regulated remodeling of *Francisella tularensis* subspecies *novicida* lipid A characterized by tandem mass spectrometry. *J. Am. Soc. Mass Spectrom*. **2007**, *18*(6): 1080-1092.
- Shang, W.; Xiao, Z.; Yu, Z.; Wei, N.; Zhao, G.; Wei, M.; Wang, X.; George, A and Tiehai, L. Chemical synthesis of outer core oligosaccharide of Escherichia coli R3 and immunological evaluation. *Organic & biomolecular chemistry*. **2015**, *13*(14):4321-4330.
- Shi, S.D.; Drader, J. J.; Hendrickson, C. L.; and Marshall, A.G. Fourier transform ion cyclotron resonance mass spectrometry in a high homogeneity 25 tesla resistive magnet. *J. Am. Soc. Mass Spectrom.* **1999**, ***10***: 265-8.

- Shukla, A. K.; and Futrell, J. H. Tandem mass spectrometry: Dissociation of ions by collisional activation. *J. Mass Spectrom*. **2000**, *35*: 1069-1090.
- Silhavy, J.T.; Kahne, D.; and Walker, S. The bacterial cell envelope. *Biol*. **2010**, *192*: 3713-3721.
- Sleno, L.; and Volmer, D. A. Ion activation methods for tandem mass spectrometry. *J. Mass Spectrom*. **2004**, *39*: 1091-1112.
- Sleno, L.; and Volmer, D. A. Ion activation methods for tandem mass spectrometry. *J. Mass Spectrom*. **2004**, *39*: 1091-1112.
- Smith, R. D.; Tang. K.; and Shen, Y. Ultra-sensitive and quantitative characterization of proteomes. *Mol. BioSyst*. **2006**, *2*: 221-230.
- Stafford, G. C.; Kelley, P. E.; Syka., J. E.; Reynolds, W. E.; and Todd, J. F. J. Determination of positions, velocities, and kinetic energies of resonantly excited ions in the quadrupole ion trap mass spectrometer by laser photodissociation. *Int. J. Mass Spectrom. Ion Processes*. **1984**, *60*: 85.
- Stafford, G. Ion trap mass spectrometry: A personal perspective. *J Am Soc Mass Spectrom*. **2002**, *13*: 589.
- Steel, S.; and Henchman, M. Understanding the quadrupole mass filter through computer simulation. *J. Chem. Ed*. **1998**, 75, 1049.
- Stephens, W. E. *A Pulsed Mass Spectrometer with Time Dispersion. Phys. Rev.* **1946**, 69: 691.
- Suda, Y.; Kim, Y. M.; Ogawa, T.; Yasui, N.; Hasegawa, Y.; Kashihara, W.; Shimoyama, T.; Aoyama, K.; Nagata, K.; Tamura, T.; and Kusumoto, S. Chemical structure and biological activity of a lipid A component from *Helicobacter pylori* strain 206. *J Endotoxin Res*. **2001**, *7*(2): 95-104.
- Sullam, K.; Essinger, S.; Lozupone, C. Connor, P. M.; Rosen, G.; Knight, R.; Kilham, S.; Russell, J. Environmental and ecological factors that shape the gut bacterial communities of fish: a meta-analysis. *Molecular ecology*. **2012**, *21*(13):3363-3378.

- Takáts, Z.; Wiseman, J. M.; Gologan, B.; and Cooks, R. G. Mass spectrometry sampling under ambient conditions with desorption electrospray ionization. *Science.* **2004**, *306* (5695): 471- 473.
- Tanaka, T.; Waki, H.; Ido, Y. Akita, S.; Yoshida, Y.; Yoshida, T.; and Matsuo, T. Protein and polymer analyses up to *m/z* 100 000 by laser ionization time-of-flight mass spectrometry. *Rapid Commun. Mass. Spectrom.* **1988**, *2*, 151.
- Thomson, J. J.; Bakerian lecture: Rays of positive electricity. *Proceedings of the Royal Society of London. Series A, Containing Papers of a Mathematical and Physical Character*. **1913**: 1-20.
- Verentchikov, A. N.; Ens, W.; and Standing, K. G. Reflecting time-of-flight mass spectrometer with an electrospray ion source and orthogonal extraction. *Analy. Chem*. **1994,** *66*(1): 126-133.
- Vickerman, C. J. Molecular imaging and depth profiling by mass spectrometry-SIMS, MALDI or DESI?. *Analyst*. **2011**,*136*: 2199-2217.
- Viertel, T. M.; Ritter, K.; and Horz, H. T. Viruses versus bacteria-novel approaches to phage therapy as a tool against multidrug-resistant pathogens. *J Antimicrob Chem*. **2014**, *69*(9): 2326-2336.
- Vukelića, Z.; Zamfira, A.; Bindilaa, L.; Froescha, M.; Peter-Katalinića, J.; Usukib, S.; Yub, R.; Peltz, C.; Drahos, L.; and Vékey, K. SORI excitation: collisional and radiative processes. *J. Am. Soc.Mass Spectrom*. **2007**, *18*: 2119-2126.
- Wang, W.; Quinn, P. J.; and Yan, A. Kdo2-lipid A: structural diversity and impact on immunopharmacology. *Biol. Rev*. **2015**, *90*, 408.
- Wei, H.; and Virol, S. Bacteriophages, revitalized after 100 years in the shadow of antibiotics. *Virologica Sinica.* **2015**, *30*: 1.
- Wells, J. M.; McLuckey, S. A. Collision-induced dissociation (CID) of peptides and proteins. *Meth. Enzymol*. 2005, 402: 148-85.
- Wieboldt, R.; Campbell, D.; Henion, J. LC/MS/MS Quantitation of Orlistat in Human Plasma with an ion Trap and a triple Quadrupole Spectrometer: A Comparative Study. 45th

ed.; ASMS Conference on Mass Spectrometry and Allied Topics, palm Springs, CA, **1997**: 1-5.

- Williams, A. H.; and Raetz, C.R. Structural basis for the acyl chain selectivity and mechanism of UDP-N-acetylglucosamine acyltransferase. *Proc Natl Acad Sci USA*. **2007**, *104*: 13543-50.
- Wysocki, V. H.; Ding, J. M.; and Jones, J. L. Surface-induced dissociation in tandem quadrupole mass spectrometers: A comparison of three designs. *J. Am. Soc. Mass Spectrom*. **1992**, *3*: 27-32.
- Yang, Q.; Wang, H.; Maas, J. D.; Chappell, W. J.; Manicke, N. E.; Cooks, R. G.; and Ouyang, Z. Paper spray ionization devices for direct, biomedical analysis using mass spectrometry. *Inter. J. Mass Spectrom*. **2011,** *312*, 201-207.
- Yost, R. A.; and Enke, C. G. Selected ion fragmentation with a tandem quadrupole mass spectrometer. *J. Am. Chem. Soc*. **1978**, 100: 2274.
- Zähringer, U.; Lindner, B.; and Rietschel, E. T. Chemical structure of lipid A: recent advances in structural analysis of biologically active molecules, in Endotoxin in Health and Disease. (Eds: H. Brade, S. M. Opal, S. N. Vogel, D. C. Morrison), Marcel Dekker, New York. **1999**: 93-114.
- Zaikin, V.; Halket, J. Review: Derivatization in mass spectrometry 8. Soft ionization mass spectrometry of small molecules. *Eur. J. Mass Spectrom*. **2006**. *12*(1): 79-115.
- Zhang-Sun, W.; Augusto, L. A.; Zhao, L.; and Caroff, M. *Desulfovibrio desulfuricans* isolates from the gut of a single individual: Structural and biological lipid A characterization. *FEBS Letters*. **2015**, *589*: 165-171.
- Zubarev, R. A.; Kelleher, N. L.; McLafferty. F. W. Electron captures dissociation of multiply charged protein cations. A nonergodic process. *J. Am. Chem. Soc*. **1998**. *120*(13): 3265-66.

Appendix:

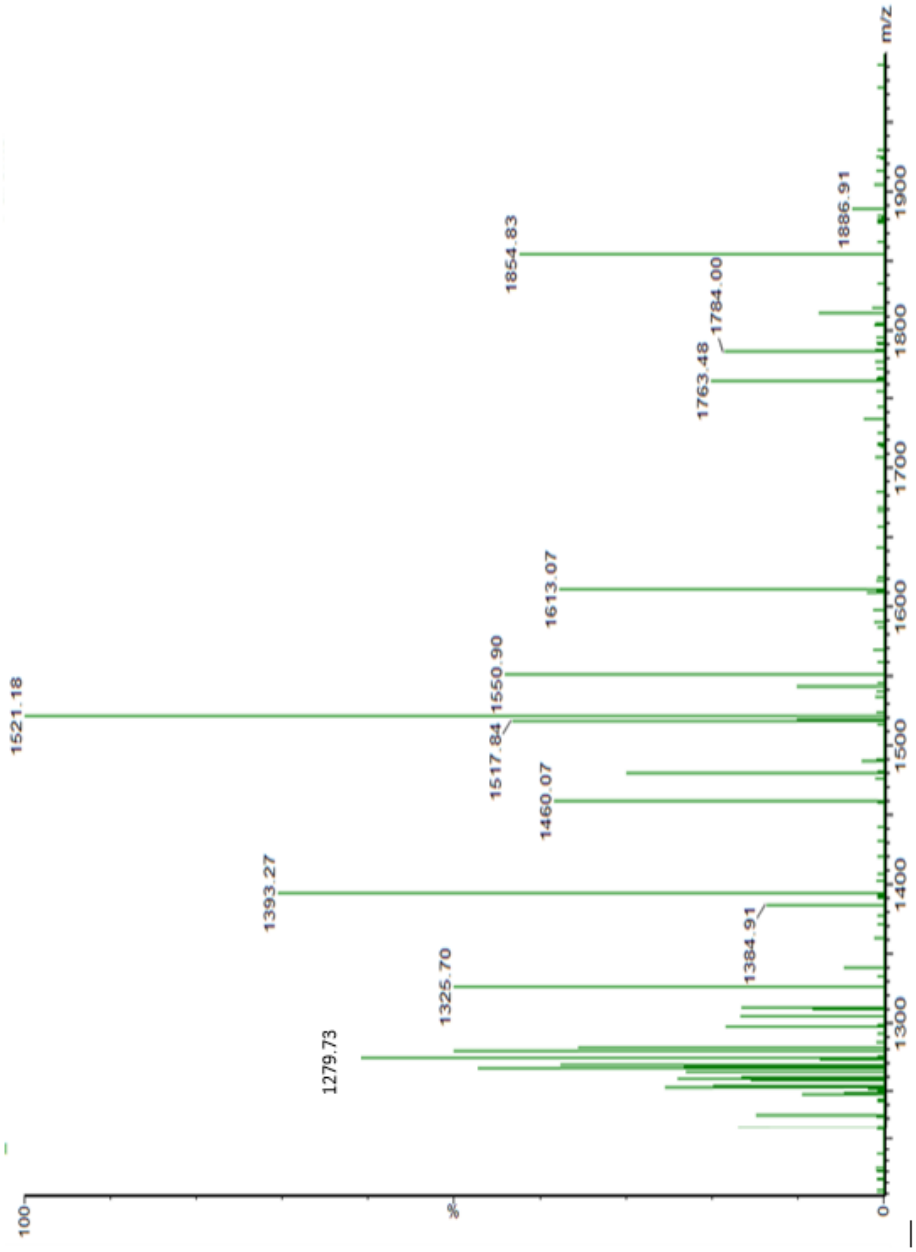

Appendix1: The ESI-QqQ-MS precursor ion scan of the deprotonated molecules at *m/z* 1279.73 obtained from LPS isolated from SJ-19a.

Appendix 2: The ESI-QqQ-MS precursor ion scan of the deprotonated molecules at *m/z* 1688.26 obtained from LPS isolated from SJ-55a.

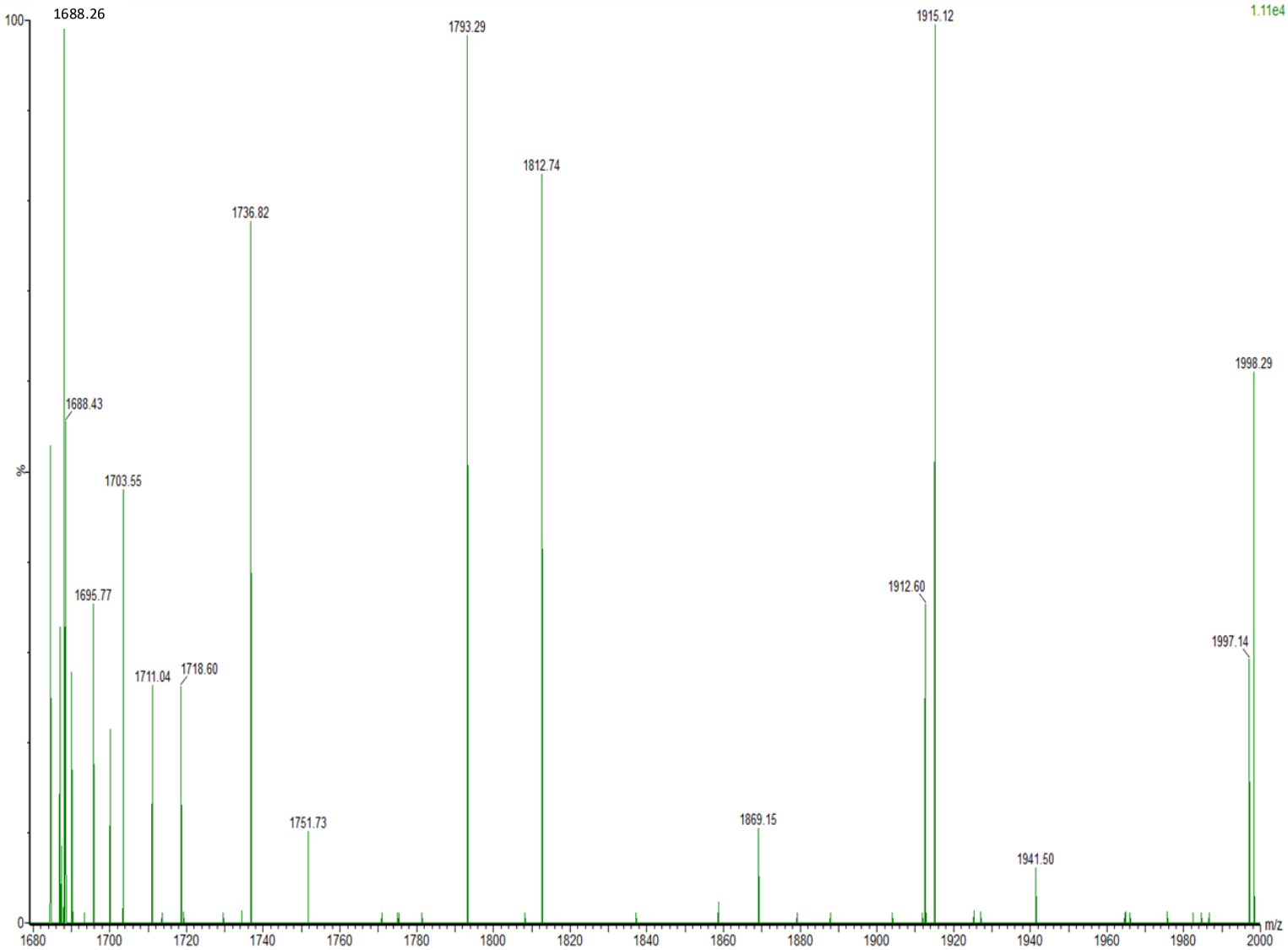

Appendix3: The ESI-QqQ-MS precursor ion scan of the deprotonated molecules at *m/z* 1506.09 obtained from LPS isolated from SJ-113a.